SEISMO-ACOUSTIC ROUGH INTERFACE SCATTERING OF SURFACE-GENERATED AMBIENT NOISE IN A STRATIFIED OCEAN

by

JIN-YUAN LIU
B.S. in Oceanography, National Taiwan Ocean University
(1978)
M.S. in Mechanical Engineering; M.S. in Mathematics, Univ. of Illinois at Chicago
(1982,1984)

Submitted to the Department of
Ocean Engineering
in Partial Fulfillment of the
Requirements of the Degree of

DOCTOR OF SCIENCE

at the
MASSACHUSETTS INSTITUTE OF TECHNOLOGY
1992

Signature of Author _____
Department of Ocean Engineering, 1992

Certified by _____
Professor Henrik Schmidt, Thesis Supervisor

Accepted by _____
Professor A. Douglas Carmichael
Chairman, Departmental Committee on Graduate Students

Seismo-Acoustic Rough Interface Scattering of Surface-Generated Ambient Noise in a Stratified Ocean

Jin-Yuan Liu

Department of Ocean Engineering

Massachusetts Institute of Technology

Cambridge, MA

TO

MY PARENTS AND PARENTS-IN-LAW

MY WIFE

AND

MY SON AND DAUGHTER

FOR THEIR

HELP

UNDERSTANDING

AND

ENCOURAGEMENT

THROUGHOUT THE YEARS AT

MIT

Acknowledgments

I am gratefully indebted to Professor Henrik Schmidt for suggesting this thesis problem and for guiding it to its completion. His guiding hand is evident throughout this thesis. As faculty advisor, he encouraged individual expression by granting complete freedom in developing the analysis, yet was *always* available for judicial advice. In an average of one visit per week in his office throughout this study, *never* had I left his office without gaining more understanding of the investigated problem. His dedication and commitment to guidance of his students have almost completely changed my view for being a mentor, and I hope, some of his approaches are now also my own. My indebtedness to him extends far more beyond my capability of exercising this language.

I would also like to express my gratitude to the members of my thesis review committee, Professor Arthur B. Baggeroer and Dr. Yueping Guo at MIT, and Dr. James F. Lynch at the Woods Hole Oceanographic Institution for their time and suggestions. My special thanks go to Professor Baggeroer; in particular, I have greatly benefited from his advice in the Part II doctoral examinations in the area of signal processing.

Special thanks are also due to my fellow colleagues Dr. Kevin LePage, from him I have learned many things during the course of this study, and Mr. Ken Rolt, for many editorial comments and proofreading the manuscript. Also, I would like to thank all of my friends in Room 5-007 for their kind suggestions whenever appropriate.

The work was supported in part by NOARL through contract N00014-88-K-6009 and the Office of Naval Research, Arctic Program Office; to them I would like to express my profound thanks for their financial support.

Finally, I wish to express my most grateful thanks to my wife, Ming-Yu, for maintaining morale and taking care of the family, to my son, Ben, and my daugh-

ter, Yenting, for their cheerful smile and *pressure-release* giggle. To my parents and parents-in-law, I owe them so much for their spiritual and financial support throughout the years at MIT. Without their understanding and support I would not have been able to give full attention to this work and to complete it successfully.

Abstract

There is strong experimental evidence that seismic interface waves are important carriers of low frequency surface-generated ambient noise in shallow, as well as deep, ocean environments. In shallow water the excitation of these evanescent wavefield components can be explained by direct coupling through the evanescent field produced by the surface sources. However, in deep water the vertical separation of the surface sources and the elastic bottom is too large for the direct coupling to occur, and therefore the theory assuming horizontal stratification cannot account for the experimentally observed seismic components.

This thesis theoretically investigates the hypothesis that the strong seismic components in the deep ocean noise field are due to scattering by rough interfaces in the bottom, coupling the vertically propagating field produced by the primary sources into evanescent waves in the bottom. The analysis combines a previously developed perturbation theory for rough interface scattering and a model for the noise field in a stratified ocean due to random surface sources, to derive the cross-spectral correlation function of the scattered noise field in a horizontally stratified ocean environment. The model was first applied in a simple three-layer ocean model, to examine the fundamental spectral features of the scattered seismic noise. It was demonstrated that since the secondary sources provided by the scattering are placed close to the bottom interfaces where the seismic interface waves have their maximum excitation, these waves will dominate not only the scattered field, but also the total noise field. As a result, the model predicts an increase in the noise level close to the bottom, which is consistent with experimental observations.

The model was then used to analyze a recent experimental data set collected in the Pacific Ocean. Using a realistic bottom model of a thick sediment layer over

a hard crustal subbottom, it was demonstrated that a rough interface between the sediment and the subbottom provides strong coupling of the noise field into the various seismic modes, in turn yielding a sharp rise in the noise level below a certain transition frequency, the value of which is dependent on the sediment thickness and shear properties. This behavior is also consistent with the experimental observations, and as has been demonstrated earlier for shallow water environments these results strongly suggests that the waveguide propagation mechanisms must be eliminated before the noise data are used to infer the spectral level of the surface sources.

Finally the spatial correlation of the noise fields was investigated. It was demonstrated that for roughness correlation lengths shorter than the acoustic wavelength, the scattering has the effect of decreasing the horizontal spatial coherence of the total noise field relative to the plane stratified case. This in turn suggests that the spatial coherence of the deep ocean noise field may be used as a basis for inversion for subbottom roughness. The effects of non-isotropy of the roughness on the noise field directivity were examined by solving a fully three-dimensional geometry with a realistic roughness spectral model.

Contents

List of Figures

Nomenclature

a	constant used in Eq. (1.5)
A	scattered operator defined by Eq. (2.35)
b	constant used in Eq. (1.5) and Eq. (1.10)
B	boundary operator defined by Eq. (2.10)
c	sound speed
C	correlation function
d	depth of water column
D	diagonal matrix defined by Eq. (3.23), or *fractal dimension* defined in Eq. (4.11)
e	diagonal matrix containing vertical exponential defined in Eq. (2.31)
f	frequency in Hz
F_0	constant used in Eq. (1.4)
g	acceleration due to gravity, or depth-dependent Green's function
G	Green's function
h	root-mean-square height of the roughness
I	scattering operator defined by Eq. (2.17) and (2.18)
j	phase factor
$\mathbf{k}$	horizontal wavevector
k_n	characteristic wavenumber in the Goff-Jordan roughness spectrum defined in Eq. (4.13)
k_s	characteristic wavenumber in the Goff-Jordan roughness spectrum defined in Eq. (4.13)
K	medium wavenumber

ℓ	interface roughness correlation length
M	interface roughness correlation function
N	ocean surface roughness correlation function
P_b	interface roughness spectrum
P_s	ocean surface roughness spectrum
q	modulus of scattered wavevector
$\mathbf{q}$	scattered horizontal wavevector
Q	normalized source level, or matrix defined by Eq. (4.10)
$\mathbf{r}$	coordinate in range
s	scattered field potential
S	source strength, or salinity in Eq. (1.2), or frequency spectrum in Eqs. (1.11) and (1.12)
t	time
$\mathbf{t}$, $\mathbf{T}$	traction vector
T	temperature
u, U	displacement in x-coordinate, or U is the wind speed in Eqs. (1.11) and (1.12)
v, V	displacement in y-coordinate
w, W	vertical displacement
z	depth coordinate (positive downward)
z', z_s	source depth

Greek Symbols

α	an angular parameter used in Eq. (1.10), or vertical component of the compressional wavevector, $\alpha = \sqrt{k^2 - K^2}$

β vertical component of the shear wavevector

γ roughness elevation

δ Dirac delta function

ζ transformed variable in Eq. (4.5), or a parameter in Goff-Jordan roughness power spectrum defined in Eq. (4.13)

κ acoustic wavenumber of the medium

λ Lame constant, or wavelength

Λ field potential for shear wave

μ Lame constant

ν parameter in Goff-Jordan roughness power spectrum defined in Eq. (4.8), or spreading factor defined in Eq. (1.10)

ρ density

σ stress

φ field potential

ϕ field potential for compressional wave

Φ general field potential

Ψ field potential used in Eq. (1.1)

χ field potential

ψ field potential for shear wave

ω angular frequency

Superscripts

$-$ (overbar) quantities in the absence of roughness

t for "total" field

$+$ upgoing wave

$-$ downgoing wave

r	radial direction
T	transpose of a vector/matrix
θ	tangential direction

Subscript

i	i^{th} layer
p	quantities for compressional wave
s	quantities for shear wave
ω	quantities at frequency ω

Special Symbols

$\tilde{}$	Fourier coefficients of the related quantities
$\langle\,\rangle$	ensemble average

Legends for Figures

CL	roughness correlation length
F	frequency
Nu	ν
RD	receiver depth
RMS R	root-mean-square roughness
SD	source depth
ST	sediment thickness
WD	water depth

... I have only knocked on
the door of *Ocean Acoustics* [Chemistry], and I see
how much remains to be said.

— with poetic license from *The Six-Colored Snowflake*,
Johannes Kepler, 1611.

Chapter 1

Introduction

— in which the idea is conceived.

1.1 Background and Motivation

Ambient noise is an important part of underwater sound. It plays a significant role in practical applications in that it essentially limits the effectiveness of any device which relies on acoustic signals as a means of communication, detection, or exploration in the ocean. For example, the detection or estimation of an either known or unknown waveform is dependent upon the ratio of signal to noise, and the design of filters for estimating a random process containing a desired signal depends upon the time or spatial coherence of the ambient noise. Recently, noise itself is being studied as a diagnostic of other ocean processes and properties, such as processes that occur at the air-sea interface or geophysical properties probed by noise interacting with the ocean bottom. Hence, noise is of great interest both as interference and signal.

The deep ocean ambient noise spans the frequency range from ultra low frequency below $1\,Hz$ to some $100\,k\,Hz$. At the high frequency end, the contribution to the ambient noise field may be due to various processes such as wind waves, radial oscillation of bubbles, and thermal noise, *etc.* At the intermediate to high frequencies, the primary sources are shipping noise, surface processes, and rain noise. In the low extreme below $1\,Hz$, the ambient noise may be generated by non-linear wave interaction, atmospheric turbulence or seismic events. For example, the theories due to Longuet-Higgins [1] and Hasselmann [2] predict that the pressure fluctuations resulting from nonlinear wave-wave interactions at the ocean surface may propagate in the ocean, and reach the ocean sea floor, thus creating microseismic motion on, or within, the sea bed.

Above $1\,Hz$, and within the infrasonic regime (below $20\,Hz$), the spectrum of the ambient noise measured near the sea bed of a deep ocean tends to show a consistent increase of 8 to $10\,dB$ per octave toward the lower frequency end, yet the origins of this noise or the processes involved are largely unknown. A recent experimental study [3] in the deep ocean has shown that seismic interface-wave components exist beyond the frequency range predicted by the classical elastic waveguide theory, and that these components in fact dominate the ocean bottom noise field. The authors suggested that the dominance of seismic interface waves may be due to scattering processes; however, no theoretical support for this hypothesis has so far been provided.

In a shallow water environment, it has been shown that direct radiation from the sea surface noise may be coupled into seismic waves [4, 5] through modal matching, either in the propagating or evanescent part of the wave spectrum. However, in a deep ocean, the vertical separation of the surface sources and the elastic bottom is too large to allow for direct excitation of the seismic interface waves. Since direct coupling cannot account for this phenomenon, other coupling mechanisms must be

responsible. Potential mechanisms may include

- continental slopes;
- sea bed facets;
- sea bed random inhomogeneities;
- sea bed roughness.

The continental slopes are unlikely coupling mechanisms since the propagation of seismic interface waves is almost unaffected by changes in water depth. Sea bed facets are possible candidates and should be identifiable in the data since the interface waves produced would have clear directional properties. The isotropic component of the seismic noise field must be due to a diffuse mechanism such as the last two mentioned, the random inhomogeneities and the roughness of the sea bed. Research proceeds in both areas, and preliminary results have indicated that, at least qualitatively, both mechanisms may explain the large interface wave component observed.

1.2 Objectives and Approaches

Motivated by the experimental observations and aforementioned conjecture, this dissertation investigates the possible coupling of the surface generated ambient noise into seismic waves by rough interfaces on and/or within the sea bed. We therefore postulate that *the strong excitation of the evanescent seismic components is due to scattering of the surface generated noise by rough interfaces in the sea bed.*

We shall first verify the above hypothesis, then analyze the experimental data

using the present theory, and finally extend our analysis to the spatial properties of the noise fields. Thus, the objectives of this research are to

- derive a combined noise-scattering formulation suitable for the study of the basic physics of rough interface scattering of ambient noise;
- devise a numerical scheme to compute rough interface scattering of the seismo-acoustic noise field;
- implement the numerical procedure to solve a canonical ocean waveguide problem for analyzing the fundamental physics of the scattering processes;
- solve a deep ocean problem, and compare the theoretical prediction with the available experimental data;
- analyze the experimental data based upon the scattering model developed in this study and the theory of seismo-acoustic propagation;
- study the spatial correlation and directivity of the noise field due to the rough interface scattering.

The various approaches dealing with the interface scattering processes were reviewed in Ref. [6] and these will be discussed in Sec. 1.3.1. The most common approaches are perturbation methods for small roughness and the Kirchhoff approximation (tangent plane methods) for large and smooth roughness. In this study we are mainly interested in scattering of low frequency sound (between 1 to $20\,Hz$), which has acoustic wavelengths larger than the roughness, making the perturbation approach an appropriate choice. The approach we take to describe rough interface scattering in a stratified medium with stochastically rough interfaces is based on the previously developed theory by Kuperman and Schmidt [7]. Their method employs

matrix operators describing a pair of boundary conditions which govern the mean (coherent) field and scattered (incoherent) field, respectively. The use of matrix operators has not only greatly reduced the amount of algebra as one would normally encounter in perturbation analysis, but it has also been compatible to the existing algorithm for the unperturbed problem, making the formulation particularly attractive for numerical implementation. For the modeling of surface generated ambient noise, we utilize the approach developed by Kuperman and Ingenito [8] in studying noise fields generated by a random distribution of surface sources.

We combine these two theories to derive the spatial correlation function for the noise field as a summation of the correlation of the mean noise field produced in a stratified ocean and the correlation of the scattered noise field due to the interface roughness. The resulting formulation is capable of treating the wave scattering problem in an environment with any number of, and any type of, rough interfaces in a stratification of fluid and elastic layers, and generated by the random sources in an infinite plane near the ocean surface. Thus the present analysis is valid for analyzing the seismo-acoustic noise field in the ocean environment illustrated in Fig. 1.1.

1.3 Relevant Issues and Related Literature

The study of wave propagation in an environment shown in Fig. 1.1 represents a combined effort which draws theories from at least the following three separate fields:

- Theories of wave scattering from random rough surfaces.
- Theories on seismo-acoustic wave propagation in a stratified medium.
- Methods for description of rough interfaces.

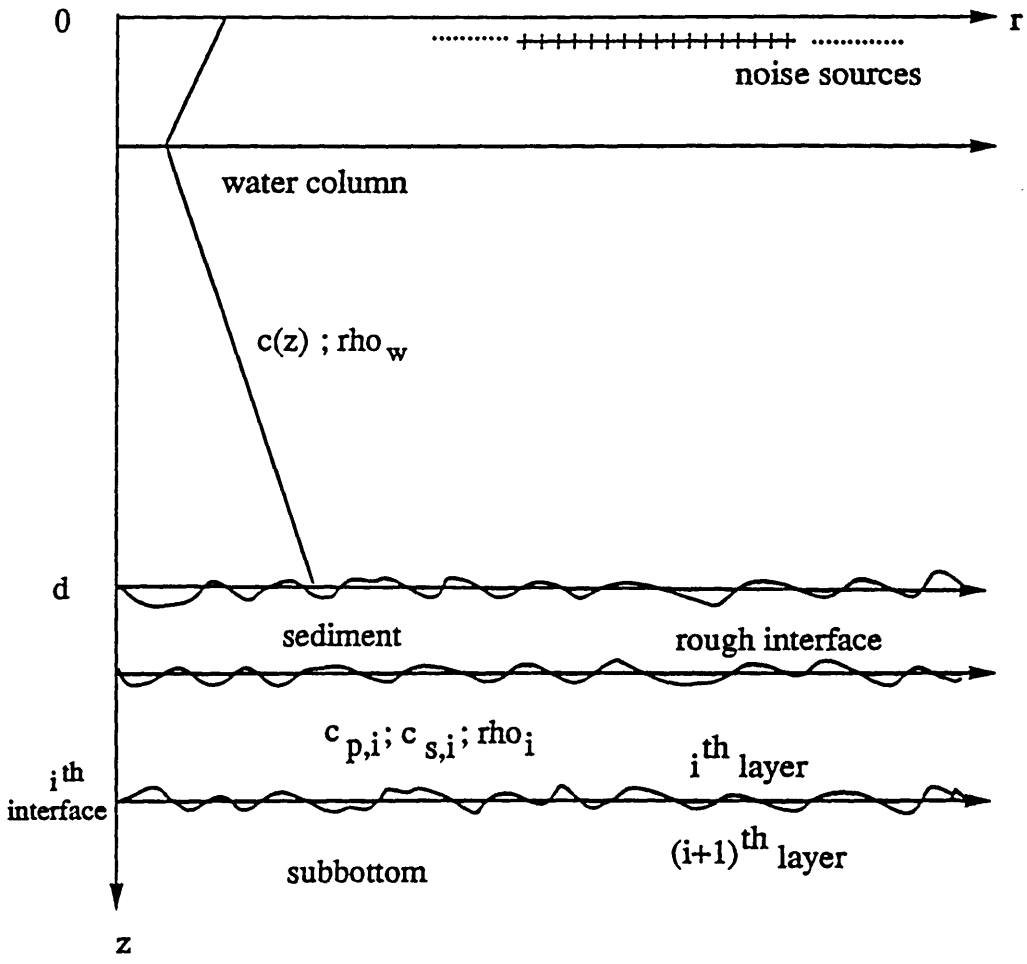

Figure 1.1: Environmental model for simulating surface-generated ambient noise in a horizontally stratified medium with rough interfaces.

In this section we discuss some related issues and literature in each of the above disciplines. This review and discussion serve the purpose of defining the basic assumptions and justifying the bases of employing the first-order perturbation theory and the direct-global-matrix numerical technique in this study, by comparing the advantages/disadvantages of various methods available in the current literature.

Some useful results from the literature relevant to the present analysis are presented with comments. The vast volume of the literature in each of the above-mentioned disciplines prohibits an extensive coverage on all aspects of the problem in a single section. Thus it is stressed that only those which bear close relation with the present study are discussed here.

1.3.1 Wave Scattering From Rough Surfaces

Wave scattering from rough surfaces has been a subject of intensive research for nearly 150 years [9] due to its wide applications in many areas such as acoustics, electromagnetics, and seismology. In this section we concentrate our discussion only on the *methodology* in treating rough surface scattering problems rather than the actual physical problems because we use one of the approaches reviewed here in the present analysis.

Most of the theoretical work on the methods of rough surface scattering can be classified into two categories: *approximation methods* such as perturbation theory and Kirchhoff theory, or more *rigorous methods* such as integral equation techniques, variational methods and Green's function approaches. In the former category, the Kirchhoff theory has gained more attention in the field due to its simplicity; however the justification of its use is often overlooked. In the latter category, although these

theories are more rigorous, they are seldom used, especially in comparison with experiments because they are mathematically abstract and often subject to unrealistic approximations, leading to difficulties in establishing their ranges of validity. In this review we emphasize the discussion on the perturbation theory, in particular, lower-order perturbation analysis, because it is the main tool which will be used in this study.

About the Perturbation Theory

The perturbation theory was originally developed by Rayleigh [10] for studying the wave scattering of a normal incident plane-wave onto a sinusoidally corrugated rough surface. The theory is particularly useful for low frequency wave (equivalently, large wavelength) scattering. The basic idea is simple: since the roughness is "small" in comparison with the "scale" of the problem for slightly perturbed surfaces, the resulting wave field is expected to deviate from the unperturbed ones at most the order of the scale of the roughness. Thus, by the theory of Taylor series expansion, the total field at a point may be expressed as an unperturbed solution with an addition of small correction due to the perturbation. To be more specific, the unknown scattered field (for simplicity, we consider acoustic field) may be written as a sum of *outgoing* plane waves,

$$\Psi(\mathbf{x}) = \Psi_0(\mathbf{x}) + (\kappa h)\Psi_1(\mathbf{x}) + \frac{(\kappa h)^2}{2!}\Psi_2(\mathbf{x}) + \ldots + \frac{(\kappa h)^n}{n!}\Psi_n(\mathbf{x}) + \ldots, \qquad (1.1)$$

where $\Psi(\mathbf{x})$ represents the value of a field variable at a point $\mathbf{x}$, and $\Psi_0(\mathbf{x})$ is the solution for the unperturbed problem; κ is the vertical component of the acoustic wavenumber and h is the root-mean-square (RMS) height of the rough surface. The outgoing wave representation is assumed to be valid arbitrarily close to the rough surface, an assumption usually referred to as the Rayleigh hypothesis. Retaining N terms in the expansion, the resulting scattering cross section, which is found from a

second moment of the scattered field, is correct to order of $(\kappa h)^N$.

The derivation of the formalism is straightforward, but it is the validity of the approach which concerns us the most. It is often cited that the perturbation theory is valid if the RMS height is "small" compared with the wavelength, *i.e.*, $\kappa h \ll 1$, or more appropriately, $Ra = kh\cos\theta_i \ll 1$ (Ra - a parameter referred to as Rayleigh parameter), where θ_i is the angle of incidence. This seems to be obvious from Eq. (1.1) as we also assume that the perturbed variables Ψ_n for $n = 1, 2, 3, ..$ are at most in the order of $(\kappa h)^n$, making the contributions from the higher-order terms negligible. On the other hand, questions were raised as to whether the smallness of κh compared to 1 guarantees the success of the perturbation theory, and what defines the explicit criterion. Recent study by Thorsos and Jackson [11] gave us a clue for these issues, and since these issues are important to us, we pay a particular attention on this paper.

Thorsos-Jackson Analysis. In their study [11], the authors used the perturbation method to study a two-dimensional (1-D roughness) acoustic wave scattering from a pressure-release surface with a Gaussian roughness spectrum (a discussion on this spectrum will be given in Sec. 1.3.3). Emphasis was placed on the first-order perturbation theory, *i.e.*, only two terms on the right-hand-side of Eq. (1.1) were retained. Using an integral equation method (will be discussed later) and higher-order analysis, the authors concluded that the often-cited criterion, $\kappa h \ll 1$, is not sufficient to guarantee the success of the first-order perturbation theory. Another parameter $\kappa\ell$, where ℓ is the roughness correlation length, plays an important role in defining the region of validity. For example, there are cases which demonstrated that for a fixed value of κh, increasing $\kappa\ell$ (equivalently reducing the RMS slope) worsens the performance of the theory particularly for the backward scattering. A detailed discussion for the $\kappa\ell$ factor is provided in their paper; the fact is that increasing

$\kappa\ell$ will reduce the resonance wavenumber for the fourth-order term, leading to a contribution larger than the second-order term. However, the performance of the low-order theory (first- or second-order) is in general very good in *forward scattering*, an important conclusion which supports the use of the perturbation theory in this study; this is elaborated in a later chapter. Moreover, it should be remembered that since their analysis is based upon the *Gaussian roughness spectrum*, the results may not necessarily apply to roughness spectra that exhibit power laws. We shall examine this effect in Chapter 5.

The explicit criteria which define the region of validity were established in the paper. An important guideline is that if Gaussian roughness spectrum is used the low-order analysis is appropriate for $\kappa h \ll 1$ and $\kappa\ell \leq 6$. We shall check our conditions against this criterion whenever a situation is suitable to fit into this framework.

Perturbation Theory vs. Kirchhoff Approximation

Another popular approximate method is the Kirchhoff theory, originated from the study of light diffraction through an aperture by Kirchhoff [12]. The formulation is based upon the exact integral formulation, but approximation to the wave field is made *on the surface of the scatterer*. The basic idea is that, at any point on a scatterer, the surface is treated as though it is part of an infinite plane, parallel to the local surface tangent. Thus the theory is exact for an infinite, smooth, plane scatterer but is approximate for scatterers that are finite-sized, non-planar, or rough. It is expected that the method performs well if the surface is "gently undulating." A detailed discussion of the method may be found in many books, which will be discussed later in this section. Here we would like to discuss some issues in relation to the perturbation theory.

There are always some ambiguities about which result is correct (or better) when

the smallness condition is satisfied for both the perturbation theory and the Kirchhoff theory, but the results differ. Some investigators claim the perturbation theory is more correct. However, it has been pointed out by Labianca and Harper [13] that it is unnecessary and highly undesirable to make the Kirchhoff approximation in conjunction with the small waveheight (perturbation) approximation. It is added by Thorsos and Jackson [11] that if the surface is such that the Kirchhoff approximation is valid ($\kappa\ell > 6$ for the Gaussian spectrum with average slope less than 20°), then the complete Kirchhoff approximation is superior to the perturbation approximation when $\kappa h \ll 1$. Moreover the Kirchhoff result gives us a way of easily including terms of higher order in κh, which presents great difficulties with the standard perturbation theory.

Therefore, a general conclusion may be drawn: if $\kappa h \ll 1$, the Kirchhoff approximation may or may not yield a better result. And if it does, then higher-order terms should be included when perturbation theory is employed, thus making the Kirchhoff theory a better choice in this case. However, if $\kappa h \ll 1$ and $\kappa\ell \leq 6$, then the higher-order terms make little contribution, and thus perturbation theory is the preferred approach. Again, it should be noted that the condition $\kappa\ell \leq 6$ was derived for the case of Gaussian roughness spectrum.

Perturbation Theory vs. Integral Equation Techniques

The use of integral equations to study surface scattering problems have been done by many investigators, *e.g.*, [14, 15]. It was mentioned that the integral equation method is a rigorous approach, thus the results are often regarded as "exact solutions" if the assumptions render a solution feasible. But, very often these assumptions are so restrictive, such as long correlation length, lack of correlation *etc.*, thus limiting the scope of realistic problems. Nonetheless, if the problem is solvable, the technique

often provides great physical insight. For example, the integral equation technique offers great potential for studying multiple scattering, a problem which can not be handled by perturbation theory because of the Rayleigh assumption (outgoing plane waves).

One advantage of perturbation theory over integral equation techniques is on computational efficiency and simplicity for realistic problems. This may be due in part to the formalisms and the solution methods employed. While roughness enters the perturbation formulation in terms of power spectra, in the integral equation method using a Monte Carlo calculation procedure for example, a sufficient number of realizations must be used to guarantee stability of the solution.

In summary, in spite of the fact that perturbation theory, particularly low-order theory, presents certain limits, it does provide a convenient and efficient technique and offer good results as long as we stay inside the region of applicability. Thus caution will be used to guard against the misuse of the theory, by appropriately justifying the conditions. It is worth noting that the low-order perturbation theory is in general robust in the forward scattering if one stays not too far away from the valid region.

Some Other References

Theories on wave scattering from random rough surfaces have been the subject of several books and numerous research papers, both theoretical and experimental. The most common quoted book is probably that by Beckmann and Spizzichino [16]. It considers the Kirchhoff solution to scalar wave scattering from periodic or random rough surfaces. Most of the results in this book may be equally well applied to electromagnetic waves or acoustic waves, with the scattered field representing either the electric, magnetic, or the acoustic field. Although written over a quarter of a

century ago, this volume remains a standard reference in use today as a basis for solutions. Later Beckmann [17] summarized the theories in Ref. [16], and briefly discussed composite surfaces and shadowing functions. A more recent book by Bass and Fuks [18] considers both the perturbation methods and Kirchhoff theory. This book considers more complete effects such as the effects due to self-shadowing and multiple scales of roughness; also multiple scattering is included.

Most recently, Ogilvy discussed the related theories and experimental results in a review article [6], and in a book on the subject [19]. The book summarizes in one place, virtually all of the current theoretical knowledge on scattering from rough surfaces. The insights offered by the mathematical methods and approximation also appeal to the study of scattering from three-dimensional bodies.

A survey of literature on acoustic wave scattering from the sea surface was conducted by Fortuin [20], in which he discussed both the perturbation and the Kirchhoff theory and compared the theoretical prediction with the experimental results of sea surface scattering. Other reviews on the subject may also be found in [21, 22].

The articles which bear direct application on the present analysis on rough interface scattering in an oceanic environment are those due to Kuperman and Ingenito [23, 24]. Following the idea developed by Bass and Fuks [18], a new set of perturbed boundary conditions was derived to replace the unperturbed ones, and was then used to study the specular reflection and transmission of an acoustic wave at a randomly rough two-fluid interface. It was shown that, when appropriate limits were invoked, the results reduced to those by earlier investigators using the Kirchhoff approximation. The approach taken in Ref. [24] was extended and generalized by Kuperman and Schmidt [7] to include elasticity and "nonlocality" of the boundary conditions into the formalism under the framework of the perturbation theory. More informa-

tion about Ref. [7] will be given in later sections as it becomes pertinent to various aspects of the present study.

1.3.2 Wave Propagation in a Stratified Medium

Many physical problems fall into this discipline by their own right in that the media, which support the waves propagating in them, are stratified either horizontally or range-wise, or both. This is evident in all of the three natural large-scale media: the atmosphere, the oceans, and the Earth. Even though the local variation of the wave-related properties of the medium is in general small, it has a profound effect on long-range propagation, notably due to refraction of the wave as it encounters discontinuities in a discretely or continuously stratified medium.

The study of wave propagation in a stratified medium is much more laborious in comparison with a uniform, homogeneous one, because of its complexity. Before the advent of modern high speed computers, the physical problems which could be solved analytically were limited to relatively few simple idealized geometries and the resultant expressions were often long and tedious. With the assistance of high speed computers and newly-developed numerical techniques our capacity in solving more realistic problems has been greatly enhanced; thus solutions to many problems which were hampered by unavailable efficient numerical algorithms and computational facilities are now possible. Since virtually all of the results presented in this thesis are generated by numerical computation, in this section we place our emphasis on reviewing the various numerical algorithms, and to justify the choice of the numerical algorithms adopted in this study.

The Ocean as a Horizontally Stratified Medium

The ocean environment is by-and-large horizontally stratified because most of the properties of the ocean such as temperature, salinity, density, sound speed *etc.*, vary much more significantly in the vertical (or depth) direction than in the lateral direction. This is supported by many oceanographic surveys, *e.g.* [25]. Among the physical properties, the one which concerns us the most is the sound speed variation. The sound speed c is a function of temperature, salinity, and pressure according to the empirical formula [25]

$$\begin{aligned} c &= 1449.2 + 4.6\,T - 0.055\,T^2 + 0.00029\,T^3 \\ &\quad +(1.34 - 0.01\,T)(S - 35) + 0.016\,z, \end{aligned} \tag{1.2}$$

where T is temperature in $^\circ C$, S is salinity in parts per thousand (ppt), and z is depth in meters, and sound velocity is in meters per second. The above equation is claimed valid for $0^\circ \leq T \leq 35^\circ C$, $0 \leq S \leq 45\,ppt$, and $0 \leq z \leq 1000\,m$. Another more complicated equation due to Wilson may be found in Ref. [26].

In the regions close to the water surface the variation of the sound speed is affected by the local conditions such as the seasonal change of the local temperature, or by storms which promote surface mixing. In the Arctic region the ice covering the surface has also a profound effect on the propagation.

Even though the variation of sound speed is relatively small, ranging between $1450\,m/s$ and $1540\,m/s$, and varying about $16\,m/s$ per $1\,km$ vertical (depth) distance, it has the most significant effect on long-range propagation of sound wave in a deep ocean. Due to refraction, the sound waves may be trapped inside a definite layer, avoiding interactions with the ocean bottom and surface. This produces an efficient sound-propagation channel known as *underwater sound channel* (USC), in which the sound wave decays in range very slowly.

There are situations in which lateral (range-wise) variations become appreciable, then the lateral variation in the stratification has to be taken into consideration. In that case, the present analysis needs to be further developed.

Numerical Solution Algorithm

The mathematical model describing wave propagation in a horizontally stratified medium will be reviewed in Chapter 2. The solution method using integral transform is also demonstrated there. Here we present some basic ideas and discuss the advantages of the numerical technique employed for this study over some other methods previously developed.

The use of digital computers for numerically solving the field problems in continuous media requires some kind of discretization. The two most notable discretization schemes are the finite difference method and the finite element method. In the former approach, the exact governing equations for the medium are first established, and subsequently discretized to give an approximate version of the governing equations suitable for numerical determination. In the latter approach, the medium itself is discretized, and in-effect the computer determines exact solution of now approximate problem. From the topological point of view, if the medium is composed of a finite number of horizontal layers, then the problem is well suited for the finite element approach. In this regard, the integral transform solution of the wave equation for horizontally stratified environment to be reviewed here is of the 'finite element' category.

The use of integral transform techniques to solve the wave equation in a horizontally stratified fluid or elastic environments is well established in underwater acoustics and seismology. By expressing the physical displacement and stress quantities in each layer by integral representations in the horizontal wavenumber, accounting for

both source contribution and unknown field satisfying homogeneous wave equation, a linear system for the unknown field amplitudes is formed by requiring the appropriate boundary conditions to be satisfied. The approach was used in the early stage to treat simple two- and three-layered models by Pekeris [27], Jardetzky [28], and Ewing, Jardetzky, and Press [29].

Before the large digital computers and associated solver software become available, the Green's function computation was tackled by propagator matrix methods introduced into seismology by Thomson [30], and later modified by, for example, Haskell [31]. However, as was realized very early, the original propagator matrix methods suffer the problem of numerical instability in the evanescent regime for high frequencies and large layer thickness, requiring special treatment and time-consuming algorithms to ensure numerical stability. This problem was attacked by Kennett [32] with improvement but unconditional stability was still not ensured; however, it was overcome later by Kennett [33] and Ha [34].

Advancement has been made by Schmidt *et al.* [35, 36] since the early 80's, using a direct global matrix (DGM) approach, which combined the original integral transform method [29] with efficient numerical techniques adopted from modern finite-element programs, *e.g.* [37]. By employing the local coordinate system for the "wave elements", the boundary condition equations are straightforwardly assembled to form a banded, positive-definite, global matrix. The global system is then solved efficiently by Gaussian elimination. Through appropriate organization, the numerical schemes are unconditionally stable. Despite the analytic equivalence between local propagator and direct global matrix solutions for the depth-dependent Green's function, there are number of important advantages of the latter technique [36]:

- Any number of sources can be conveniently treated because the fields produced by multiple sources are simply superimposed, and no dummy interfaces have to be introduced at the source depths.
- Any number of receiver depths can easily be treated, with only one solution pass, since the wavefield potentials are found in all layers simultaneously.
- In contrast to the situation for techniques based upon propagator matrices, mixed fluid/solid/vacuum cases are easily treated in an efficient manner.
- Time-consuming stability assurance problems do not arise, because they are removed automatically by choosing an appropriate coordinate system within each layer together with a proper organization of the global system.

The numerical scheme has been fully implemented in a computer code SAFARI [38], standing for *Seismo-Acoustic Fast Field Algorithms for Range Independent Environments*, and is accessible through the Acoustics Research Group of Ocean Engineering Department at MIT. The SAFARI scheme forms the basis for the numerical algorithm used in this thesis.

Some Related References

Related literature on the subject is abundant. The most notable book with ocean acoustics application is probably that by Brekhovskikh [39]. Since its publication, it has attracted a great deal of attentions in underwater acoustic community. It provides a systematic exposition of the theory of the propagation of elastic and electromagnetic waves in layered media. An earlier classic by Ewing, Jardetzky, and Press [29] establishes the integral transform solution of the wave equation in horizontally stratified media, forming the base for many subsequent studies. A more recent volume by Aki and Richards [40] attempts to give a unified treatment of those

methods of seismology that are currently used in interpreting actual data. The book develops the theory of seismic-wave propagation in realistic Earth models, in which the medium properties vary only with depth; it presents the specialized theories of fracture and rupture propagation in a horizontally stratified medium.

Traditionally, the problems of rough surface scattering and wave propagation in a stratified medium have been treated separately. However, Kuperman and Ingenito [24] have presented a self-consistent perturbation approach for normal mode propagation in a waveguide with a rough fluid bottom. Later, the approach was extended by Kuperman and Schmidt [41] where elasticity was introduced into the formalism by combining the waveguide perturbation procedure with Schmidt's elastic full-wave propagation method [42, 43]. In Ref. [41], it restricted itself to the decay of the coherent component of the acoustic field in a quasi-Kirchhoff perturbation limit, which involves only the leading term of the expansion of the correlation function of the interface roughness. These restrictions were eliminated in a later paper by the same authors in Ref. [7], where the authors extended the previous results in Ref. [41] to allow for arbitrary surface roughness spectra and computation of the mean (coherent) field as well as scattered (incoherent) field. Since we have followed the development in Ref. [7], the important results in Ref. [7] are summarized in Chapter 2.

1.3.3 Description of Rough Interfaces

This dissertation concerns wave scattering from rough surfaces. Our interests are to predict the scattered acoustic fields resulting from irregular interfaces such as an ocean sea bed, or those within the stratified sea floor. In view of their random nature, these interfaces are more appropriately treated as samples of a random process, even though it is a single well-defined (but unknown) deterministic function. Moreover, as

will be seen in the formulation, the parameterization of rough interfaces and ocean surface in terms of their roughness power spectra (or simply roughness spectra) is the most useful representation for describing acoustic scattering from such surfaces.

Several second-moment statistical models in terms of roughness power spectra which are useful in describing rough surfaces in the ocean environment are presented and discussed in this section. Some of these models will be used in the later chapters, and comparisons of results using different roughness spectra will be investigated in Chapter 5.

Gaussian Spectrum

Among all available models, the Gaussian spectrum has probably gained the most attention in application. The definition of the roughness spectrum in relation to the spatial correlation function is given in Eq. (2.20). The Gaussian spectrum for 1-D rough surfaces is

$$P_b(\kappa) = \sqrt{2\pi}\ell\, e^{-\kappa^2\ell^2/2}. \tag{1.3}$$

Even though it may not be appropriate for describing the natural rough surfaces under consideration, in the application of perturbation theory for rough surface scattering, the Gaussian spectrum is a useful simplification for several reasons. First, it restricts the surface to a single horizontal spatial scale, giving a convenient and often-used test for scattering theory approximation. Second, in comparison with the power law spectra, the latter introduces surface relief extending beyond the perturbation limits, in all but the low frequencies. Third, it is intrinsically interesting for a number of rough surface scattering problems, notably in electromagnetic scattering. And fourth, results from the Gaussian spectrum suggest how the first-order perturbation theory becomes inaccurate for backscattering from natural surfaces when the level of the roughness spectral density is very low near the acoustic wavenumber [11].

We use the Gaussian spectrum for the test case in the theoretical model, in particular, in the investigation of fundamental mechanisms. The results from the Gaussian case may be considered as a benchmark solution.

Power Law Spectra

Natural rough surfaces such as the ocean sea floor tend to extend their high frequency components beyond the limits describable by the Gaussian spectrum. In some cases, they are more appropriate described by a power law spectrum. Bell [44, 45] considered a power law spectrum with functional form

$$P_b(\kappa) = \frac{F_0}{\kappa^2 + \kappa_0^2}, \tag{1.4}$$

where F_0 is a parameter determined by the RMS roughness, and κ_0 is a characteristic wavenumber separating a "white" spectrum at low wavenumber from a "red" spectrum at high wavenumber with a length scale κ_0^{-1} corresponding to its transition. At large wavenumber ($\kappa \gg \kappa_0$), this spectrum decays at the rate κ^{-2}, which is much slower than the Gaussian spectrum. However, Fox and Hayes [46] argued that spectral slopes other than order -2 are observed on bathymetric profiles, and subsequently they proposed a two-parameter model

$$P_b(\kappa) = a^2 \kappa^{-2b}. \tag{1.5}$$

Even though this model extends to an arbitrary decay rate, it suffers the problem that at low frequency, extrapolating the power law too far towards zero frequency leads to large values of topographic variance, in conflict with the overall flatness of the ocean bottom at long wavelength. The model was later extended to include angular dependency in a form

$$P_b(\kappa) = a(\theta) \kappa^{b(\theta)}. \tag{1.6}$$

This *ad hoc* model, although simple, is not sufficient to account consistently for many aspects of an anisotropic topography.

Goff-Jordan Model

Hinted by the Bell, Fox and Hayes models, Goff and Jordan [47] proposed a five-parameter anisotropic model. This five-parameter model behaves with power law decay rate at the high frequency, and is suitable to account for RMS roughness, two length scales, mountain strike orientation, and characteristics of the roughness in terms of *fractal dimension* [48]. The model was tested through the use of inversion techniques from the real data, and showed in general satisfactory agreement. This spectrum forms the basis for the modeling of deep ocean sea floor in the present analysis, and thus deserves a special attention. A review is provided in Sec. 4.3 in conjunction with a simulation for a deep ocean waveguide.

Sea Surface Roughness

In this study we have treated the random surface waves as the ambient noise generators. It enters the formulation in terms of wavenumber spectrum of the ocean surface roughness for monochromatic wave scattering. Most of the available results refer to the frequency spectra, but keep in mind that the dispersion relation for deep ocean gravity waves relates wavenumber and frequency in a form

$$\omega^2 = g\kappa, \tag{1.7}$$

where ω is the angular frequency of the surface wave and g is the gravitational acceleration. For this case, the ocean surface roughness spectrum due to the wind waves can be expressed as [49]

$$P_s(\kappa) = \frac{\sqrt{g}}{2\sqrt{\kappa^3}} S(\sqrt{g\kappa}) K(\kappa, \alpha), \tag{1.8}$$

where $S(\sqrt{g\kappa}) = S(\omega)$ is the frequency spectrum (to be given below). The parameter $K(\kappa, \alpha)$ is a function of the angular distribution of sea wave energy normalized so that

$$\int_{-\pi}^{\pi} K(\kappa, \alpha)\, d\alpha = 1, \tag{1.9}$$

where α is the angle between the average direction of the wind and the direction of propagation of a surface wave with wavenumber κ. The experimental data are satisfactorily described by [50]

$$K(\kappa, \alpha) \;=\; \begin{cases} b\cos^{\nu(\kappa)}\alpha, & |\alpha| \le \frac{\pi}{2} \\ 0, & |\alpha| > \frac{\pi}{2} \end{cases} \tag{1.10}$$

where $\nu(\kappa)$ varies from 10 at low frequencies to 2 at high frequencies. The factor b is determined from the normalization condition. Sometimes values of $\nu = 2$ or $\nu = 4$ are used for all κ.

For *fully-developed* wind waves, the frequency spectrum of the surface waveheight may be satisfactorily described by the *Pierson-Moscovitz spectrum* [51]

$$S(\omega) = C_{pm} \cdot \frac{g^2}{\omega^5}\, exp\left[-0.74\left(\frac{g}{\omega U}\right)^4\right], \tag{1.11}$$

where $C_{pm} = 8.1 \times 10^{-3}$, and U is the wind speed in m/s. Another model referred to as *Pierson-Neumann spectrum* can also be found in literature [52]; it is given by

$$S(\omega) = C_{pn} \cdot \omega^{-6}\, exp\left[-2\left(\frac{g}{\omega U}\right)^2\right], \tag{1.12}$$

where $C_{pn} = 2.4\, m^2/s^5$. The frequency spectrum $S(\omega)$ has unit m^2-s.

It is noted that the wavenumber spectrum of the surface waveheight is generally colored. However, in this initial attempt to model rough sea floor scattering due to surface-generated ambient noise, we have placed our attention on the coloring effect on the ambient noise due to rough sea floor, taking a white spectrum for

surface random sources for simplicity. Thus care must be exercised in interpreting the results derived from the white noise assumption. We shall discuss this in Sec. 4.6.

Some Related References

In Chapter 2 of Ref. [19] the statistical methods used to describe random rough surfaces are discussed. The concepts of the height probability distribution and the height correlation function are introduced. A more general discussion of various statistical models of rough surfaces is also provided by Ref. [53].

Previous works in the study of sea floor morphology using statistics included Agapova [54], who generated mean, variance, skewness, and kurtosis statistics from measurement of slopes of a transect of the mid-Atlantic ridge. Heezen and Holcombe [55] calculated the average distribution of slopes without regard to spatial frequency for a physiographic province over a large portion of the North Atlantic Ocean. Krause and Menard [56] studied depth distribution from many profiles in the east Pacific Ocean and found them to be normally distributed. The distribution of slopes in a small area of the eastern North Pacific was investigated by Larson and Spiess [57] using a deep-towed instrument package, and cumulative frequency plots of slopes in two areas of the East Pacific Rise were generated by Krause *et al.* [58]. They found a very consistent power law form to describe their distributions and concluded that marine geomorphology could be described using only a few parameters.

Furthermore, Neidell [59] obtained the spectral estimates of bathymetric profiles from Atlantic and Indian oceans. All the spectra showed a "red noise" in nature; that is, in a power law description, and the power decreases with increasing spatial frequencies. Berkson [60] also attempted to fit a variety of bottom types with a power law form and found that the power law form seemed to be consistent over many types of topography. A polar autocorrelation function was developed by McDonald and

Katz [61] attempting to describe the directional dependence. Caly and Leong [62] studied the relationship between the spatial coherence and sea floor roughness, and estimated the RMS roughness of microtopography ($< 0.2\,km$). Akal and Hovem [63] used two sets of stereo-pair bottom photography to generate a two-dimensional spectrum of sea floor roughness and developed a contoured bathymetric chart. Recently, Naudin and Prud'homme [64] described bottom morphologies for several areas based upon the multibeam sonar data collected by the SEABEAM system. Earlier work of Berkson [60] was extended to estimate the sediment-basaltic interface roughness by Berkson and Matthews [65].

In summary, there are several stochastic models based upon second-order statistics for the sea floor morphology, but all are under the most fundamental assumption of *stationarity*; in reality this may not be appropriate. Thus in using the above model, one should judiciously pick a region so that the required condition is met; a procedure of which has been described in Ref. [46].

1.4 Scope of the Dissertation

In Chapter 2 of this dissertation, the perturbation theory that combines rough surface scattering with elastic wave propagation in a horizontally stratified medium developed in Ref. [7] is summarized. Also, the approach developed by Kuperman and Ingenito in Ref. [8] for noise field generated by surface random sources is outlined. The combination of the two theories results in a general formalism for the cross-spectral correlation function of the scattered noise field. Here we also discuss the underlined assumptions and interpret the formulation with respect to the waveguide environment under analysis.

In Chapter 3, we apply the derived formulation to analyze the scattering mechanisms of surface-generated ambient noise. The main theme of this chapter is to investigate the basic coupling mechanisms between the surface-generated ambient noise with the elastic sea bed. In order not to obscure the objectives, the model geometry is kept simple: a canonical waveguide with a uniform water column bounded above by vacuum, and below by a semi-infinite elastic sea bed. Wavenumber spectrum is the main subject of the investigation because it is illustrative in identifying various waves. Physical interpretation of the scattering mechanisms is provided.

In Chapter 4, we then analyze a deep ocean data set from the Pacific using a simulated deep ocean model. Comparison is made between the predicted frequency spectra and the spectra from experiments. Our efforts are devoted to interpret the characteristics of the observed frequency spectra, and to assess the performance of the present theory. Comments are made in relation to the assumptions which have been applied in the theoretical prediction.

The spatial properties of the noise fields are studied in Chapter 5. Horizontal correlation, vertical correlation, effects of various roughness spectra and of variation of the sound speed throughout the water column, and directionality of the noise fields are among the subjects of interest. The dissertation is concluded with a summary and a suggestion of further developments in Chapter 6.

Chapter 2

Theory

— in which the related theories are reviewed,
and the desired formulations
are derived.

2.1 Introduction

In this chapter we derive a combined noise-scattering formulation suitable for studying rough interface scattering of surface-generated ambient noise for an environment shown in Fig. 1.1. We first state the basic assumptions which are made throughout this study, then review the basic mathematical model for wave propagation in a homogeneous, isotropic, and horizontally stratified medium with unperturbed boundaries. Since the related literature for this problem is abundant, *e.g.* [29, 66], only a brief outline of the features relating to the present study will be given.

The problem under analysis shown in Fig. 1.1 may be treated as a superposition of two subproblems as shown in Figs. 2.1 and 2.2, each of which has been studied previously in Ref. [7] and Ref. [8], respectively. Since we utilize the results from the above two references extensively, the theory developed in Ref. [7] for perturbed boundary is summarized with an interpretation of the formulations specific to the present study, and the method developed in Ref. [8] for a noise field generated by random surface sources is briefly outlined. Finally, by combining the results in Ref. [7] and Ref. [8] we derive an expression for the cross-spectral correlation function of the scattered noise field.

2.2 Basic Assumptions

In Sec. 1.3 we have discussed the relevant issues for the present analysis, and justified the bases for choosing the perturbation theory for rough surface scattering analysis. The theory performs well under appropriate assumptions, and here we summarize the basic assumptions which are made throughout this study:

1. The ocean environment is horizontally stratified, and because the contrast between air and water is so large that we assume it is vacuum above the ocean.

2. We assume that the roughness scales of the sea bed/floor are within the range of applicability of the first-order perturbation theory. In particular, the RMS roughness and correlation length are small enough so that the conditions are met. While there are no explicit results for the region of validity for a general roughness spectrum, and general boundary conditions, we use the results derived by Thorsos and Jackson [11] as a guideline, *i.e.* $\kappa\sqrt{\langle\gamma^2\rangle} \ll 1$ and $\kappa\ell < 6$, where $\sqrt{\langle\gamma^2\rangle}$ is the RMS roughness of the sea floor.

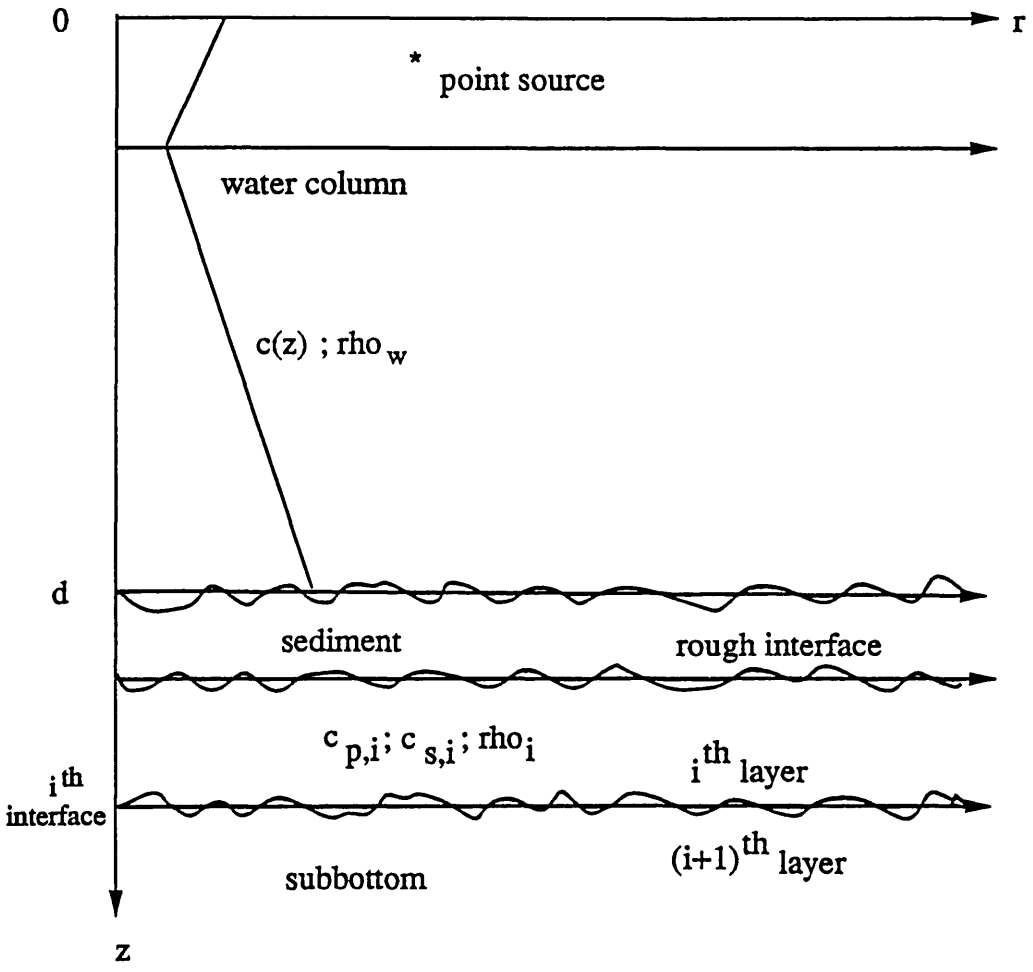

Figure 2.1: Model geometry for a point source in a horizontal stratified medium with rough interfaces.

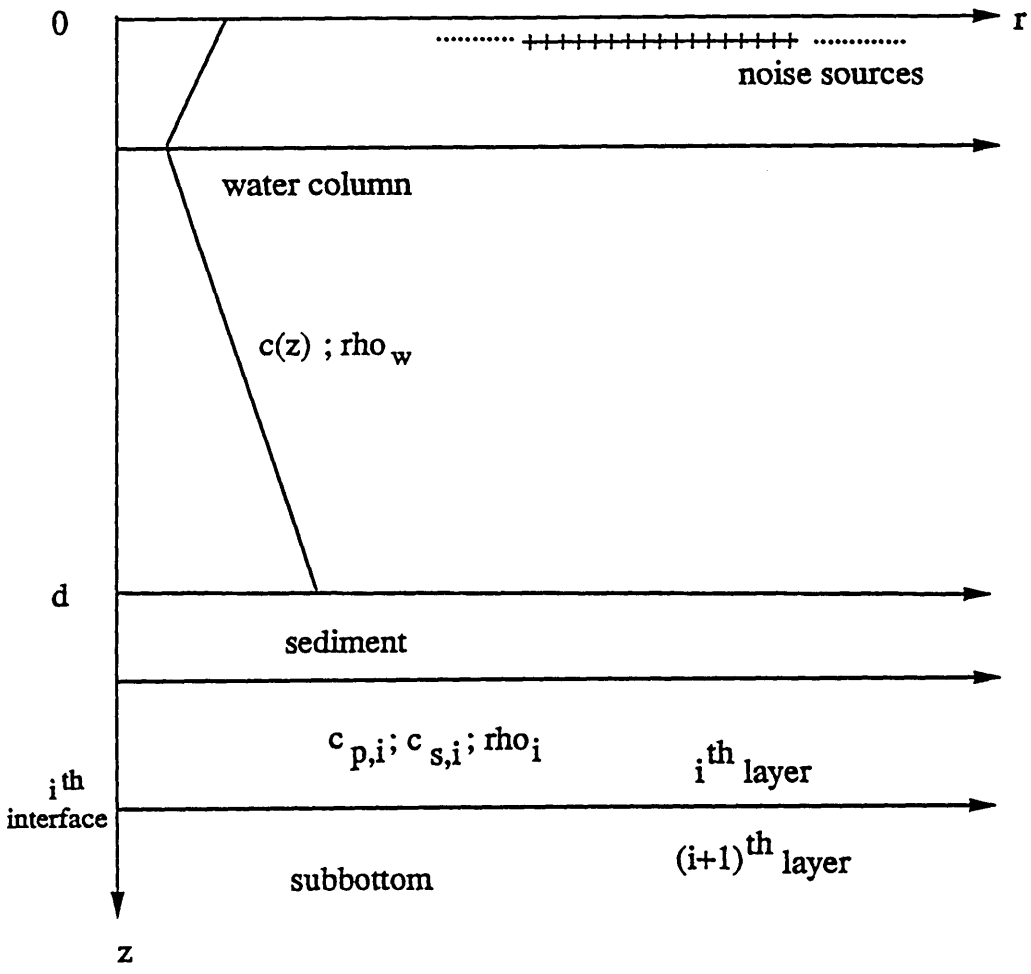

Figure 2.2: Model geometry for an infinite plane of random sources in a horizontal stratified medium with plane interfaces.

3. Both the sea floor and surface roughness are stationary, and they are independent. The independency assumption is realistic because the separation between the two surfaces are so large that surface activities are unlikely to affect a change of the sea floor topography in a time period of our interest.

Specific assumptions when applying the following theory to a particular problem may be invoked, and shall be stated when they are appealed.

2.3 Solution of Wave Equation for an Unperturbed Problem

The wave propagation in a homogeneous and isotropic medium is governed by wave equation of the form:

$$\nabla^2\Phi = \frac{1}{c^2}\frac{\partial^2\Phi}{\partial t^2}, \tag{2.1}$$

where $\Phi(\mathbf{r}, z, t)$ may be a scalar or a vector potential, and c is the speed of wave propagation. The time dependence may be separated through Fourier transform in time defined as

$$\chi_\omega(\mathbf{r}, z) = \frac{1}{\sqrt{2\pi}}\int dt\, \Phi(\mathbf{r}, z, t)e^{-j\omega t} \tag{2.2}$$

$$\Phi(\mathbf{r}, z, t) = \frac{1}{\sqrt{2\pi}}\int d\omega\, \chi_\omega(\mathbf{r}, z)e^{j\omega t}. \tag{2.3}$$

Application of the above transform on Eq. (2.1) yields the Helmholtz equation (or the reduced wave equation):

$$\nabla^2\chi_\omega + K^2\chi_\omega = 0, \tag{2.4}$$

where $\chi_\omega = \chi_\omega(\mathbf{r}, z)$ is the a potential which, for frequency ω, depends on space only; $K = \omega/c$ is the medium wavenumber. In a fluid only one scalar potential

exists, whereas for an elastic medium, the field may be described by three scalar displacement potentials [67]: $\phi(\mathbf{r}, z), \psi(\mathbf{r}, z)$, and $\Lambda(\mathbf{r}, z)$, corresponding to compressional (P), vertically polarized (SV), and horizontally polarized shear waves (SH), respectively.

Assuming the medium properties vary only in depth (thus, $K = K(z)$), we may separate the horizontal and vertical dependence using a two-dimensional spatial Fourier transform defined by

$$\tilde{\chi}_\omega(\mathbf{k}, z) = \frac{1}{2\pi} \int \chi_\omega(\mathbf{r}, z) e^{j\mathbf{k}\cdot\mathbf{r}} d^2\mathbf{r} \tag{2.5}$$

$$\chi_\omega(\mathbf{r}, z) = \frac{1}{2\pi} \int \tilde{\chi}_\omega(\mathbf{k}, z) e^{-j\mathbf{k}\cdot\mathbf{r}} d^2\mathbf{k}. \tag{2.6}$$

The application of the spatial Fourier transform on Eq. (2.4) leads to the depth-separated wave equation:

$$\left(\frac{d^2}{dz^2} - [k^2 - K^2(z)] \right) \tilde{\chi}_\omega(\mathbf{k}, z) = 0, \tag{2.7}$$

with $k = |\mathbf{k}|$ being the horizontal wavenumber. The subscript ω signifies the related quantities being evaluated at frequency ω, and since it is implied throughout the following presentation, the subscript ω is dropped for brevity.

The depth-separated wave equation, Eq. (2.7), is a linear ordinary differential equation in z, with the horizontal wavenumber k being a parameter. Therefore, the general solution for the depth dependence of the field, the so-called depth-dependent Green's function, takes the form

$$\tilde{\chi}(\mathbf{k}, z) = \mathcal{A}^-(\mathbf{k}) \tilde{\chi}^-(\mathbf{k}, z) + \mathcal{A}^+(\mathbf{k}) \tilde{\chi}^+(\mathbf{k}, z) + \tilde{\tilde{\chi}}(\mathbf{k}, z), \tag{2.8}$$

where $\mathcal{A}^-(\mathbf{k})$ and $\mathcal{A}^+(\mathbf{k})$ are arbitrary coefficients to be determined, and $\tilde{\tilde{\chi}}(\mathbf{k}, z)$ is a particular solution to account for the source field if a source is present in the medium.

For a stratification of isovelocity layers with the propagation in each layer being governed by Eq. (2.7) with $K(z) = K_i$, the solutions of Eq. (2.7) are of exponential form. Thus the homogeneous solution for the layer i has the integral representation:

$$\chi_i(\mathbf{r}, z) = \frac{1}{2\pi} \int d^2\mathbf{k} e^{-j\mathbf{k}\cdot\mathbf{r}} [\tilde{\chi}_i^-(\mathbf{k}) e^{-\alpha z} + \tilde{\chi}_i^+(\mathbf{k}) e^{\alpha z}], \tag{2.9}$$

where $\alpha = \sqrt{k^2 - K_i^2}$. The subscript i stands for i^{th} layer. Equation (2.9) may be interpreted as decomposition of the acoustic field into up- and down-going plane waves with horizontal wavevector $\mathbf{k}$ and amplitudes $\tilde{\chi}_i^+(\mathbf{k})$ and $\tilde{\chi}_i^-(\mathbf{k})$, respectively.

Equation (2.9) is the general solution of the Helmholtz equation for isovelocity layer with the unknown amplitudes $\tilde{\chi}_i^-$ and $\tilde{\chi}_i^+$ yet to be determined from the physical constraints of the problem. In the present context, these constraints are continuities of stresses and displacements at the interfaces. Using a differential operator notation B_i introduced in Ref. [7], these conditions can be expressed as:

$$B_i(\chi_{i;i+1}) = 0, \; i = 1, 2, ..., N-1, \tag{2.10}$$

where N is the total number of layers, including the upper and lower half-spaces, and $\chi_{i;i+1}$ is a vector containing the displacement potentials in layer i and $i+1$.

Again, the Fourier transform is applied to the boundary conditions, Eq. (2.10), replacing the differential operators by algebraic operators,

$$\tilde{B}_i(\mathbf{k})[\tilde{\chi}_{i;i+1}^{\mp}(\mathbf{k}) + \hat{\tilde{\chi}}_{i;i+1}^{\mp}(\mathbf{k})] = 0, \; i = 1, 2, ..., N-1, \tag{2.11}$$

with $\tilde{\chi}_{i;i+1}^{\mp}(\mathbf{k})$ being a vector containing the unknown plane-wave amplitudes for the homogeneous solution in the layers i and $i+1$, and $\hat{\tilde{\chi}}_{i;i+1}(\mathbf{k})$ is added to account for the amplitudes of the source field in the two layers. It should be noted that the linear system, Eq. (2.11), cannot be directly solved locally at interface i since the number of unknowns $\tilde{\chi}_{i;i+1}^{\pm}$ is larger than the number of equations. However, these local systems

may be assembled to form a global system similar to the that in the finite-element program [37], which when supplemented by the radiation conditions for $z \rightarrow \pm\infty$ may be directly solved for the unknown plane-wave amplitudes, and the solution of the Helmholtz equation is then determined by carrying out the wavenumber integral, Eq. (2.9). The above procedure known as *direct global matrix* (DGM) approach was incorporated in the SAFARI code [38].

The advantages of the numerical solution technique, based upon DGM approach taken by SAFARI, over some other methods such as recursive propagator matrix techniques were summarized in Sec. 1.3.2. Dependent on the time/frequency and range/depth requirements, the determination of the depth dependent Green's function may have to be performed a substantial number of times. The efficiency of the code is therefore highly dependent on this part, and it is precisely here - in the global matrix approach - that the SAFARI code differs in computational approach from previously developed codes of the same type. The details are documented in Ref. [38].

2.4 Solution for Rough Boundaries

Next, we review the boundary perturbation approach developed in Ref. [7] for the model geometry shown in Fig. 2.1, which extends the application of the spectral field representation in Eq. (2.11) to a stratification with small interface roughness.

Suppose that the interface at mean depth z_i between the two layers i and $i+1$ is randomly rough with elevation described by a function $\gamma(\mathbf{r}) = z - z_i$, with $\langle\gamma(\mathbf{r})\rangle = 0$ as shown in Fig. 2.3. For this case, the boundary conditions must be applied at $z = \gamma(\mathbf{r}) + z_i$ rather than at the nominal interface depth z_i, and the boundary

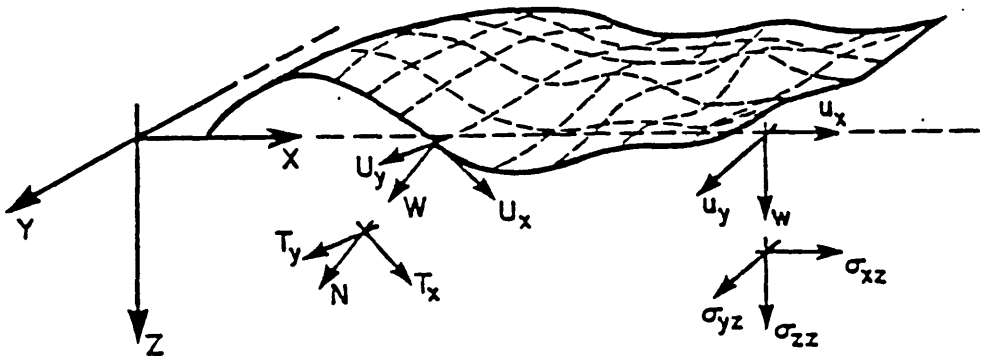

Figure 2.3: Coordinate system of a rough surface.

conditions must be represented in a rotated system defined by the local tangent plane of the rough interface.

Let the upper case letters, $W, \mathbf{U}, N$ and $\mathbf{T}$ represent the displacements and stresses in the rotated coordinate system, corresponding to the unperturbed parameters $w, \mathbf{u} = (u_x, u_y), n = \sigma_{zz}$, and $\mathbf{t} = (\sigma_{xz}, \sigma_{yz})$, respectively. Assuming the slope of the surface is small, *i.e.* $|\gamma'| \ll 1$, where γ' is the gradient of the surface defined as

$$\gamma'(\mathbf{r}) = (\gamma_{,x}, \gamma_{,y}) = \left(\frac{\partial \gamma(\mathbf{r})}{\partial x}, \frac{\partial \gamma(\mathbf{r})}{\partial y} \right), \tag{2.12}$$

then the rotation transformation of displacements and stresses is [7]

$$\begin{aligned} W &= w - \gamma' \cdot \mathbf{u}, \\ \mathbf{U} &= \mathbf{u} + \gamma' w, \\ N &= n - 2\gamma' \cdot \mathbf{t}, \\ \mathbf{T} &= \mathbf{t} + (\gamma_{,x}[\sigma_{zz} - \sigma_{xx}] - \gamma_{,y}\sigma_{xy}\,,\, \gamma_{,y}[\sigma_{zz} - \sigma_{yy}] - \gamma_{,x}\sigma_{xy}), \end{aligned} \tag{2.13}$$

where only the terms to the first order of the roughness are retained. The rotated boundary conditions can now be expressed as a perturbation of the the original conditions, Eq. (2.10), as

$$B_i^*(\chi_{i;i+1}) = B_i(\chi_{i;i+1}) + \gamma' \circ b_i(\chi_{i;i+1}), \tag{2.14}$$

where the operator symbol $\circ$ represents the various operations in Eq. (2.13).

Now, in treating the wave scattering due to the perturbation, the total field in the layer i is decomposed into the coherent or mean field $\langle \chi_i \rangle$, and the incoherent or scattered field s_i,

$$\chi_i = \langle \chi_i \rangle + s_i \tag{2.15}$$

where the scattered field is assumed to be order of γ. Following the development in Ref. [7], one then arrives at a set of equations which must be satisfied by the

solutions of mean and scattered fields at the average interface depth z_i, respectively. The equation for the mean field is

$$\left\{\bar{B}_i(\mathbf{k}) + \frac{\langle\gamma^2\rangle}{2}\frac{\partial^2}{\partial z^2}\bar{B}_i(\mathbf{k}) + I_1(\mathbf{k}) + I_2(\mathbf{k})\right\}\langle\bar{\chi}^{\mp}_{i;i+1}(\mathbf{k})\rangle = 0, \tag{2.16}$$

where $I_1(\mathbf{k})$ and $I_2(\mathbf{k})$ are scattering integrals given by

$$\begin{aligned} I_1(\mathbf{k}) &= -\frac{\langle\gamma^2\rangle}{2\pi}\int d^2\mathbf{q}P_b(\mathbf{q}-\mathbf{k})\frac{\partial\bar{B}_i(\mathbf{q})}{\partial z} \\ &\quad \times\bar{B}_i^{-1}(\mathbf{q})\left(\frac{\partial\bar{B}_i(\mathbf{k})}{\partial z} - j(\mathbf{q}-\mathbf{k})\circ\tilde{b}_i(\mathbf{k})\right), \end{aligned} \tag{2.17}$$

$$\begin{aligned} I_2(\mathbf{k}) &= -\frac{\langle\gamma^2\rangle}{2\pi}\int d^2\mathbf{q}P_b(\mathbf{q}-\mathbf{k})j(\mathbf{q}-\mathbf{k})\circ\tilde{b}_i(\mathbf{k}) \\ &\quad \times\bar{B}_i^{-1}(\mathbf{q})\left(\frac{\partial\bar{B}_i(\mathbf{k})}{\partial z} - j(\mathbf{q}-\mathbf{k})\circ\tilde{b}_i(\mathbf{k})\right). \end{aligned} \tag{2.18}$$

The equation for the scattered field is

$$\begin{aligned} \bar{B}_i(\mathbf{q})\tilde{s}_{i;i+1}(\mathbf{q}) &= -\frac{1}{2\pi}\int d^2\mathbf{k}\tilde{\gamma}(\mathbf{q}-\mathbf{k}) \\ &\quad \times\left[\frac{\partial\bar{B}_i(\mathbf{k})}{\partial z} - j(\mathbf{q}-\mathbf{k})\circ\tilde{b}_i(\mathbf{k})\right]\langle\bar{\chi}^{\mp}_{i;i+1}(\mathbf{k})\rangle. \end{aligned} \tag{2.19}$$

In the above expressions, $\langle\bar{\chi}^{\mp}_{i;i+1}\rangle$ and $\tilde{s}_{i;i+1}$ are vectors containing the unknown plane-wave amplitudes in layers i and $i+1$ for coherent and incoherent components, respectively. $P_b(\mathbf{q})$ is the interface roughness power spectrum defined by

$$\langle\gamma^2\rangle P_b(\mathbf{q}) = \frac{1}{2\pi}\int d^2\bar{\mathbf{r}}M(\bar{\mathbf{r}})e^{j\mathbf{q}\cdot\bar{\mathbf{r}}}, \tag{2.20}$$

with $M(\bar{\mathbf{r}}) = \langle\gamma(\mathbf{r})\gamma(\mathbf{r}')\rangle$ being the surface correlation function for a spatially stationary stochastic random surface, and $\bar{\mathbf{r}} = \mathbf{r}-\mathbf{r}'$. It is also noted that the above equations are based upon the expansion of the rotated boundary condition, Eq. (2.14), in a Taylor series to second order in the roughness parameter γ. Thus, the results are correct to $O\left[\left(\kappa\sqrt{\langle\gamma^2\rangle}\right)^2\right]$.

Equation (2.19) provides an expression for the spectral components of the scattered field in terms of the mean field and therefore forms a cornerstone for the noise

scattering theory described in the following. Equation (2.19) is clearly a special version of the global matrix equations (2.11), with the source term in the unperturbed formulation replaced by the convolution integral on the right hand side of Eq. (2.19). Therefore, once the mean field is determined, the scattered field is found by solving the unperturbed problem with the field being generated by a sheet of *secondary sources* at the depth of the rough interface, with a spectral shading given by the convolution integral. The above formulation clearly demonstrates that using the above simple operator representation, Eqs. (2.16)-(2.19) are totally compatible with the algorithms for the corresponding unperturbed problem presented in the previous section.

2.4.1 Physical Interpretation of Scattering in a Waveguide Environment

In applying the above formalisms in a waveguide environment, it is necessary first to generalize Eq. (2.19). This is due to the fact that the derivation of Eq. (2.16)-(2.19) is based on the assumption that only scattered waves propagating away from the rough interface are involved in the boundary conditions for the mean field [7], corresponding to the case of the rough interface separating two infinite halfspaces. Therefore, the scattered field reflected from other interfaces is not involved in the formulation, with the boundary operator $\tilde{B}_i(\mathbf{q})$ in Eq. (2.19) representing the *local* boundary conditions at mean depth of the rough interface. In contrast, the operator $\bar{B}_i(\mathbf{k})$ in Eq. (2.16) for the mean field represents the *global* boundary conditions, including all waveguide effects. For a stochastic representation of the rough interface this assumption makes sense due to the fact that, for the ocean waveguide, the important reflectors such as the free surface are far away from the rough interface, with the reflected scattered field

returning at large horizontal offsets compared to the roughness correlation length, producing an insignificant secondary scattered field. However, once generated, the scattered field must propagate through the environment according to the waveguide physics described by the *global* boundary operator. The spatial properties of the scattered field are therefore controlled by both the generating mechanism described by Eqs. (2.16)-(2.19) and the modal structure of the waveguide propagation.

It is therefore to be emphasized here that the noise scattering theory described in the following is based on the fundamental assumption that the *local* boundary operator in Eq. (2.19) can be directly replaced by the *global* operator for the full waveguide. In physical terms this corresponds to assuming that the *secondary sources* are unaffected by the presence of the other interfaces and therefore give rise to a source field traveling away from the rough interface only. On the other hand these interfaces, being part of the waveguide, have a critical effect on determining the modal structure of scattered wave field as soon as it is generated by the roughness. In addition, the waveguide propagation of the scattered field ignores secondary scattering due to the fact that the global operator $\tilde{B}_i(\mathbf{q})$ is that of the unperturbed problem.

2.5 Noise Field Generated by Random Surface Sources

The noise field resulting from a random distribution of surface sources in a stratified environment with plane interfaces as shown in Fig. 2.2 is described by the theory of Kuperman and Ingenito [8]. Here, we briefly summarize the procedure of the derivation and its results.

Let $G(\mathbf{r}, \mathbf{r}'; z, z')$ be a Green's function, representing a displacement potential due to a harmonic monopole of unit strength located at $(\mathbf{r}', z')$, satisfying the Helmholtz equation,

$$\nabla^2 G + K^2(z)G = -\delta(\mathbf{r} - \mathbf{r}')\delta(z - z'). \tag{2.21}$$

As described in Sec. 2.3, the Green's function is given by the integral representation,

$$G(\mathbf{r}, \mathbf{r}'; z, z') = \frac{1}{2\pi} \int d^2\mathbf{k} g(\mathbf{k}; z, z') e^{i\mathbf{k}\cdot(\mathbf{r}-\mathbf{r}')}, \tag{2.22}$$

where g is the depth-dependent Green's function satisfying the equation

$$\left(\frac{d^2}{dz^2} - [k^2 - K^2(z)] \right) g = -\frac{\delta(z - z')}{2\pi}. \tag{2.23}$$

The total potential due to contribution of all sources of strength $S_\omega(\mathbf{r}')$ in an infinite plane located at $z = z'$ is then equal to the integration of the Green's function $G(\mathbf{r}, \mathbf{r}'; z, z')$ over the source plane

$$\overline{\varphi}(\mathbf{r}, z) = \int d^2\mathbf{r}' S_\omega(\mathbf{r}') G(\mathbf{r}, \mathbf{r}'; z, z'), \tag{2.24}$$

where the overbar indicates the field in the absence of roughness.

Next, to obtain the cross-spectral density we form the product of $\overline{\varphi}(\mathbf{r}_1, z_1)$ and $\overline{\varphi}^*(\mathbf{r}_2, z_2)$, and then take the ensemble average

$$\begin{aligned} \langle \overline{\varphi}(\mathbf{r}_1, z_1) \overline{\varphi}^*(\mathbf{r}_2, z_2) \rangle &= \int\int d^2\mathbf{r}' d^2\mathbf{r}'' \langle S_\omega(\mathbf{r}') S_\omega^*(\mathbf{r}'') \rangle \\ &\quad \times G(\mathbf{r}_1, \mathbf{r}'; z_1, z') G^*(\mathbf{r}_2, \mathbf{r}''; z_2, z'). \end{aligned} \tag{2.25}$$

Substituting Eq. (2.22) into Eq. (2.25) yields

$$\begin{aligned} \langle \overline{\varphi}(\mathbf{r}_1, z_1) \overline{\varphi}^*(\mathbf{r}_2, z_2) \rangle &= \int\int d^2\mathbf{r}' d^2\mathbf{r}'' \langle S_\omega(\mathbf{r}') S_\omega^*(\mathbf{r}'') \rangle \\ &\quad \times \frac{1}{(2\pi)^2} \int\int d^2\mathbf{k} d^2\mathbf{k}' \, g(\mathbf{k}; z_1, z') g^*(\mathbf{k}'; z_2, z') \\ &\quad \times e^{j\mathbf{k}\cdot(\mathbf{r}_1 - \mathbf{r}')} e^{-j\mathbf{k}'\cdot(\mathbf{r}_2 - \mathbf{r}'')}. \end{aligned} \tag{2.26}$$

Now, we assume that the strength of random surface noise sources is spatially stationary, *i.e.* its correlation function is spatially invariant, being function of separation only, not absolute position. So, let $\bar{\mathbf{r}} = \mathbf{r}_1 - \mathbf{r}_2$, $\bar{\mathbf{r}}' = \mathbf{r}' - \mathbf{r}''$, and denote the correlation function by $N(\bar{\mathbf{r}}') = \langle S_\omega(\mathbf{r}')S_\omega^*(\mathbf{r}'')\rangle$. Then, substituting for $\mathbf{r}_1$ and $\mathbf{r}'$ in Eq. (2.26) and integrating over $\mathbf{r}''$ and $\mathbf{k}'$ results in

$$\begin{aligned}\langle\overline{\varphi}(\mathbf{r}_1,z_1)\overline{\varphi}^*(\mathbf{r}_2,z_2)\rangle &= \int\int d^2\bar{\mathbf{r}}'d^2\mathbf{k} \\ &\quad\times N(\bar{\mathbf{r}}')g(\mathbf{k};z_1,z')g^*(\mathbf{k};z_2,z')e^{j\mathbf{k}\cdot(\mathbf{r}-\mathbf{r}')}. \qquad (2.27)\end{aligned}$$

Here we have used an identity

$$\frac{1}{(2\pi)^2}\int d^2\mathbf{r}e^{j\mathbf{r}\cdot\mathbf{k}} = \delta(\mathbf{k}). \qquad (2.28)$$

Finally, expressing $N(\bar{\mathbf{r}}')$ by its Fourier transform

$$\langle S_\omega^2\rangle P_s(\mathbf{k}) = \frac{1}{2\pi}\int d^2\bar{\mathbf{r}}'N(\bar{\mathbf{r}}')e^{j\mathbf{k}\cdot\mathbf{r}'}, \qquad (2.29)$$

and integrating over $\bar{\mathbf{r}}'$ yields the cross-spectral correlation function of the noise field

$$\overline{C}_\omega(\bar{\mathbf{r}},z_1,z_2) = 2\pi\langle S_\omega^2\rangle\int d^2\mathbf{k}P_s(\mathbf{k})g(\mathbf{k};z_1,z')g^*(\mathbf{k};z_2,z')e^{-j\mathbf{r}\cdot\mathbf{k}}, \qquad (2.30)$$

where $\langle S_\omega^2\rangle$ and $P_s(\mathbf{k})$ are, respectively, the mean-square source strength and power spectrum of the random noise sources. In the present context, these correspond to mean-square waveheight and wavenumber spectrum of the ocean surface waves. It is noted that the parameter $\langle S_\omega^2\rangle$ is still unknown and arbitrary. A normalization can be made so that it yields a specified level in an infinitely deep ocean, independent of the actual source depth. The condition will be given in Sec. 3.2.

2.6 Rough Interface Scattering of Surface Generated Ambient Noise

Our objective is to derive the cross-spectral correlation function of the scattered field resulted from rough interface scattering of surface-generated ambient noise. By the same concept of plane wave decomposition as in Eq. (2.9), the scattering potential at a point $(\mathbf{r}_1, z_1)$ in the layers separated by a rough interface i due to a point source of strength S_ω at $(\mathbf{r}'_s, z')$ may be represented by

$$s_i^{ps}(\mathbf{r}_1, z_1; \mathbf{r}'_s, z') = \frac{1}{2\pi} \int d^2\mathbf{q}_1 S_\omega(\mathbf{r}'; z') e^{-j\mathbf{q}_1\cdot(\mathbf{r}_1-\mathbf{r}'_s)} e_i(z_1, \mathbf{q}_1)\tilde{s}_i(\mathbf{q}_1, z'), \qquad (2.31)$$

where the superscript *ps* stands for "point source" solution; $e_i(z, \mathbf{q})$ is a diagonal matrix containing the vertical exponentials in Eq. (2.9), and $\tilde{s}_i(\mathbf{q}_1, z')$ is a vector containing the amplitudes of the up- and down-going waves of the scattered field determined from Eq. (2.19). The total contribution from an infinite plane of random monopoles located at $z = z'$ is then determined by integration over the source plane

$$s_i(\mathbf{r}_1, z_1; z') = \frac{1}{2\pi} \iint d^2\mathbf{r}'_s d^2\mathbf{q}_1 S_\omega(\mathbf{r}'_s; z') e^{-j\mathbf{q}_1\cdot(\mathbf{r}_1-\mathbf{r}'_s)} e_i(z_1, \mathbf{q}_1)\tilde{s}_i(\mathbf{q}_1, z'), \qquad (2.32)$$

with the cross-spectral density of the scattered noise following as

$$\begin{aligned} \langle s_i(\mathbf{r}_1, z_1) s_i^*(\mathbf{r}_2, z_2)\rangle \;=\; & \frac{1}{(2\pi)^2} \iiiint d^2\mathbf{r}'_s d^2\mathbf{r}''_s d^2\mathbf{q}_1 d^2\mathbf{q}_2 \\ & \times e^{-j\mathbf{q}_1\cdot(\mathbf{r}_1-\mathbf{r}'_s)} e^{j\mathbf{q}_2\cdot(\mathbf{r}_2-\mathbf{r}''_s)} e_i(z_1, \mathbf{q}_1) e_i^*(z_2, \mathbf{q}_2) \\ & \times \langle S_\omega(\mathbf{r}'_s) S_\omega^*(\mathbf{r}''_s) \tilde{s}_i(\mathbf{q}_1) \tilde{s}_i^*(\mathbf{q}_2)\rangle, \end{aligned} \qquad (2.33)$$

where the constant source depth z' is implied. Substitution of Eq. (2.19) into Eq. (2.33) now yields

$$\begin{aligned}\langle s_i(\mathbf{r}_1,z_1)s_i^*(\mathbf{r}_2,z_2)\rangle &= \frac{1}{(2\pi)^4}\int\int\int\int\int\int d^2\mathbf{r}_s' d^2\mathbf{r}_s'' d^2\mathbf{q}_1 d^2\mathbf{q}_2 d^2\mathbf{k}_1 d^2\mathbf{k}_2 \\ &\times[A(z_1,\mathbf{q}_1,\mathbf{k}_1)e^{-j\mathbf{q}_1\cdot(\mathbf{r}_1-\mathbf{r}_s')}] \\ &\times[A(z_2,\mathbf{q}_2,\mathbf{k}_2)e^{-j\mathbf{q}_2\cdot(\mathbf{r}_2-\mathbf{r}_s'')}]^* \\ &\times\langle S_\omega(\mathbf{r}_s')S_\omega^*(\mathbf{r}_s'')\tilde{\gamma}(\mathbf{q}_1-\mathbf{k}_1)\tilde{\gamma}^*(\mathbf{q}_2-\mathbf{k}_2)\rangle, \end{aligned} \tag{2.34}$$

where

$$\begin{aligned}A(z,\mathbf{q},\mathbf{k}) &= e_i(z,\mathbf{q})\tilde{B}^{-1}(\mathbf{q}) \\ &\times\left\{\frac{\partial\tilde{B}_i(\mathbf{k})}{\partial z} - j(\mathbf{q}-\mathbf{k})\circ\tilde{b}_i(\mathbf{k})\right\}\langle\tilde{\chi}_i(\mathbf{k})\rangle. \end{aligned} \tag{2.35}$$

Here, one may recognize that the operator $A(z,\mathbf{q},\mathbf{k})$ represents the scattered components with wavevector $\mathbf{q}$ corresponding to an incoming wave with wavevector $\mathbf{k}$. Like the case for the single source discussed in Sec. 2.4, it is clear from Eq. (2.35) that the effect of the roughness is effectively represented by a distribution of sources along the interface i, with a spectral shading given by the terms in the curly bracket. These *secondary* sources then radiate energy into the ocean environment according to the waveguide response represented by the operator $B^{-1}(\mathbf{q})$. This observation is important for the physical interpretation of the numerical results presented below.

The rough surface amplitude spectrum is given by the Fourier transform of the roughness,

$$\tilde{\gamma}(\mathbf{q}) = \frac{1}{2\pi}\int d^2\mathbf{r}_b'\gamma(\mathbf{r}_b')\,e^{j\mathbf{q}\cdot\mathbf{r}_b'}, \tag{2.36}$$

the substitution of which into Eq. (2.34) yields a 16-dimensional convolution integral,

$$\langle s_i(\mathbf{r}_1, z_1) s_i^*(\mathbf{r}_2, z_2)\rangle =$$
$$\frac{1}{(2\pi)^6}\int\int\int\int\int\int\int\int d^2\mathbf{r}_s' d^2\mathbf{r}_s'' d^2\mathbf{r}_b' d^2\mathbf{r}_b'' d^2\mathbf{q}_1 d^2\mathbf{q}_2 d^2\mathbf{k}_1 d^2\mathbf{k}_2$$
$$\times[A(z_1,\mathbf{q}_1,\mathbf{k}_1)e^{-j\mathbf{q}_1\cdot(\mathbf{r}_1-\mathbf{r}_s')}][A(z_2,\mathbf{q}_2,\mathbf{k}_2)e^{-j\mathbf{q}_2\cdot(\mathbf{r}_2-\mathbf{r}_s'')}]^*$$
$$\times e^{j(\mathbf{q}_1-\mathbf{k}_1)\cdot\mathbf{r}_b'} e^{-j(\mathbf{q}_2-\mathbf{k}_2)\cdot\mathbf{r}_b''}$$
$$\times\langle S_\omega(\mathbf{r}_s')S_\omega(\mathbf{r}_s'')\gamma(\mathbf{r}_b')\gamma(\mathbf{r}_b'')\rangle. \tag{2.37}$$

To proceed, we assume that the randomness of the roughness and of the surface source are statistically independent, and both spatially stationary, *i.e.*

$$\begin{aligned}\langle S_\omega(\mathbf{r}_s')S_\omega(\mathbf{r}_s'')\gamma(\mathbf{r}_b')\gamma(\mathbf{r}_b'')\rangle &= \langle S_\omega(\mathbf{r}_s')S_\omega(\mathbf{r}_s'')\rangle\,\langle\gamma(\mathbf{r}_b')\gamma(\mathbf{r}_b'')\rangle \\ &= N(\bar{\mathbf{r}}_s)M(\bar{\mathbf{r}}_b),\end{aligned} \tag{2.38}$$

where $\bar{\mathbf{r}}_b = \mathbf{r}_b' - \mathbf{r}_b''$ and $\bar{\mathbf{r}}_s = \mathbf{r}_s' - \mathbf{r}_s''$. Then using the identity in Eq. (2.28), Eq. (2.37) reduces to 12-dimensional integral,

$$\begin{aligned}\langle s_i(\mathbf{r}_1, z_1) s_i^*(\mathbf{r}_2, z_2)\rangle &= \frac{1}{(2\pi)^2}\int\int\int\int\int\int d^2\bar{\mathbf{r}}_s d^2\bar{\mathbf{r}}_b d^2\mathbf{q}_1 d^2\mathbf{q}_2 d^2\mathbf{k}_1 d^2\mathbf{k}_2 \\ &\quad\times[A(z_1,\mathbf{q}_1,\mathbf{k}_1)e^{-j\mathbf{q}_1\cdot\mathbf{r}_1}][A(z_2,\mathbf{q}_2,\mathbf{k}_2)e^{-j\mathbf{q}_2\cdot\mathbf{r}_2}]^* \\ &\quad\times e^{j\mathbf{q}_1\cdot\mathbf{r}_s}\,\delta(\mathbf{q}_1-\mathbf{q}_2)e^{j(\mathbf{q}_1-\mathbf{k}_1)\cdot\mathbf{r}_b} \\ &\quad\times\delta((\mathbf{q}_1-\mathbf{k}_1)-(\mathbf{q}_2-\mathbf{k}_2)) \\ &\quad\times N(\bar{\mathbf{r}}_s)\,M(\bar{\mathbf{r}}_b).\end{aligned} \tag{2.39}$$

Inserting the power spectra of random roughness and source strength in Eq. (2.20) and Eq. (2.29) into Eq. (2.39), the expression for the correlation is further simplified to

$$\begin{aligned}\langle s_i(\mathbf{r}_1, z_1) s_i^*(\mathbf{r}_2, z_2)\rangle &= \langle\gamma^2\rangle\langle S_\omega^2\rangle\int\int\int\int d^2\mathbf{q}_1 d^2\mathbf{q}_2 d^2\mathbf{k}_1 d^2\mathbf{k}_2 \\ &\quad\times P_s(\mathbf{q}_1)P_b(\mathbf{q}_1-\mathbf{k}_1) \\ &\quad\times[A(z_1,\mathbf{q}_1,\mathbf{k}_1)e^{-j\mathbf{q}_1\cdot\mathbf{r}_1}][A(z_2,\mathbf{q}_2,\mathbf{k}_2)e^{-j\mathbf{q}_2\cdot\mathbf{r}_2}]^* \\ &\quad\times\delta(\mathbf{q}_1-\mathbf{q}_2)\,\delta((\mathbf{q}_1-\mathbf{k}_1)-(\mathbf{q}_2-\mathbf{k}_2)).\end{aligned} \tag{2.40}$$

Equation (2.40) can be directly integrated over $\mathbf{q}_1$ and $\mathbf{k}_2$ to yield

$$\begin{aligned} C_\omega(\bar{\mathbf{r}}, z_1, z_2) &= \langle s_i(\mathbf{r}_1, z_1) s_i^*(\mathbf{r}_2, z_2) \rangle \\ &= \langle \gamma^2 \rangle \langle S_\omega^2 \rangle \int\int d^2\mathbf{q} d^2\mathbf{k} P_s(\mathbf{q}) P_b(\mathbf{q} - \mathbf{k}) \\ &\quad \times A(z_1, \mathbf{q}, \mathbf{k})\, A^*(z_2, \mathbf{q}, \mathbf{k}) e^{-j\bar{\mathbf{r}}\cdot\mathbf{q}}, \end{aligned} \tag{2.41}$$

where $\bar{\mathbf{r}} = \mathbf{r}_1 - \mathbf{r}_2$. The simplification of the formulation, reducing from 16-dimensional in Eq. (2.37) to 4-dimensional convolution integral in the above equation, relies completely on the assumption of stationarity of both random noise sources and interface roughness, which in turn leads to a horizontally stationary scattered field.

Equation (2.41) is the key result of this study. It is seen that the cross-spectral correlation function of the scattered noise field is a convolution integral of the interface roughness spectrum, a condition often referred to as Bragg's law. The correlation is directly proportional to the mean-square roughness and source strength. It is also noted when $\bar{\mathbf{r}}$ is set to zero, and $z_1 = z_2 = z$, it yields a quantity proportional to the intensity of the noise field at z.

2.7 Total Noise Field and Born Approximation

The total noise field is the sum of the mean and the scattered noise fields

$$\chi_i(\mathbf{r}, z) = \overline{\chi}_i(\mathbf{r}, z) + s_i(\mathbf{r}, z) \tag{2.42}$$

with $\overline{\chi}_i(\mathbf{r}, z)$ representing the mean noise field resulting from rough interface scattering due to the distributed random noise sources given by

$$\overline{\chi}_i(\mathbf{r}, z) = \frac{1}{2\pi} \int\int d^2\mathbf{r}_s' d^2\mathbf{k} S_\omega(\mathbf{r}_s') e^{-j\mathbf{k}\cdot(\mathbf{r}-\mathbf{r}_s')} e_i(z, \mathbf{k}) \langle \bar{\chi}_i^{\pm}(\mathbf{k}) \rangle, \tag{2.43}$$

where $\langle\tilde{\chi}_i^{\pm}(\mathbf{k})\rangle$ is the solution of Eq. (2.16). It should not be confused that, while $\langle\tilde{\chi}_i^{\pm}(\mathbf{k})\rangle$ is a constant, the mean noise field $\overline{\chi}_i(\mathbf{r}, z)$ is a random variable due to the fact that the noise sources are random. Therefore, when we refer to the mean field in this study we are in fact implying the mean noise field created by the scattering processes due to an infinite plane of random sources.

With vanishing expectation value for the scattered field, $\langle s_i(\mathbf{r}, z)\rangle = 0$, the cross-spectral correlation function of the total noise field C_ω^t is

$$\begin{aligned} C_\omega^t(\bar{\mathbf{r}}, z_1, z_2) &= \langle\chi_i(\mathbf{r}_1, z_1)\chi_i^*(\mathbf{r}_2, z_2)\rangle \\ &= \langle\overline{\chi}_i(\mathbf{r}_1, z_1)\overline{\chi}_i^*(\mathbf{r}_2, z_2)\rangle + \langle s_i(\mathbf{r}_1, z_1)s_i^*(\mathbf{r}_2, z_2)\rangle, \end{aligned} \tag{2.44}$$

where the first term in Eq. (2.44) is the mean field correlation function. By a parallel argument as it was presented in Sec. 2.5, the correlation of the mean field is given by Eq. (2.30) with $g(\mathbf{k}; z_1, z')$ replaced by $e_i(z, \mathbf{k})\langle\tilde{\chi}_i(\mathbf{k})\rangle$, which inserted together with Eq. (2.41) into Eq. (2.44) yields

$$\begin{aligned} C_\omega^t(\bar{\mathbf{r}}, z_1, z_2) &= \langle S_\omega^2\rangle \int d^2\mathbf{q} P_s(\mathbf{q}) \\ &\quad \times \Big\{\langle\gamma^2\rangle \int d^2\mathbf{k}[P_b(\mathbf{q}-\mathbf{k})A(z_1, \mathbf{q}, \mathbf{k})\, A^*(z_2, \mathbf{q}, \mathbf{k})] \\ &\quad + 2\pi e_i(z_1, \mathbf{q})e_i^*(z_2, \mathbf{q})|\langle\tilde{\chi}_i(\mathbf{q})\rangle|^2\Big\} e^{-j\mathbf{r}\cdot\mathbf{q}}. \end{aligned} \tag{2.45}$$

Within the limits of the perturbation approximation, Eq. (2.45) is completely general in terms of dimensionality, the number of layers in the stratification, and the statistics of the rough interfaces and random noise sources apart from the assumption of stationarity.

In evaluating the cross-spectral correlation function by Eq. (2.45), aside from the computational efforts needed to carry out the double integral, a significant amount of *extra* time is required to solve for the mean field solution $\langle\tilde{\chi}_i(\mathbf{k})\rangle$ *in comparison with the time needed for the plane interface case.* This is due to the fact that the

perturbed boundary condition, Eq. (2.16), is much more complicated than the one for the smooth interface, since it involves evaluating the wavenumber integrals in Eqs. (2.17) and (2.18) for every value of the mean field wavevector $\mathbf{k}$. In this regard, we shall apply the *Born approximation.* Instead of solving the *self-consistent* mean field equation, Eq. (2.16), we apply the solution of the corresponding problem with smooth interfaces as the mean field solution. That is, only the first term in Eq. (2.16) is retained, and Eq. (2.19) remains the equation for the scattered field. This approximation inevitably overestimates both the mean and the scattered fields. However, it may be shown, *e.g.* by the order-of-magnitude analysis, that the Born approximation will affect the mean and the scattered noise field solutions in the order of $\left(\kappa\sqrt{\langle\gamma^2\rangle}\right)^2$ and $\left(\kappa\sqrt{\langle\gamma^2\rangle}\right)^3$, respectively, which are relatively insignificant for the sound waves in the frequency regime of our interest. *It is more important to recognize that the qualitative spectral characteristics required for identifying the fundamental scattering mechanisms are unaffected by the approximation.*

With the Born approximation, Eq. (2.45) becomes

$$\begin{aligned} C_\omega^t(\bar{\mathbf{r}}, z_1, z_2) &= \langle S_\omega^2\rangle \int d^2\mathbf{q} P_s(\mathbf{q}) \\ &\quad \times \Big\{ \langle\gamma^2\rangle \int d^2\mathbf{k} [P_b(\mathbf{q}-\mathbf{k}) A(z_1,\mathbf{q},\mathbf{k})\, A^*(z_2,\mathbf{q},\mathbf{k})] \\ &\quad + 2\pi e_i(z_1,\mathbf{q}) e_i^*(z_2,\mathbf{q}) |g_i(\mathbf{q})|^2 \Big\} e^{-j\bar{\mathbf{r}}\cdot\mathbf{q}} \end{aligned} \tag{2.46}$$

with $g_i(\mathbf{q})$ being the amplitudes of up- and down-going for the depth-dependent Green's function for the plane interface problem. Also, $\langle\tilde{\chi}_i(\mathbf{k})\rangle$ in the operator A is now replaced by $g_i(\mathbf{k})$.

2.8 Summary

After reviewing the related theories in literature, we have derived the cross-spectral correlation function for the noise field generated by random surface sources in a horizontally stratified medium with rough interfaces. The present analysis differs from the previous study by Kuperman and Schmidt [7] in that we have incorporated the distributed sources into the scattering formalism in contrast to the discrete sources treated in Ref. [7]. This is particularly useful in simulating the combined noise-scattering effect on the ambient noise induced by the natural processes such as ocean surface waves in an irregular medium. While the present formulation shares many similar expressions as those in Ref. [7] in particular the integration kernels, there exists intrinsic difference between the resultant cross-spectral correlation function for the case of distributed sources and that for the discrete sources, leading to a different interpretation for the significance of the various peaks in wavenumber spectra. This will be discussed in Sec. 3.7.

An important scattering operator A defined by Eq. (2.35) which enables a clear physical interpretation in terms of the scattering processes was derived. Equation (2.45) is the final result of the derivation, which expresses the cross-spectral correlation function of the total noise field as a summation of the correlation of the mean noise field and that of the scattered noise field. The basic assumption which greatly simplifies the formulation is the stationarity of both the random noise sources and the interface roughnesses. This assumption in turn leads to a stationary noise field. Important implications for directly replacing the local operator by the global operator in Eq. (2.19) for scattering in a waveguide environment are discussed in Sec. 2.4.1. For small roughness, the Born approximation, which replaces the mean field solution of the perturbed boundaries by the corresponding unperturbed one,

may be invoked in order to save computational efforts. It is expected that this assumption will lead to some degree of numerical variation, but the qualitative properties of the noise fields, which are our primary interests, should not be affected.

The cross-spectral correlation function will facilitate computation of various quantities of our interests such as noise power intensity and spatial correlation, which are the subjects of the following chapters.

Chapter 3

Canonical Seismo-Acoustic Ocean Waveguide

— in which the basic mechanism of the scattering processes is unveiled.

3.1 Introduction

Recent ambient noise data [3] recorded in the deep ocean have indicated that for the frequencies below $10\,Hz$, the noise measured by the hydrophones or geophones has a significant interface wave component. Below $1\,Hz$ in the deep ocean, this may be explained by the direct ensonification of the surface sources due to, *e.g.*, non-linear interaction between the surface gravity waves. Above $1\,Hz$, however, the excitation of interface modes by surface noise sources is not accounted for by this mechanism,

simply because the distance is too large for direct excitation. In the next chapter we shall use the present theory to simulate the noise field in a real ocean environment and compare to the experimental data. However, in this chapter we will first focus on the basic physics of the noise scattering problem by applying the developed theory to a canonical seismo-acoustic ocean waveguide environment.

The main theme of this chapter is to investigate the fundamental mechanisms of the scattering processes. After presenting the physical environment, the details of the related operators for the linear systems are derived, followed by a few remarks regarding the numerical procedure and a brief review of the basic structure of the wavenumber spectrum. Then the efforts are devoted to generate the wavenumber spectra both for the acoustic fields and the seismic fields. The scattering processes of surface-generated ambient noise are then interpreted in terms of basic physical principles. Finally the noise intensities of the noise fields throughout the water column are computed and analyzed.

Specific Assumptions

Before proceeding, we state some specific assumptions invoked. The basic assumptions were stated in Sec. 2.2. Here are some specific assumptions:

- The Born approximation is invoked for the rest of this study.
- The sea floor roughness spectrum is taken to be Gaussian, and isotropic. Thus the criteria: $\kappa\sqrt{\langle\gamma^2\rangle} \ll 1$ and $\kappa\ell \leq 6$ will be used as a reference.
- The surface sources are assumed to be completely random for the rest of this study. The wavenumber spectrum of the surface sources may be incorporated without much ado, but is considered not to be the primary interest of the present analysis.

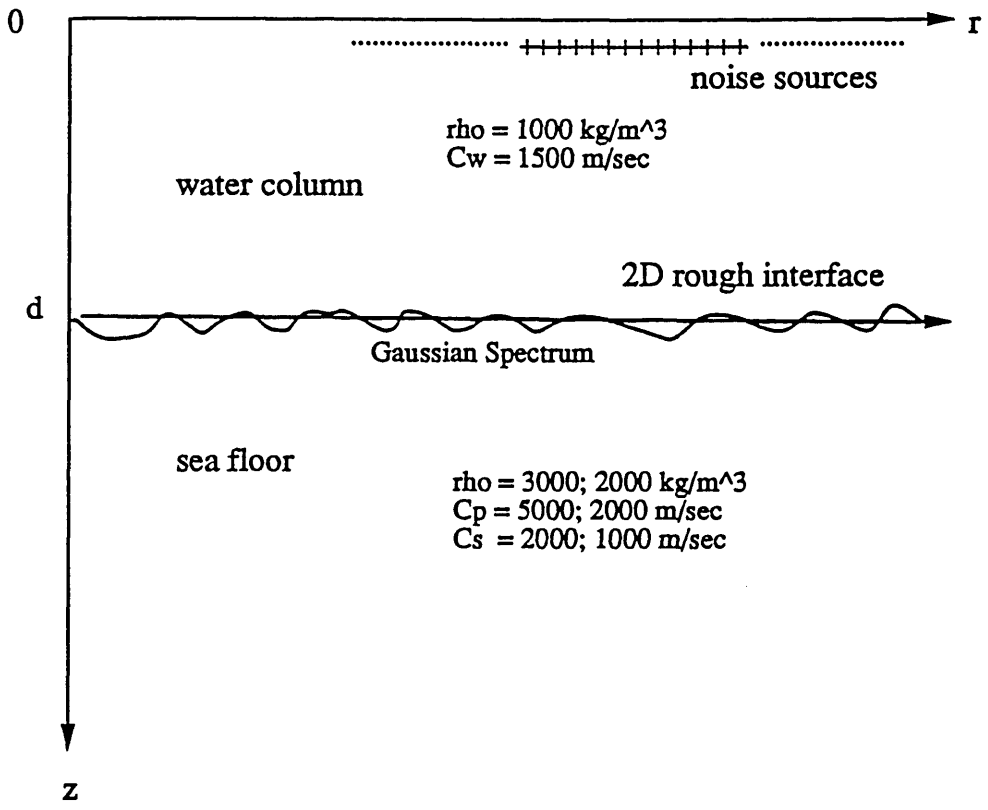

Figure 3.1: Canonical seismo-acoustic ocean waveguide.

3.2 Canonical Seismo-Acoustic Waveguide

In order not to obscure the fundamental features, we shall first analyze the scattering of surface generated noise for a three-layer canonical problem as shown in Fig. 3.1. An ocean waveguide is bounded above by a pressure-release surface and below by a rough, homogeneous elastic sea bed. We base the analysis on the Born approximation to reduce the computational efforts. Moreover, the spatial frequency spectrum of the surface sources is assumed to be completely random. In this case, the correlation

function is given by [68]

$$N(\bar{\mathbf{r}}_s) = \langle S_\omega^2 \rangle \frac{2\delta(|\bar{\mathbf{r}}_s|)}{K^2|\bar{\mathbf{r}}_s|}, \tag{3.1}$$

with the corresponding power spectrum

$$P_s(\mathbf{q}) = \frac{2}{K^2}. \tag{3.2}$$

The interface between the water column and the elastic medium is assumed to be rough with an isotropic Gaussian spectrum,

$$P_b(\mathbf{q}) = \ell^2 e^{-|\mathbf{q}|^2\ell^2/2}, \tag{3.3}$$

where ℓ is the roughness correlation length. The spectrum is properly normalized so that

$$\frac{1}{2\pi}\int\int P_b(\mathbf{q})\, d\mathbf{q} = 1. \tag{3.4}$$

With the above two assumptions, *i.e.* completely random source distribution and isotropic roughness power spectrum, it is clear that the resultant mean and scattered noise fields are also isotropic. Thus the integrand in Eq. (2.46) is independent of azimuthal angle with respect to the variable $\mathbf{q}$, and the integration over the azimuthal angle may then be carried out to yield

$$\begin{aligned} C_\omega^t(\bar{\mathbf{r}}, z_1, z_2) \;=\; & 2\pi\langle S_\omega^2\rangle \int_0^\infty dq\, q\, J_0(|\bar{\mathbf{r}}|\, q) P_s(q) \\ & \times\{\langle\gamma^2\rangle \int_{-\infty}^{\infty} d^2\mathbf{k}[P_b(\mathbf{q}-\mathbf{k}) A(z_1,\mathbf{q},\mathbf{k})\, A^*(z_2,\mathbf{q},\mathbf{k})] \\ & +2\pi g(z_1,q) g^*(z_2,q)\}, \end{aligned} \tag{3.5}$$

where $J_0(z)$ is the zeroth-order Bessel function of the first kind. To eliminate the dependence on the unknown source depth z', the monopole source strength $\langle S_\omega^2\rangle$ is normalized to yield the pressure level Q in an infinitely deep ocean, independent of the actual value of z'. This is accomplished to first order in z' if $\langle S_\omega^2\rangle$ is assigned the value [5]

$$\langle S_\omega^2\rangle = \frac{Q^2}{16\pi(z')^2}. \tag{3.6}$$

This makes adjustment of the unknown source strength relatively easy. For example, when requiring a noise source level of 70 dB in the far field, we merely need to set the value of Q to be 70, resulting in a uniform 70-dB pressure level in a homogeneous semi-infinite half-space.

3.3 Linear Systems

The linear systems governing the mean and scattered noise fields, Eqs. (2.16) and (2.19) are expressed in terms of the boundary operator $\tilde{B}(\mathbf{k})$ and the rotational operator $\tilde{b}(\mathbf{k})$. In this section we give a detailed derivation for these operators for the case of an isovelocity water column overlying an elastic halfspace shown in Fig. 3.1.

3.3.1 Wavenumber Integrals

The solution of Helmholtz equation, Eq. (2.4), has the integral representation as given in Eq. (2.9). It should be remembered that the present analysis considers the scattering from a *two-dimensional* rough surface. One must therefore expect that the resultant scattered fields generated by *an incoming wave* with wavevector $\mathbf{k}$ are in general *three-dimensional*, even though the overall noise field resulting from a completely random source distribution and an isotropic rough surface is axisymmetric. In this case it is convenient to employ a rectangular coordinate system. Thus, for a fluid medium, say layer i, the solution of the compressional potential has the following integral representation

$$\phi_i(\mathbf{r}, z) = \frac{1}{2\pi} \int d^2\mathbf{k} e^{-j\mathbf{k}\cdot\mathbf{r}} [\tilde{\phi}_i^-(\mathbf{k}) e^{-z\alpha_i} + \tilde{\phi}_i^+(\mathbf{k}) e^{z\alpha_i}]. \tag{3.7}$$

In an elastic medium, say layer $i+1$, in addition to the compressional potential, there are two shear potentials, which have the similar representation

$$\psi_{i+1}(\mathbf{r},z) = \frac{1}{2\pi}\int d^2\mathbf{k}e^{-j\mathbf{k}\cdot\mathbf{r}}[\tilde{\psi}^-_{i+1}(\mathbf{k})e^{-z\beta_{i+1}} + \tilde{\psi}^+_{i+1}(\mathbf{k})e^{z\beta_{i+1}}], \tag{3.8}$$

$$\Lambda_{i+1}(\mathbf{r},z) = \frac{1}{2\pi}\int d^2\mathbf{k}e^{-j\mathbf{k}\cdot\mathbf{r}}[\tilde{\Lambda}^-_{i+1}(\mathbf{k})e^{-z\beta_{i+1}} + \tilde{\Lambda}^+_{i+1}(\mathbf{k})e^{z\beta_{i+1}}], \tag{3.9}$$

where $\alpha_i = \sqrt{k^2 - k^2_{p,i}}$ and $\beta_{i+1} = \sqrt{k^2 - k^2_{s,i+1}}$ with $k_{p,i}$ and $k_{s,i+1}$ being the compressional and shear wavenumber in the layer i and $i+1$, respectively. The amplitudes $\tilde{\phi}^{\mp}_i, \tilde{\psi}^{\mp}_{i+1}$ and $\tilde{\Lambda}^{\mp}_{i+1}$ are arbitrary functions of the wavenumber.

The displacement components are obtained from the potentials by

$$u_i = \frac{\partial\phi}{\partial x_i} + \varepsilon_{ijk}\frac{\partial\Psi_j}{\partial x_k} \tag{3.10}$$

where $\Psi_i = \left(\frac{\partial\Lambda}{\partial y}, -\frac{\partial\Lambda}{\partial x}, \psi\right)$, and ε_{ijk} is the permutation tensor. Carrying out the tensor operation yields

$$\begin{aligned} u &= \frac{\partial\phi}{\partial x} + \frac{\partial\psi}{\partial y} + \frac{\partial^2\Lambda}{\partial x\partial z}, \\ v &= \frac{\partial\phi}{\partial y} - \frac{\partial\psi}{\partial x} + \frac{\partial^2\Lambda}{\partial y\partial z}, \\ w &= \frac{\partial\phi}{\partial z} - \frac{\partial^2\Lambda}{\partial x^2} - \frac{\partial^2\Lambda}{\partial y^2}. \end{aligned} \tag{3.11}$$

The stress components are derived according to the constitutive relation

$$\sigma_{ij} = \lambda\frac{\partial u_k}{\partial x_k}\delta_{ij} + \mu\left(\frac{\partial u_i}{\partial x_j} + \frac{\partial u_j}{\partial x_i}\right), \tag{3.12}$$

where λ and μ are the Lame constants, and δ_{ij} is the Kronecker delta. Again, carrying out the tensor operation results in

$$\sigma_{xx} = \lambda\left(\frac{\partial^2\phi}{\partial x^2} + \frac{\partial^2\phi}{\partial y^2} + \frac{\partial^2\phi}{\partial z^2}\right) + 2\mu\frac{\partial}{\partial x}\left(\frac{\partial\phi}{\partial x} + \frac{\partial\psi}{\partial y} + \frac{\partial^2\Lambda}{\partial x\partial z}\right),$$

$$
\begin{aligned}
\sigma_{yy} &= \lambda\left(\frac{\partial^2\phi}{\partial x^2}+\frac{\partial^2\phi}{\partial y^2}+\frac{\partial^2\phi}{\partial z^2}\right)+2\mu\frac{\partial}{\partial y}\left(\frac{\partial\phi}{\partial y}-\frac{\partial\psi}{\partial x}+\frac{\partial^2\Lambda}{\partial y\partial z}\right),\\
\sigma_{zz} &= \lambda\left(\frac{\partial^2\phi}{\partial x^2}+\frac{\partial^2\phi}{\partial y^2}+\frac{\partial^2\phi}{\partial z^2}\right)+2\mu\frac{\partial}{\partial z}\left(\frac{\partial\phi}{\partial z}-\frac{\partial^2\Lambda}{\partial x^2}-\frac{\partial^2\Lambda}{\partial y^2}\right), \qquad (3.13)\\
\sigma_{xy} &= \mu\left[2\frac{\partial^2\phi}{\partial x\partial y}-\left(\frac{\partial^2\psi}{\partial x^2}-\frac{\partial^2\psi}{\partial y^2}\right)+2\frac{\partial}{\partial x}\left(\frac{\partial^2\Lambda}{\partial y\partial z}\right)\right],\\
\sigma_{zx} &= \mu\left[2\frac{\partial^2\phi}{\partial z\partial x}+\frac{\partial^2\psi}{\partial y\partial z}-\frac{\partial}{\partial x}\left(\frac{\partial^2\Lambda}{\partial x^2}+\frac{\partial^2\Lambda}{\partial y^2}-\frac{\partial^2\Lambda}{\partial z^2}\right)\right],\\
\sigma_{zy} &= \mu\left[2\frac{\partial^2\phi}{\partial z\partial y}-\frac{\partial^2\psi}{\partial x\partial z}-\frac{\partial}{\partial y}\left(\frac{\partial^2\Lambda}{\partial x^2}+\frac{\partial^2\Lambda}{\partial y^2}-\frac{\partial^2\Lambda}{\partial z^2}\right)\right].
\end{aligned}
$$

For the present environment, the integral representation of the existing wavefield potentials are

$$
\begin{aligned}
\phi_2(\mathbf{r},z) &= \frac{1}{2\pi}\int d^2\mathbf{k}e^{-j\mathbf{k}\cdot\mathbf{r}}\left[e^{-\alpha_2 z}A_2^-(\mathbf{k})+e^{\alpha_2 z}A_2^+(\mathbf{k})\right],\\
\phi_3(\mathbf{r},z) &= \frac{1}{2\pi}\int d^2\mathbf{k}e^{-j\mathbf{k}\cdot\mathbf{r}}e^{-\alpha_3 z}A_3^-(\mathbf{k}),\\
\psi_3(\mathbf{r},z) &= \frac{1}{2\pi}\int d^2\mathbf{k}e^{-j\mathbf{k}\cdot\mathbf{r}}e^{-\beta_3 z}B_3^-(\mathbf{k}),\\
\Lambda_3(\mathbf{r},z) &= \frac{1}{2\pi}\int d^2\mathbf{k}e^{-j\mathbf{k}\cdot\mathbf{r}}e^{-\beta_3 z}C_3^-(\mathbf{k}),
\end{aligned}
$$

with $k^2=k_x^2+k_y^2$, $\alpha_2=\sqrt{k^2-k_{p,2}^2}$, $\alpha_3=\sqrt{k^2-k_{p,3}^2}$, and $\beta_3=\sqrt{k^2-k_{s,3}^2}$, where the radiation conditions are applied to eliminate the upgoing waves in the layer 3.

It should be noted that if a source is present in a particular layer, the wavefield should be supplemented by a particular solution. Here we assume the source is in the water column at depth z_s, thus the source field is

$$
\hat{\phi}_2(\mathbf{r},z;z_s)=\frac{1}{2\pi}\int d^2\mathbf{k}e^{-j\mathbf{k}\cdot\mathbf{r}}\hat{\tilde{\phi}}_2(\mathbf{k},z), \qquad (3.14)
$$

where

$$
\hat{\tilde{\phi}}_2(\mathbf{k},z)=\frac{S_\omega}{4\pi\alpha_i}e^{-\alpha_2|z-z_s|}. \qquad (3.15)
$$

3.3.2 Unperturbed Problem

The unknown wavefield amplitudes are determined from the boundary conditions. For an interface separating two fluids, the normal displacement w and stress σ_{zz} must be continuous. These conditions degenerate into only one condition for fluid-vacuum interface, in which it requires vanishing normal stress. For an interface separating a fluid medium and an elastic medium, in addition to the requirements of continuities of normal displacement w and stress σ_{zz}, the shear stresses σ_{zx} and σ_{xy} must vanish, since the fluid cannot sustain shear stresses. Thus for the three-layer problem the conditions are:

At the sea surface:

$$\sigma_{zz,2}|_{z=0} = 0. \tag{3.16}$$

At the sea bed:

$$w_2|_{z=d} = w_3|_{z=d}, \tag{3.17}$$

$$\sigma_{zz,2}|_{z=d} = \sigma_{zz,3}|_{z=d}, \tag{3.18}$$

$$\sigma_{zx,3}|_{z=d} = 0, \tag{3.19}$$

$$\sigma_{zy,3}|_{z=d} = 0. \tag{3.20}$$

When the above displacements and stresses are written in terms of potentials, and related kernels are inserted, these conditions result in a linear system of equations in the wavefield amplitudes

$$\tilde{B}_g(\mathbf{k})\tilde{\chi}_g^{\mp}(\mathbf{k}) = \tilde{C}(\mathbf{k}), \tag{3.21}$$

where $\tilde{\chi}_g^{\mp}(\mathbf{k})$ is a column vector containing the unknown amplitudes

$$\{\tilde{\chi}_g^{\mp}(\mathbf{k})\}^T = \{\tilde{\phi}_2^-(\mathbf{k}), \tilde{\phi}_2^+(\mathbf{k}), \tilde{\phi}_3^-(\mathbf{k}), \tilde{\psi}_3^-(\mathbf{k}), \tilde{\Lambda}_3^-(\mathbf{k})\}, \tag{3.22}$$

and $\tilde{B}_g(\mathbf{k})$ is the coefficient matrix which may be written as

$$\tilde{B}_g(\mathbf{k}) = \tilde{B}'_g(\mathbf{k})\, D, \tag{3.23}$$

with

$\tilde{B}'_g(\mathbf{k}) =$

$$\begin{bmatrix} -\rho_2\omega^2 e^{\alpha_2 d} & -\rho_1\omega^2 e^{-\alpha_2 d} & 0 & 0 & 0 \\ -\alpha_2 & \alpha_2 & \alpha_3 & 0 & -k^2 \\ -\rho_2\omega^2 & -\rho_2\omega^2 & -\mu(2k^2 - k_{s,3}^2) & 0 & 2\mu k^2\beta_3 \\ 0 & 0 & 2\mu k_x\alpha_3 & j\mu k_y\beta_3 & -j\mu k_x(2k^2 - k_{s,3}^2) \\ 0 & 0 & 2\mu k_y\alpha_3 & -j\mu k_x\beta_3 & -j\mu k_y(2k^2 - k_{s,3}^2) \end{bmatrix}$$

and

$$D = \begin{bmatrix} e^{-\alpha_2 d} & 0 & 0 & 0 & 0 \\ 0 & e^{\alpha_2 d} & 0 & 0 & 0 \\ 0 & 0 & e^{-\alpha_3 d} & 0 & 0 \\ 0 & 0 & 0 & e^{-\beta_3 d} & 0 \\ 0 & 0 & 0 & 0 & e^{-\beta_3 d} \end{bmatrix}.$$

The column vector $\tilde{C}(\mathbf{k})$ representing the integration kernel for the source field for a source in the water at depth z_s, is

$$\tilde{C}(\mathbf{k}) = \begin{Bmatrix} \frac{S_\omega \rho_2 \omega^2}{4\pi\alpha_2} e^{-\alpha_2|z_s|} \\ \frac{S_\omega}{4\pi} e^{-\alpha_2|d-z_s|} \\ \frac{S_\omega \rho_2 \omega^2}{4\pi\alpha_2} e^{-\alpha_2|d-z_s|} \\ 0 \\ 0 \end{Bmatrix}.$$

3.3.3 Perturbed Problem

The total field in the layer i is decomposed into coherent and scattered components. So, for the problem at hand, we have:

In layer 2, *i.e.*, water column:

$$\chi_2^{\mp} = \langle \chi_2^{\mp} \rangle + s_2^{\mp} = \begin{cases} \langle \phi_2^- \rangle + p_2^- \\ \langle \phi_2^+ \rangle + p_2^+ . \end{cases}$$

In layer 3, *i.e.*, elastic sea-floor:

$$\chi_3^{\mp} = \chi_3^- = \langle \chi_3^- \rangle + s_3^- = \begin{cases} \langle \phi_3^- \rangle + p_3^- \\ \langle \psi_3^- \rangle + q_3^- \\ \langle \Lambda_3^- \rangle + r_3^- . \end{cases}$$

The local vectors containing plane-wave amplitudes are

$$\langle \tilde{\chi}_{1;2}^{\mp} \rangle^T = \{ \tilde{\phi}_2^-, \tilde{\phi}_2^+ \}, \tag{3.24}$$

$$\langle \tilde{\chi}_{2;3}^{\mp} \rangle^T = \{ \tilde{\phi}_2^-, \tilde{\phi}_2^+, \tilde{\phi}_3^-, \tilde{\psi}_3^-, \tilde{\Lambda}_3^- \}, \tag{3.25}$$

$$\tilde{s}_{1;2}^{\mp,T} = \{ p_2^-, p_2^+ \}, \tag{3.26}$$

$$\tilde{s}_{2;3}^{\mp,T} = \{ p_2^-, p_2^+, p_3^-, q_3^-, r_3^- \}, \tag{3.27}$$

where the radiation condition has eliminated the upgoing components in the bottom halfspace.

Next, the expression for the local operators $\tilde{B}_i(\mathbf{k})$ for the smooth boundary, and rotation boundary operator $\tilde{b}_i(\mathbf{k})$ will be presented. In the previous section, we have derived the global system for all three layers, which is obviously assembled from the local systems for various interfaces. The local operator $\tilde{B}_2(\mathbf{k})$, at the rough sea bed is simply the lower 4 rows at the matrix in Eq. (3.23), $\tilde{B}_2(\mathbf{k}) = \tilde{B}_2'(\mathbf{k})D'$, with the depth derivative following as $\frac{\partial \tilde{B}_2(\mathbf{k})}{\partial z} = \tilde{B}_2'(\mathbf{k})\frac{\partial D'}{\partial z}$.

The rotation boundary operator $\tilde{b}_2(\mathrm{k})$ is derived in a similar way, representing the discontinuities of the following field parameters according to Eq. (2.13):

$$\tilde{b}_{2,x}(\mathrm{k})\tilde{\chi}^{\mp}_{2;3}(\mathrm{k}) = \left\{ \begin{array}{c} -\tilde{u}_2 + \tilde{u}_3 \\ -2\tilde{\sigma}_{xz,2} + 2\tilde{\sigma}_{xz,3} \\ \tilde{\sigma}_{zz,2} - \tilde{\sigma}_{xx,2} - \tilde{\sigma}_{zz,3} + \tilde{\sigma}_{xx,3} \\ -\tilde{\sigma}_{xy,2} + \tilde{\sigma}_{xy,3} \end{array} \right\}, \tag{3.28}$$

$$\tilde{b}_{2,y}(\mathrm{k})\tilde{\chi}^{\mp}_{2;3}(\mathrm{k}) = \left\{ \begin{array}{c} -\tilde{v}_2 + \tilde{v}_3 \\ -2\tilde{\sigma}_{yz,2} + 2\tilde{\sigma}_{yz,3} \\ -\tilde{\sigma}_{xy,2} + \tilde{\sigma}_{xy,3} \\ \tilde{\sigma}_{zz,2} - \tilde{\sigma}_{yy,2} - \tilde{\sigma}_{zz,3} + \tilde{\sigma}_{yy,3} \end{array} \right\}. \tag{3.29}$$

By inserting the wavenumber kernel for the displacements and stresses, we get

$$\tilde{b}_{2,x}(\mathrm{k}) = \tilde{b}'_{2,x}(\mathrm{k})\, D, \tag{3.30}$$

$$\tilde{b}_{2,y}(\mathrm{k}) = \tilde{b}'_{2,y}(\mathrm{k})\, D, \tag{3.31}$$

where

$$\tilde{b}'_{2,x}(\mathrm{k}) = \begin{bmatrix} jk_x & jk_x & -jk_x & -jk_y & jk_x\beta_3 \\ 0 & 0 & 4j\mu k_x\alpha_3 & 2j\mu k_y\beta_3 & -2j\mu k_x(2k^2 - k_{s,3}^2) \\ 0 & 0 & -2\mu(\alpha_3^2 + k_x^2) & -2\mu k_x k_y & 2\mu(k^2 + k_x^2)\beta_3 \\ 0 & 0 & -2\mu k_x k_y & \mu(k_x^2 - k_y^2) & 2\mu k_x k_y \beta_3 \end{bmatrix}$$

and

$$\tilde{b}'_{2,y}(\mathrm{k}) = \begin{bmatrix} jk_y & jk_y & -jk_y & jk_x & jk_y\beta_3 \\ 0 & 0 & 4j\mu\alpha_3 k_y & -2j\mu\beta_3 k_x & -2j\mu(2k^2 - k_{s,3}^2)k_y \\ 0 & 0 & -2\mu k_x k_y & \mu(k_x^2 - k_y^2) & 2\mu k_x k_y \beta_3 \\ 0 & 0 & -2\mu(\alpha_3^2 + k_y^2) & 2\mu k_x k_y & 2\mu(k^2 + k_y^2)\beta_3 \end{bmatrix}.$$

3.4 Numerical Considerations

To determine the correlation function of the scattered field, Eq. (2.41), for a general case, we need to numerically evaluate two integrals, each of which are two-dimensional. The integrand involves solving a linear system for each value of the wavevector $\mathbf{q}$ being sampled. This linear system with coefficient matrix $\tilde{B}(\mathbf{q})$ has singularities due to the existence of poles corresponding to the normal modes in the waveguide. Furthermore, there also exist poles corresponding to the interface modes at the fluid-solid interfaces known as *Scholte waves* (or *Stoneley waves* in seismology) [29]. While the normal modes exist only when the frequency is higher than the corresponding cut-off frequency, the Scholte wave mode (fundamental mode) is never cut off. However, as a practical consideration, one often includes a small amount of viscous attenuation, usually in terms of dB per wavelength, in the compressional and/or shear properties of the elastic media. This will result in moving the poles away from the real wavenumber axis, ensuring that neither pole creates numerical problems for the evaluation of integrals.

It should also be noted that attenuation must be included into the system for its own right to ensure a finite value of cross-spectral density function. This may be reasoned from an energy point of view. Sound trapped by the layered medium suffers cylindrical spreading ($\sim \frac{1}{\sqrt{r}}$) while the amount of energy radiated by the uncorrelated noise ring sources increases linearly with range ($\sim r$) from the field points. Thus, the contribution of distant sources to the intensity increases in range, making the total intensity integral diverge. By adding any amount of attenuation to the system, the intensity will decay exponentially with range, ensuring convergence of the integral.

Other problems relating to the numerical integration of wavenumber integrals include aliasing caused by undersampling in space/wavenumber domains. This problem

can be solved by moving the integration contour away from the poles, *i.e.* smoothing the kernels. The techniques have been discussed in details in SAFARI manual [38].

3.5 A Brief Review for Three Spectral Regimes

For wave propagation in an elastic waveguide environment, the wavenumber spectra are characterized by three distinct spectral regimes. Since the understanding of which plays a crucial role in the present study, we pause to review some basic features of the wavenumber spectra; Ref. [69] contains an extensive discussion.

The various waves propagating inside a medium have distinct features depending upon where the wavenumber lies in a particular regime in the wavenumber spectra. In general the wavenumber spectrum may be divided into three regimes: *continuous spectrum*, *modal spectrum*, and *evanescent spectrum*. These are schematically shown in Fig. 3.2.

Here we consider a canonical waveguide with the following specification: the medium 1 is a water column with acoustic sound speed c_1, which overlies a semi-infinite elastic medium (medium 2) with compressional speed c_p and shear speed c_s, where $c_1 < c_s < c_p$ (referring to as hard bottom case later). As was shown in Eq. (2.9), because the solutions of the depth-separated wave equation are of exponential form, the variation of a wave in the vertical direction depends upon the quantity $\eta^2 = k^2 - k_m^2$, where $k = \omega/c$ is the horizontal wavenumber and $k_m = \omega/c_m$ is the medium wavenumber, which can be either compressional or shear wavenumber. If η^2 is positive, *i.e.* $k^2 < k_m^2$, the waves vary exponentially in the vertical direction in the medium with medium wavenumber k_m, and in effect decays exponentially away from the interface in this case. These waves are called *evanescent waves*. On the

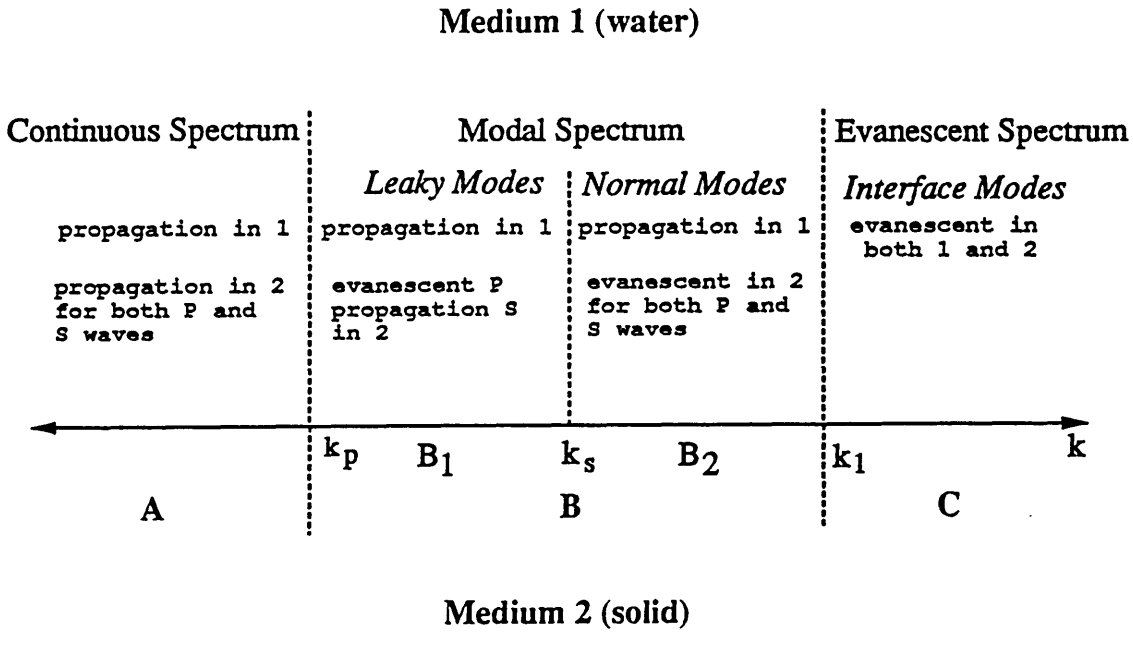

Figure 3.2: Three spectral regimes.

other hand, if η^2 is negative, *i.e.* $k^2 > k_m^2$, the waves vary sinusoidally, and these are the propagating waves.

In Region A of Fig. 3.2, where $k < k_p$ (and $k < k_s < k_1$, in this case), the waves propagate in both media. Thus a wave with wavenumber k propagating in medium 1 will continuously lose its energy into medium 2 through transmission of both compressional and shear waves, thus forming a *continuous spectrum* in wavenumber domain. Region B is the *modal spectrum* regime, which can be subdivided into two subregions in this case. In Region B_1 where the horizontal wavenumber k satisfies $k_p < k < k_s$, the wave can transit through medium 2 by shear wave only, thus waves in medium 1 can form a weak modal structure; these are called *leaky modes.* In Region B_2 where $k_s < k < k_1$, the medium 2 can support evanescent waves only. Thus waves in medium 1 are completely trapped in this medium. The resultant interference is such that only some plane waves with particular angles interfere constructively, and the so-called *normal modes* are formed. Normal modes which correspond to poles in the wavenumber integral exhibit discrete structure in the wavenumber domain, and are the most efficient waves for long-range propagation, because energy is not lost by surface interactions. Physically, these correspond to waves traveling in a shallow grazing angle so that total reflection is resulted.

Finally, in Regime C where $k > k_1$, these waves are evanescent in both media. It has been shown, for example in Ref. [29], that there exist poles in the wavenumber integral corresponding to these waves for interfaces involving elasticity. These are the interface waves, or referred to as inhomogeneous waves in seismology, which propagate along the interfaces and their energy is confined in a region close to the interface. These waves only exist for interfaces involving shear property, and are the most interesting feature for the present study.

3.6 Wavenumber Spectra

With the above review in mind we are here to examine the wavenumber spectra for the present problem. The wavenumber spectra are illustrative in identifying the specific waves, which allow us analyzing the fundamental mechanisms. In this section we devote ourselves to investigate the basic coupling mechanisms between the surface-generated ambient noise and the elastic waves.

The wavenumber spectra to be presented below correspond to the terms covered by the curly bracket in Eq. (3.5) with $z_1 = z_2$. For convenience, the factor $2\pi\langle S_\omega^2\rangle$ is also included. Thus we plot the values of

$$2\pi\langle S_\omega^2\rangle\langle\gamma^2\rangle \int_{-\infty}^{\infty} d^2\mathbf{k}[P_b(\mathbf{q}-\mathbf{k})|A(z,\mathbf{q},\mathbf{k})|^2]$$

as a function of q for the scattered field wavenumber spectra, and likewise

$$4\pi^2\langle S_\omega^2\rangle|g(z,\mathbf{q})|^2$$

for the mean field.

The waveguide is taken to be a water column with sound speed $1500\,m/s$ and density $1.0\,g/cm^3$. We consider both a hard and soft bottom example. The hard bottom is represented by a elastic half-space with compressional speed $5000\,m/s$ and shear speed $2000\,m/s$. The attenuation is $0.1\,dB/\lambda$ and $0.3\,dB/\lambda$ for compressional and shear, respectively, and the density is $3.0\,g/cm^3$. The soft bottom has compressional speed $2000\,m/s$, shear speed $1000\,m/s$, and density $2.0\,g/cm^3$. We have chosen a source strength $Q = 70$ so that it yields $70\,dB$ relative to $\mu\,Pa$ in an infinitely deep ocean.

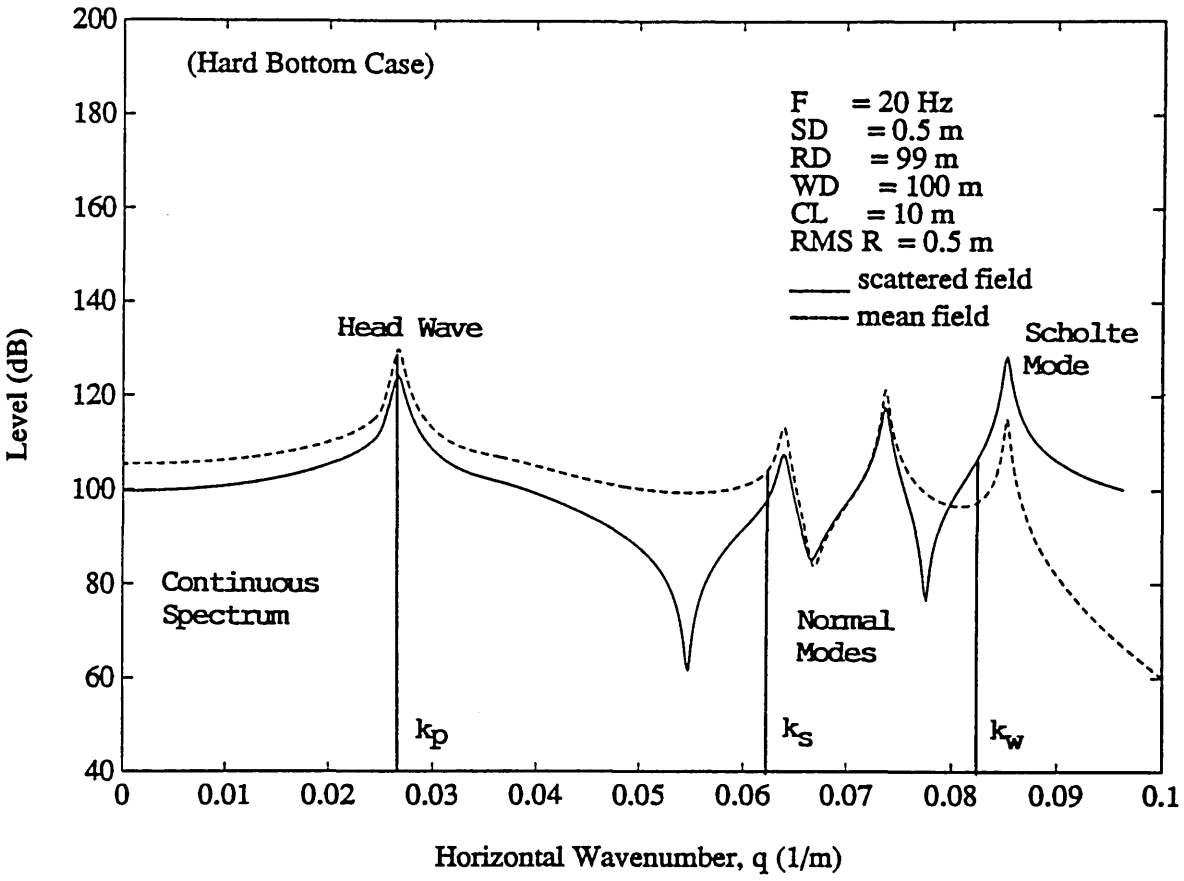

Figure 3.3: Pressure wavenumber spectra: shallow water, hard bottom case

3.6.1 Acoustic Fields

We first examine the wavenumber spectra for the acoustic noise field in order to identify the important propagation mechanisms. It is noted that the sound pressure for a monotonic wave is related to the field potential by a factor of $\rho\omega^2$. Figure 3.3 shows the pressure wavenumber spectrum of both the mean field (dashed line) and scattered noise field (solid line) *near the sea bed* in a hard bottom, shallow water environment of depth $100\,m$. The frequency is $20\,Hz$, the RMS roughness is $0.5\,m$, and the correlation length is $10\,m$. The spectrum for the mean field solution has

peaks corresponding to normal modes between the shear wavenumber, $0.0628\,m^{-1}$ and the water wavenumber, $0.083\,m^{-1}$, and a head wave contribution at the critical wavenumber for the compressional wave, $0.0251\,m^{-1}$. For this hard bottom case, an evanescent Scholte mode exists with wavenumber larger than the water wavenumber. Due to its evanescent nature, the excitation of this interface wave decreases exponentially with the distance between the source and the interface. At $20\,Hz$, the sea bed is within two-wavelength away, so it is *acoustically near*; thus the Scholte mode with wavenumber $0.0879\,m^{-1}$ wave is directly excited in the mean field as shown in the Fig. 3.3. The scattered field has contribution from both the normal modes and the Scholte wave, but with the energy shifted towards the latter compared to the mean field.

Figure 3.4 shows the corresponding results for $500\,m$ water depth. As expected, more normal modes exist in the water column. At $20\,Hz$, the sea bed now is several wavelengths away from the surface, implying it is *acoustically far away*; thus the excitation of the Scholte wave is insignificant in the mean field. However, the Scholte wave mode is the eminent feature in the spectrum of the scattered field, where it clearly provides the most significant contribution.

Figures 3.5 and 3.6 show the similar results for the soft bottom example. Here, the normal modes are leaky, continuously losing their energy through shear-wave transmission, thus making the corresponding spectral peaks weaker than the ones in the hard bottom case. For the low shear speed, the Scholte wave in the mean field is much weaker than the previous case, and totally disappearing in the deep water case (dashed curve in Fig. 3.6). Again the Scholte wave contribution is dramatic in the scattered noise field, totally dominating the noise field near the rough interface.

The results in Figs. 3.3 - 3.6 strongly suggest that the Scholte wave component

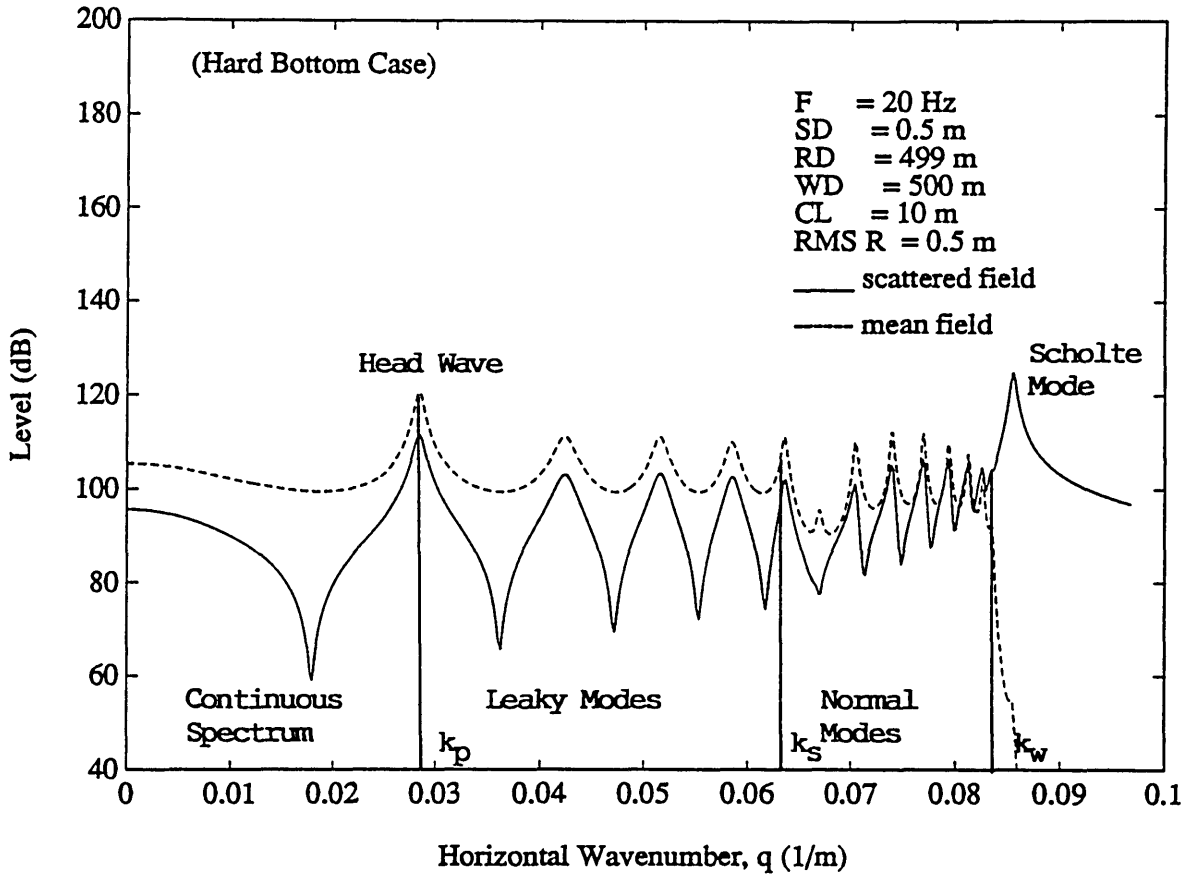

Figure 3.4: Pressure wavenumber spectra: deep water, hard bottom case.

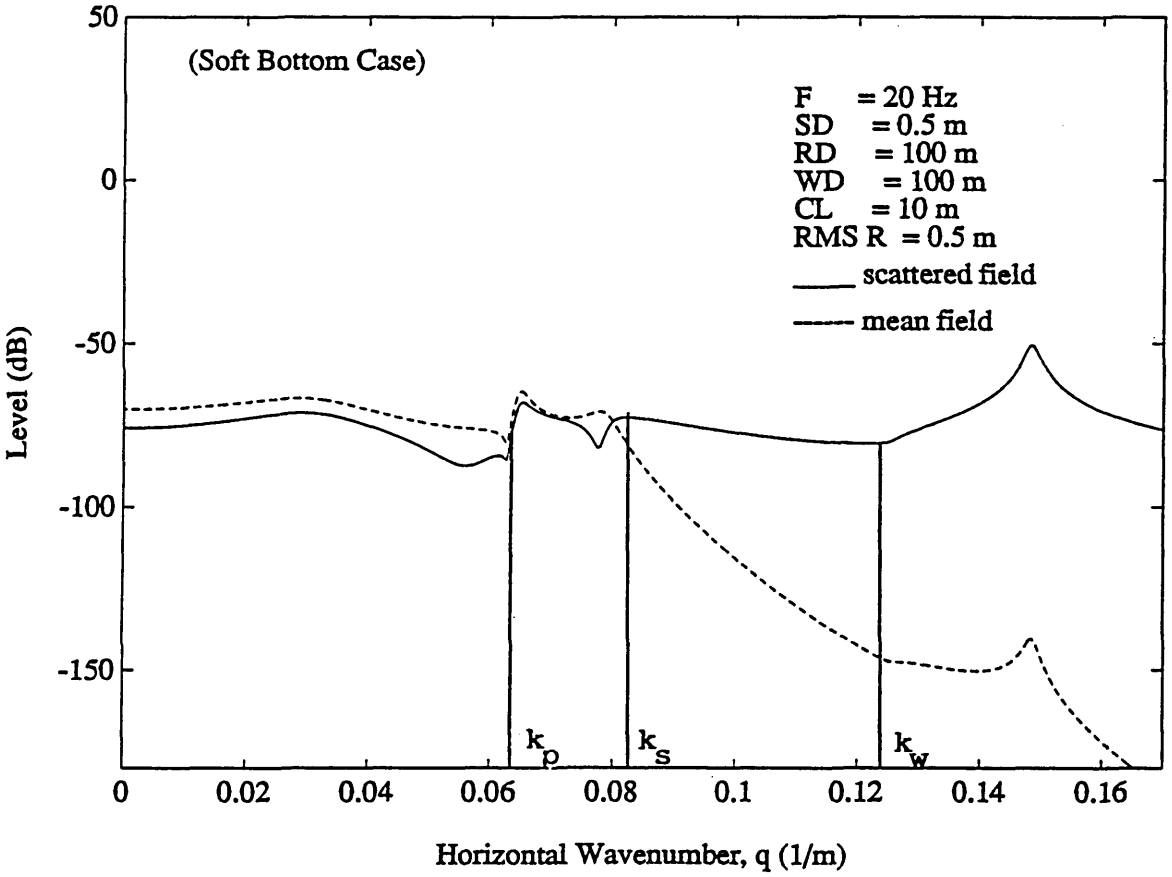

Figure 3.5: Pressure wavenumber spectra: shallow water, soft bottom case.

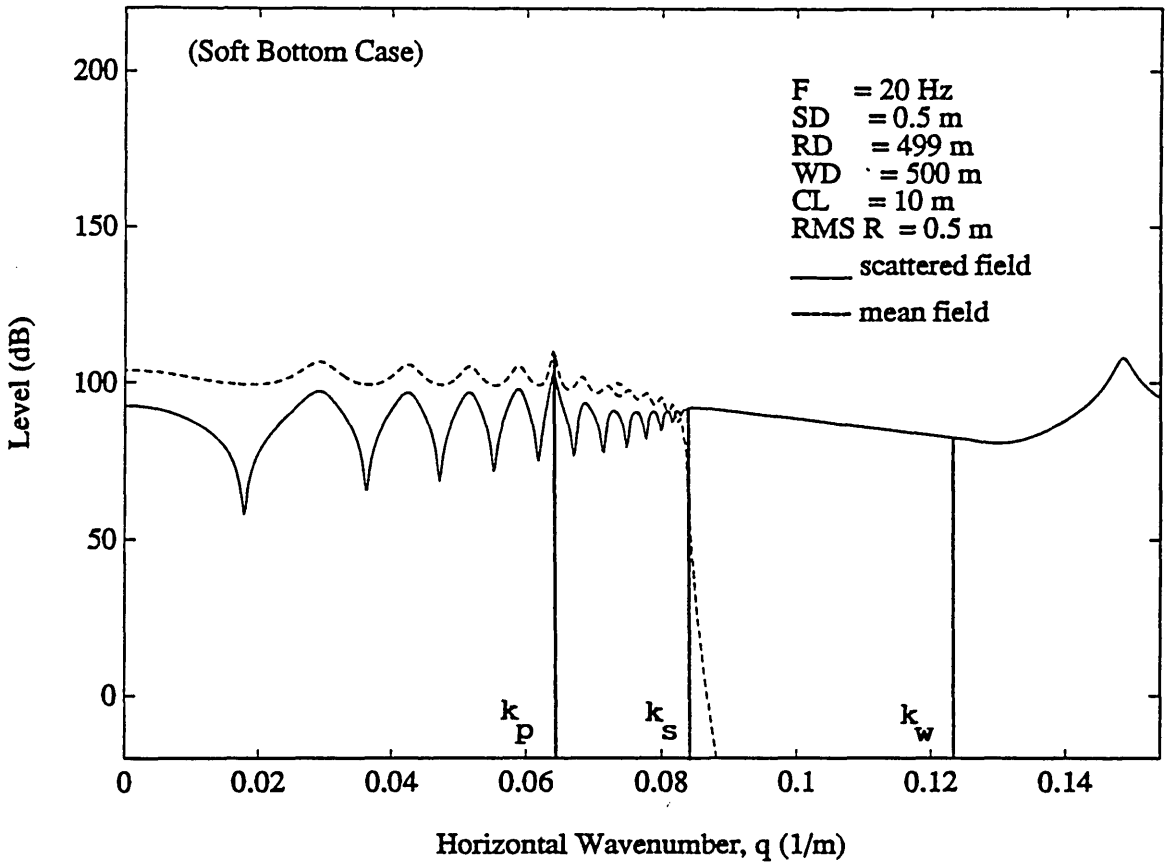

Figure 3.6: Pressure wavenumber spectra: deep water, soft bottom case.

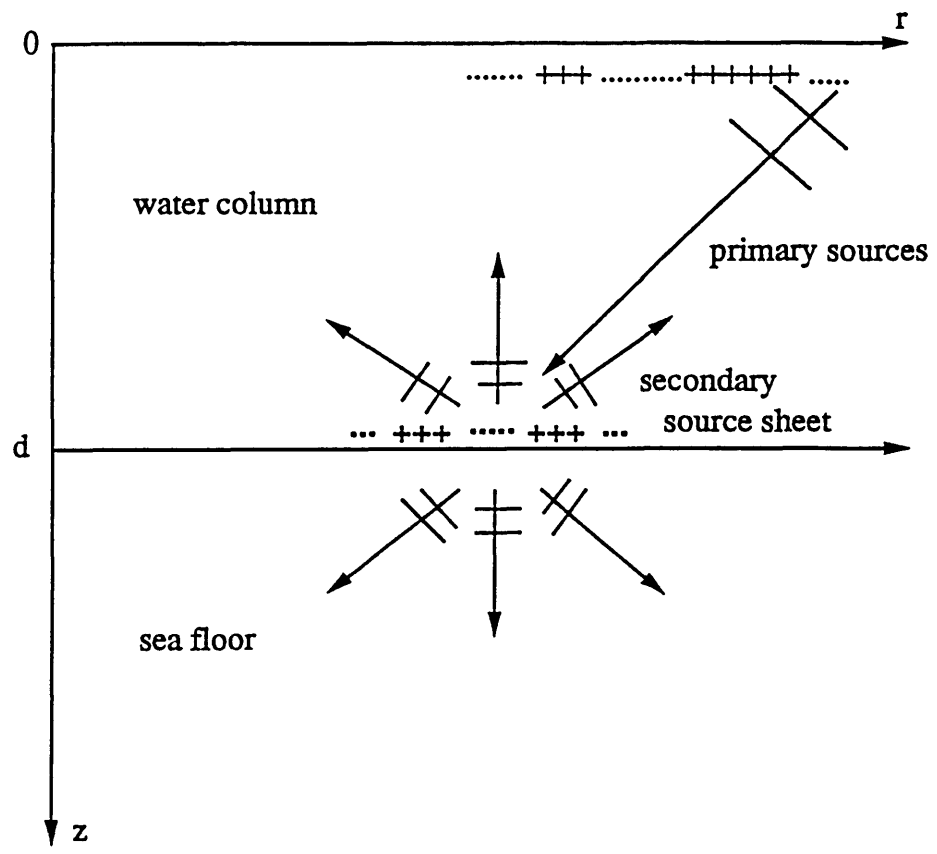

Figure 3.7: Schematic diagram of the scattering processes.

of the surface-generated ambient noise at least qualitatively can be accounted for by scattering from the rough interface. A schematic diagram for the scattering processes is illustrated in Fig. 3.7. The physical interpretation of this phenomenon is as follows. As a downward traveling wave with wavevector k arrives at the rough interface, it scatters into a wide wavevector spectrum, which as described earlier can be considered as generated by a sheet of secondary sources at the depth of the rough interface. These secondary sources excite the modes of the waveguide *depending on the modal amplitude at the "source" depth.* Since the seismic interface modes have maximum amplitude at the sea bed, they become strongly excited by the secondary

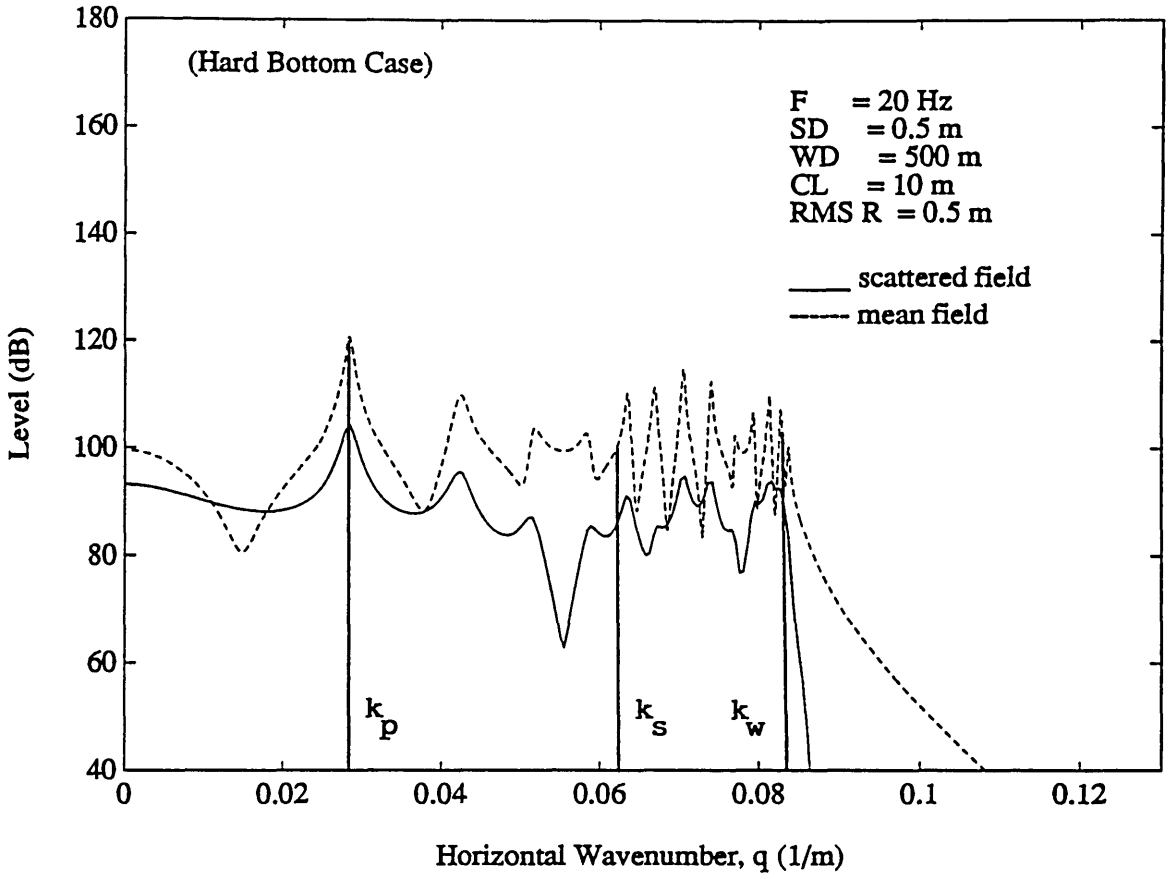

Figure 3.8: Pressure wavenumber spectra for RD = $100\,m$.

sources. Therefore the scattering process has a tendency of shifting energy towards the evanescent spectrum as is evident in Figs. 3.3 - 3.6.

Figure 3.8 shows the pressure wavenumber spectra for a receiver depth of $100\,m$, which is several wavelength away from the rough sea floor. In this case, the mean field (dashed curve) has the similar characteristics for the propagation modes as in Fig. 3.4, except in the evanescent regime. Here the mean field receives contribution from the evanescent part of the source field because it is close to the source, giving a "tail" as shown in the figure. For the scattered field (solid curve), however, the Scholte mode is of no significance because the receiver is too far away from the sea

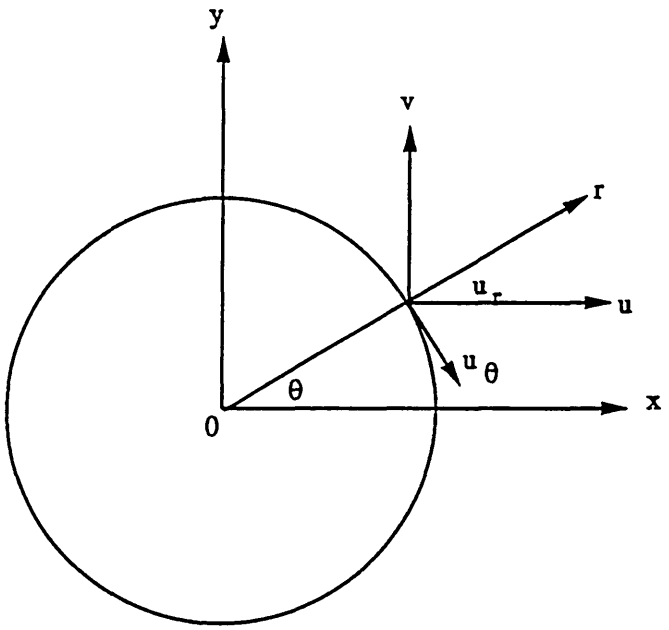

Figure 3.9: Coordinate system for displacements and stresses of the seismic fields.

bed, thus receiving no contribution as expected.

3.6.2 Seismic Fields

For the acoustic field, the sound pressure is related to its potential by a simple factor $\rho\omega^2$. However, the displacements and stresses of the seismic fields need to be evaluated from Eq. (3.11) and (3.13), which are a combination of all three potentials. Since the problem is axisymmetric, it is convenient to present the displacements and stresses in a polar coordinate as shown in Fig. 3.9, where the radial, tangential, and

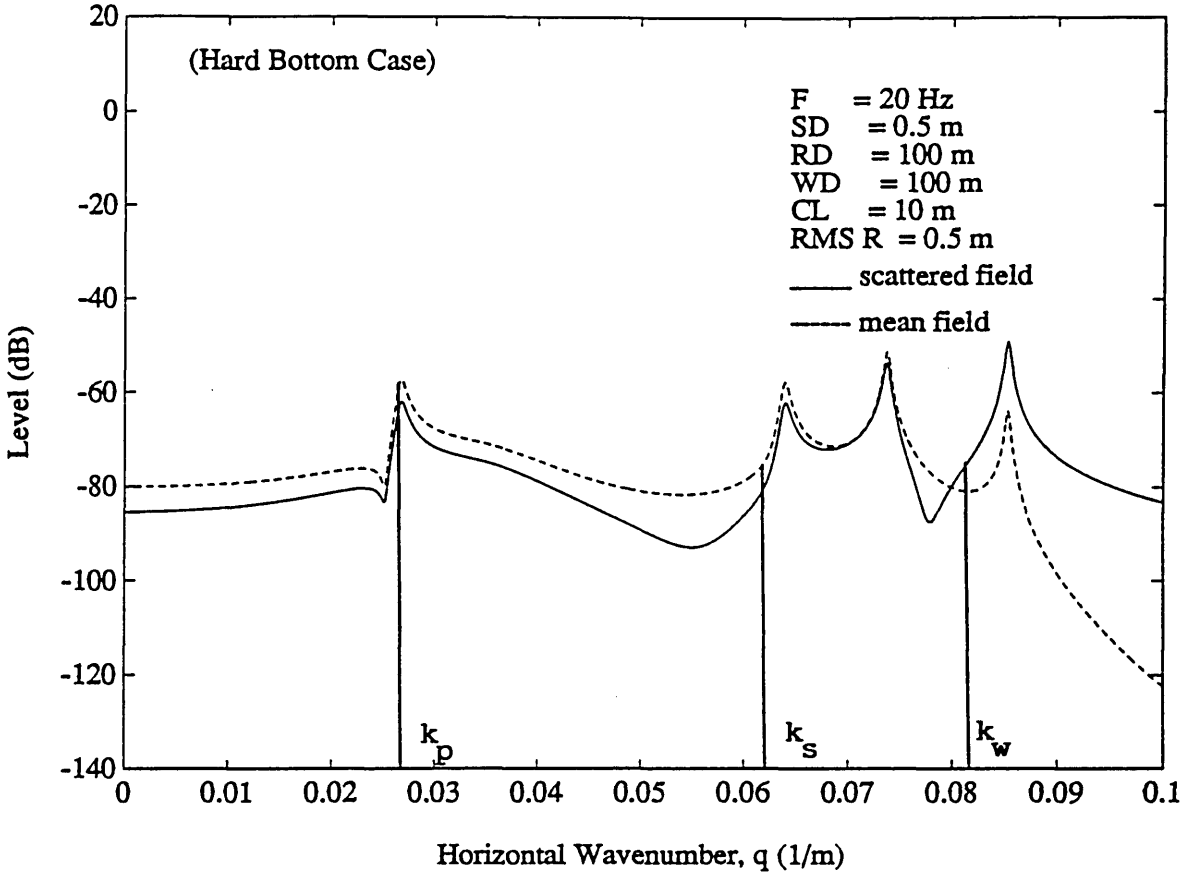

Figure 3.10: Vertical displacement spectra: hard bottom, shallow water case.

vertical component are given by

$$u_r = u\cos\theta + v\sin\theta,$$

$$u_\theta = u\sin\theta - v\cos\theta, \tag{3.32}$$

$$u_v = w, \tag{3.33}$$

and similarly for the stress components. Since the seismic fields are generally measured by a velocity-sensitive geophone, and it is noted that the velocities differ from the displacements by a multiplicative constant $i\omega$, thus we shall here present the results for the displacements only. All the displacement spectral levels are in terms of dB relative to $1\,m$.

We first consider the hard bottom case. Figure 3.10 and 3.11 show, respectively, the vertical and the radial displacement spectra received directly on the water-sea

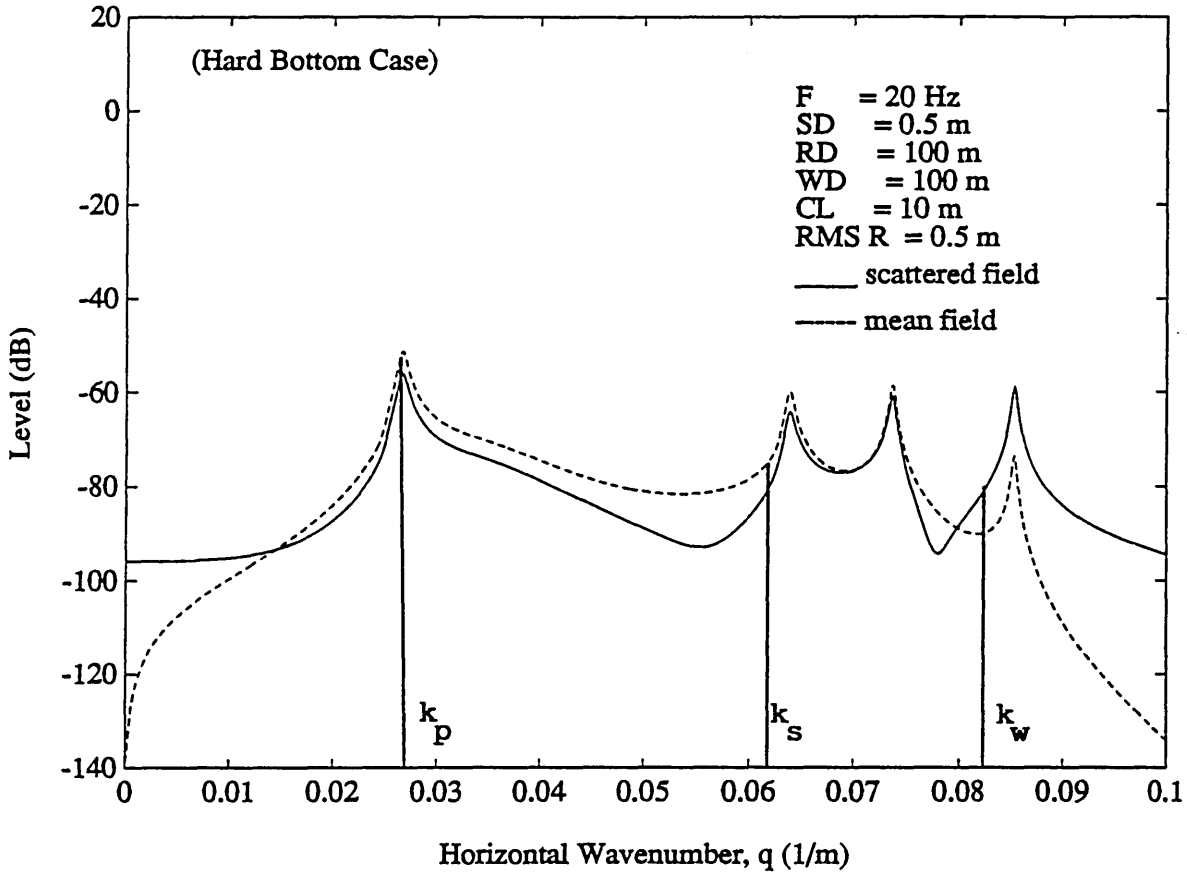

Figure 3.11: Radial displacement spectra: hard bottom, shallow water case.

floor interface. The mean fields (dashed curves) for the both figures are similar except near the zero horizontal wavenumber, where the radial displacement component diminishes. This is because of the axisymmetric nature of the environment and the isotropy of the noise sources, which in turn result in cancellation of the particle motion in the radial direction for the wave propagating vertically. It is seen that, through phase matching, there exist a head wave, normal modes, and an interface wave at the corresponding wavenumbers for those in the water column. For the scattered fields (solid curves), the results show that the energy is scattered into various waves corresponding to the mean fields. It is also noticed that the interface mode is highly excited in the scattered field, not unlike that in the water column.

Next we consider the out-of-plane scattering. Figure 3.12 shows the tangential displacement spectra. The figure shows that there is no tangential displacement component in the mean field. This is expected because there exist only the compressional sources in the mean field which can only excite P and SV potentials. However, the existence of the roughness is equivalent to distributing the various sources, compressional or shear, along the interface, resulting in the excitation of the out-of-plane scattering in the direction corresponding to the shear critical angle. It is interesting to note that the waves propagating vertically are mainly associated with the tangential displacement component.

The corresponding results for the deep water case are shown in Figs. 3.13, 3.14, and 3.15. These results exhibit the similar characteristics corresponding to Figs. 3.10-3.12, except for the higher number of modes due to the larger water depth.

Two representative results for the soft bottom case are shown in Figs. 3.16-3.17.

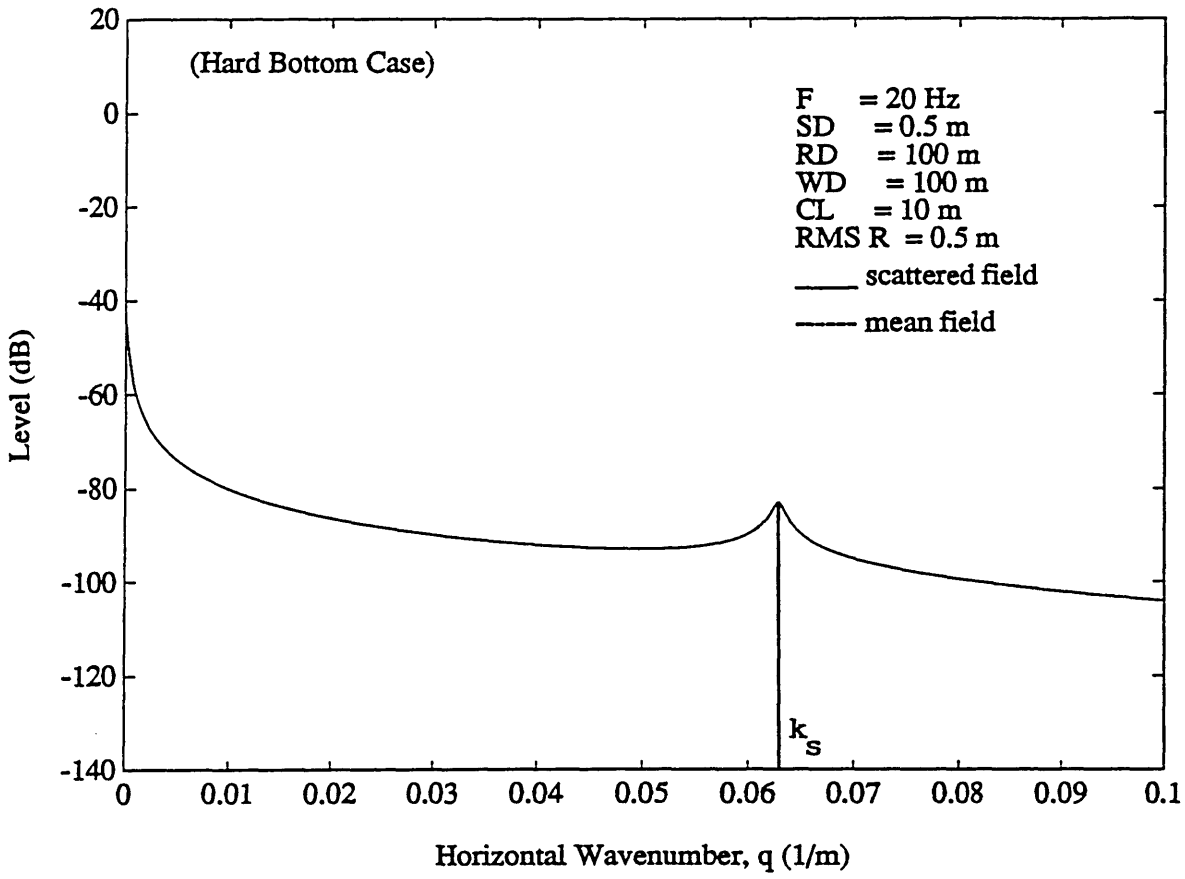

Figure 3.12: Tangential displacement spectra: hard bottom, shallow water case.

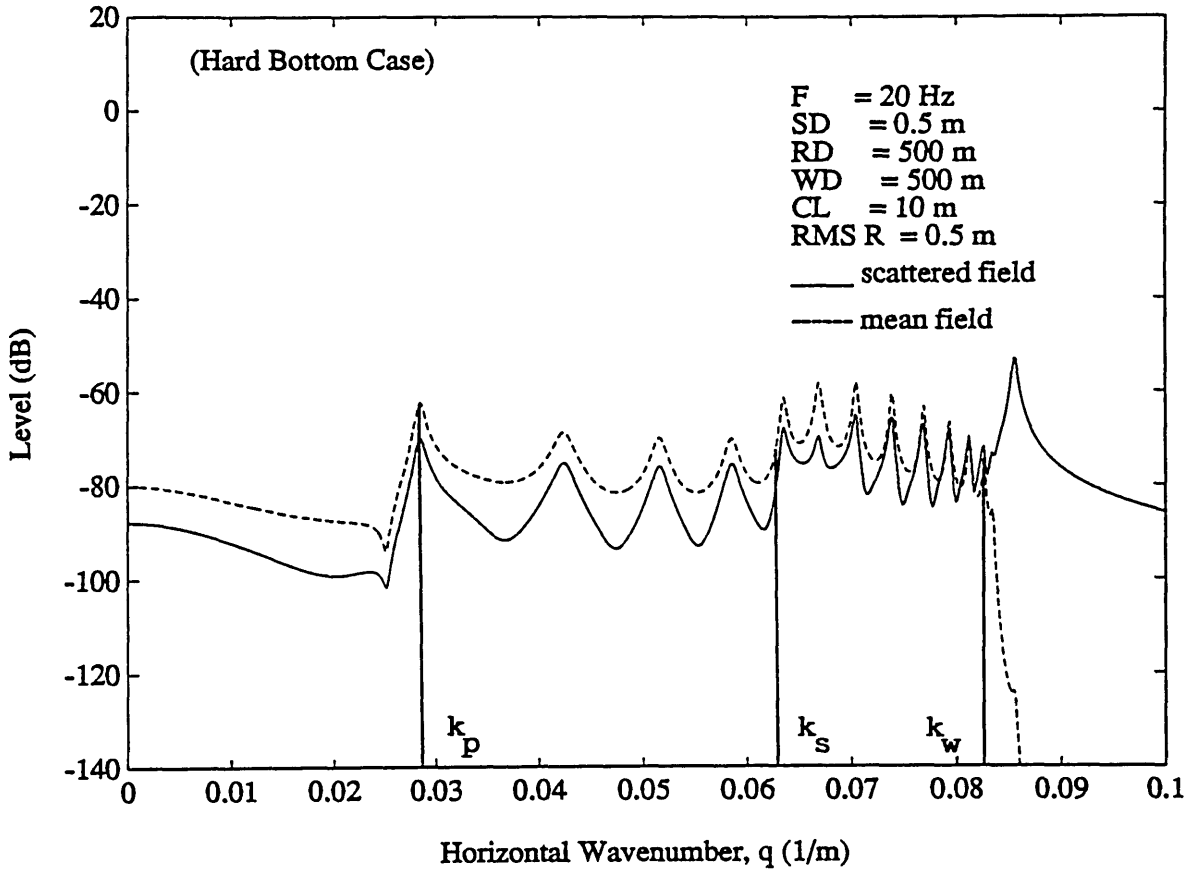

Figure 3.13: Vertical displacement spectra: hard bottom, deep water case.

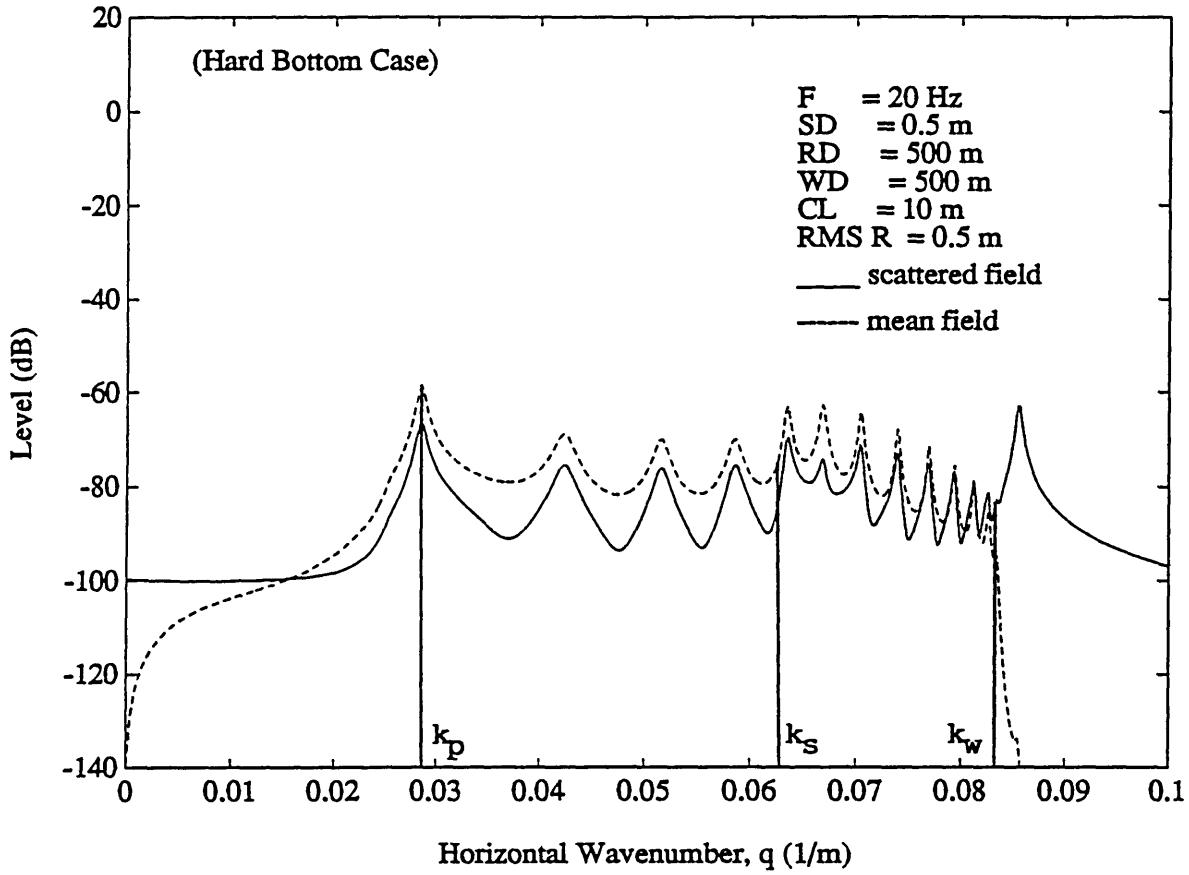

Figure 3.14: Radial displacement spectra: hard bottom, deep water case.

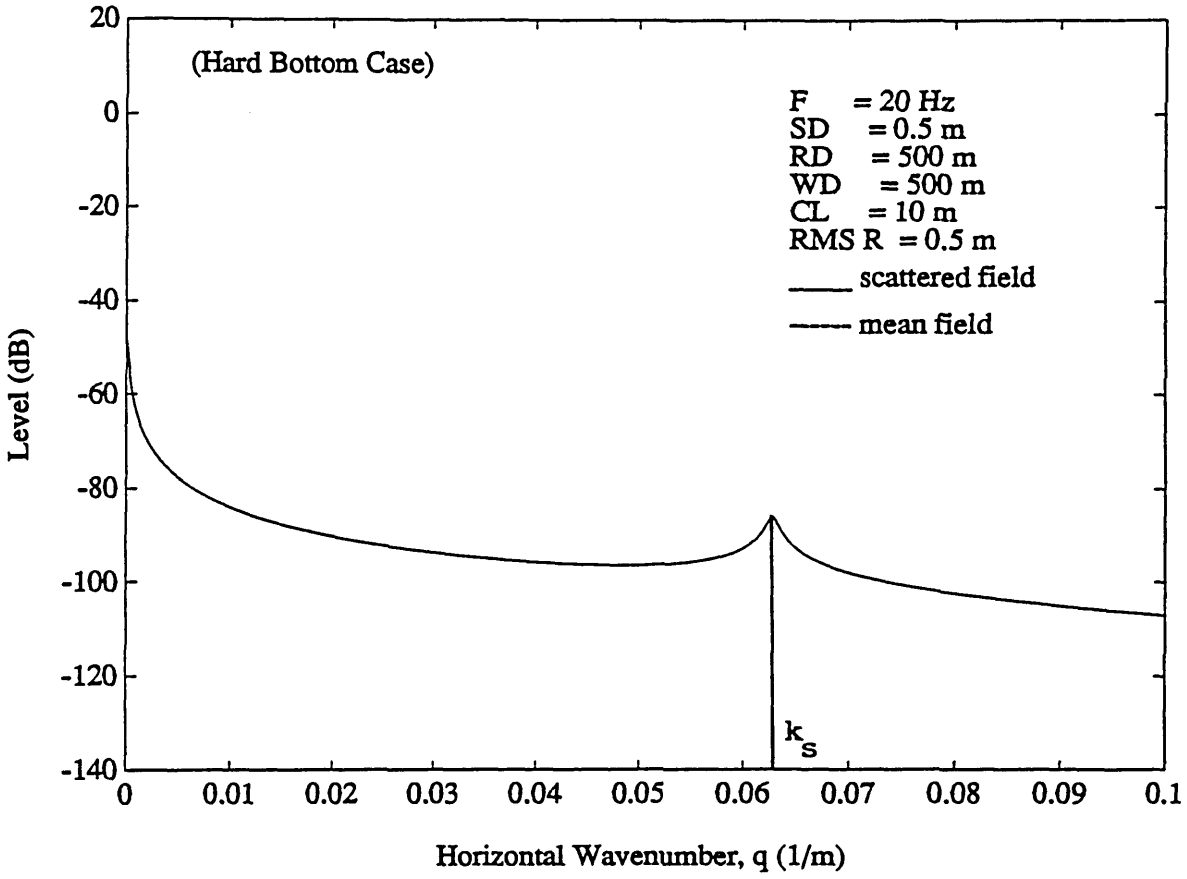

Figure 3.15: Tangential displacement spectra: hard bottom, deep water case.

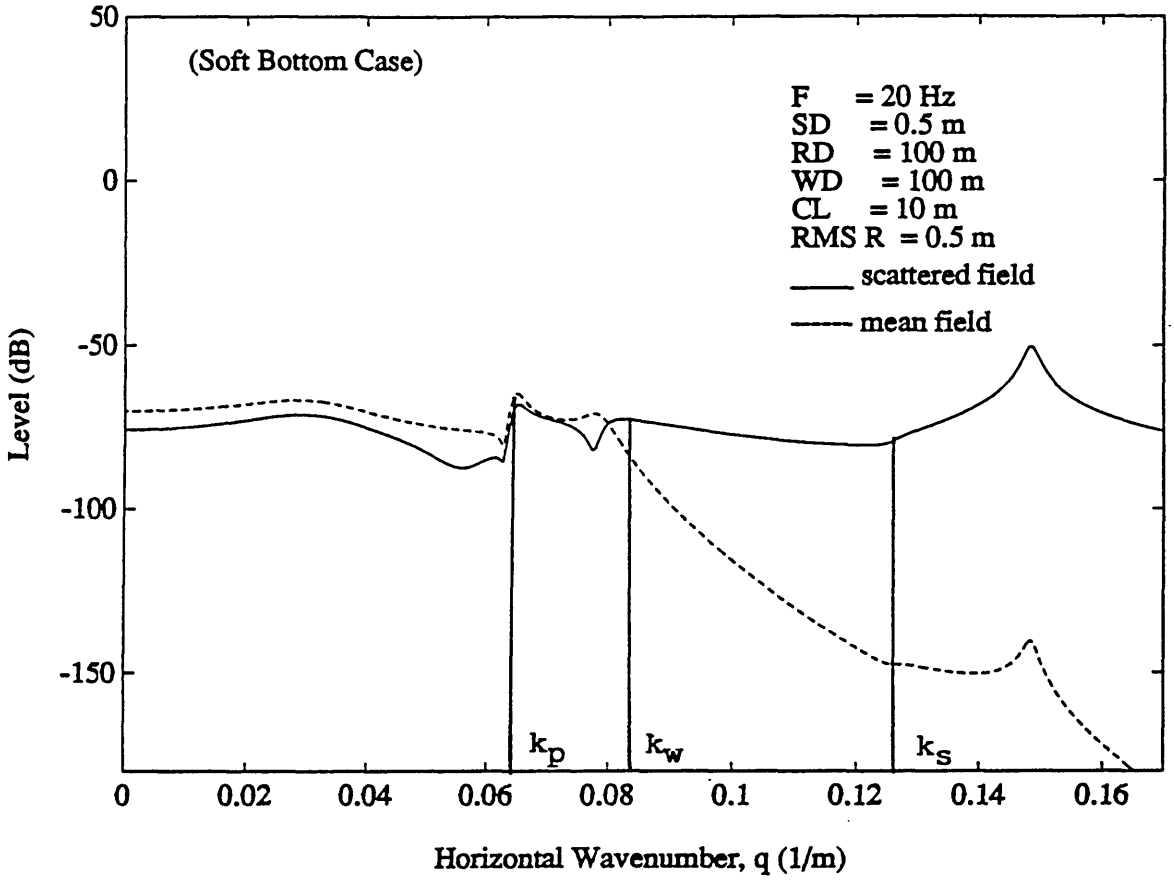

Figure 3.16: Vertical displacement spectra: soft bottom, shallow water case.

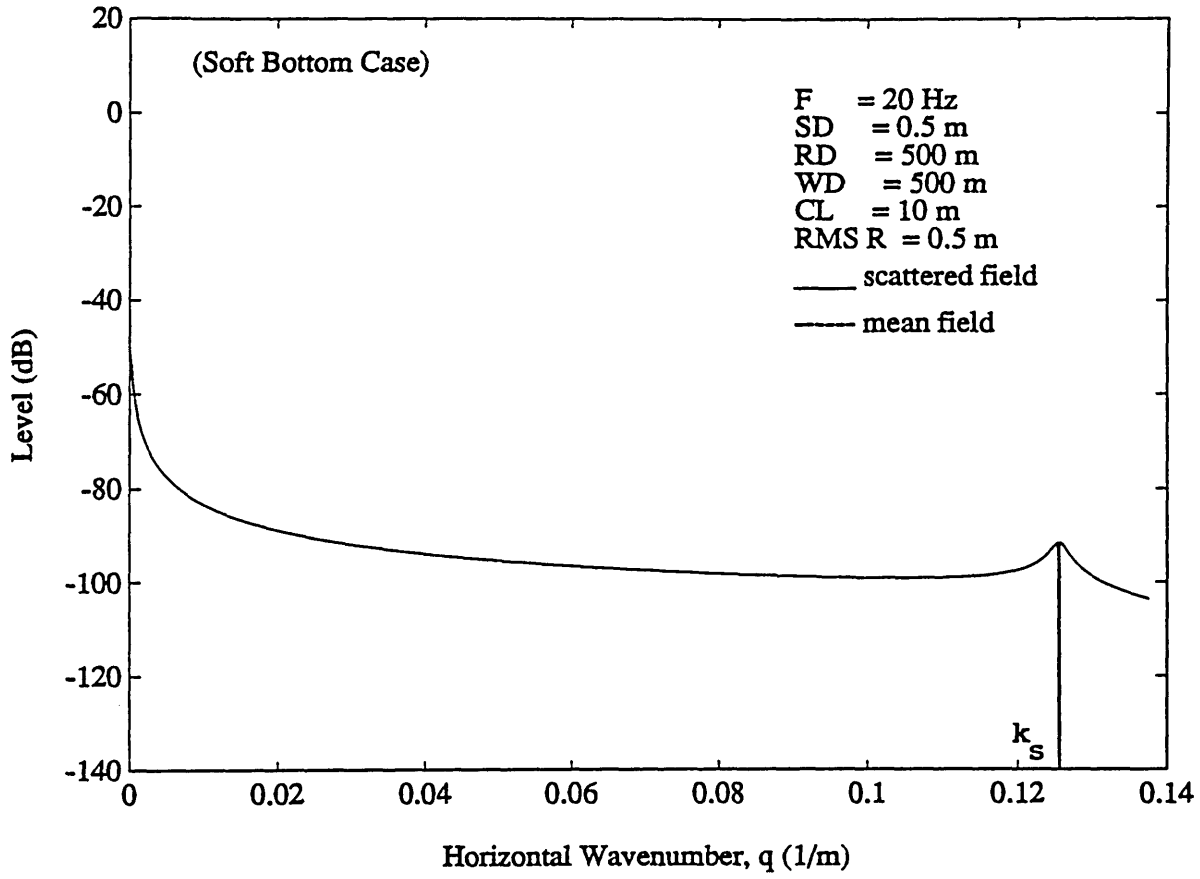

Figure 3.17: Tangential displacement spectra: soft bottom, shallow water case.

3.7 Noise Intensities

In this section we study the vertical distribution of the noise intensities throughout the water column, which may shed light on the region where the scattered field is important. The noise intensity is proportional to the correlation function given by Eq. (3.5) with $\bar{\mathbf{r}} = 0$, and $z_1 = z_2 = z$, *i.e.*,

$$\begin{aligned} I_\omega^t(z) &= C_\omega^t(0,z) \\ &= 2\pi\langle S_\omega^2\rangle \int_0^\infty dq\, q\, P_s(q) \\ &\quad \times\{\langle\gamma^2\rangle \int_{-\infty}^\infty d^2\mathbf{k}[P_b(\mathbf{q}-\mathbf{k})|A(z,\mathbf{q},\mathbf{k})|^2] \\ &\quad +2\pi|g(z,q)|^2\}. \end{aligned} \tag{3.34}$$

Before we examine the distribution of the noise intensities, it is relevant to note the difference in interpreting the various peaks in the wavenumber spectra presented in the previous section for the case of signal propagation from discrete sources and for the present case of propagation from horizontally distributed sources. In the case of a discrete signal, the kernel is multipled by an oscillating exponential function $exp(-iqr)$ or a Bessel function $J_0(qr)$. As a result of cancellation, this has the effect that, for long ranges r, a wide peak in the kernel will contribute less than a narrow peak, or in other words, the width of a peak is a measure of the range attenuation of the corresponding mode. In the present case, however, the integration over the horizontal source plane eliminates the oscillating exponential or Bessel functions. Thus, as seen in Eq. (3.34), the wavenumber integration is performed directly on the kernel amplitudes. A wide peak therefore contributes not only according to its peak level, but also as a result of its width.

It is also helpful to recognize the general structure of of the noise intensity distri-

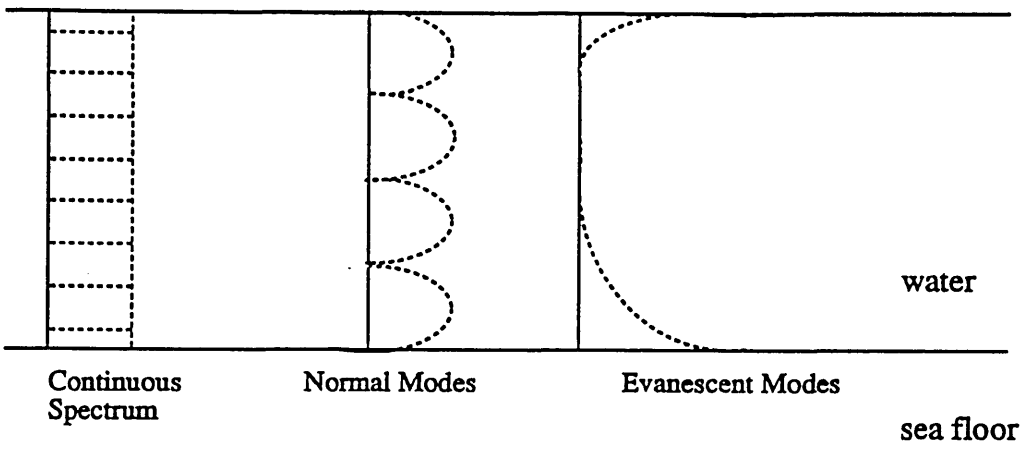

Figure 3.18: Vertical distribution of noise intensities from the three different parts of the wavenumber spectra.

bution contributed by the various parts in the wavenumber spectra, because it will benefit our understanding for the results to be presented below. As we have seen in the previous sections, the noise energy at each point in the water column is derived from three components: continuous spectrum, normal/leaky modes, and evanescent spectrum. Each component may be isolated by properly selecting the range of integration in the wavenumber integral. Figure 3.18 shows schematically the vertical distribution of noise intensities from the three different parts of the wavenumber spectra. The contribution due to continuous spectrum is roughly uniform through-

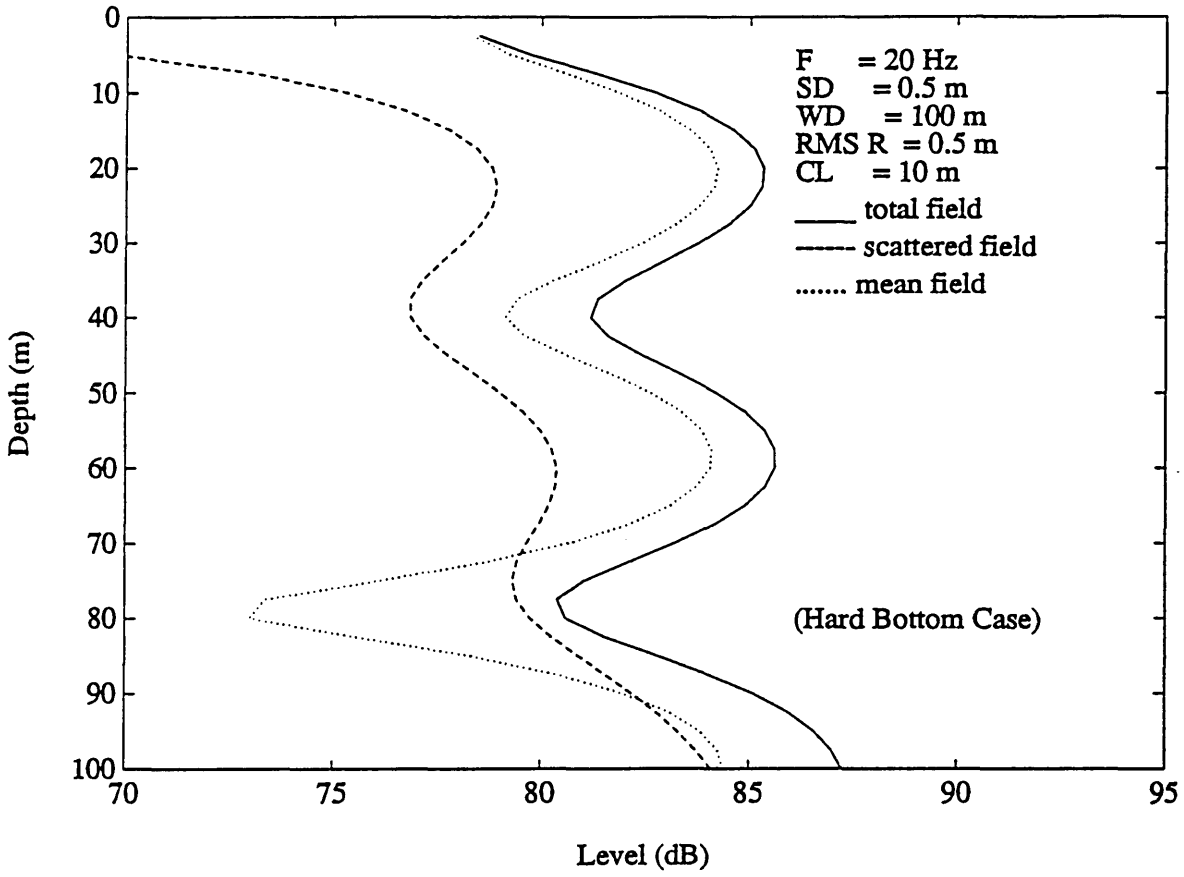

Figure 3.19: Noise intensities: hard bottom, shallow water case.

out the water column, whereas the normal mode contribution exhibits a sinusoidal behavior. For the contribution from the evanescent part of the wavenumber spectra, it confines in a region near the interface due to the excited Scholte waves (lower part of the figure), or in the vicinity of the source (top part of the figure), both with an exponentially-decaying variation.

With the above picture in mind, let us consider the distribution of the noise intensities for the present problem. Figures 3.19 and 3.20 show the noise intensities (the dotted curves for the mean noise fields, the dashed curves for the scattered noise fields, and solid curves for the total noise fields) as a function of depth for the water

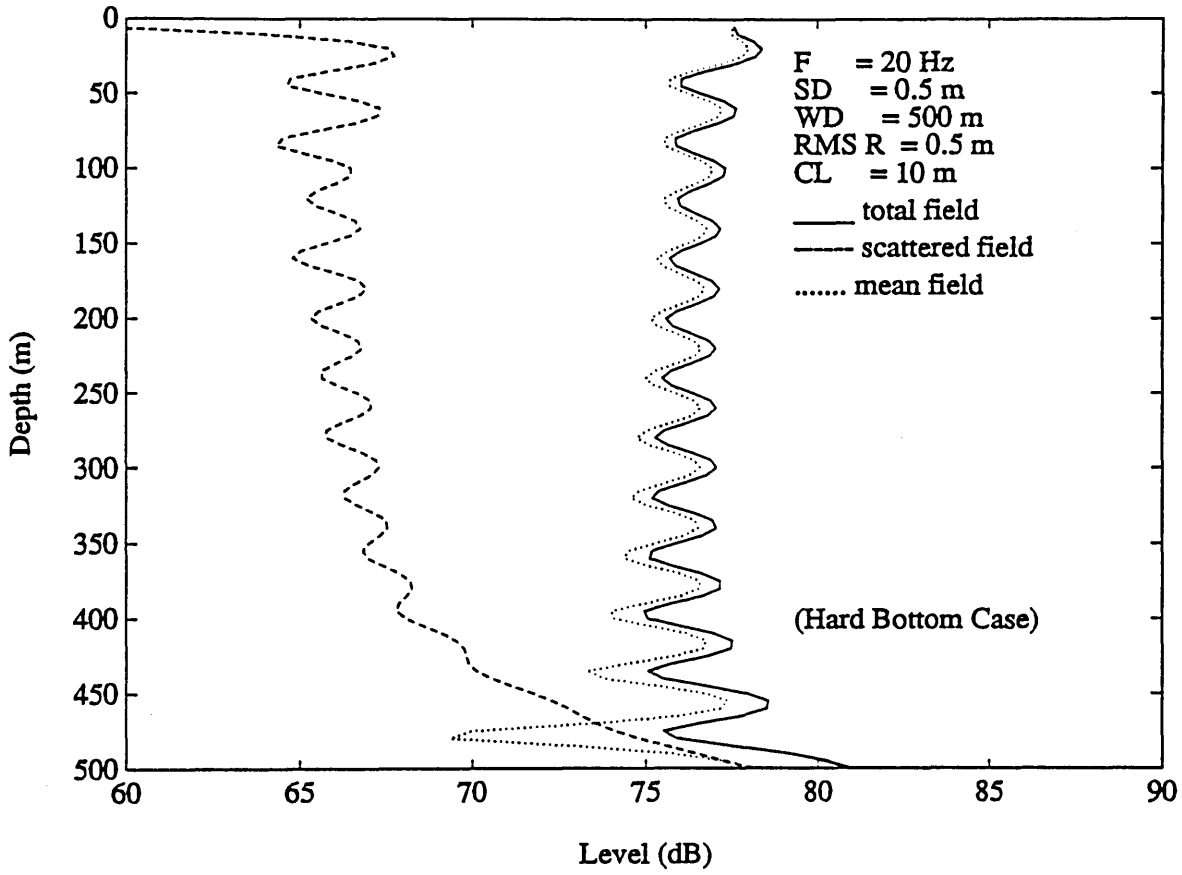

Figure 3.20: Noise intensities: hard bottom, deep water case.

column of $100\,m$ and $500\,m$, respectively. It is seen that the mean field level stays relatively constant as a function of depth apart from the modal shape, with a slight decrease in the deep water case because of the increasing distance from the noise sources, and therefore decreasing evanescent components of the direct source field. The latter effect, in the shallow water case, is counter-balanced by the excitation of the Scholte wave along the sea bed, resulting in an overall uniform distribution in this case.

The scattered fields in both cases are characterized by a low intensity near the surface, and a gradual increase in intensity towards the sea bed. This is particularly evident in the deep water case, where the non-modal structure near the sea bed clearly indicates that the interface wave is the dominant component in the scattered field near the sea bed. This is consistent with the wavenumber spectra shown in Fig. 3.21 for the deep water case for three different receiver depths. As expected, the Scholte wave is clearly decaying away as the receiver is raised from the sea bed.

The overall intensity is the sum of the mean and scattered fields. By comparing the two components, it is seen that the overall intensity is dominated by the mean noise field near the top of the water column, and gradually affected by the contribution from the scattered noise field as the depth is increased, and finally resulting in the dominance of the scattered component near the sea bed. In summary, the overall noise level decreases slightly first, then reaches a minimum, and finally increases toward the sea bed. At least qualitatively, this result is consistent with experimental observations. It should be pointed out here that the fact the scattered noise intensity is significantly larger than that of the mean field near the sea bed may appear to violate the basic assumption of the perturbation theory. As will be discussed in the following section, this is actually not the case.

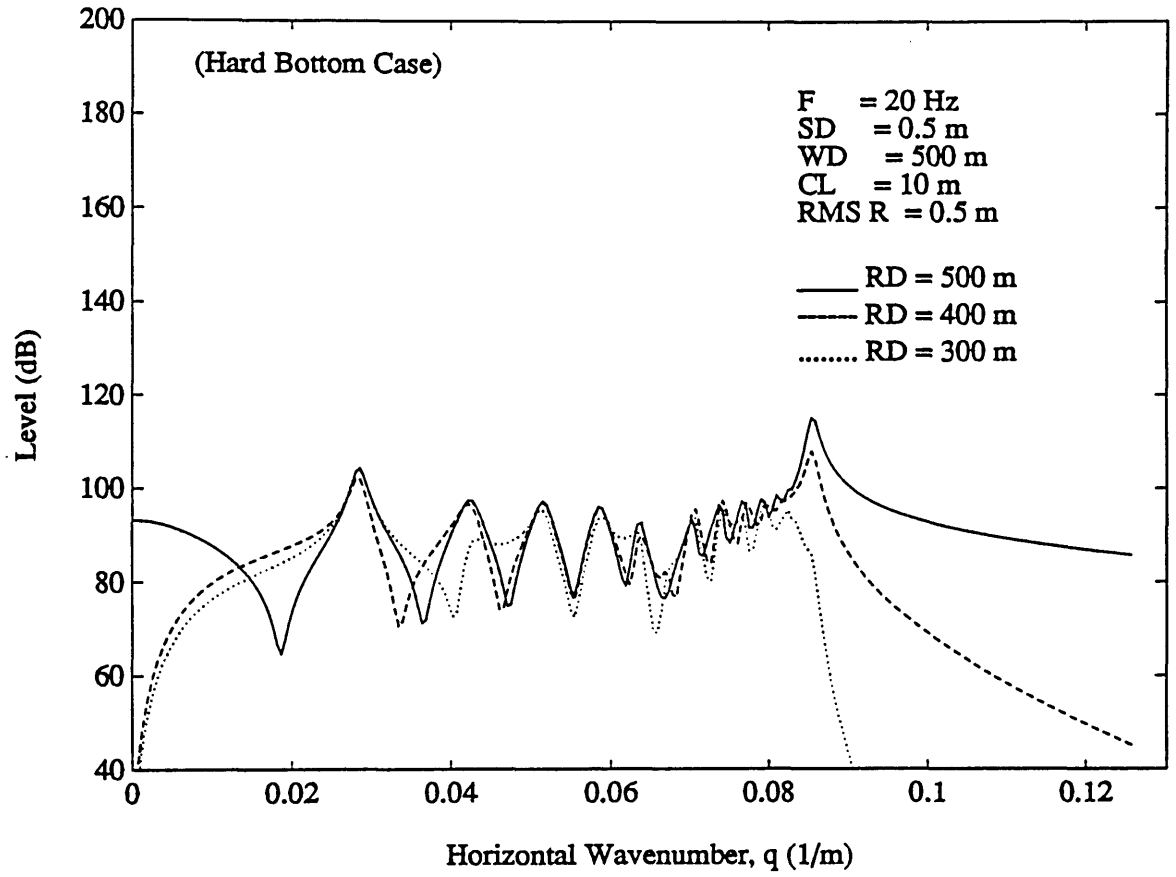

Figure 3.21: Pressure wavenumber spectra (scattered fields) for three different receiver depths.

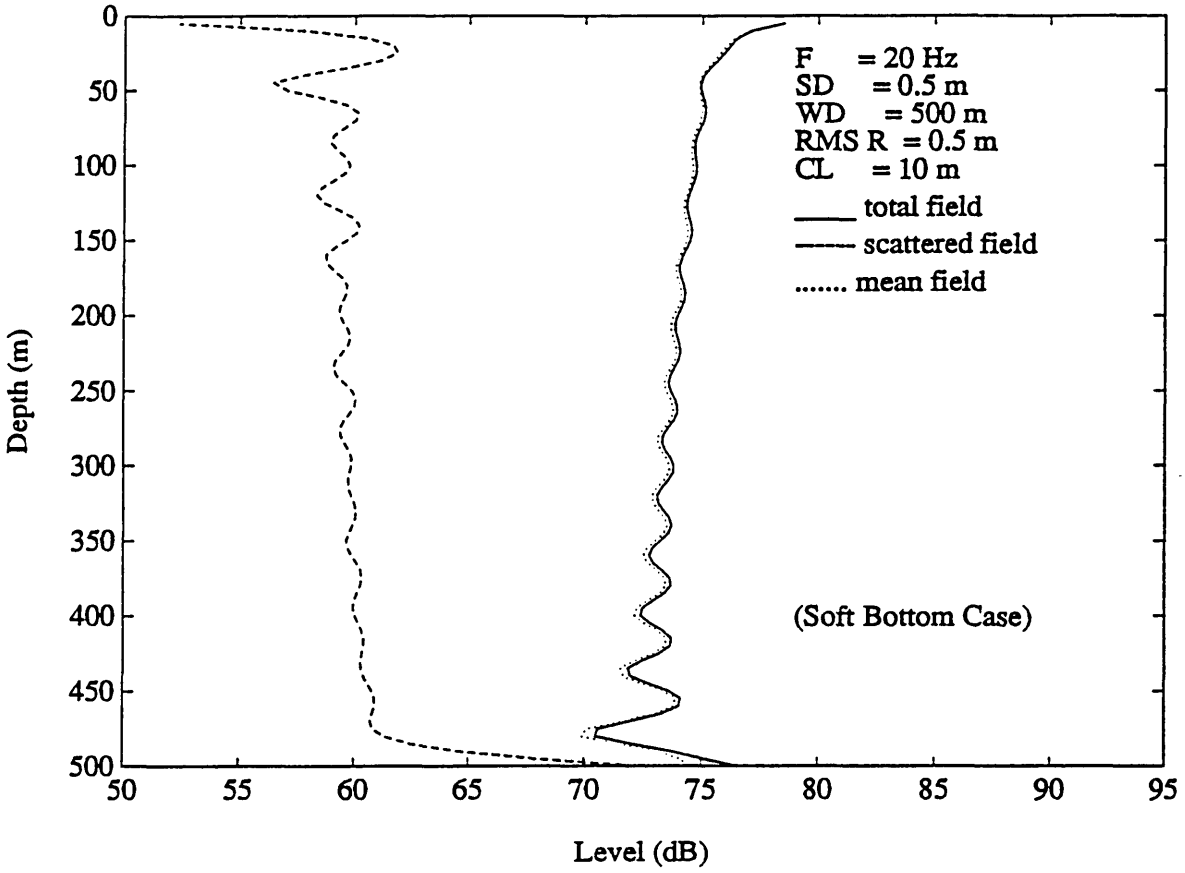

Figure 3.22: Noise intensities: soft bottom, deep water case.

The effect of the sea floor properties on the noise intensity is shown in Fig. 3.22. It is seen that due to the leaky nature of the waveguide, the mean field noise intensity (dotted curve) has demonstrated a weakly modal structure, and decreases as the receiver depth increases. Again this is due to a decrease of the contribution from the evanescent part of the source field. The scattered field (dashed curve) maintains relatively uniform distribution in the most part of the water column, except near a short distance from the sea floor, where the noise intensity increases dramatically due to the Scholte wave contribution. The reduced contrast in the sea floor properties has led to a shallow penetration of the Scholte wave in comparison with the hard

bottom case shown in Fig. 3.19.

One interesting feature is found as one compares the total noise intensity near the top of the water column between Fig. 3.20 and Fig. 3.22. It is seen that, for the hard bottom case (Fig. 3.20), the noise intensity varies sinusoidally, indicating the contribution due to normal modes is more important than the evanescent part from the source field. This is contrary to the soft bottom case (Fig. 3.22), for which the domination is taken over by the evanescent waves from the source field, because the normal modes are weakly excited, resulting in an exponentially decaying behavior near the source region.

3.8 Discussion on the Validity of the Theory

About the Perturbation Theory

A few issues in relation to the validity of the perturbation methods employed are discussed in this section. The fact that the scattered component dominates the near-bottom noise field may appear to violate the requirement that the scattered field should be small compared to the mean field for the perturbation approach to be valid. However, here it should be remembered that the level of the scattered field is controlled by two effects, the actual scattering process and the waveguide propagation effect. As described earlier, the scattering process is represented by the wavenumber integral on the right hand side of Eq. (2.19), whereas the waveguide propagation effect is accounted for by the global matrix operator $B_i(\mathbf{q})$. The dominance of the scattered field is primarily due to the waveguide mechanism of selectively exciting the modes according to their amplitude at the rough interface, in turn leading to a dominance of the evanescent seismic modes in the wavenumber spectrum for the

scattered field. In other words, the high level of the scattered noise near the bottom is primarily a product of the distribution of the scattered field dictated by the waveguide physics. As is clear from Eq. (2.19) the generation of the scattered field is a local effect represented by the secondary source distribution corresponding to the wavenumber integral in Eq. (2.19), independent of the waveguide physics controlling the propagation once the scattered field has been generated. Therefore, the validity of the perturbation approach concerns only the source strengths of the secondary sources, *i.e.* the value of the wavenumber integral in Eq. (2.19). Except for the different mean field, this integral is identical for the waveguide and the halfspace problems for which the perturbation approach was originally developed, and the requirements to the roughness for the theory to be valid are therefore the same, *i.e.* $\sqrt{\langle|\gamma'|^2\rangle} \ll 1$ and $\kappa\sqrt{\langle\gamma^2\rangle} \ll 1$, conditions which are satisfied for all cases treated in this study.

As has been shown by Thorsos and Jackson [11], perturbation theories can be applied well beyond their theoretical limit for modeling forward scattering. The present noise problem is almost entirely a forward scattering problem due to the fact that the scattered field is dominated by modes excited by distant sources, with backscattering playing an insignificant role. It is therefore expected that the predictions produced by the present model are valid for strongly rough interfaces as well, at least in a qualitative sense.

In addition to the approximation introduced in the perturbation approach, we have here generated numerical results using the Born approximation, replacing the mean noise field by the unperturbed field. This has the effect of overestimating the levels of both the mean and scattered components. However, within the limits imposed by the perturbation approach, the spectral composition of the mean and scattered fields is qualitatively correct to at least first order in the roughness parame-

ter. For the small roughness considered here, even the quantitative errors introduced by the Born approximation are within a fraction of a dB.

About the Conservation of Energy

A word about energy conservation is in order. The large noise energy increase near the bottom might raise concern regarding overall energy balance, in view of the fact that scattering only serves as a means of *redistributing* energy rather than *creating* energy. So, where does the increased energy come from? As we have pointed out earlier the bottom magnification of the noise field is attributed to the effect of the waveguide physics. In other words, the large increase in the bottom noise field is due to energy carried by the seismic interface waves with *cylindrical* spreading; energy which in the case of smooth interface would in part penetrate into the bottom according to a *spherical* spreading law. Thus, the scattering merely provides a mechanism for capturing additional energy to remain within the waveguide, resulting in an increase in the total trapped noise energy. Therefore, there is no violation of the fundamental energy conservation principle, except for that imposed by the Born approximation which in the present analysis is insignificant.

3.9 Summary

The objectives of this chapter have been to verify our hypothesis set forth for this study. That is, *the evanescent seismic components of the noise field may be excited by the rough interface scattering processes in a deep ocean.* To achieve this objective, we have implemented the formulation developed in the previous chapter to a simplified ocean environment.

The important mechanisms are illuminated by the wavenumber spectra of both the acoustic fields and the seismic fields. The results have indicated that the seismic interface wave components, exclusively for an elastic sea bed, may be generated by the rough interface scattering, either in a shallow or deep water environment, and it is important for both hard and soft bottom case. This is due to the fact that the effective secondary sources are placed at where the Scholte wave has the largest amplitudes, leading to a strong excitation provided by the waveguide propagation effect. Since the Scholte wave component is the dominant energy carrier, and it decays exponential away from the guiding interface, its major contribution is confined in a layer close to the interface whose thickness depends upon the contrast of the properties between the water column and the elastic sea bed. While the excitation of the Scholte wave offers no surprise for the shallow water case by direct coupling, this mechanism cannot be activated without a rough interface in a deep water environment.

The results for the pressure intensities reiterate the importance of the Scholte wave. The distributions of the noise intensities have shown a significant increase as the receiver approaches the sea bed, in contrast to the plane interface case where the distributions demonstrate a gradual decrease throughout the water column. It is important to recognize that the present magnification of the scattered field is mainly attributed to the waveguide propagation effect triggered by the scattering processes.

The consistency of the above results with the experimental observations has clearly fulfilled our conjecture on the coupling between the surface-generated ambient noise and the seismic interface waves. In the next chapter we shall refine the canonical model to study an actual deep ocean waveguide and then compare the results with the available experimental data, with the hope that the role of rough interface scattering in deep-ocean ambient noise generation may be established.

Chapter 4

Rough Sea Bed Scattering in a Deep Ocean

— in which the performance of the theory is assessed,
and a physical interpretation of the
observed spectral characteristics
of ambient noise is offered.

4.1 Introduction

The canonical waveguide described in the previous chapter has served for understanding the basic physics of the noise scattering processes. In this chapter, the objective is to determine whether the present theory may partially account for the high ambient noise intensity observed in the infrasonic regime (between 1 and 20 Hz) in noise

experiments conducted in deep ocean environments. We begin with a description of a deep ocean waveguide, followed by a presentation of the related operators for this environment. We shall here adopt a recently developed stochastic model [47] for the sea floor roughness in view of its generality in describing a non-isotropic topography; thus Ref. [47] is briefly summarized.

We then concentrate on the analysis of the frequency spectra. We first outline the characteristics of some recent experimental data, followed by the theoretical prediction by the present model. A comparison is then made, and a physical interpretation of the spectral characteristics is offered after a careful analysis.

4.2 Deep Ocean Waveguide

The simplified environmental model used for the noise modeling in a deep ocean waveguide is shown in Fig. 4.1. The environment is assumed to consist of 5 layers with a vacuum layer (layer 1) above the ocean. The water column is represented by two layers (layer 2 and 3); each with pseudo-linear sound speed profile of the form

$$c(z) = \frac{1}{\sqrt{\rho_w(a_i z + b_i)}}, \tag{4.1}$$

where i represents the number of a particular layer. The parameters a_i and b_i are found by matching the sound speed at the interfaces. Let c_1', c_2', and c_3' be the sound speeds at depth $z = z_1 = 0$ (sea surface), $z = z_2$ (sound channel axis), $z = z_3$ (sea bottom), respectively, then

$$a_i = \frac{1}{z_i - z_{i-1}}\left(\frac{1}{\rho_w c_i'} - \frac{1}{\rho_w c_{i-1}'}\right), \tag{4.2}$$

$$b_i = \frac{1}{\rho_w c_{i-1}'}. \tag{4.3}$$

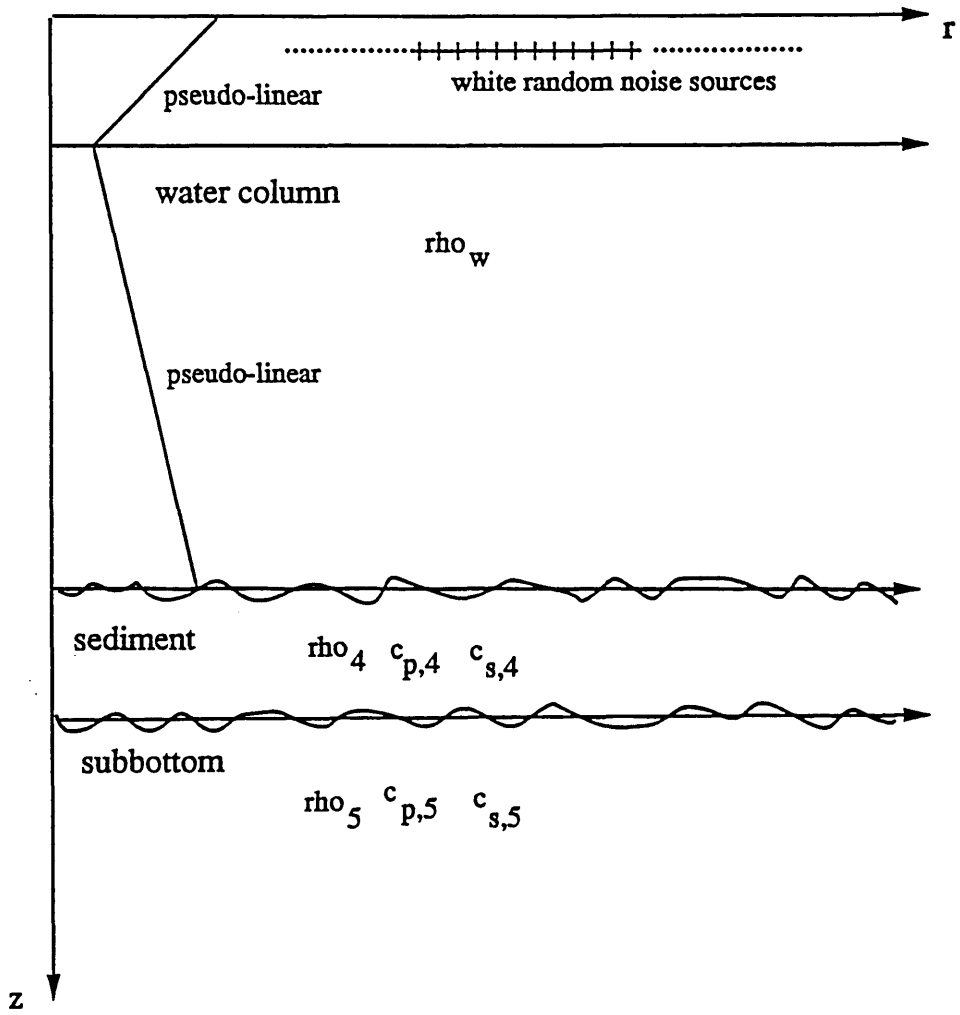

Figure 4.1: Deep ocean waveguide.

We have employed this sound speed profile for two reasons. Firstly, it may reasonably fit the sound speed variations of the ocean in most practical applications. And secondly, this sound speed variation renders the depth-dependent Green's function a closed form solution [38]. The density of the water column is assumed to be constant.

The ocean bottom is assumed to consist of a uniform elastic sediment layer (layer 4) of density ρ_4, compressional speed $c_{p,4}$, and shear speed $c_{s,4}$, overlying a semi-infinite elastic subbottom (layer 5) of density ρ_5, compressional speed $c_{p,5}$, and shear speed $c_{s,5}$, with randomly rough interfaces at either of the two bottom interfaces.

The derivation of the related operators for the present environment is similar to that for the three-layer problem presented in the previous chapter. The major difference is that for the water column the solutions are now those for the pseudo-linear sound speed profile. For this sound speed variation the depth-separated wave equation, Eq. (2.7), becomes [38]

$$\left\{\frac{d^2}{dz^2} - \left[k^2 - \rho_w\omega^2(a_i z + b_i)\right]\right\}\phi(k,z) = 0. \tag{4.4}$$

By introducing the transformation,

$$\begin{aligned}\zeta &= (\rho_w\omega^2 a_i)^{-2/3}[k^2 - \rho_w\omega^2(a_i z + b_i)] \\ &= c_i^{-2/3}[k^2 - \rho_w\omega^2(a_i z + b_i)],\end{aligned} \tag{4.5}$$

Eq. (4.4) becomes

$$\left(\frac{d^2}{d\zeta^2} - \zeta\right)\phi(\zeta) = 0. \tag{4.6}$$

Equation (4.6) is a special form of the Bessel differential equation, for which two independent solutions are the Airy functions $Ai(\zeta)$ and $Bi(\zeta)$ [70]. The details of the derivation for the various operators are presented in Appendix A.

4.3 Description of Rough Sea Floor

For the statistical model of the randomly rough sea floor, most perturbation approaches assume a Gaussian spectrum for simplicity. In spite of its popularity, most experimental data have shown that the spectrum of the sea floor topography tends to be a power-law rather than a Gaussian distribution [44, 46]. Thus, we shall adopt a recently proposed model by Goff and Jordan [47] which behaves as power law at the high frequency components. The model may well represent a non-isotropic sea floor topography having stationarity with respect to an elliptic 'window' by five parameters: root-mean-square height H, a roughness parameter ν, two characteristic wavenumbers, k_s and k_n, and an orientation parameter ζ_s. Since we use this model extensively, Ref. [47] is briefly summarized here.

The above-mentioned five parameters are incorporated in an autocovariance function of the form

$$C_{hh}(\mathbf{x}) = H^2 \frac{G_\nu(r(\mathbf{x}))}{G_\nu(0)}, \tag{4.7}$$

with $G_\nu(r)$ defined as

$$G_\nu(r) = r^\nu K_\nu(r), \qquad 0 \le r < \infty \qquad \nu \in [0,1] \tag{4.8}$$

where K_ν is the modified Bessel function of the order ν. This correlation function describes the azimuthal variation through the dimensionless ellipsoidal norm

$$r(\mathbf{x}) = \left[\mathbf{x}^T Q \mathbf{x}\right]^{1/2} = \sqrt{q_{11}x_1^2 + 2q_{12}x_1x_2 + q_{22}x_2^2} \tag{4.9}$$

where Q is a positive-definite, symmetric matrix whose Cartesian elements q_{ij} have dimension of (length)$^{-2}$. In terms of its eigenvalues $k_n^2 \ge k_s^2$ and its normalized eigenvectors $\hat{\mathbf{e}}_n$ and $\hat{\mathbf{e}}_s$, Q may be expressed as

$$Q = k_n^2 \hat{\mathbf{e}}_n \hat{\mathbf{e}}_n^T + k_s^2 \hat{\mathbf{e}}_s \hat{\mathbf{e}}_s^T. \tag{4.10}$$

The parameters k_n and k_s play the same role as the correlation length in defining the topographic characteristics; thus $2\pi/k_n$ and $2\pi/k_s$ represent, respectively, the characteristic length of the minor and major axis of the ellipsoidal topography. The variable ζ_s is an orientation parameter which is conveniently chosen to be the angle between the major axis and north, measured clockwise from north. This model is capable of describing the non-isotropic feature of the sea floor morphology such as the local strikes formed by the abyssal hills commonly found on the ocean floor.

The roughness parameter ν determines the behavior of the autocovariance function as r approaches to zero lag, which also determines the roll-off rate of the power spectra at the high frequencies. In the physical terms, ν measures the degree of the roughness, with the limiting cases of unity and zero corresponding to a random surface with continuous derivative and one which is "space-filling", respectively. All realizations of this covariance model are bounded self-affine fractal surfaces (appendix of [47]), with the special case $\nu = 1.0$ being a bounded self-similar. It was shown [47] that ν relates to the *Hausdorff-Besicovitch* dimension D (or *fractal* dimension [48]) as

$$D = 3 - \nu. \tag{4.11}$$

The corresponding power spectrum may be obtained by a Fourier transform, and is given by [47]

$$P_b(\mathbf{k}) = 2\nu H^2 |Q|^{-1/2} [u^2(\mathbf{k}) + 1]^{-(\nu+1)}, \tag{4.12}$$

where

$$\begin{aligned} u(\mathbf{k}) &= [\mathbf{k}^T Q^{-1} \mathbf{k}]^{1/2} \\ &= \sqrt{\left(\frac{k}{k_s}\right)^2 \cos^2(\zeta - \zeta_s) + \left(\frac{k}{k_n}\right)^2 \sin^2(\zeta - \zeta_s)}, \end{aligned} \tag{4.13}$$

where k and ζ are, respectively, the modulus and azimuth of $\mathbf{k}$. An example for the power spectrum along with its realization for $k_s = 0.03\,m^{-1}$, $k_n = 0.06\,m^{-1}$,

and $\zeta_s = 60°$ is shown in Fig. 4.2. It is noted that the minor axis of the spectrum corresponds to the direction of the local strikes in its realization, which in this case is aligned along 60° counting clockwise from y-axis.

The special case of isotropic rough surface corresponds to $k_n = k_s$, which simplifies the power spectrum, Eq. (4.12), to become

$$P_b(\mathbf{k}) = \frac{2\nu H^2}{k_0^2}\left[\left(\frac{|\mathbf{k}|}{k_0}\right)^2 + 1\right]^{-(\nu+1)}, \tag{4.14}$$

where $2\pi/k_0$ is a characteristic length similar to the correlation length for the Gaussian spectrum. Equation (4.14) shows that the spectrum has a finite value as $|\mathbf{k}| \to 0$, and its decay rate for the high spatial frequencies is $k^{-2(\nu+1)}$.

Figure 4.3 presents two representative cases for the isotropic Goff-Jordan spectrum, Eq. (4.14) for $\nu = 1.0$, and Gaussian spectrum, Eq. (3.3). It is seen the Goff-Jordan spectra decay much slower than the Gaussian spectra at the high frequency components. We shall examine this effect on the scattering characteristics in the next chapter. For the time being we concentrate on the performance of the theory and interpretation of the experimental observations.

4.4 Frequency Spectra

Here we illustrate the role of rough surface scattering in shaping the frequency spectra of the ambient noise. The frequency spectra may be generated by evaluating the two integrals in Eq. (3.5) for *each* value of frequency selected in a given range. Since every value of frequency represents a completely independent run, the generation of the frequency spectra presents the most time-consuming computation.

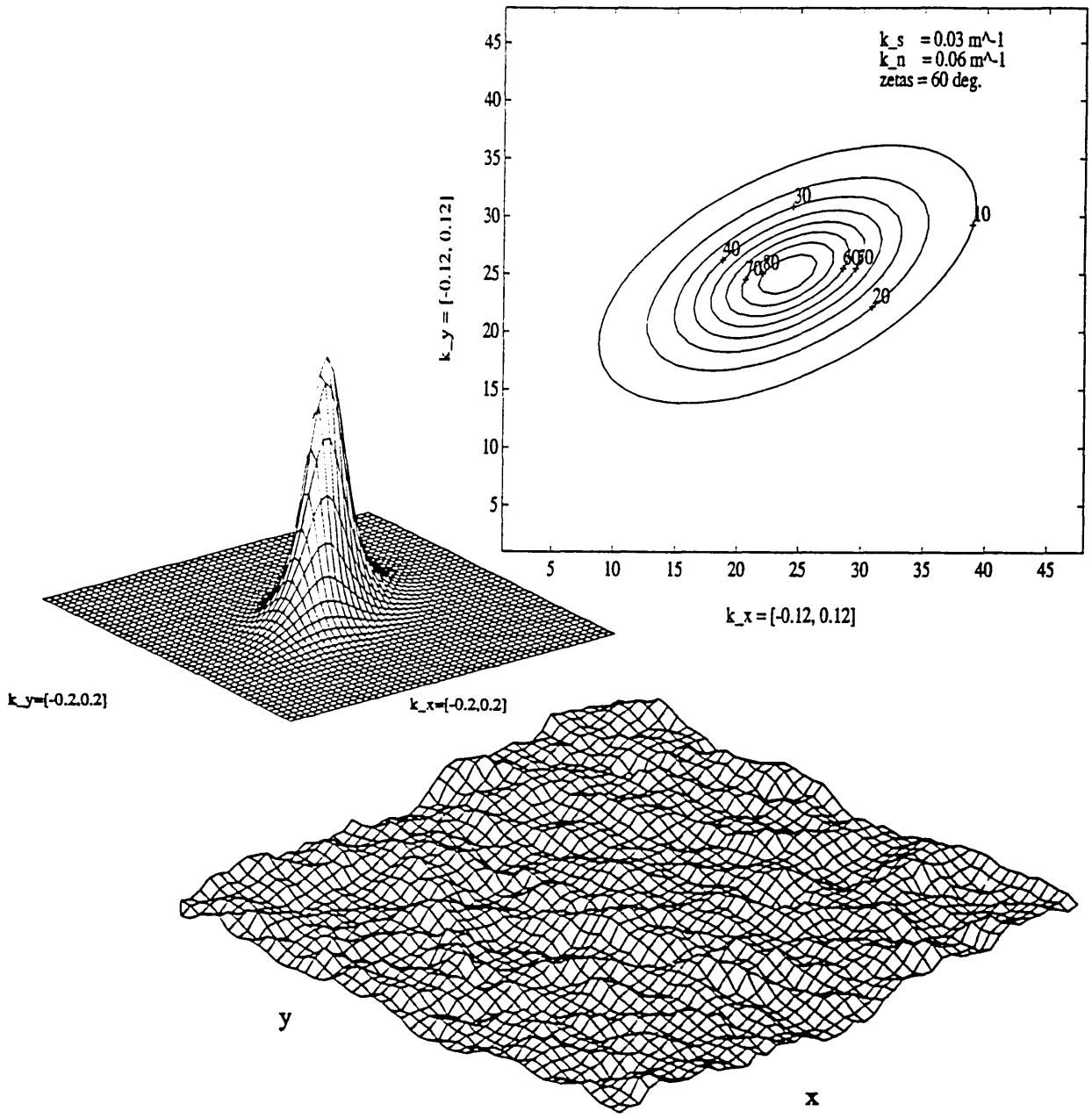

Figure 4.2: Goff-Jordan spectrum and its realization for $k_s = 0.03\,m^{-1}$, $k_n = 0.06\,m^{-1}$ and $\zeta_s = 60°$.

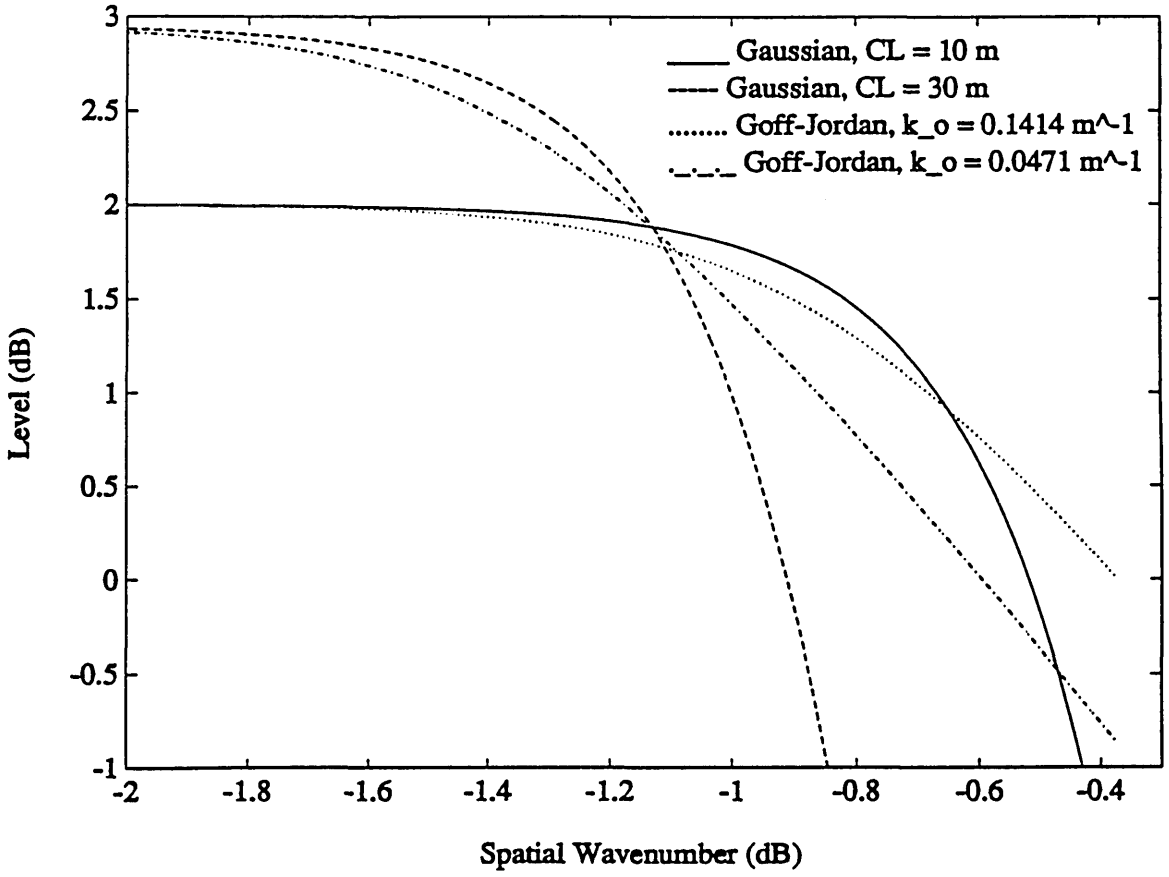

Figure 4.3: Roughness power spectra

We begin with a review of the environment for the experiment whose results are to be compared with the model prediction. Then the characteristics of the frequency spectra from the experimental data are identified and described. After presenting the wavenumber spectra, our major effort is to generate the frequency spectra using the current model with realistic environmental parameters. Comparisons are made at the end of the section.

4.4.1 Experimental Observations

The experimental data we analyze have been collected during an experiment conducted by the Marine Physical Laboratory at Scripps Institution of Oceanography (SIO), using freely drifting floats, and the results of the data analysis were reported in Ref. [71]. The experiment was conducted in the Pacific Ocean during July 1989, at 34.8° N, 122.3° W, about 150 km west-northwest of Point Arguello, California, in a region with the average depth 3800 m. The map of the sea floor morphology near the experimental site was given in Fig. 2 of Ref. [71]. A measured sound speed profile of this experiment is shown in Fig. 4.4.

The frequency spectra from the experiment is shown in Fig. 4.5. The experimental data [71] have demonstrated that the frequency spectrum in the infrasonic regime between 1 and 20 Hz is distinctly different below and above approximately 5 Hz. Above 5 Hz, the noise intensity is relatively constant at about 70 dB, whereas below that frequency, the intensity increases dramatically to about 135 dB towards the low end. The observations of this experiment are similar to those of another Pacific experiment reported in Ref. [3].

The scope of the present analysis is to understand the basic physics governing the

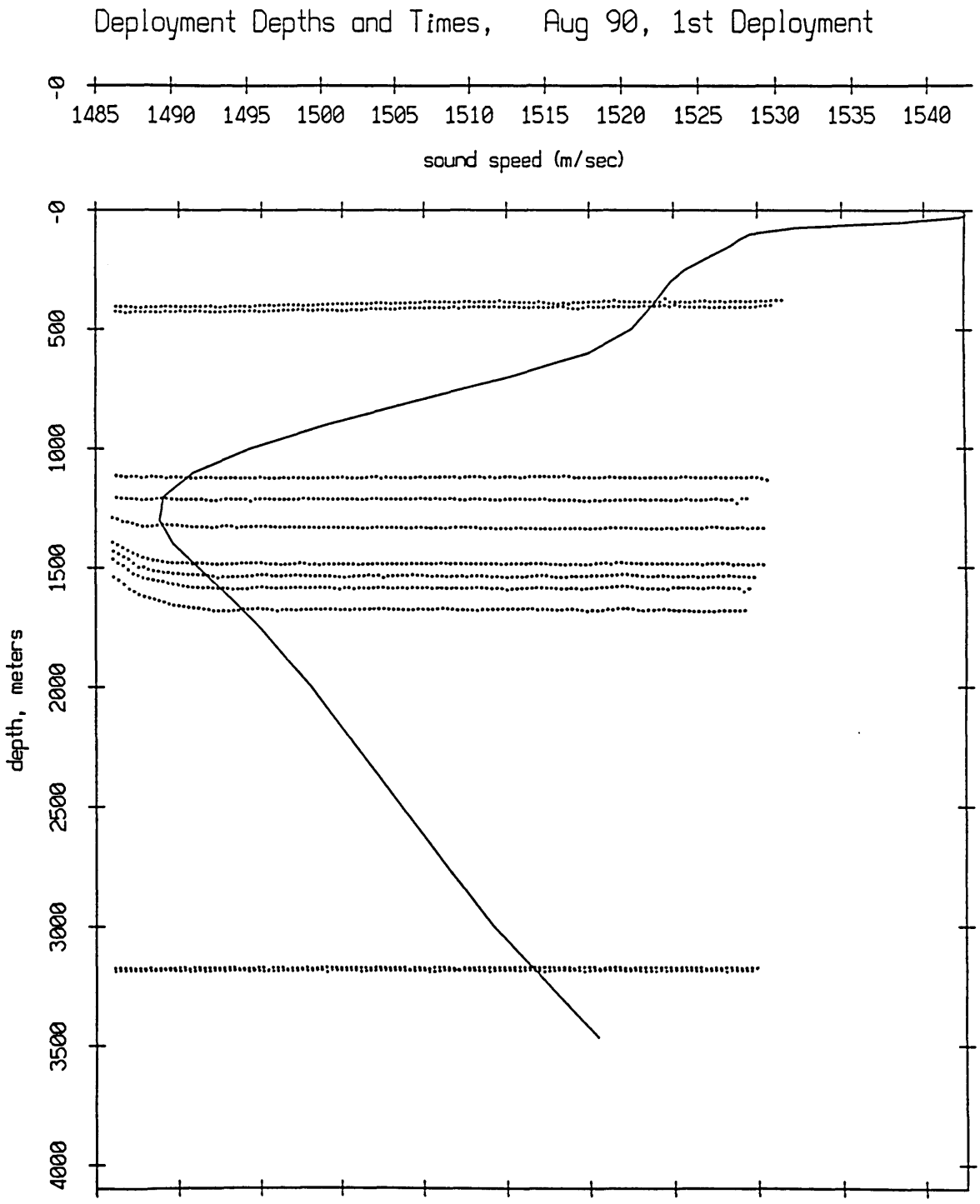

Figure 4.4: Sound speed profile of a deep ocean from Ref. [71].

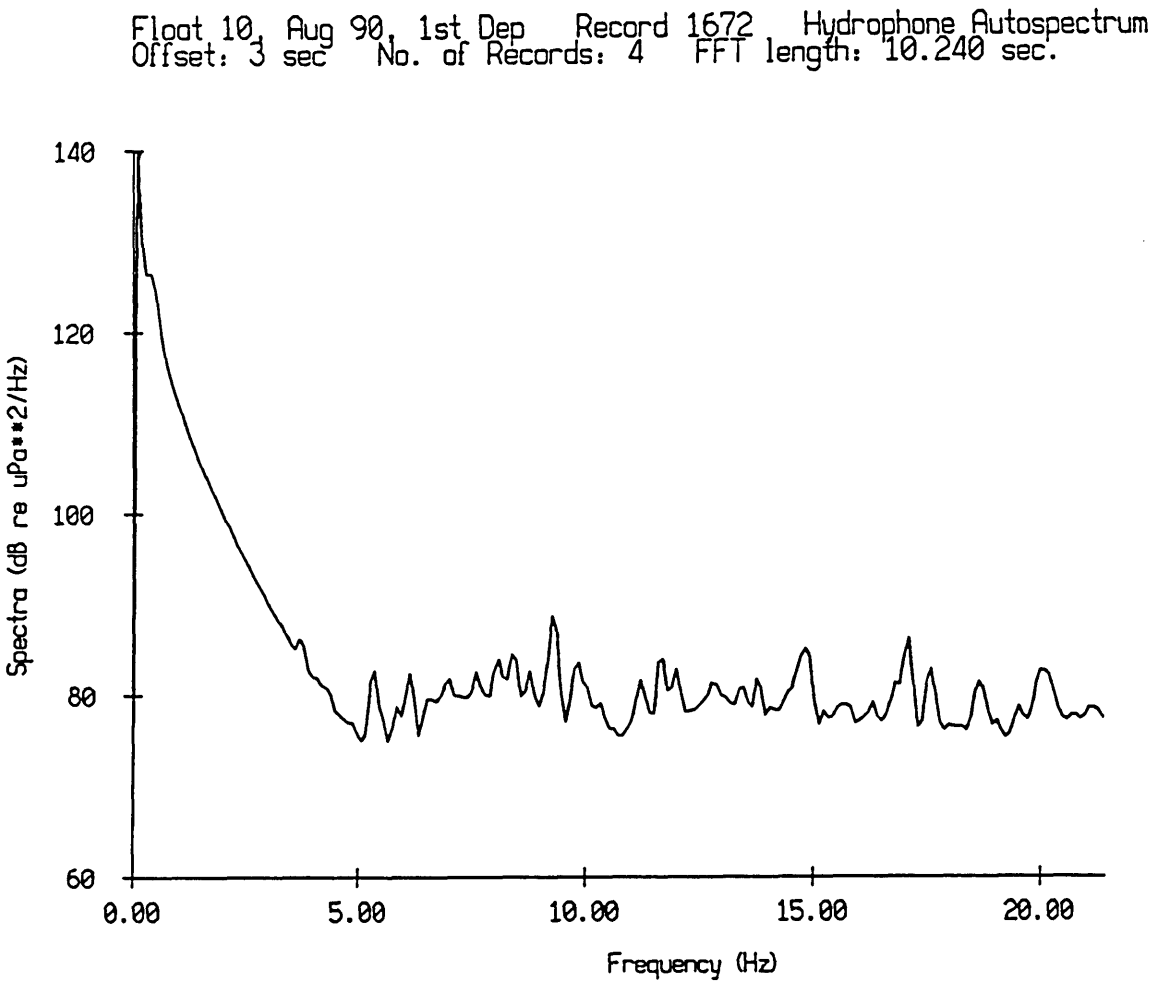

Figure 4.5: Frequency spectra: experimental data from Ref. [71].

low frequency rise of the spectral levels and provide an explanation for the existence of the transition frequency.

4.4.2 Model Prediction

About the Environment

The formulations described in Sections 4.2-4.3 are now implemented numerically. To compare with the experimental data, the parameters in Eq. (4.1) are chosen such that the two-layer water column model provides the best fit to the sound speed profile measured. In view of Fig. 4.4 the sound speed is chosen to be $1540\,m/s$ at the sea surface, decreasing pseudo-linearly to $1490\,m/s$ at $1200\,m$ depth, and then increasing to $1520\,m/s$ at depth $3180\,m/s$. This choice of parameters, although not in complete agreement with the data in details particularly in the upper part of the water column, represents a sound speed variation consistent with the experimental profile as a whole. The effect of sound speed variation throughout the water column in a deep ocean waveguide, in particular, with an excess depth will be examined later in Sec. 5.5. For the time being we choose the values to best fit the data in order to demonstrate the performance of the theory.

The sea bottom is modeled as a sediment layer overlying a semi-infinite subbottom. At the experimental site, the observations have shown that the sea bed is generally smooth, but the underlying sea floor is rough. This may be due to the fact that the topography of the Earth crust is formed by large-scale tectonic motions, forcing the continental plates to collide and to form corrugated rough surfaces. However, the sea bed is formed by long-term sedimentation of fine grain substances, and therefore is relatively flat. Thus in modeling the interfaces, we shall treat the

interface between the sea floor subbottom and the sediment layer as rough surface, while the sea water to sediment interface as flat.

The sediment density $1800\,kg/m^3$, and compressional speed $1800\,m/s$ are taken to be constant, whereas the shear speed and the sediment thickness will be varied. The attenuation is assumed to be $0.7\,dB/\lambda$ and $1.5\,dB/\lambda$ for compressional and shear, respectively. The subbottom is assumed to be basalt with compressional speed $5250\,m/s$, and shear $2500\,m/s$, with the corresponding attenuation $0.2\,dB/\lambda$ and $0.5\,dB/\lambda$. The density is $2600\,kg/m^3$. The interface between the sediment layer and the subbottom is assumed to be rough, with an isotropic Goff-Jordan power spectrum, and the RMS roughness is $10\,m$. The model environment with the chosen values of parameters is shown in Fig. 4.6.

Wavenumber Spectra

To reveal the significance of the rough sea floor scattering, we again first examine the wavenumber spectra for this simulated deep ocean environment. Figures 4.7, 4.8, and 4.9 show the wavenumber spectra (solid curves for scattered and dashed curves for mean fields) for 3, 4, and $5\,Hz$, respectively, for a receiver on the sea bed. The variation of the spectra with respect to various frequencies will be discussed in a later section, in conjunction with interpretation of the experimental data. Attention is given now to the comparisons of the mean and the scattered fields.

All the above three figures clearly indicate that while the interface waves (the right most peaks in the solid curves) are of no significance in the mean fields, they are the most outstanding feature in the scattered wavenumber spectra, consistent with the deep water case in a canonical waveguide discussed in the previous chapter. Based upon the discussion in Sec. 3.6, the interface wave modes will dominate the ambient noise near the rough sea floor. The dominance of the interface waves near

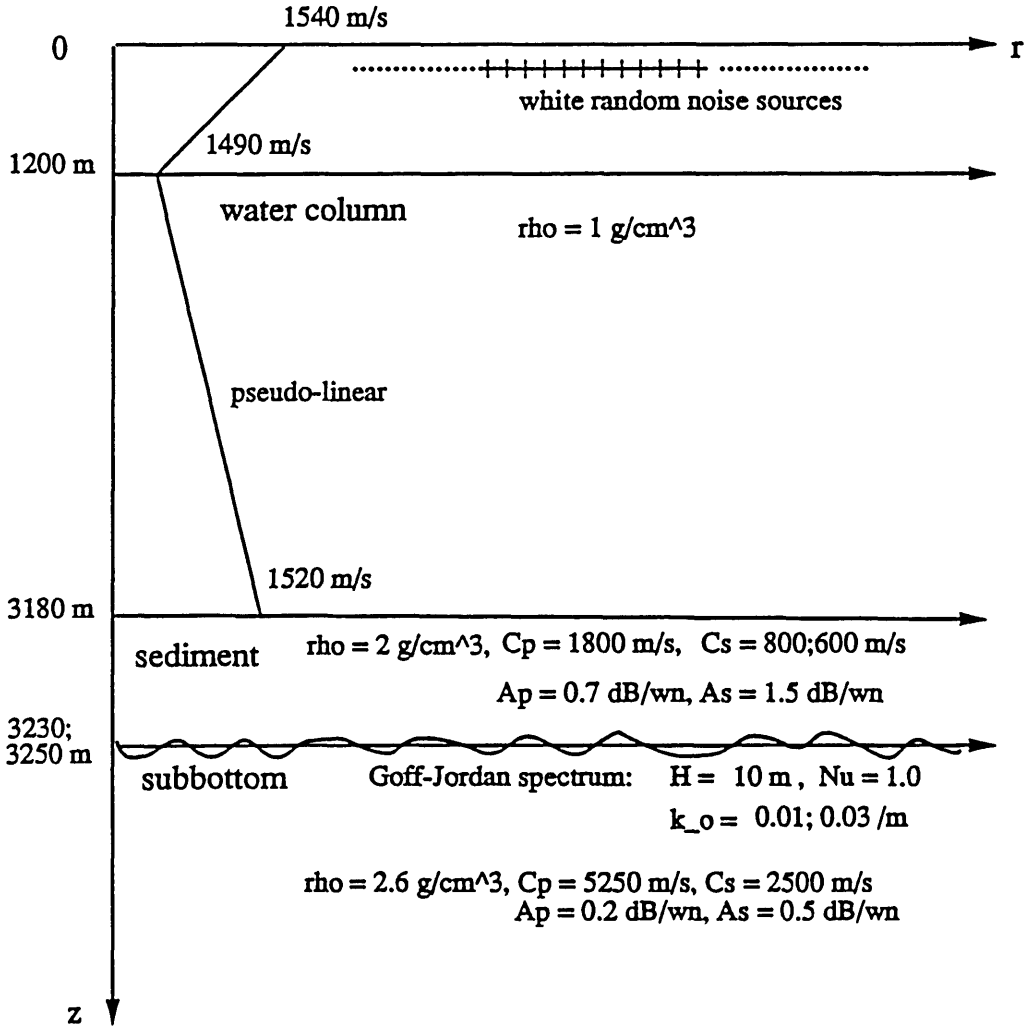

Figure 4.6: Model environment for a deep ocean waveguide.

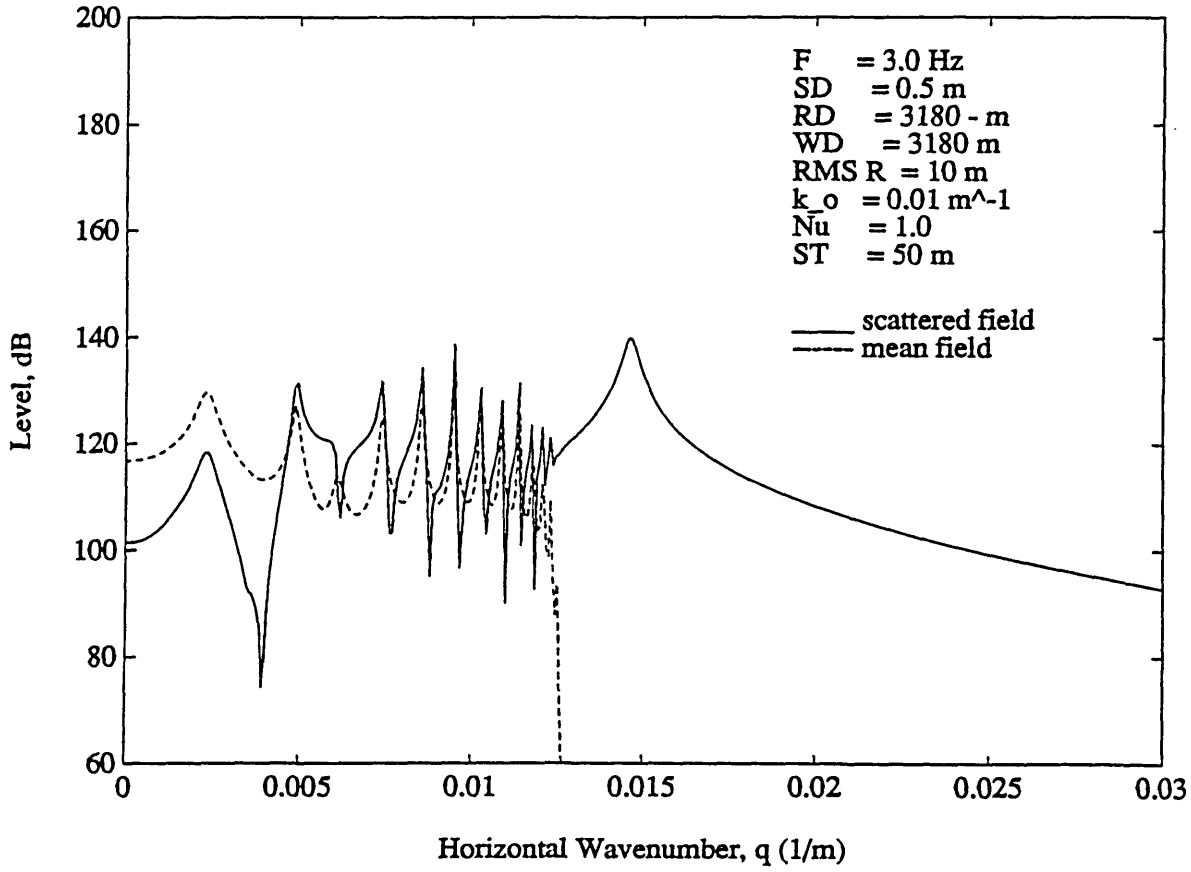

Figure 4.7: Pressure wavenumber spectra for frequency 3 Hz.

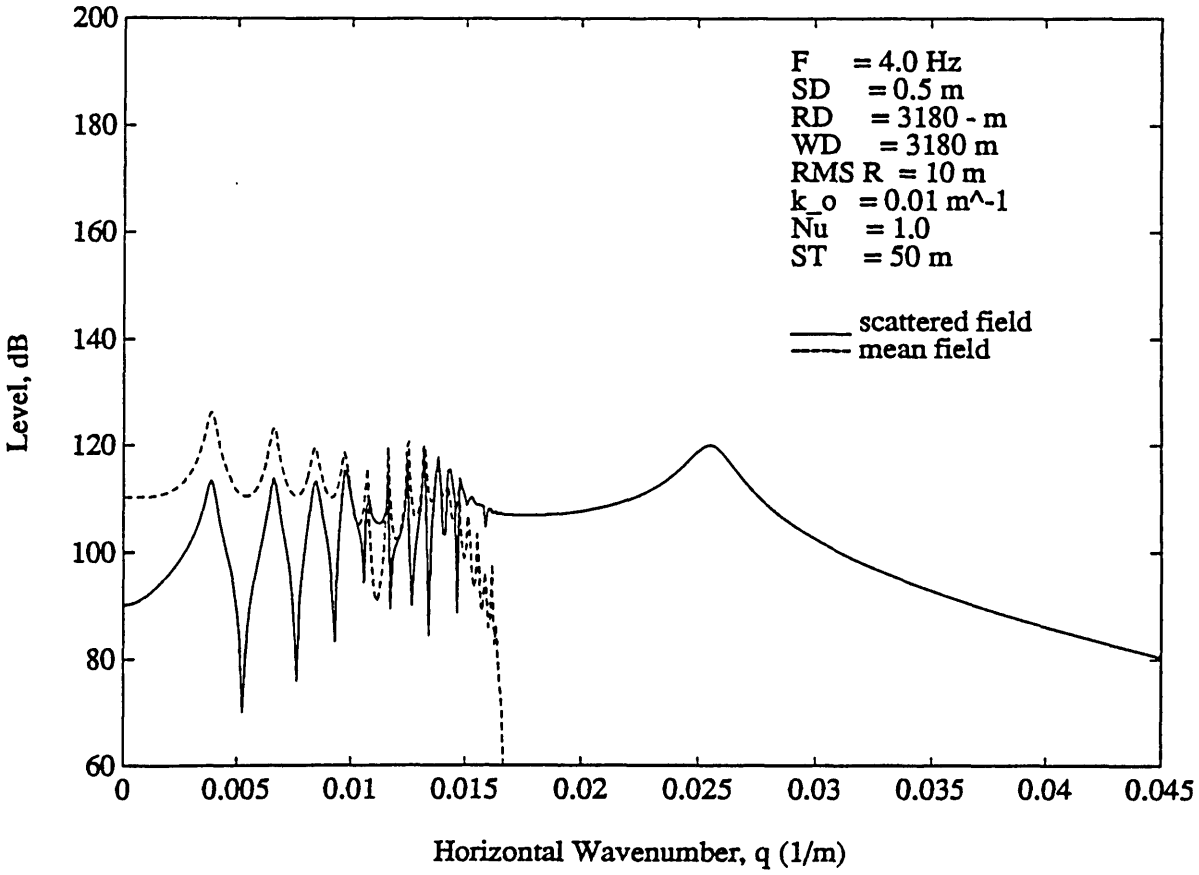

Figure 4.8: Pressure wavenumber spectra for frequency 4 Hz.

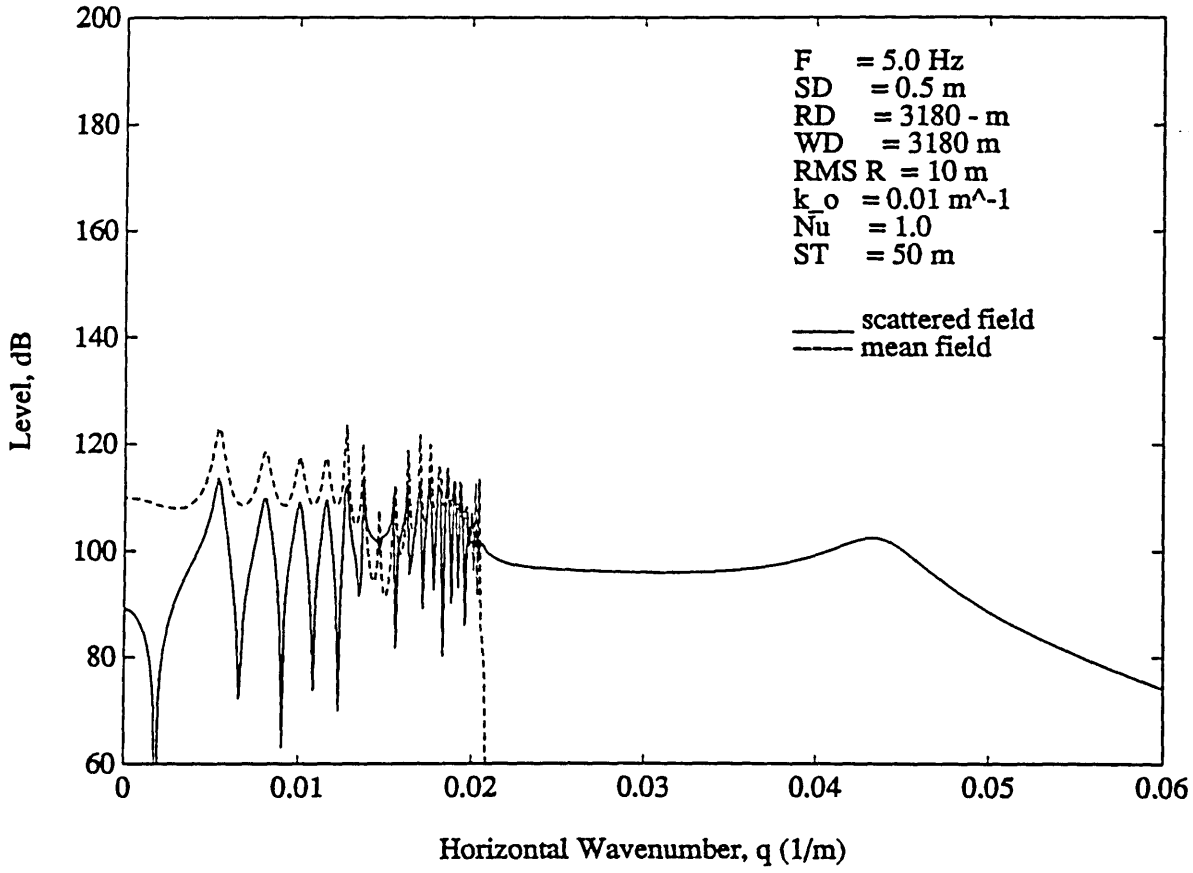

Figure 4.9: Pressure wavenumber spectra for frequency 5 Hz.

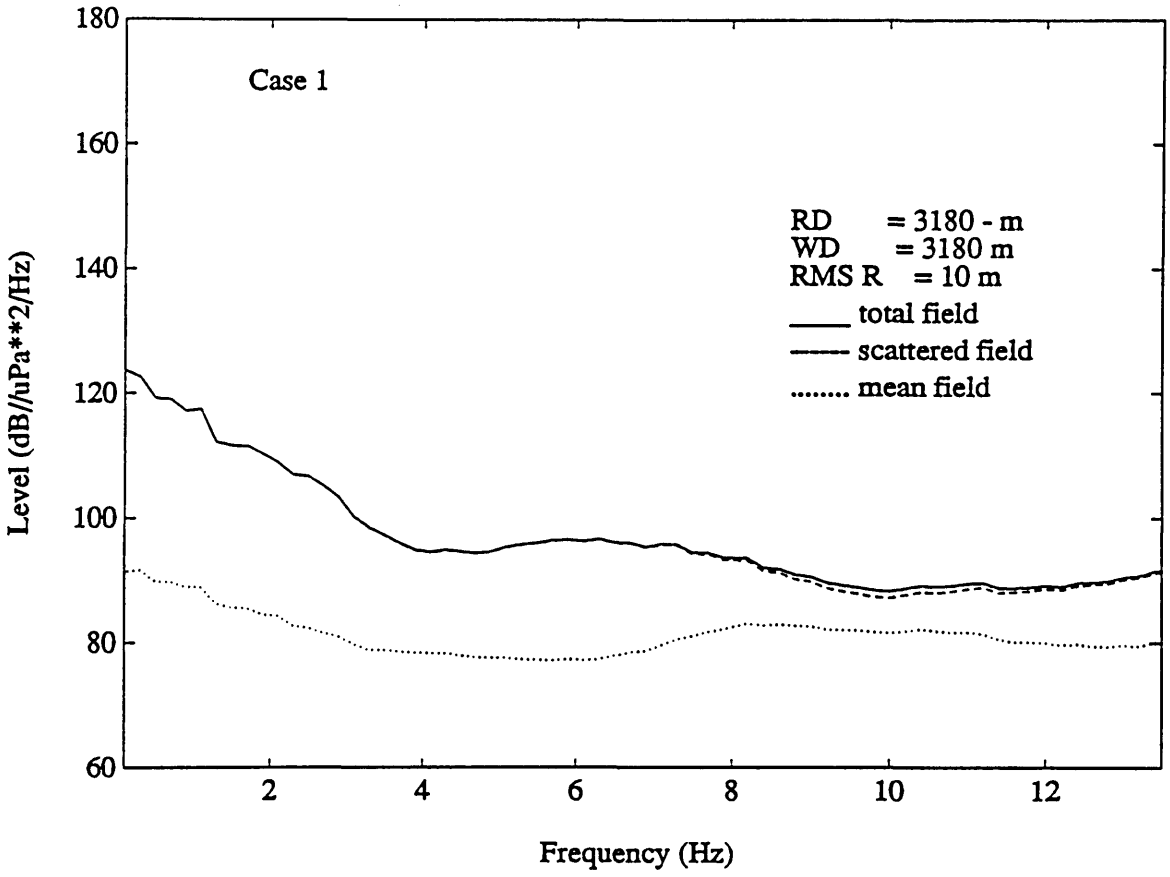

Figure 4.10: Frequency spectra: Case 1

the bottom is expected to play an important role on modifying the characteristics of deep-ocean frequency spectra to be presented in the following.

Numerical Prediction of Frequency Spectra

Figure 4.10 (Case 1) shows the frequency spectrum for sediment thickness $50\,m$, shear speed $600\,m/s$, and the characteristic wavenumber $k_0 = 0.01\,m^{-1}$ for the roughness. The noise source level $\langle S_\omega^2 \rangle$ is chosen to yield $70\,dB$ ($Q = 70$) in an infinitely deep ocean. The dotted curve shows the frequency spectrum of the mean noise field,

the dashed curve is the scattered noise field, and the solid curve is the total noise field. It is seen that the overall noise near the sea bed is completely dominated by the scattered noise field. This is particularly evident at the low frequency end, where an average of about $20\,dB$ difference between the mean noise field and the scattered noise field indicates that, according to the model, the spectral variation is a roughness effect. Qualitatively, the spectrum shown in Fig. 4.10 is consistent with the experimental observations [3, 71]. The transition frequency is approximately $4\,Hz$ in this case.

Figure 4.11 presents the frequency spectrum for two different shear velocities, with the sediment thickness fixed at $50\,m$. The solid curve corresponds to a shear speed $600\,m/s$, and the dashed curve is for shear speed $800\,m/s$ (Case 2). It shows that an increase of shear velocity results in an increase of overall noise level. Moreover, the transition, although less pronounced, takes place at higher frequency, approximately $5\,Hz$, for shear velocity $800\,m/s$ than for $600\,m/s$.

The effect of a change in sediment thickness is shown in Fig. 4.12, where the frequency spectrum is given for two different sediment thicknesses, $50\,m$ (solid curve), and $70\,m$ (dashed curve, Case 3), with a constant shear speed, $600\,m/s$. The results show that the increase of the sediment thickness decreases the transition frequency to about $3\,Hz$. Moreover, a second transition frequency appears at about $6\,Hz$.

Figure 4.13 demonstrates the effect of the characteristic wavenumber of the roughness on the frequency spectrum. The solid curve is for $k_0 = 0.01\,m^{-1}$, while the dashed curve is for $k_0 = 0.03\,m^{-1}$ (Case 4). It is illustrated that increasing the value of k_0, decreases the total noise level; however, the transition frequency is unaffected. The effect of characteristic wavenumber, or equivalently roughness correlation length, on scattered field intensity will be investigated in Sec. 5.4.

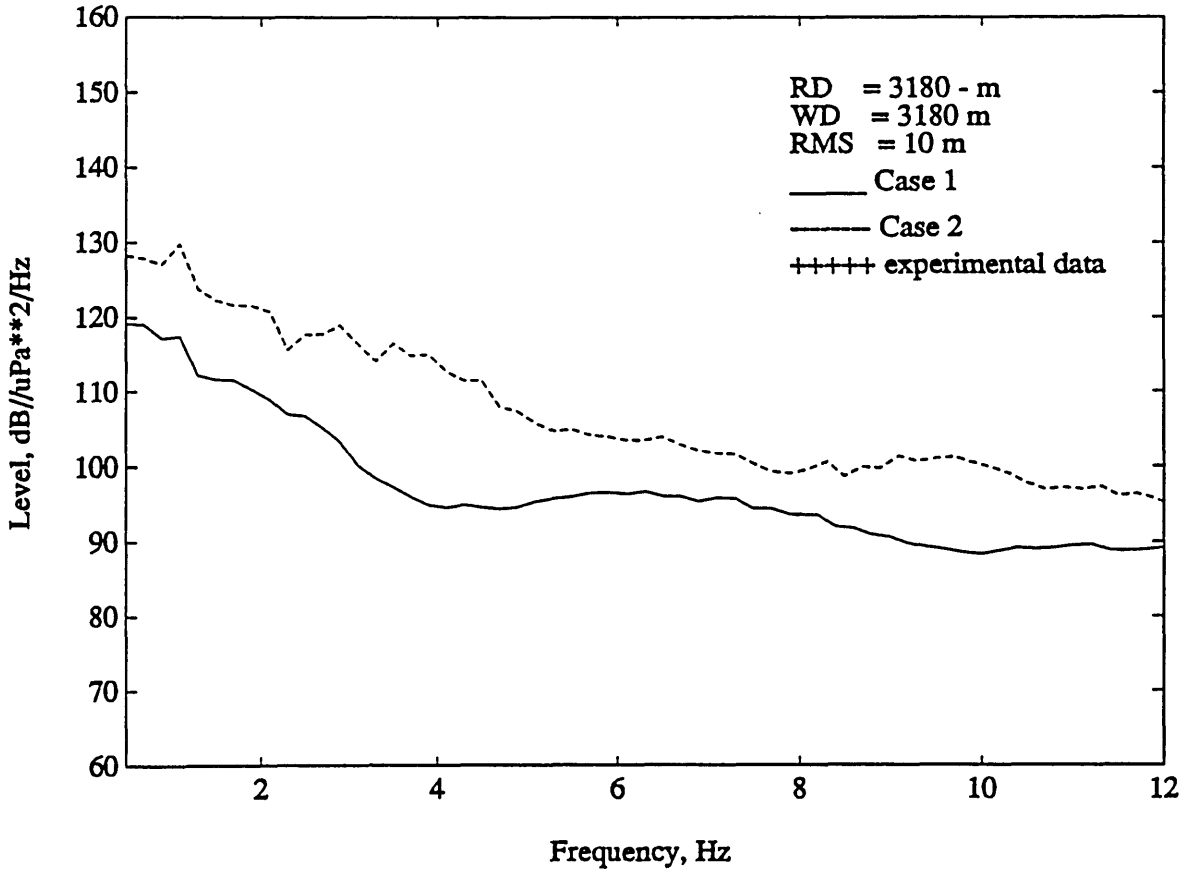

Figure 4.11: Frequency Spectra: Case 2

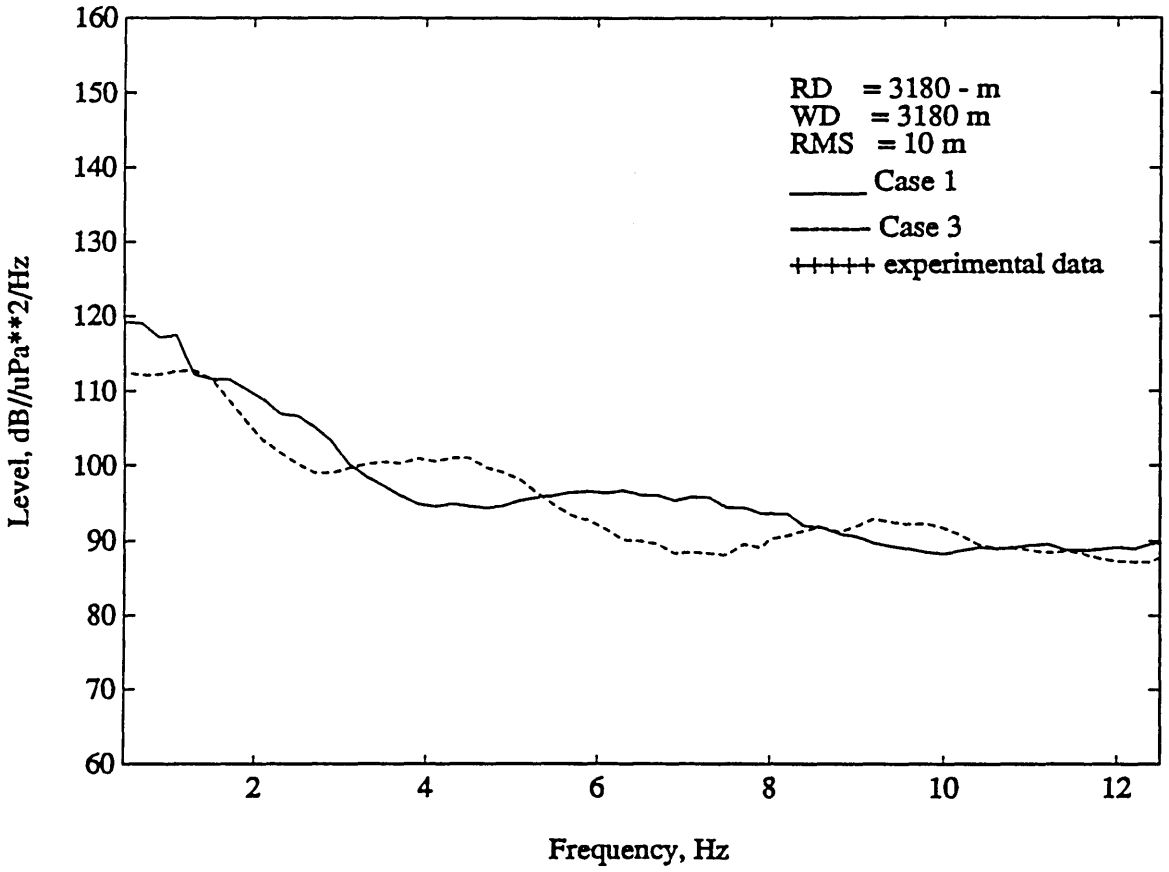

Figure 4.12: Frequency spectra: Case 3

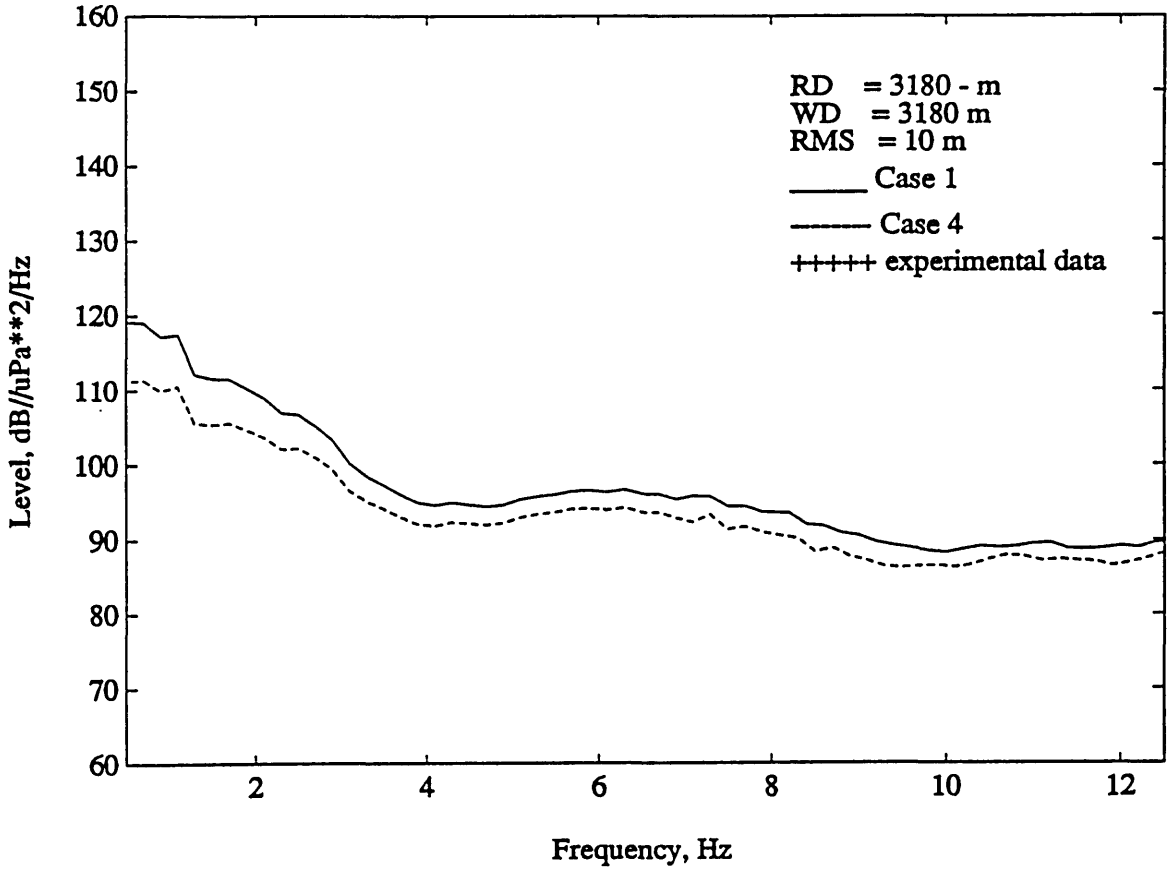

Figure 4.13: Frequency spectra: Case 4

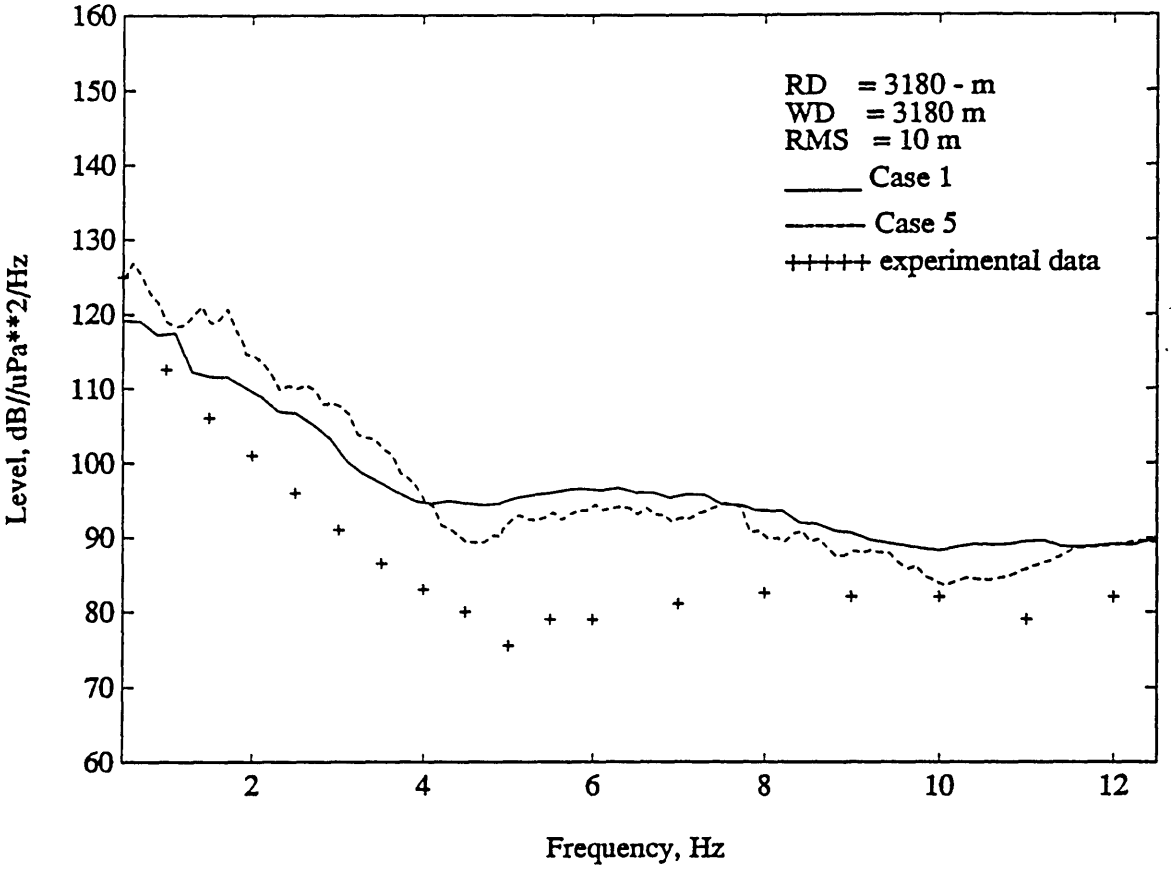

Figure 4.14: Frequency spectra: Case 1, Case 5, and experimental data

Figure 4.14 presents two cases which closely resemble the characteristics of the experimental data [71]. Case 5 corresponds to sediment thickness $70\,m$, shear speed $800\,m/s$, and subbottom compressional speed $5000\,m/s$. In this case, the Gaussian spectrum with correlation length $150\,m$ is used. These results suggest that the present theory can, in fact, closely fit the experimental data both in terms of the levels and the transition frequency in view of its flexibilities in adapting a wide range of values for the various parameters. It should be stressed here that it is by no means appropriate to do so, in that the use of the white noise spectra for the surface sources may not be realistic. However the present results are generated by the model with

realistic parameters for the environment, and the resemblance between the present noise scattering model prediction and the experimental data strongly suggests the importance of the scattering processes in shaping the ambient noise frequency spectrum. It is noted that there still exists a fair amount of discrepancies in both the levels and the roll-off rate unaccounted for by the present theory, which may be attributed to a colored source spectrum. But, the inference of the source spectrum has not been the primary goal of the present analysis. Instead it has been the intent to demonstrate the important role of rough interface scattering together with the waveguide propagation mechanisms in modifying the infrasonic noise spectrum.

4.5 Discussion

It is clear from the results shown in Figs. 4.11 to 4.13 that the qualitative behavior of the infrasonic noise spectrum is dependent on the bottom properties, but not the details of the roughness characteristics, which only have a quantitative effect on the spectral levels. On the other hand, Fig. 4.10 clearly demonstrates that the scattering mechanism is essential for the increase in level to occur towards the low frequency end below the transition frequency. The results therefore suggest that the transition frequency and the associated spectral variations are predominantly due to propagation effects, with the rough interface scattering merely being a necessary catalyst for these spectral features to become pronounced.

As described in Chapter 3, the fundamental difference between the mean and scattered components is the strong excitation of the evanescent seismic components in the latter. Since the scattered field dominates the infrasonic noise field, this in turn suggests that the spectral shape of the sea bed noise field is controlled by the

propagation characteristics of the seismic interface waves.

As discussed in Ref. [72] the dispersion of the fundamental seismic interface mode is characterized by the presence of a transition frequency below which the interface wave propagates with phase and group velocities similar to those of the fundamental Scholte mode for an interface separating a water halfspace and a halfspace of the subbottom material. The physical explanation for this is that the sediment layer becomes thin relative to the wavelengths involved, and therefore becomes insignificant. At high frequencies the evanescent "tail" of the interface wave becomes short compared to the thickness of the sediment, making the fundamental mode similar to the Scholte mode for the water-sediment interface, with phase and group velocities becoming independent of the presence of the subbottom. The transition frequency can be shown to be associated with the *thickness-shear frequency* for the sediment layer [72], *i.e.* the lowest eigenfrequency for horizontal shear vibrations [73]. If the lower sediment interface is assumed fixed, then the thickness-shear frequency is given by the relation [73]

$$f_t = \frac{c_S}{4d_S}\,, \tag{4.15}$$

where c_S is the sediment shear speed, and d_S is the thickness. For the three different sediment layers used in this study, the thickness-shear frequencies are: Case 1: $3\,Hz$, Case 2: $4\,Hz$, and Case 3: $2.14\,Hz$. The corresponding phase velocity dispersion curves are shown in Fig. 4.15, as computed by SAFARI [38]. Although the definition of the transition frequency is rather arbitrary, the dispersion relations for the various sediments are consistent with Eq. (4.15).

For the noise problem, we defined the transition frequency to be associated with the initiation of the low frequency increase in spectral level. It is easily verified that this frequency is also consistent with Eq. (4.15) in the sense that it is proportional

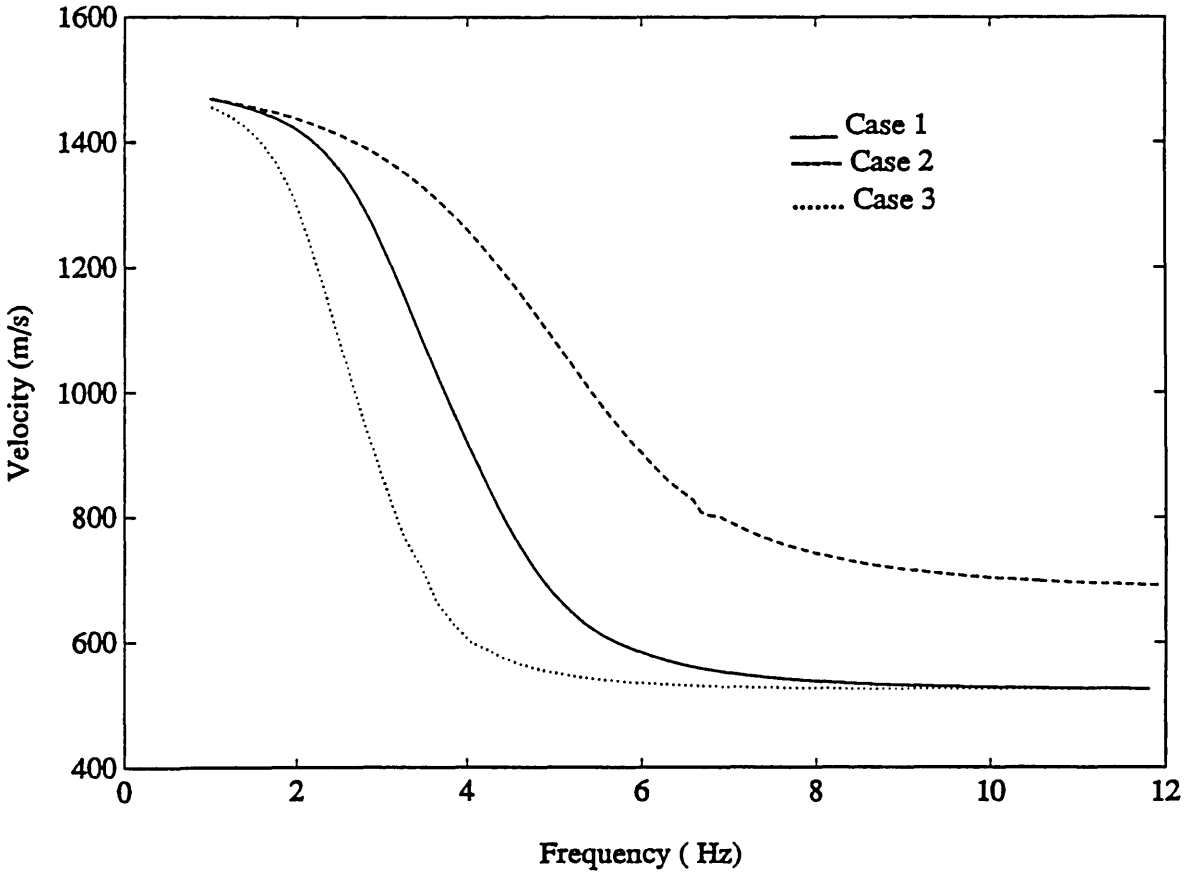

Figure 4.15: Dispersion curves.

to the shear speed and inversely proportional to the sediment thickness, *i.e.*

$$f_0 = \alpha \frac{c_S}{d_S} , \tag{4.16}$$

where the constant α for the present environmental models is approximately 1/3. Although the subbottom properties have some effect on the transition frequency, we have found that it is predominantly determined by the sediment properties through Eq. (4.16).

In summary the results indicate that the transition frequency observed in deep ocean noise experiments is controlled by the propagation characteristics of the fundamental interface mode. The less pronounced second transition frequency which can be identified at approximately $10\,Hz$ in Fig. 4.14 in both the experimental and simulated results can similarly be associated with the dispersion characteristics of a higher order seismic mode.

A physical explanation for the sharp increase in noise level below the transition frequency can be provided by analyzing the wavenumber spectra of the noise field. Fig. 4.16 shows the horizontal slowness spectrum of the scattered noise field near the bottom at frequencies 3, 4 and 5 Hz for Case 1. At 5 Hz, the slowness of the interface mode is $1.4\,s/km$, with a field that is highly evanescent in the water with slowness $0.67\,s/km$. It is clear from Eq. (2.41) that the excitation of the scattered components by a mean field component depends on the amplitude of the roughness spectrum at the difference wavenumber, $P_b(\mathbf{q} - \mathbf{k})$. Here, the mean field only has components with slowness less than $0.67\,s/km$, and the excitation of the high-slowness interface wave is therefore relatively small.

When the frequency is lowered below the transition frequency, the slowness of the interface mode rapidly approaches the water slowness as observed in Fig. 4.15, resulting in an increased excitation by scattering of wave components in the mean

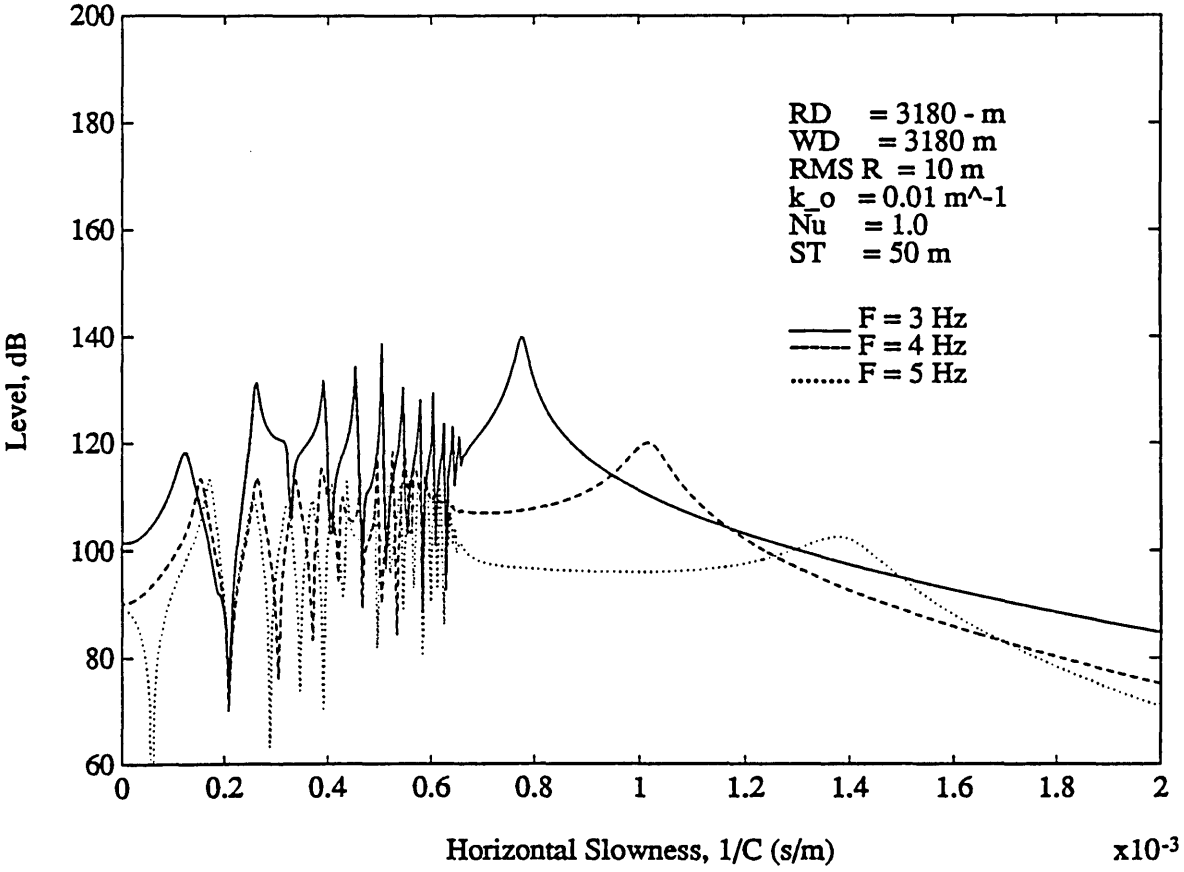

Figure 4.16: Slowness spectra (scattered field) for three different frequencies.

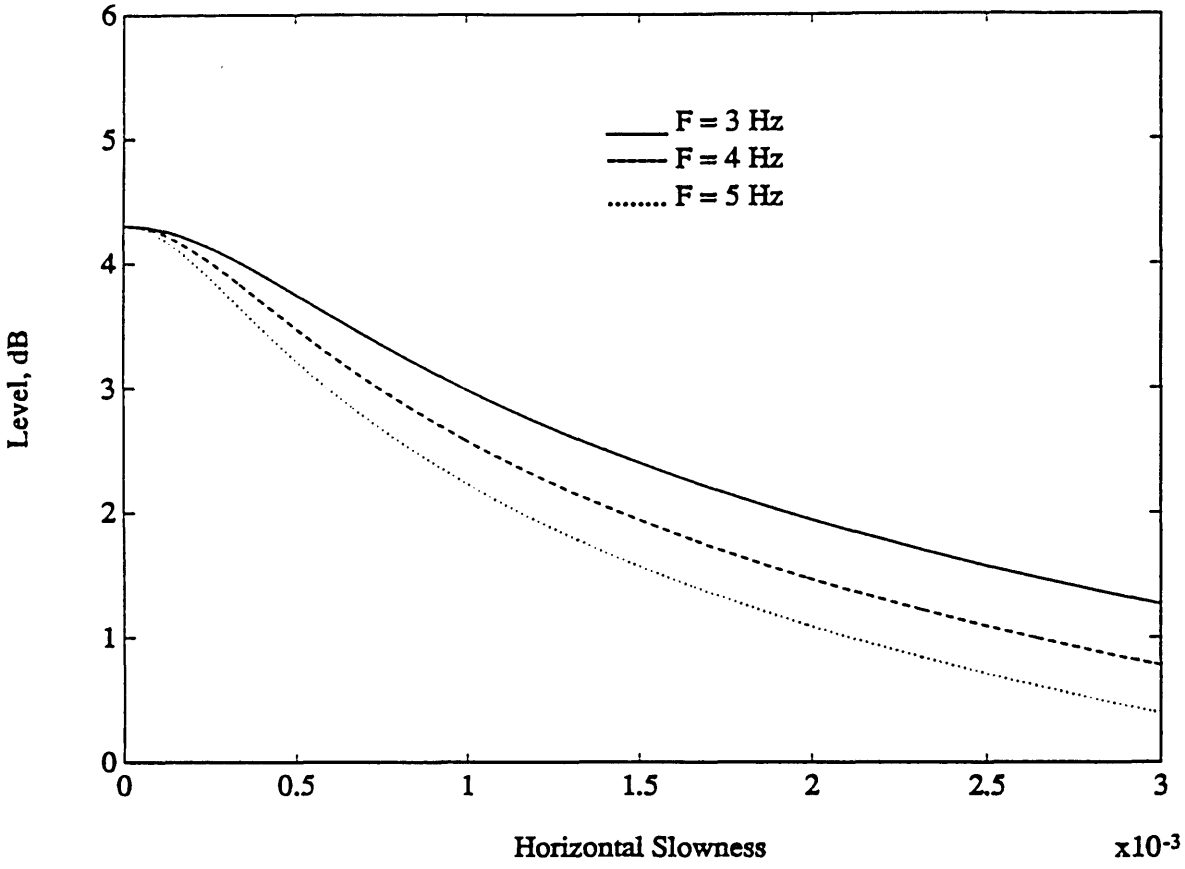

Figure 4.17: Power spectra as function of horizontal slowness.

field. In addition, the roughness spectrum will widen in terms of slowness when the frequency is lowered as shown in Fig. 4.17. The combination of these two effects yields a rapid increase in the interface wave component when the frequency is lowered, as is evident in the slowness spectra in Fig. 4.16.

4.6 Summary

In this chapter we have analyzed the bottom noise field in a deep ocean waveguide. We have obtained the frequency spectra of the surface-generated ambient noise. The formulation results in several controlling parameters including the sediment properties and thickness. By choosing these parameters appropriately the model may account for both the noise levels and the transition characteristics of the frequency spectra observed in the experiments.

The fact that the present theory can qualitatively account for the experimental data strongly suggests that rough interface scattering in combination with the seismic propagation effects have a strong coloring effect on the noise in the deep ocean. This in turn suggests that this scattering effect needs to be taken into account in using the measured seismo-acoustic data to infer the source spectrum, as has been discussed in Ref. [5]. Quantitatively, as we have mentioned that invoking the Born approximation may result in an overestimate of both the mean and the scattered noise fields. However, we don't expect to cause a dramatic difference for the present case, because the roughness we have used is so small ($10\,m$ RMS roughness relative to an average of $150\,m$ wavelength), and is well within the perturbation limit. Nonetheless, the use of the present model for prediction of the noise intensity, inference of source level, inversion of sediment properties, or rough interface statistics, *etc.*, still awaits further quantitative assessment of the assumptions in the theory as well as in the environment.

In the next chapter the spatial properties of the noise fields will be investigated. We shall extend our analysis to a full three-dimensional scattering problem so that the directionality of the noise field may be accounted for.

Chapter 5

Spatial Correlation

— in which the spatial properties of the noise fields are analyzed.

5.1 Introduction

An important characteristic of the scattered noise field is the spatial correlation of the sound field; in some cases it is used to solve the inverse problem. For example, by measuring the scattered sound field with sufficiently wide interval of sound frequencies or angles, we can estimate the spectrum of a rough surface. This occurs because the scattered sound field bears direct/indirect information about its generation constituents, particularly information on the roughness characteristics such as the correlation length, RMS roughness, anisotropy, *etc.* Moreover, the spatial correlation of the noise field is particularly important for the performance of an array, because the detection or estimation of a desired signal embedded in a noise field is

based upon the array gain, which is defined as the ratio of the signal to noise of the array output to the signal to noise of the output of a single element. The gain of the array only becomes substantial if the sensor separations are greater than the correlation length of the noise. Thus understanding the spatial structures of the scattered sound field is crucial to the design of arrays.

In this chapter we study the influence of rough interface scattering on spatial correlation of the ambient noise. In order to achieve our objectives, we still assume that the surface noise sources are completely random, thus the spatial correlation of the noise field is totally controlled by the waveguide properties and the roughness of the sea bed. We shall first demonstrate the interplay between the spatial correlation of the noise field and the correlation length of the roughness using an isotropic roughness spectrum corresponding to an isotropic random field. This is best illustrated by the horizontal correlation using isotropic Gaussian roughness spectra in a canonical waveguide environment.

We then continue to investigate the vertical correlation of the noise field. A comparison is made on the scattered noise fields for different roughness spectra, and the effect of sound speed variation throughout the water column in a waveguide is also examined. Finally, we generalize our study to investigate three-dimensional scattering resulting from an anisotropic random field. With this, we accomplish our final objective on studying directivity of the noise field due to anisotropic rough sea bed.

5.2 Horizontal Correlation

We begin with the investigation of the horizontal correlation of an isotropic noise field. The cross-spectral correlation function is given by Eq. (3.5). The normalized correlation is obtained by normalizing Eq. (3.5) such that it yields a value of unity for $\bar{r} = 0$, *i.e.*, $Re\{C_\omega^t(\bar{r}, z_1, z_2)\} / Re\{C_\omega^t(\mathbf{0}, z_1, z_2)\}$. To keep our analysis simple, we illustrate the relation between the roughness statistics and the noise correlation by evaluating Eq. (3.5) for a Gaussian roughness spectrum in the canonical waveguide environment. Here, we choose two representative correlation lengths ℓ (labelled as CL in the figures), $10\,m$ and $75\,m$, for the Gaussian spectrum function. It should be noted that the random noise sources have zero correlation length. Also, one should note that the product of the correlation length of the roughness and the wavenumber, *i.e.*, $\kappa\ell$, is the controlling parameter for the correlation of the scattered field [74].

Before we study correlation of the noise fields, we first examine the effect of the roughness correlation length on the noise intensities. This will be useful in helping us understand the effect of the scattered-field coherence on the correlation of the total noise field.

Figure 5.1 demonstrates the noise intensities for two different correlation lengths for the Gaussian spectrum. This figure shows that the mean field intensity (dotted curve) in average is about $15\,dB$ larger than the scattered fields (solid and dashed curves), except in a region close to the bottom. It also demonstrates that the scattered noise intensities near the bottom decrease about $10\,dB$ as correlation length increases from $10\,m$ to $75\,m$. A physical interpretation for the effect of different roughness correlation lengths on scattered noise intensity will be provided in Sec. 5.4. Here, we note that, for the case of $\ell = 10\,m$, the scattered field is as important as the mean field near the bottom; on the other hand, the scattered field is unimportant

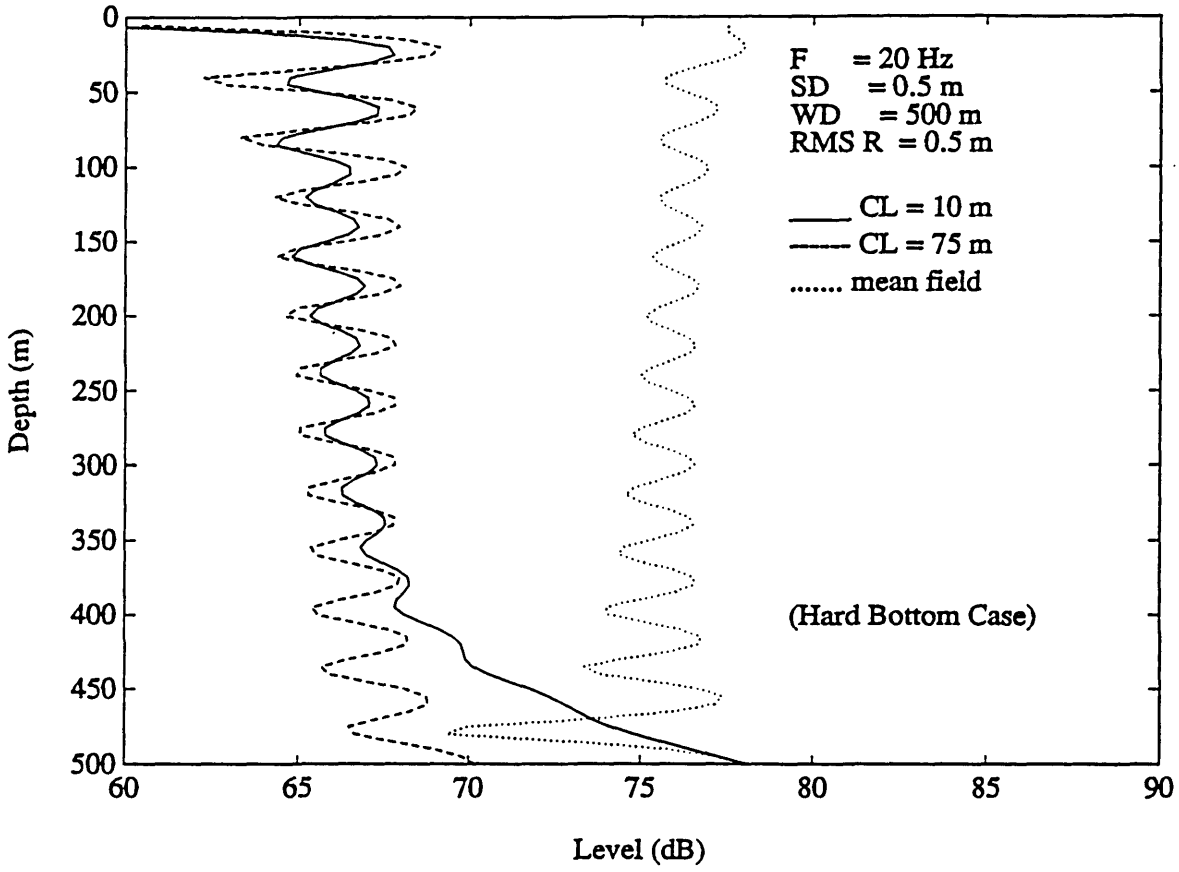

Figure 5.1: Noise intensities for two different correlation lengths of the Gaussian spectrum.

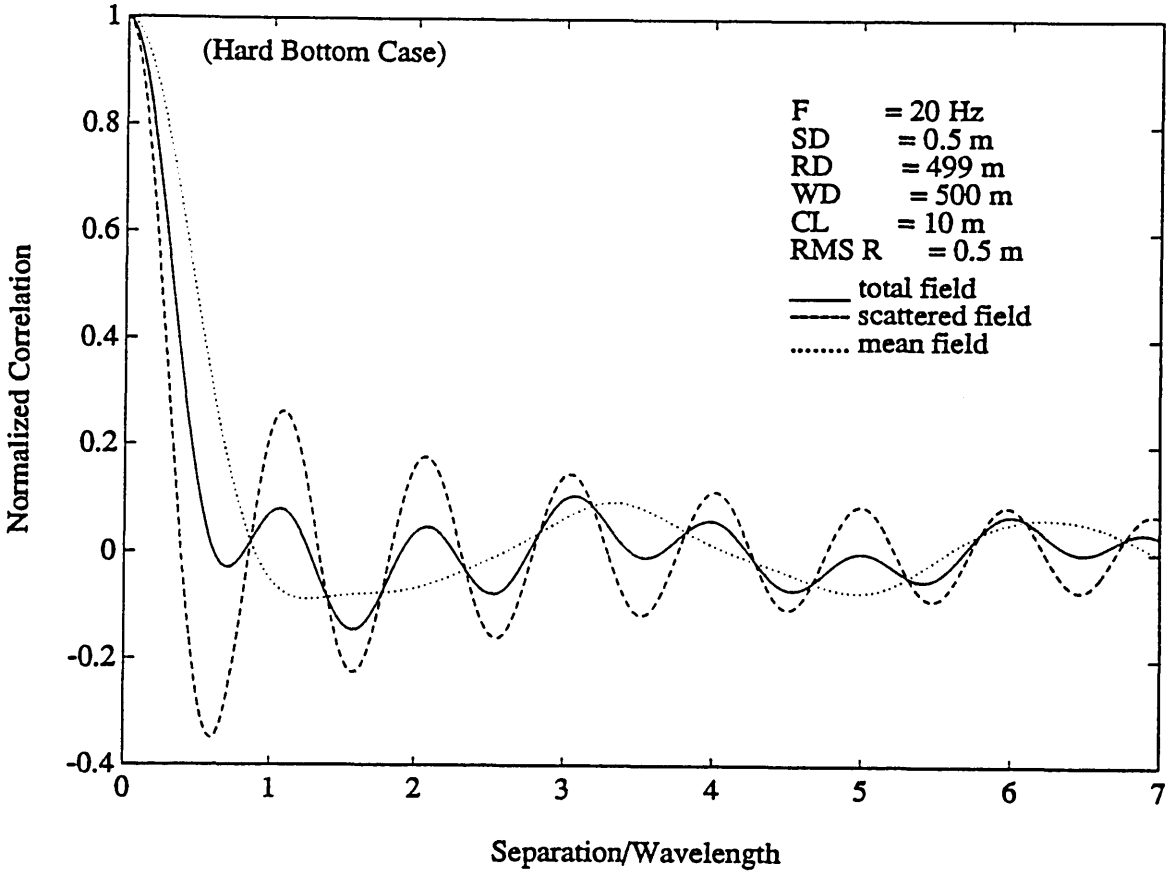

Figure 5.2: Horizontal correlation for $\ell = 10\,m$.

for $\ell = 75\,m$.

The horizontal correlation for $\ell = 10\,m$ is presented in Fig. 5.2. In this case the $\kappa\ell$ is small (about 0.835), corresponding to small-scale roughness. The correlation of the mean noise field (dotted curve) represents the horizontal correlation function for the plane sea bed, and is therefore totally controlled by the waveguide properties. In this case it has been shown that for fluid waveguide the correlation length is of the order of the acoustic wavelength [74], which is consistent with the present results if one *liberally* defines the first zero as the correlation length. Also, one should expect that this correlation length represents the limit of the total noise field correlation

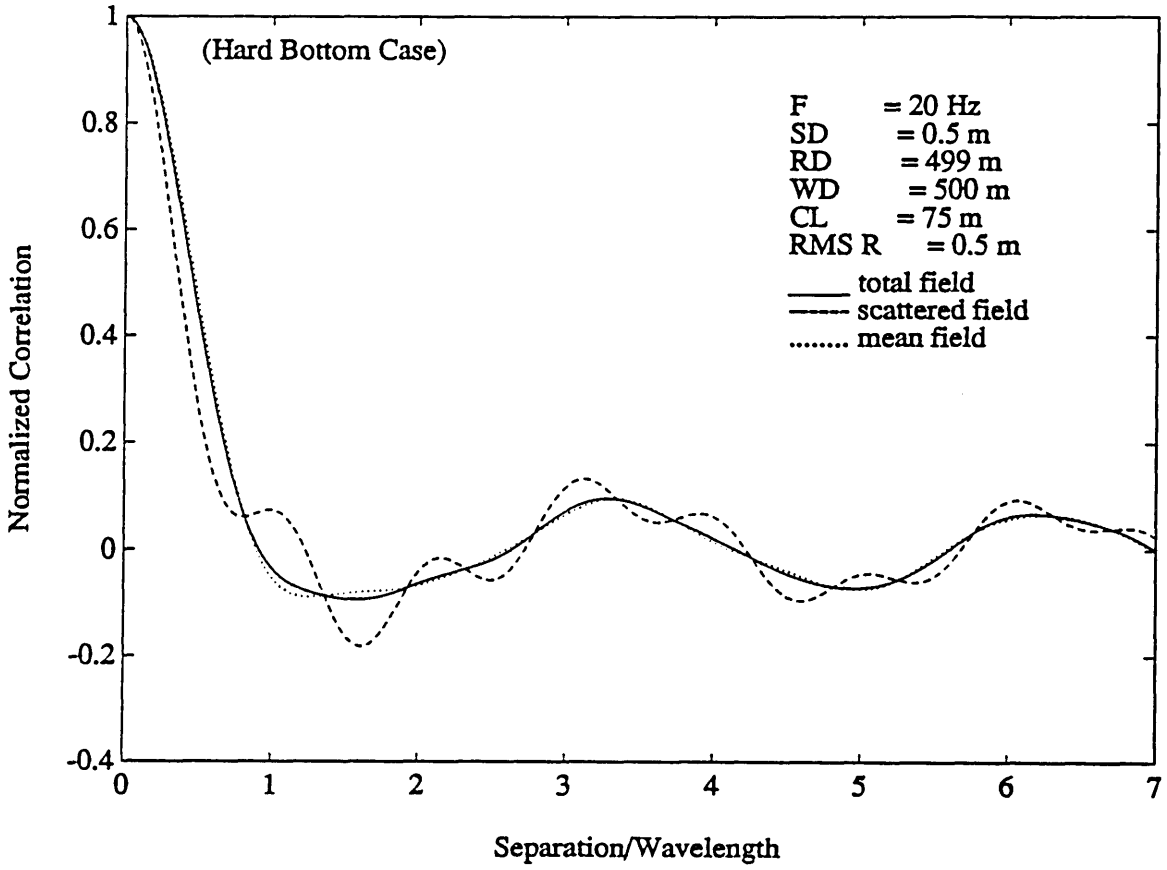

Figure 5.3: Horizontal correlation for $\ell = 75\,m$.

length as the correlation length of the roughness increases towards infinity.

The correlation length for the scattered noise field (dashed line) for this case is about half of that of the mean noise field as shown in Fig.5.1. For this roughness correlation length, there is a strong scattered field. As a result, the total noise correlation (solid line) is highly influenced by the scattering field. The overall effect is to reduce the correlation length of the noise field by about 1/3.

Figure 5.3 shows the correlation for the same parameters as Fig. 5.2, except for $\ell = 75\,m$. For this case the $\kappa\ell$ is large (about 6.26), representing a large-scale

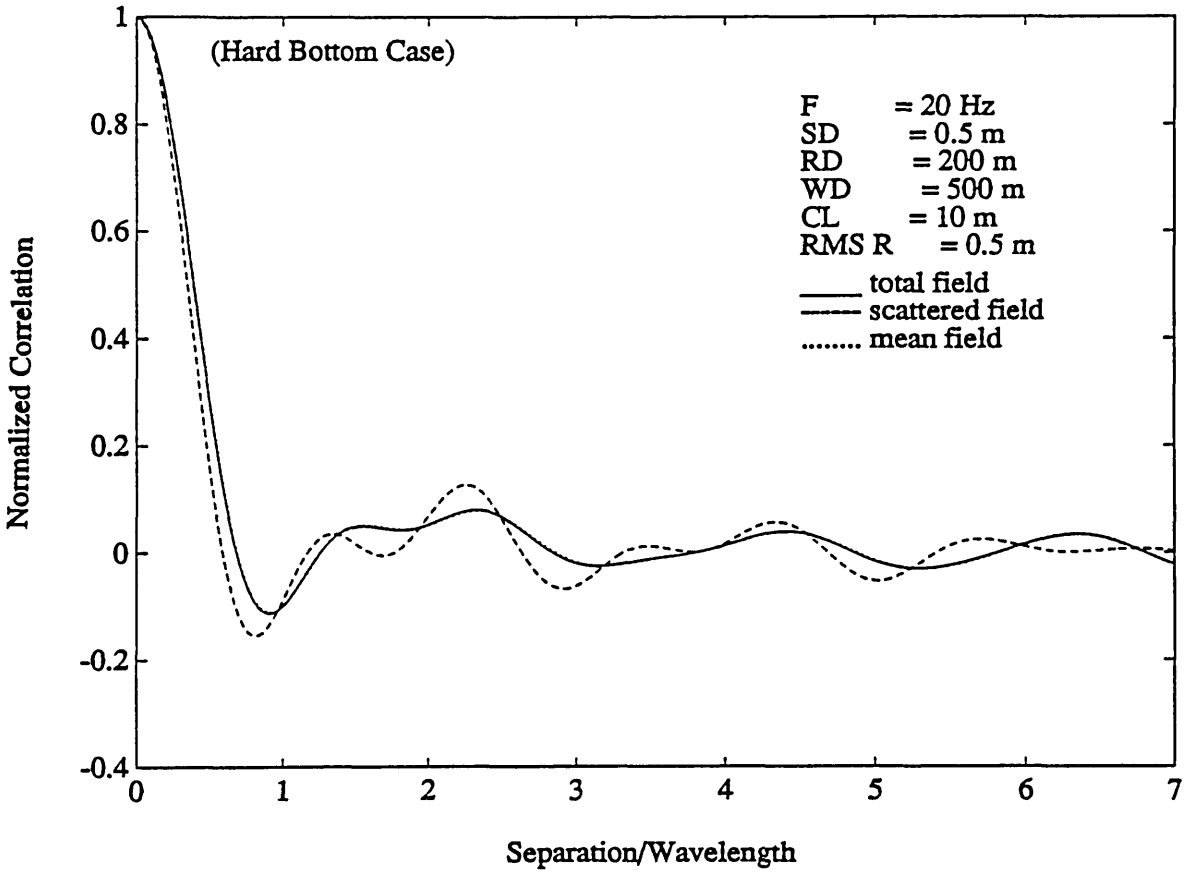

Figure 5.4: Horizontal correlation for $\ell = 10\,m$, $RD = 200\,m$.

roughness of the sea bed. Here, it is clear that the effect of the scattered field is insignificant as was shown in Fig. 5.1, and the correlation length of the total noise field is almost unaffected by the present of roughness.

The horizontal correlation for a receiver far away from the rough interface is shown in Fig. 5.4. In this case, the receiver depth is $300\,m$ away from the rough sea bed. The results show that the horizontal correlation of the scattered field (dashed curve) closely resembles that of mean field, and the solutions for the mean and total fields are the same, completely unaffected by the scattered field. This occurs due to the fact that the Scholte waves dominate the scattered field. Since Scholte waves

are confined in a thin region on the water-bottom interface, so, as the receiver is retreated from the sea bed, the total noise field is completely controlled by the mean noise field as expected.

It may be summarized from the above results shown in Fig. 5.1 - 5.4 that, in a region close to the bottom, small-scale roughness (small ℓ) scattering has profound effects on the horizontal correlation of the total noise field. It is easily understood by now that this is because of the excitation the Scholte waves generated by the secondary "sources", which significantly alters the spectral structure of the noise field. These results also agree with the observation [3], which indicates that the noise near the bottom consists predominantly of interface waves.

For a simulated deep ocean waveguide environment presented in Sec. 4.2, the horizontal correlation is shown in Fig. 5.5. It shows a similar feature as that for canonical waveguide. For a receiver near the sediment layer, the scattered noise field results in a reduction of the mean field correlation length by about one-half for the set of parameters chosen. It is noted that an isotropic Goff-Jordan roughness spectrum is used for this case. Variations of the dominance between the mean field and the scattered field may be expected by choosing different characteristic wavenumber k_0, RMS roughness, and receiver depth, as is discussed in the previous paragraphs for the canonical waveguide.

5.3 Vertical Correlation

The vertical correlation may be obtained by setting $\bar{\mathbf{r}} = 0$, and varying the vertical separations, $\bar{z} = z_1 - z_2$, in Eq. (3.5). It should be noted that the noise field is non-stationary in the vertical direction. That is, the vertical correlation depends

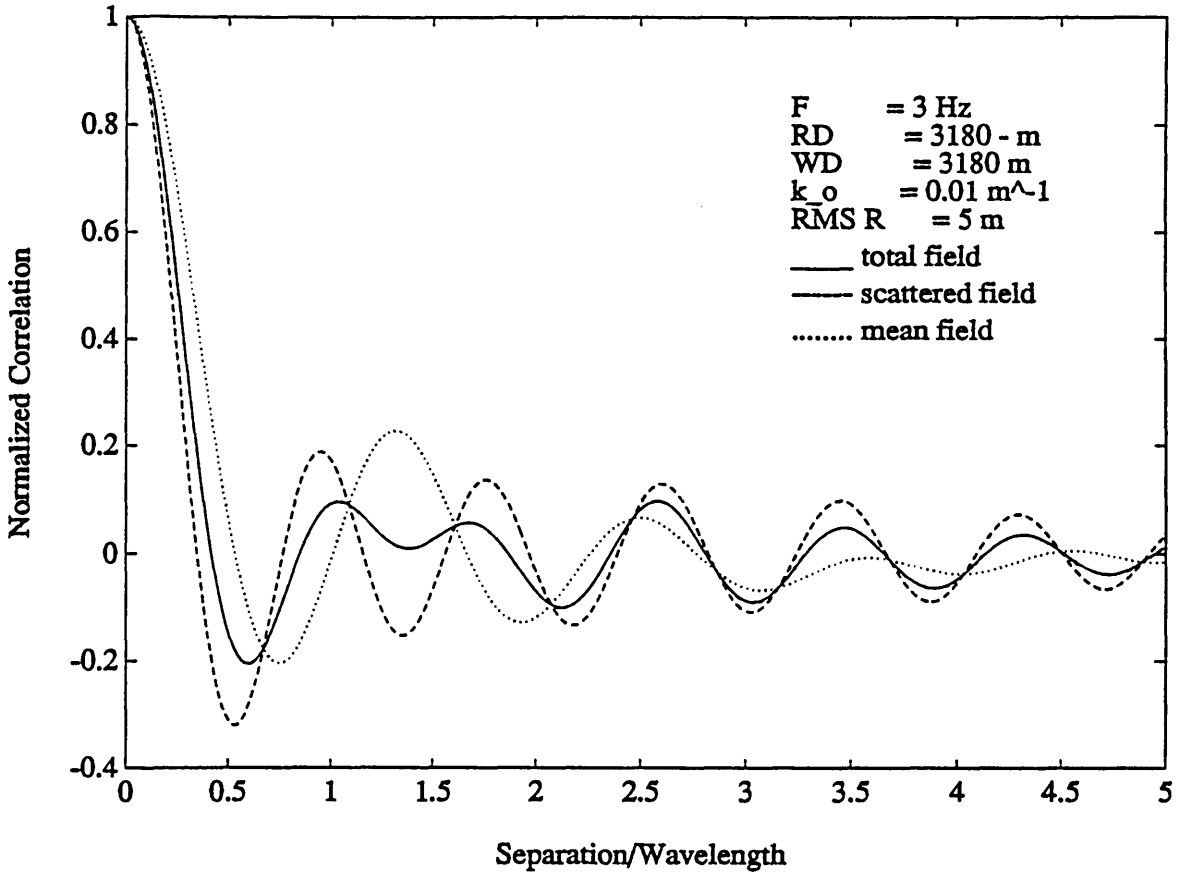

Figure 5.5: Horizontal correlation for a deep ocean waveguide.

upon not only the vertical separations, but also the absolute position of the receiver to be correlated with. Here we fix one receiver at depth z_1, and vary the depth of the second receiver throughout the water column. The correlation is normalized so that it yields a value of unity at $z = z_1$.

Figures 5.6 and 5.7 show the vertical correlation for the hard bottom deep water case for the canonical waveguide environment with an isotropic Gaussian roughness spectrum. The correlation lengths chosen for the Gaussian roughness spectra are $10\,m$ and $75\,m$, respectively. The fixed receiver is at depth $250\,m$. Both results indicate that the total correlation lengths (solid curves) are of the order of the sound wavelength, consistent with the analysis presented in Ref. [74]. Since the fixed receiver depth is far away from the rough sea bed, the total correlation lengths are completely dominated by the mean noise field, for which the correlation length is controlled by the waveguide properties. We also note that since the scattered fields (dashed curves) are composed of the same wave components as the mean field, the scattered field solution is similar to that of the mean field.

The results for the vertical correlation with respect to a fixed receiver at depth directly on the sea bed are given in Figs. 5.8 and 5.9 for $\ell = 10\,m$ and $\ell = 75\,m$, respectively. It is seen for the case of $\ell = 10\,m$, the correlation length of the scattered field (dashed curve) is about twice of that for the mean field (dotted curve). This is attributable to the fact that the major contribution is due to the Scholte waves, resulting in high value of coherence which is soon decorrelated as the separation exceeds the thin region in which the Scholte waves are dominant. The overall effect is a slight increase of the total correlation length.

As ℓ increases to $75\,m$ as shown in Fig. 5.9, the scattered field shows less coherence compared with $\ell = 10\,m$ for small separations, but maintains some degree of

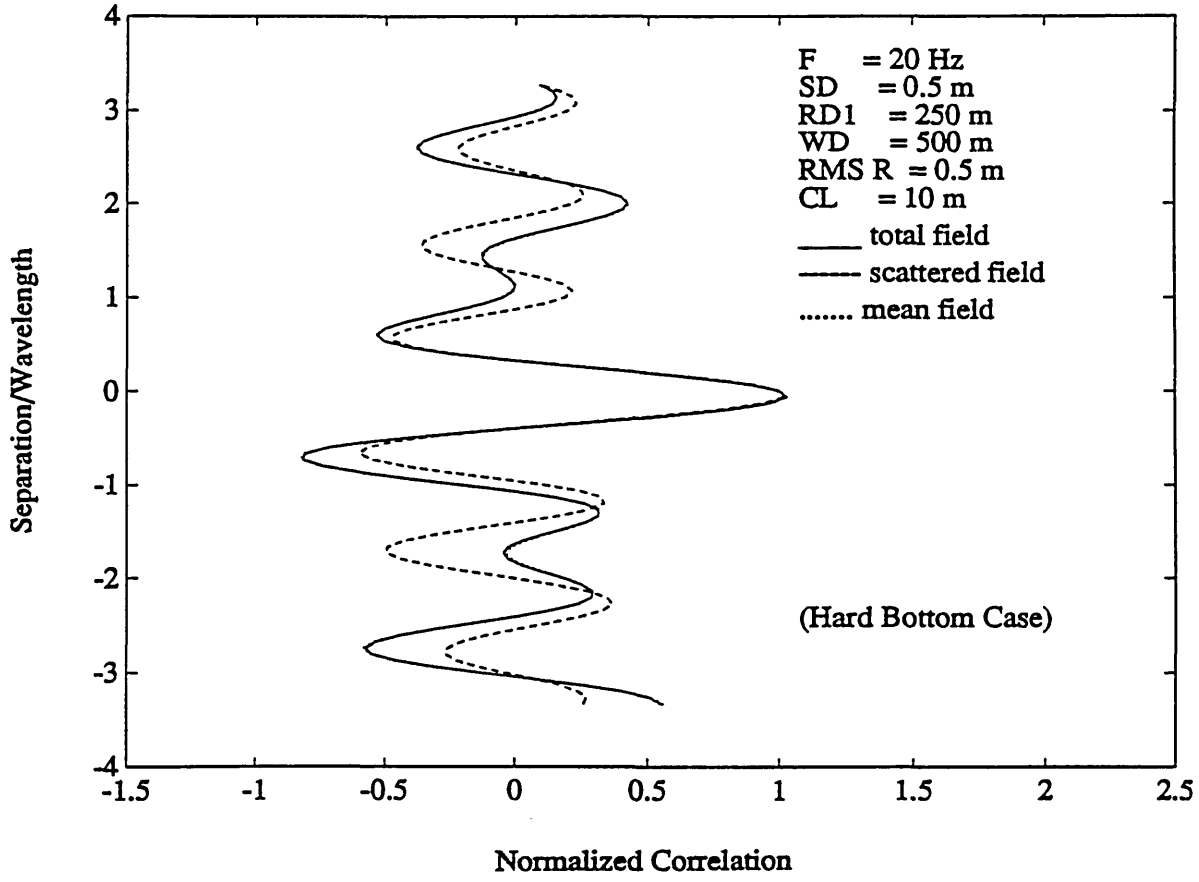

Figure 5.6: Vertical correlation for $RD_1 = 250\,m$ and $\ell = 10\,m$.

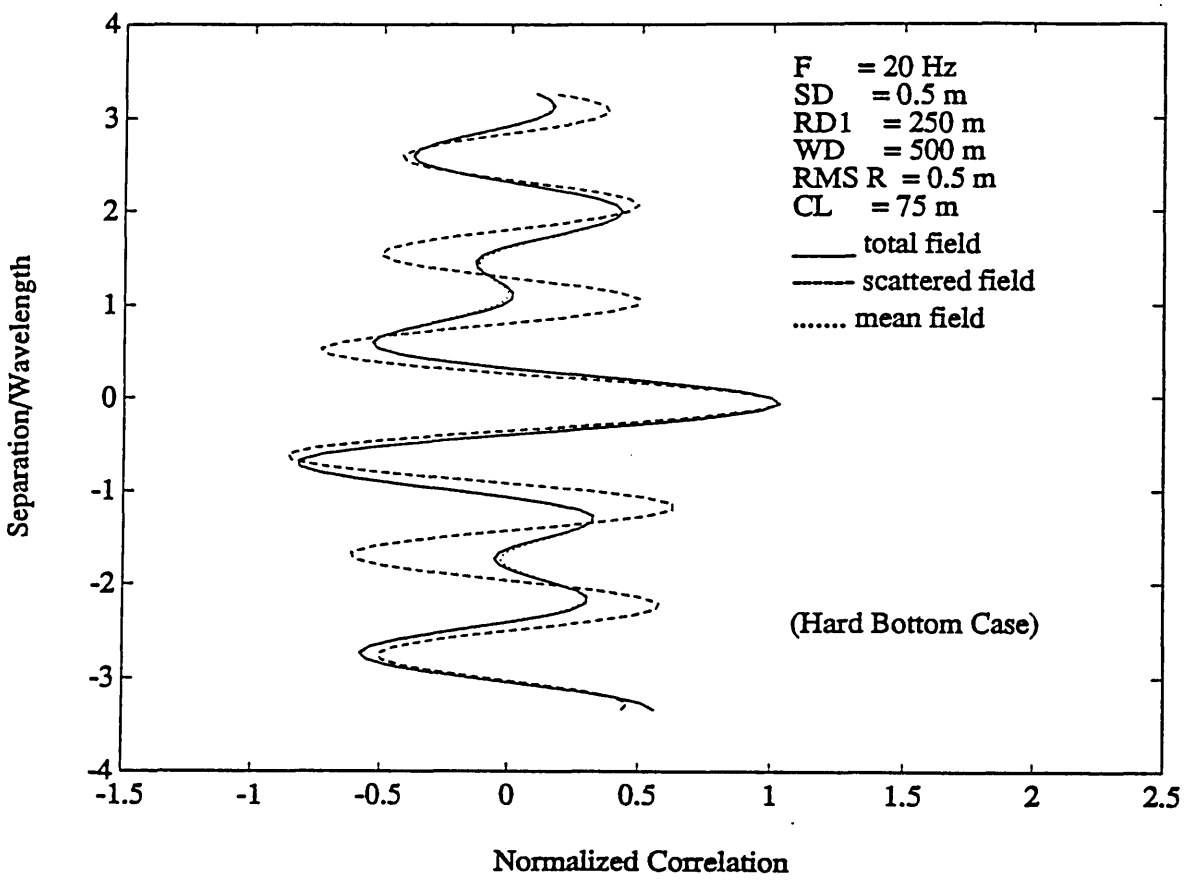

Figure 5.7: Vertical correlation for $RD_1 = 250\,m$ and $\ell = 75\,m$.

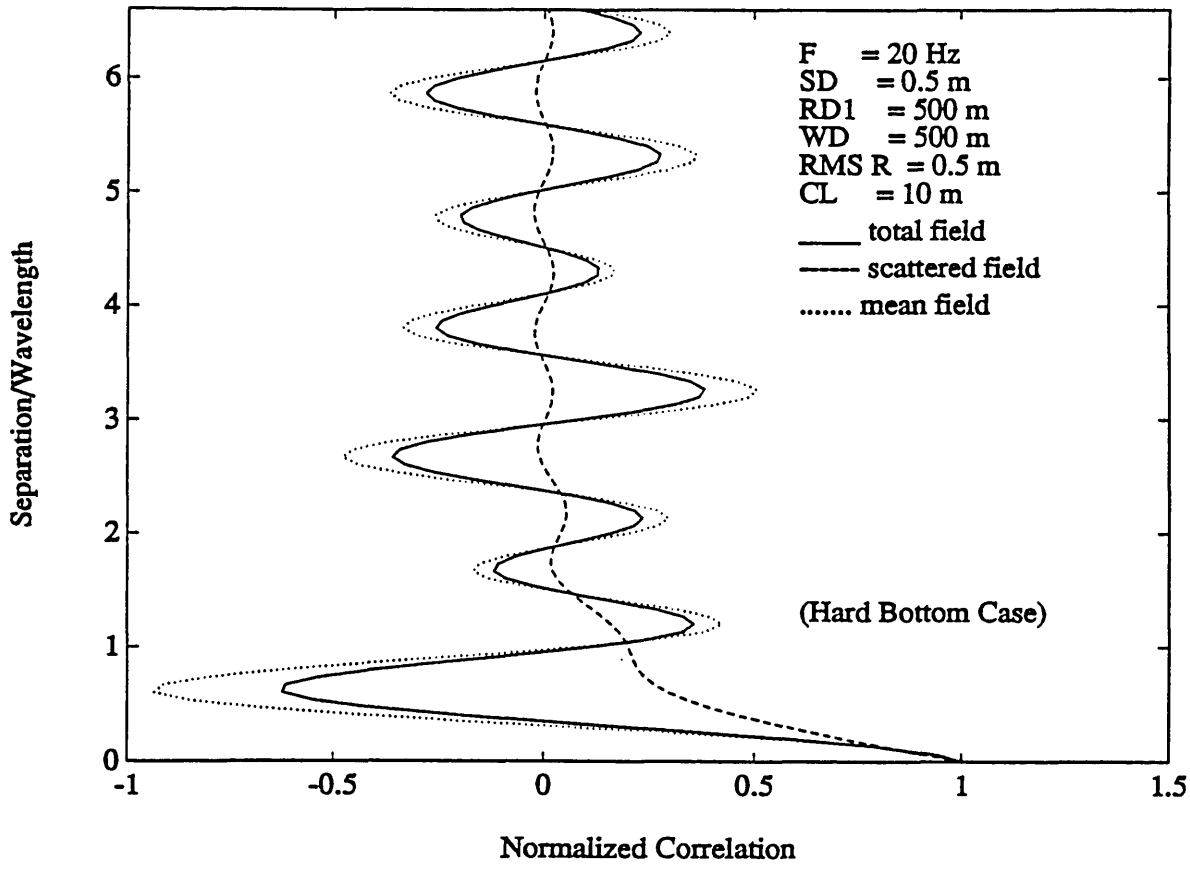

Figure 5.8: Vertical correlation for $RD_1 = 500\,m$ and $\ell = 10\,m$.

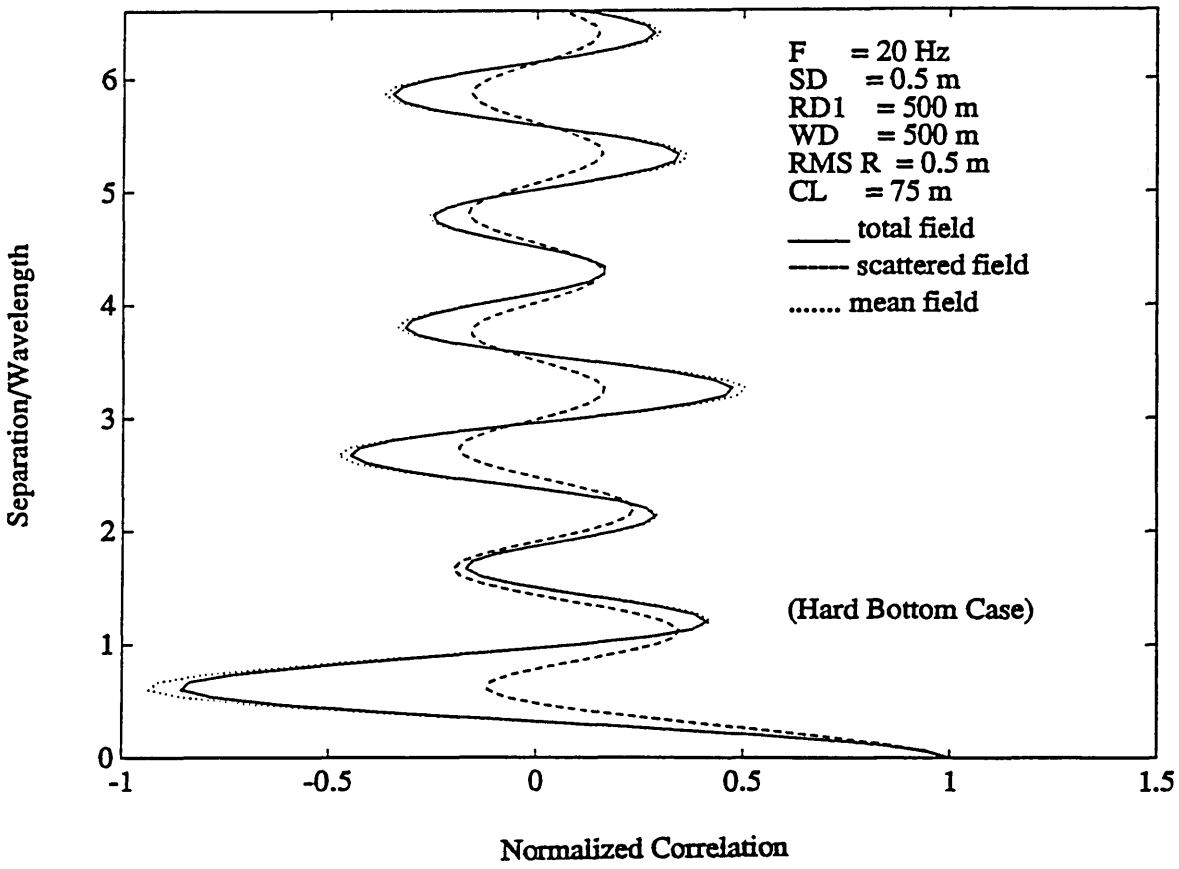

Figure 5.9: Vertical correlation for $RD_1 = 500\,m$ and $\ell = 75\,m$.

coherence over several wavelengths. Again, in this case, the insignificant scattered field makes little effect on the total noise field.

In summary, rough sea bed scattering has only minor effect on the vertical correlation of the total noise field, even in a region close to the bottom; thus the vertical correlation is mainly determined by the waveguide properties in contrast to horizontal correlation length which is sensitive to roughness.

5.4 Effects of Roughness Spectrum

The roughness power spectrum directly provides a shading over the integration kernel, as shown in Eq. (2.46). This equation indicates that the excitation of the scattered noise is proportional to the power of the roughness contained at wavenumber component equal to the *difference* of scattered wavevector $\mathbf{q}$ and incoming wavevector $\mathbf{k}$. Two types of power spectra have been used in this study: Gaussian spectra and Goff-Jordan (power-law) spectra. The major difference is that the latter contains more power for the high frequency components than the former, the effect of which is examined in this section.

We first consider the effect of different correlation lengths on the scattered noise intensities for the same power spectrum which was shown Fig. 5.1. The major difference of the noise intensity occurs near the bottom, at where the scattered noise intensity for $\ell = 10\,m$ is about $15\,dB$ higher than that for $\ell = 75\,m$. Since the Scholte wave mode is the dominant energy carrier in that region, this may be interpreted in terms of the excitation of the Scholte wave by different roughness scales.

Figure 5.10 illustrates the Gaussian power spectra for $\ell = 10\,m$ (solid curve) and

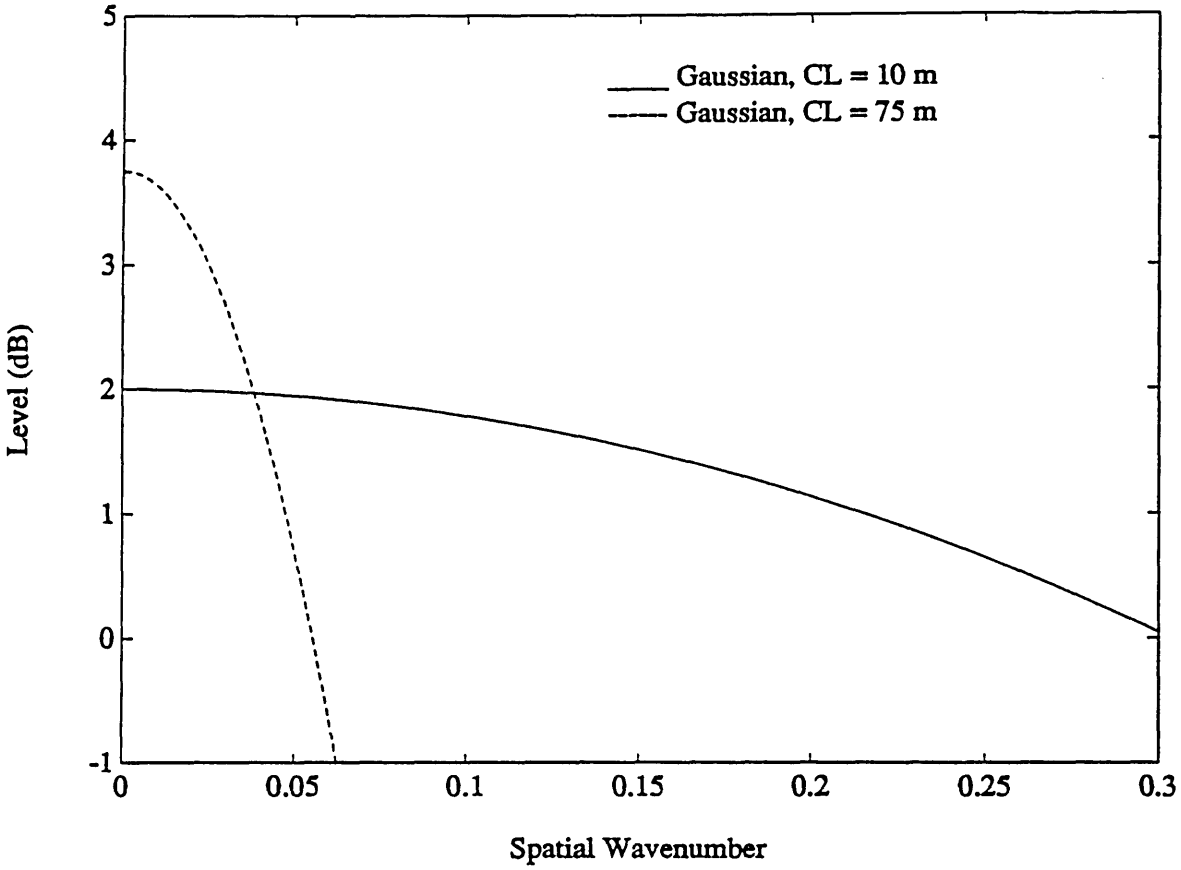

Figure 5.10: Gaussian roughness spectra with different correlation length.

for $\ell = 75$ (dashed curve). It is seen that below the spatial wavenumber equal to $0.04\,m^{-1}$, the spectrum corresponding to $\ell = 75\,m$ contains more power; however, above $0.05\,m^{-1}$, it decreases dramatically in comparison with that for $\ell = 10\,m$. We should also recall, in view of Fig. 3.3, that the major incoming horizontal wave components are less than $0.083\,m^{-1}$, and the Scholte wavenumber is about $0.0879\,m^{-1}$ in this case. Thus even through, for $\ell = 75\,m$, those shallow angle incoming wave modes (lower-order modes) excite the Scholte wave more efficiently because of the smaller values of $|\mathbf{q} - \mathbf{k}|$, the fast decay of the spectrum at high wavenumbers has made the excitation of the Scholte wave attributable to the higher-order incoming

wave modes insignificant. This is contrary to the case for $\ell = 10\,m$. Here despite the fact that the lower-order incoming wave modes are less efficient in exciting the Scholte wave, the high level of the spectrum, encompassing the major interval where $|\mathbf{q} - \mathbf{k}|$ is important, has rendered an overall higher noise intensity for $\ell = 10\,m$ than the intensity for $\ell = 75\,m$. It may be inferred from Fig. 5.10 that there exists a critical correlation length depending upon the frequency under consideration; beyond the critical correlation length, longer correlation lengths give smaller noise intensities near the bottom. Physically, a rough surface having smaller correlation length appears to be "rougher", and the higher frequency components are the better catalysts for generating a wider-angle scattering field.

Next we consider the resulting scattered noise intensities with different roughness spectra. To see the effect of high frequency components, both power spectra are normalized and the parameters are chosen so that they possess the same amount of power at zero frequency. Figure 5.11 shows the scattered noise intensities for Gaussian spectrum (solid curve) with correlation length $10\,m$, and for Goff-Jordan spectrum (dashed curve) with characteristic wavenumber $0.1414\,m^{-1}$. This figure shows that on average the noise intensity using Gaussian spectrum is $2\,dB$ higher than that using Goff-Jordan spectrum throughout the water column. This may be understood by examining the power spectra shown in Fig. 5.12, which shows that the Gaussian power spectrum is higher than that of Goff-Jordan spectrum for wavenumber less than $0.2\,m^{-1}$, which essentially includes the complete range of $|\mathbf{q}-\mathbf{k}|$ in which the important wave components exist. Thus no wave components beyond the point at where the Goff-Jordan spectrum begins to dominate over the Gaussian spectrum is excited in this case. The overall result is a 2 dB higher noise intensity with the Gaussian spectrum, as shown in Fig. 5.11.

The scattered noise intensities for large roughness correlation length are shown in

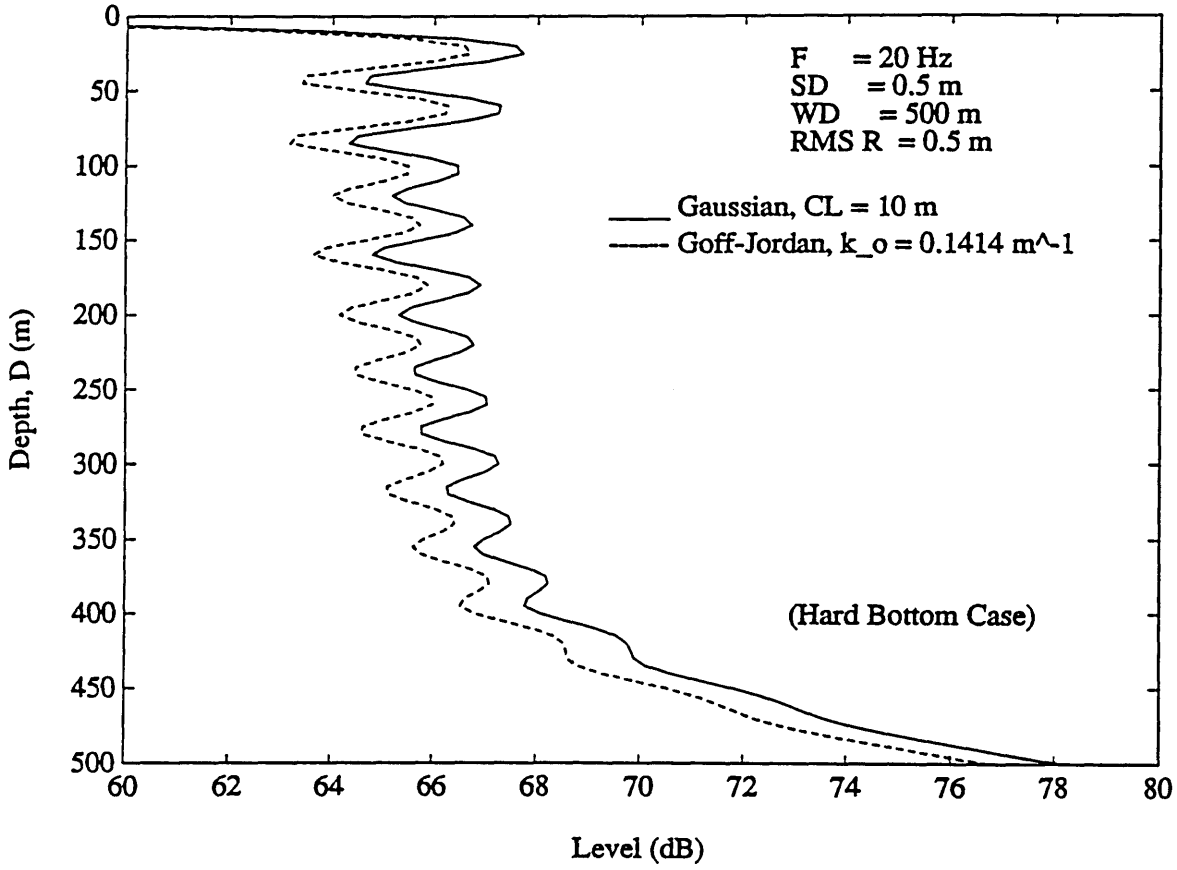

Figure 5.11: Scattered noise intensities for Gaussian spectrum with $\ell = 10\,m$ and Goff-Jordan spectrum with $k_0 = 0.1414\,m^{-1}$.

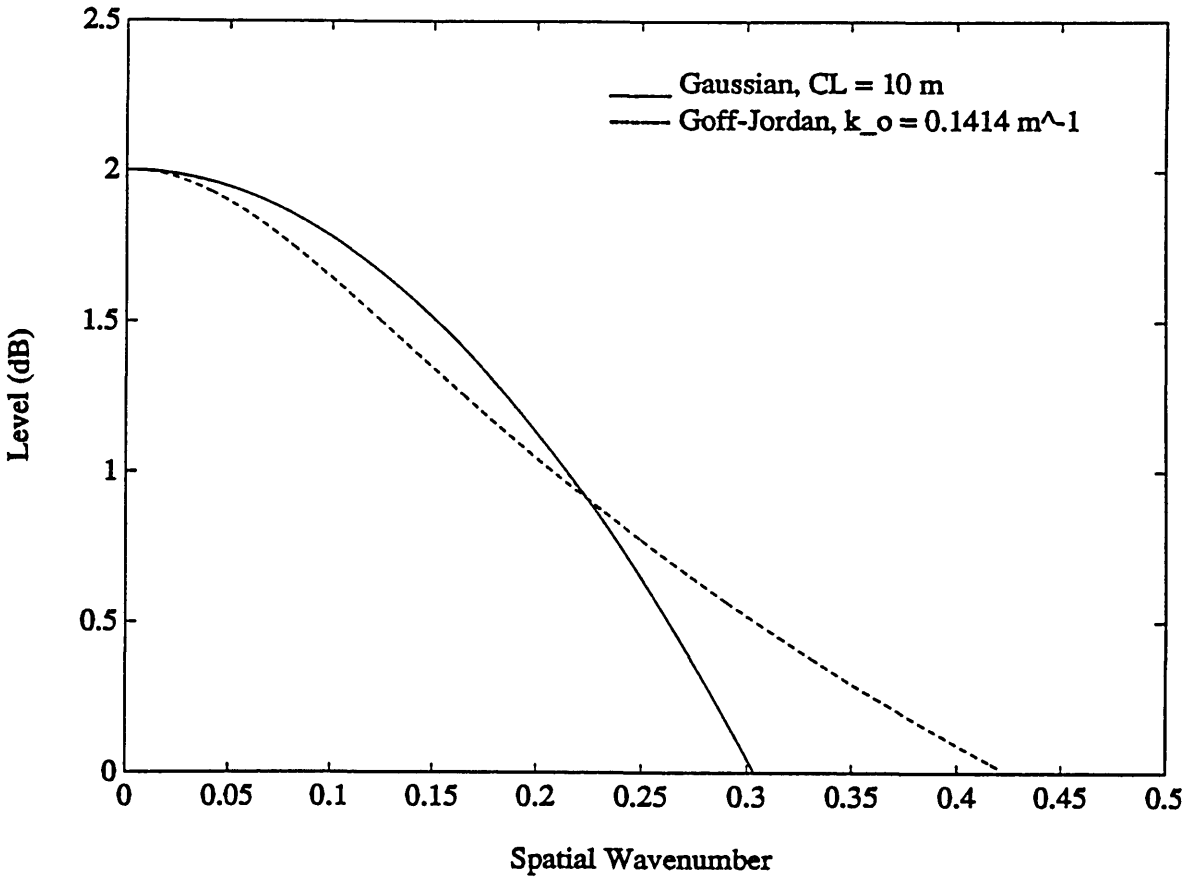

Figure 5.12: Power spectra for Gaussian spectrum with $\ell = 10\,m$ and Goff-Jordan spectrum with $k_0 = 0.1414\,m^{-1}$.

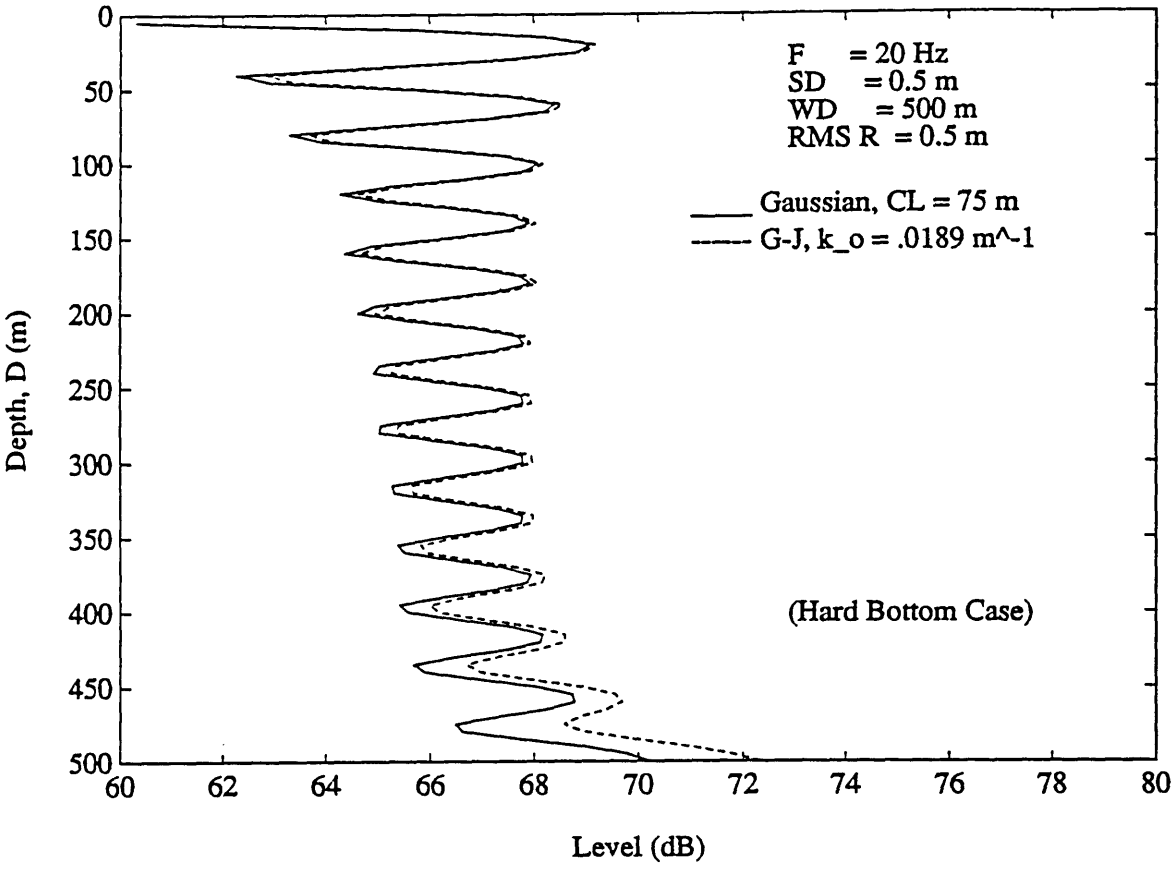

Figure 5.13: Scattered noise intensities for Gaussian spectrum with $\ell = 75\,m$ and Goff-Jordan spectrum with $k_0 = 0.0189\,m^{-1}$

Fig. 5.13 for Gaussian spectrum with $\ell = 75\,m$ (solid curve) and Goff-Jordan spectrum with $k_o = 0.0189\,m^{-1}$ (dashed curve), and the spectra are shown in Fig. 5.14. It shows that the noise intensities are comparable throughout the water column except near the sea floor. This is similar to the case discussed above for Gaussian spectrum with two different correlation lengths, except the discrepancy now has been reduced because the difference between the two spectra at larger wavenumber decreases. It is expected that the difference for the noise intensities with different spectra increases with the correlation length and frequencies.

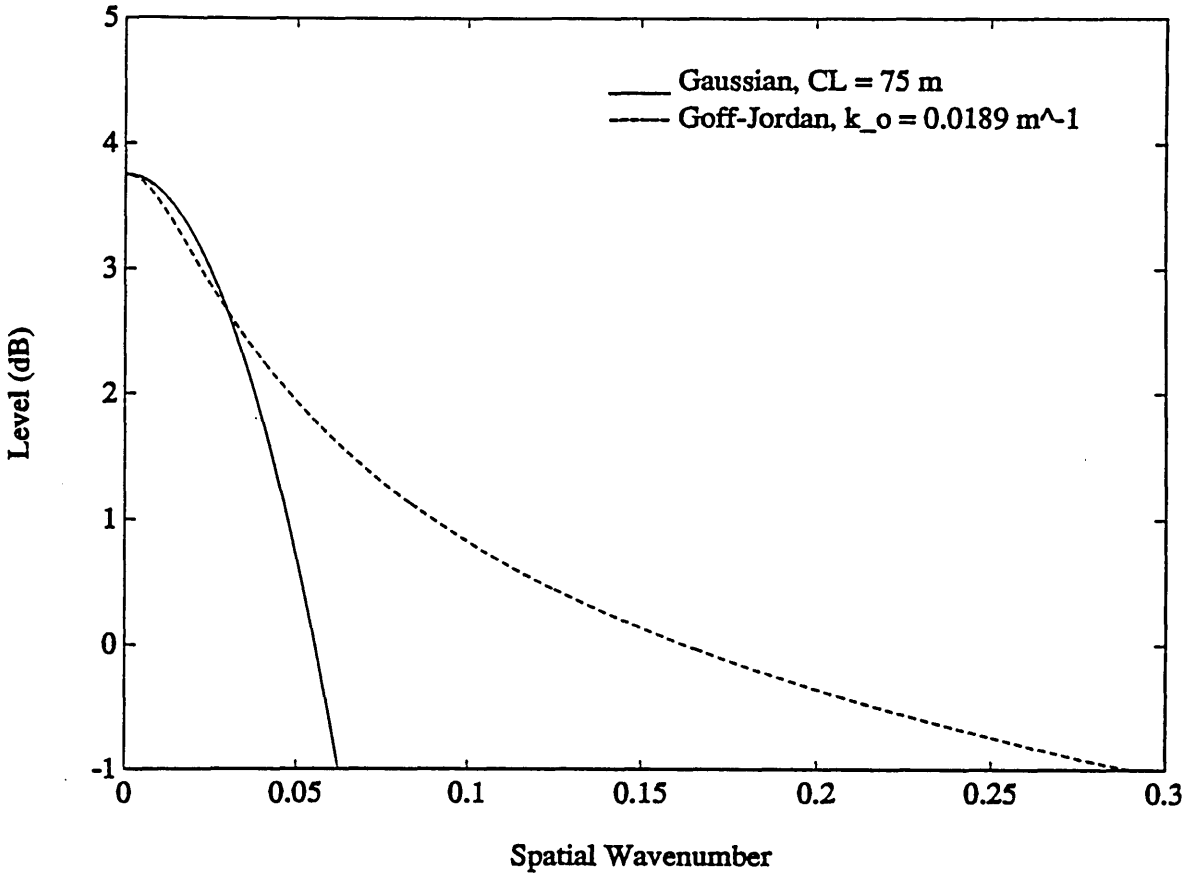

Figure 5.14: Power spectra for Gaussian spectrum with $\ell = 75\,m$ and Goff-Jordan spectrum with $k_0 = 0.0189\,m^{-1}$

From the above results, it may be summarized that the roughness correlation length has an effect on the noise intensity (or noise scattering), especially near the bottom. This is particularly evident for the Gaussian spectrum. However the difference between results with different roughness spectra is not significant in general in the frequency regime of our interest (the above results indicate that the difference is within $2\,dB$).

5.5 Effects of Sound Speed Variation

As was mentioned in Sec. 1.3.2 that sound propagation in a deep ocean environment is characterized by an efficient sound-propagation layer known as underwater sound channel resulting from refraction due to a particular variation of the sound speed. This layer may trap those rays emanating from the sources with shallower angles, depending upon the sound speed variation with depth, thus avoiding the interaction with the boundary surfaces which in turn produces slowly range-decaying sound field caused only by geometric spreading, not boundary interaction. For instance, in a deep water waveguide, if there exists an excess depth so that the sound speed at the bottom is larger than that of near the sources, the lower-order modes are likely to be trapped in the upper part of the water column. Since the scattered noise field in the present analysis is generated by the *equivalent* secondary sources at the bottom which are excited by the primary noise sources near the surface of the water column, therefore, if the primary noise field is in part trapped in the upper part of the water column, the excitation of the scattered field will become less efficient. In this section we investigate the coupling between the surface noise sources and the seismic waves in a waveguide with various sound speed distributions.

Here we consider a deep ocean waveguide model similar to that shown in Fig. 4.6, and in particular we vary the sound speed distribution by changing the value of the sound speed at the bottom (c_3). The model environment for the present analysis is shown in Fig. 5.15. The water column of $500\,m$ deep consists two layers with pseudo-linear sound speed variation, and the sea floor is composed of a layer of a sand sediment of $5\,m$ thick overlying a basalt subbottom. We shall assume that the sound speed at the surface (c_1) and at the channel axis (c_2) is fixed, and is $1500\,m/s$ and $1480\,m/s$, respectively. The sound speed at the bottom is chosen to be $1490\,m/s$, or $1520\,m/s$, for which the later case results in an excess-depth sound channel.

To see the effect of the sound speed variation on the noise fields, we first examine the noise intensity throughout the water column. Figures 5.16, and 5.17 demonstrate the intensities of the noise fields (solid curve for the total field, dashed curve for the scattered field, and dotted curve for the mean field) for $c_3 = 1490\,m/s$, and $c_3 = 1520\,m/s$, respectively. These results indicate that the mean noise intensity is relatively uniform throughout the water column for $c_3 = 1490\,m/s$, and is concentrated in the upper part of the water column for $c_3 = 1520\,m/s$. The concentration of the noise intensity in the upper part of the water column, showing about 5 to 6 dB higher, is an indication of the low-order modes being trapped in the sound channel. These lower-order hardly interact with the bottom, resulting in a very small attenuation, and therefore a significant contribution is attributable to the distant sources. This argument is supported by the wavenumber spectra shown in Fig. 5.18, where three lower-order normal modes are isolated. It is seen that the first normal mode becomes stronger and stronger as the receiver moves towards the upper part of the water column.

The coupling into the seismic waves is shown in the wavenumber spectra in Fig. 5.19 for $c_3 = 1490\,m/s$, and in Fig. 5.20 for $c_3 = 1520\,m/s$. These results

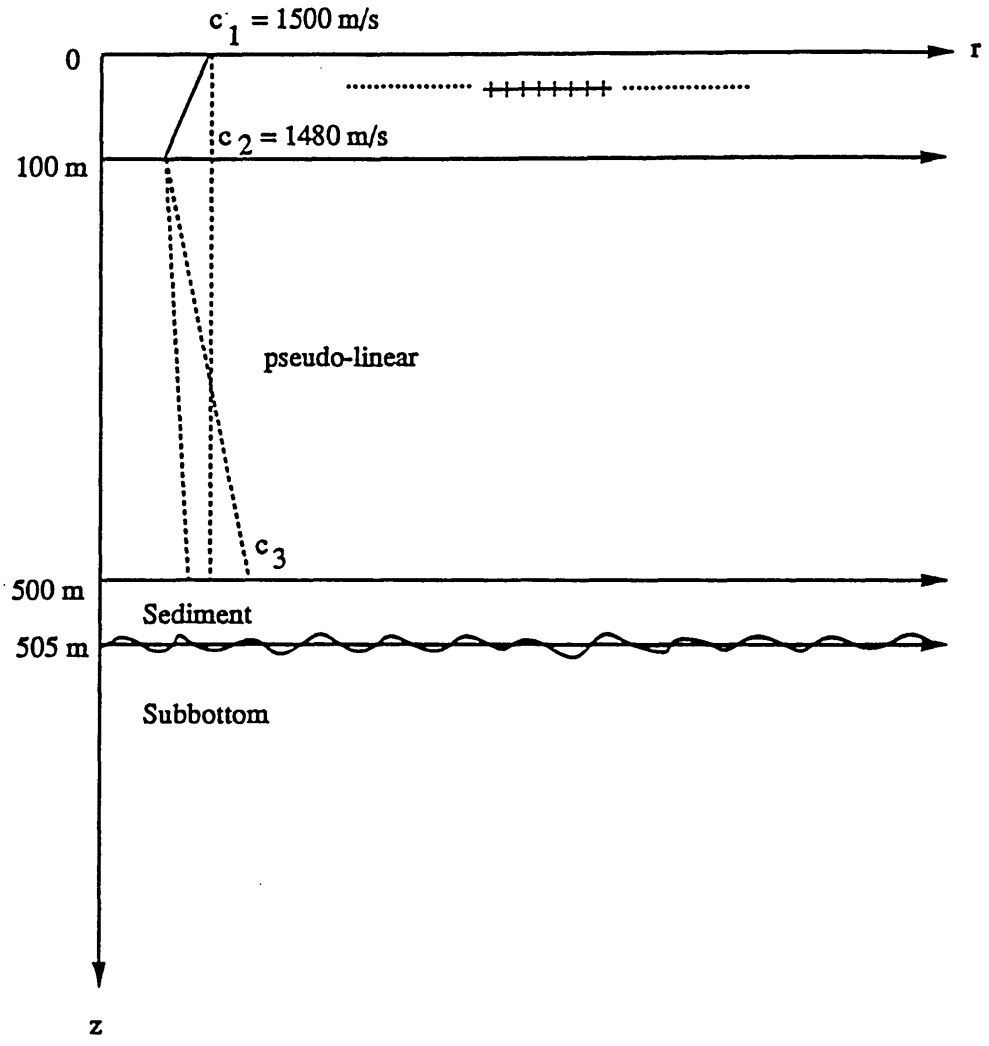

Figure 5.15: A deep ocean waveguide with various sound speed at the bottom (c_3).

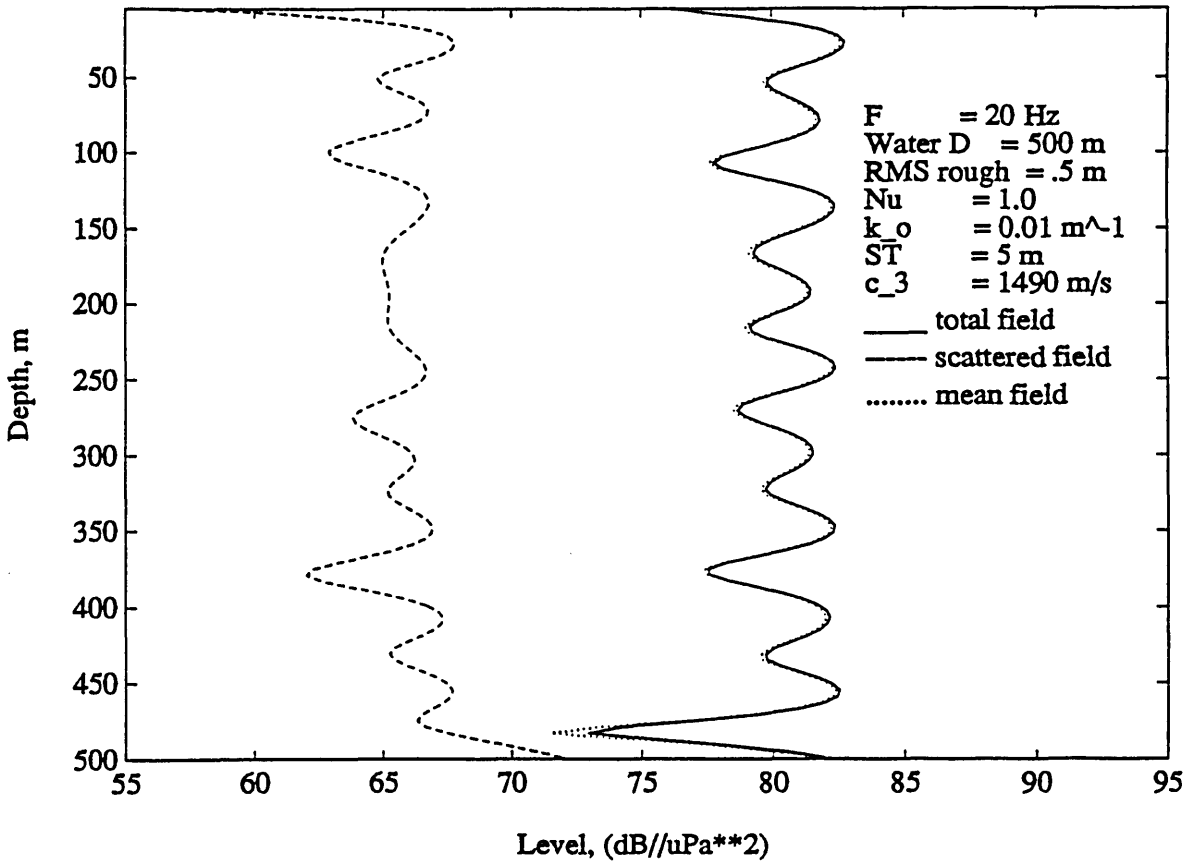

Figure 5.16: Noise intensities for a waveguide for $c_3 = 1490\, m/s$.

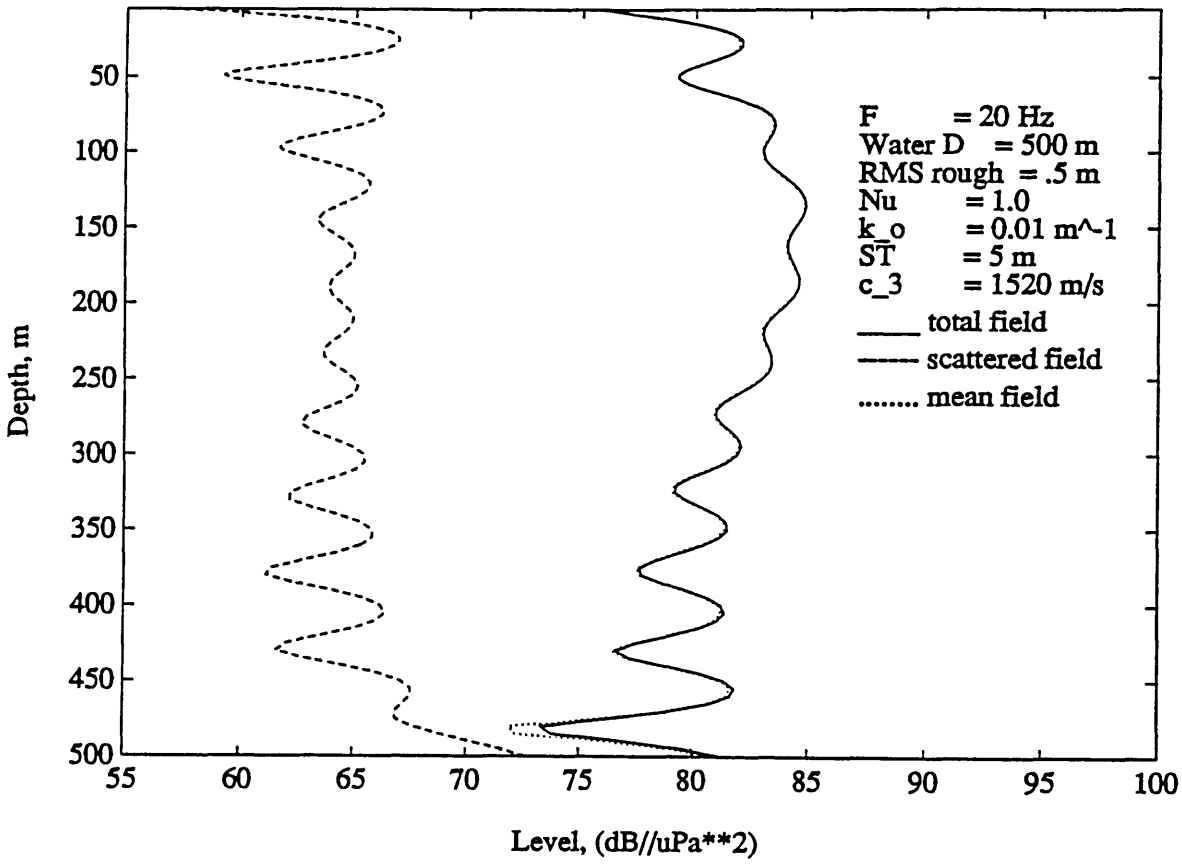

Figure 5.17: Noise intensities for a waveguide for $c_3 = 1520\,m/s$.

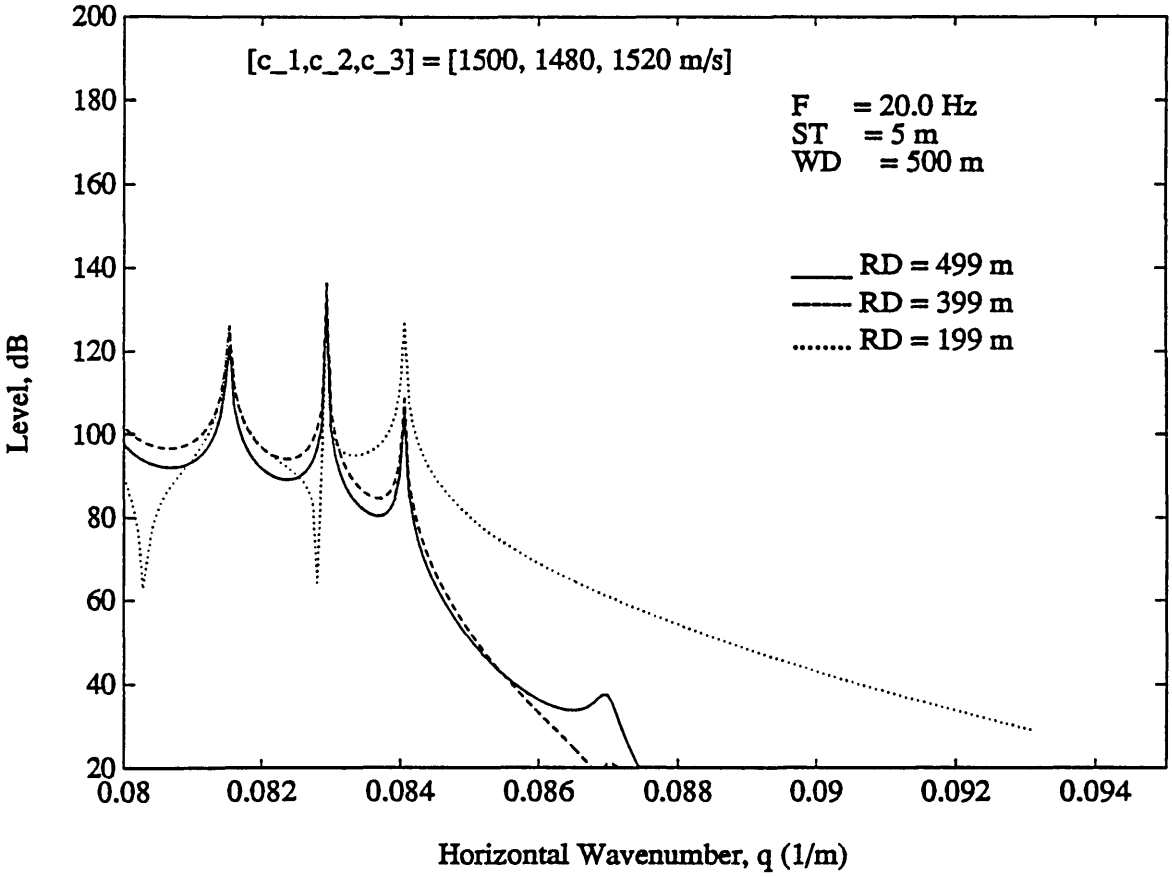

Figure 5.18: Mean field wavenumber spectra for $c_3 = 1520\,m/s$.

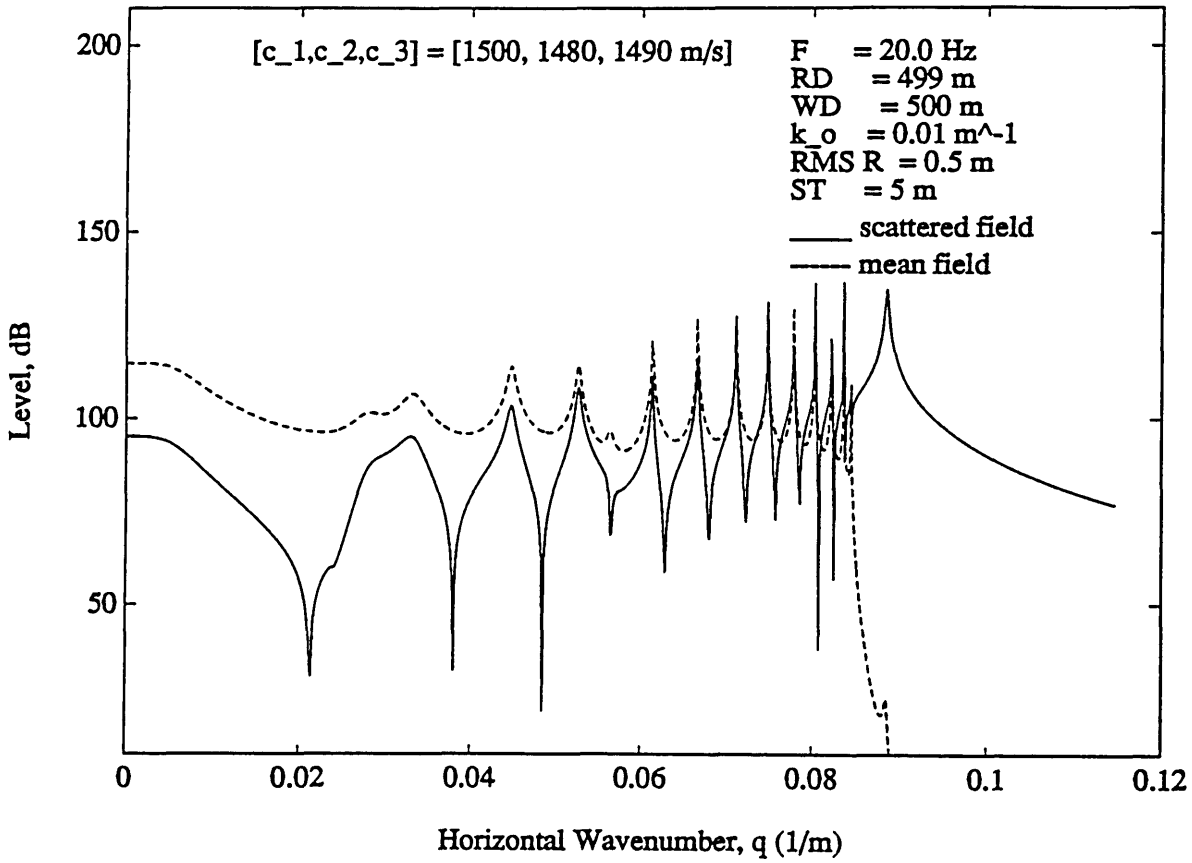

Figure 5.19: Wavenumber spectra for $c_3 = 1490\,m/s$.

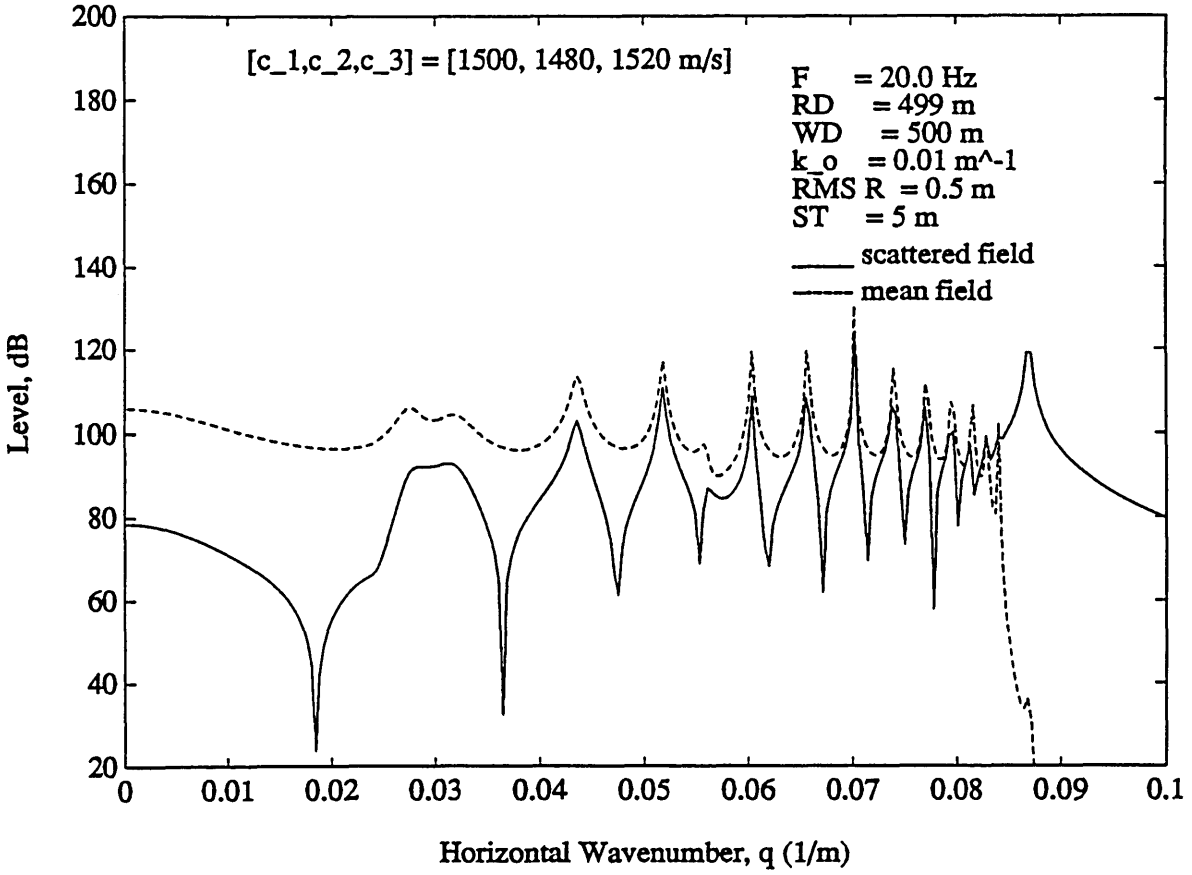

Figure 5.20: Wavenumber spectra for $c_3 = 1520\,m/s$.

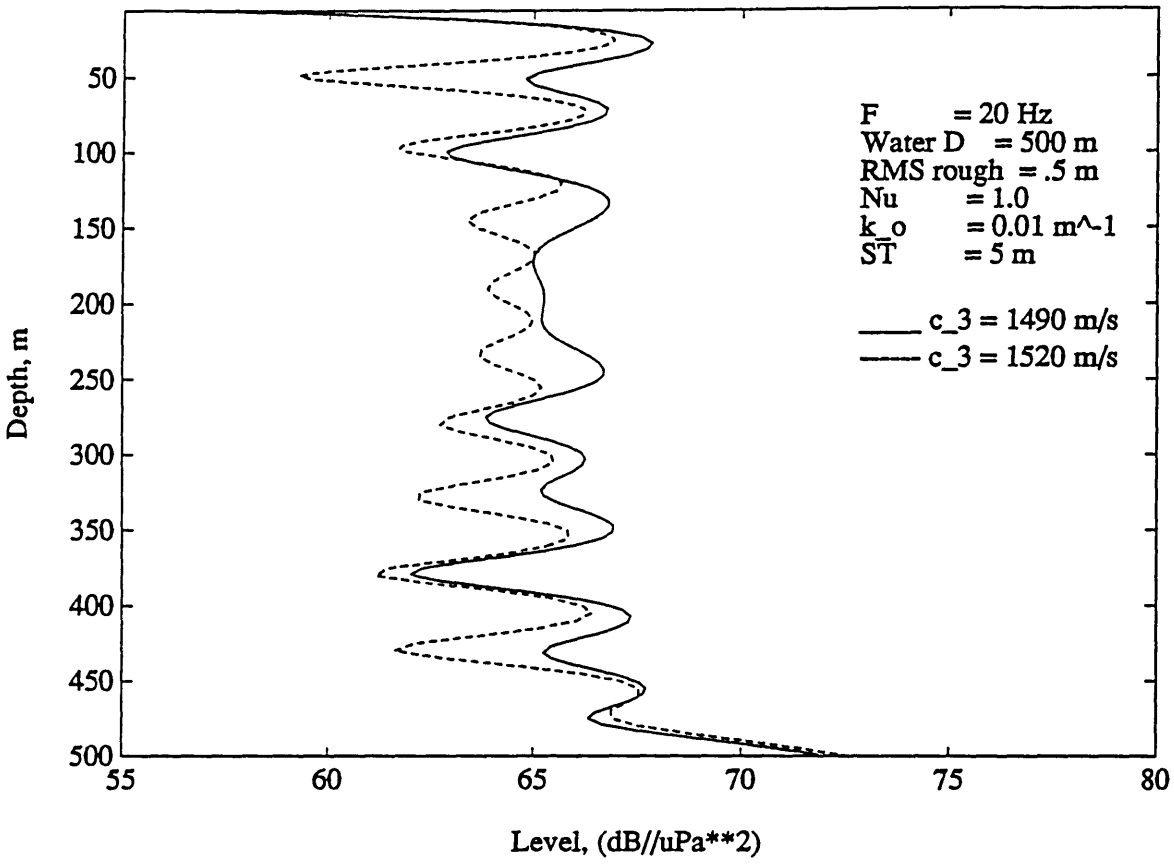

Figure 5.21: Scattered noise intensities for two values of c_3.

have shown that the excitation of the interface wave is still significant for both cases, with the interface mode being the most important feature in the wavenumber spectra for the scattered field near the bottom. This is also illustrated by Fig. 5.21, where it is seen that different values of c_3 lead to some variation of the noise intensities in the water column caused by the mean noise field. However, near the bottom the interface wave still dominates the scattered noise field, and the noise intensities are comparable for these two cases.

The interpretation of the excitation of the interface wave in this case is as follows. Since excitation of the interface wave mode is due to the complete spectrum,

continuous or *discrete*, of the mean noise field, even through the low-order modes are trapped in the waveguide, there still exists a wide spectrum in which the waves may interact with the rough surfaces. However, it is conceivable that when the variation of the sound speed and the frequency range of interest result in a situation so that many modes are trapped in the waveguide, the coupling into the seismic waves may be significantly reduced.

From the above results, one may conclude that the existence of the underwater sound channel may trap low-order normal modes of the mean noise field in the upper part of the water column, being prevented from interaction with the rough bottom which leads to a reduction of the excitation of the seismic waves. However, there are many other modes which can propagate through the ocean and reach the bottom to interact with the roughness. Thus, rough bottom scattering is still important *in general* in considering the generation of the deep ocean ambient noise, even with an excess depth in the sound channel.

5.6 Directivity of the Noise Fields

In all of the above studies, we have assumed that the interfaces are isotropic random fields for simplicity. Consequently, the resulted noise fields are isotropic. However, in reality, the noise field may possess a strong directional dependence [3]. There are many possible reasons for the directional dependence, among others, the anisotropy of the noise source fields due to directed wind fields, and that of due to anisotropic random rough interfaces are likely candidates. In this section we investigate the effect of anisotropy of the latter kind on the noise fields and demonstrate this dependence qualitatively with the canonical waveguide model.

For the sea floor topography we shall use the Goff-Jordan model shown in Eqs. (4.7) and (4.12). It is noted that anisotropy may be specified by properly choosing the model parameters k_s, k_n, and ζ_s so that the local strikes of the seamounts are aligned in the direction of ζ_s degree (0° and 90° are along x- and y-axis, respectively). Figure 5.22 shows the Goff-Jordan spectrum and its realization for the case of $k_s = 0.03\,m^{-1}$, $k_n = 0.09\,m^{-1}$, and $\zeta_s = 90°$. It is clearly seen that the seamounts are oriented preferentially along y-axis.

The horizontal correlation of the resulting noise fields for a receiver near the sea floor are shown in Figs. 5.23, 5.24, and 5.25, for the mean, scattered, and total noise fields, respectively. Because of the assumption of the Born approximation, which eliminates the effects of the rough interfaces on the mean field, the mean field remains isotropic as expected.

The results for the scattered field, Fig. 5.24, is most interesting (and expected). It shows the anisotropic nature of the noise field. It is seen that the correlation length is larger and the correlation decays faster along the strikes of the seamounts (90°) whereas, facing the seamounts (0°), the figure shows lower value of coherence for small receiver separations, but maintains some degree of coherence for several wavelengths. This is due to the fact that the random fields have a larger correlation length corresponding to the direction of the local strikes, resulting in a scattered field with a weaker strength in the corresponding direction, and vice versa in the direction facing the seamounts. The total noise field, Fig. 5.25, is the sum of mean and noise fields, and for this case the overall effect is to suppress the effect of anisotropy of the random noise fields since the total field is dominated by the mean field along the local strikes.

The effect of the orientation of the local strikes on the scattered noise field is

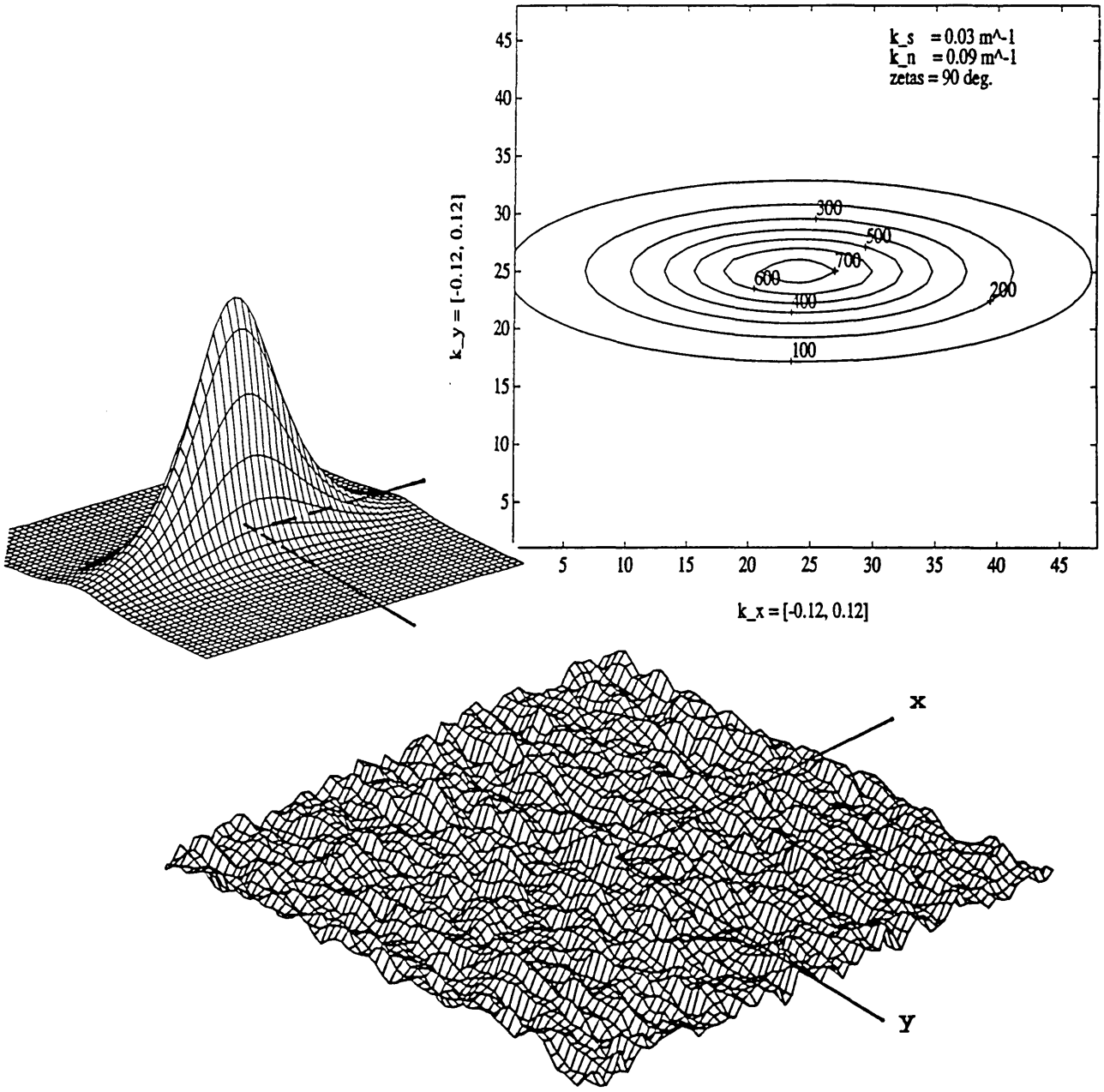

Figure 5.22: Goff-Jordan spectrum and its realization for $k_s = 0.03\,m^{-1}$, $k_n = 0.09\,m^{-1}$, and $\zeta_s = 90°$.

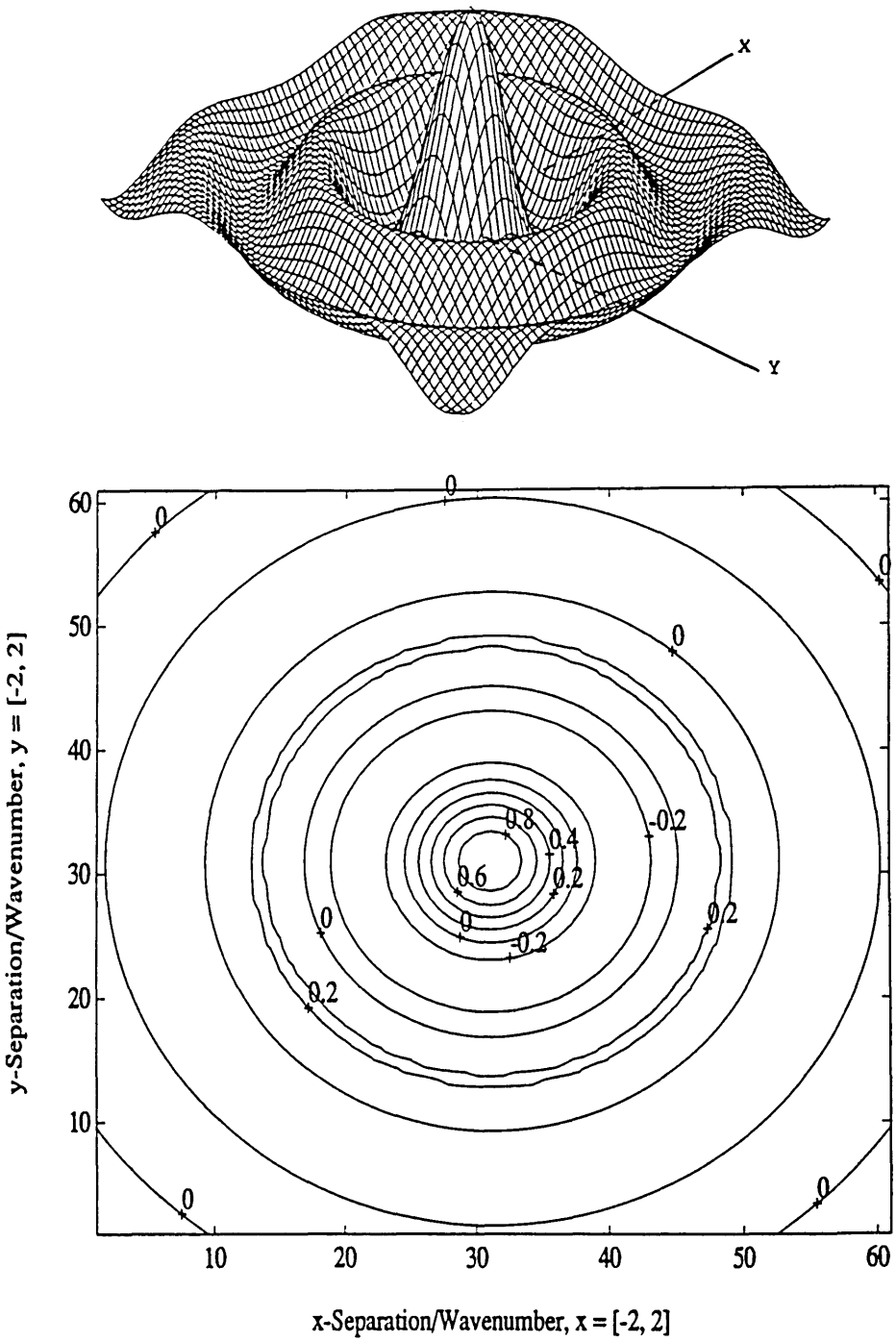

Figure 5.23: Horizontal correlation (mean field).

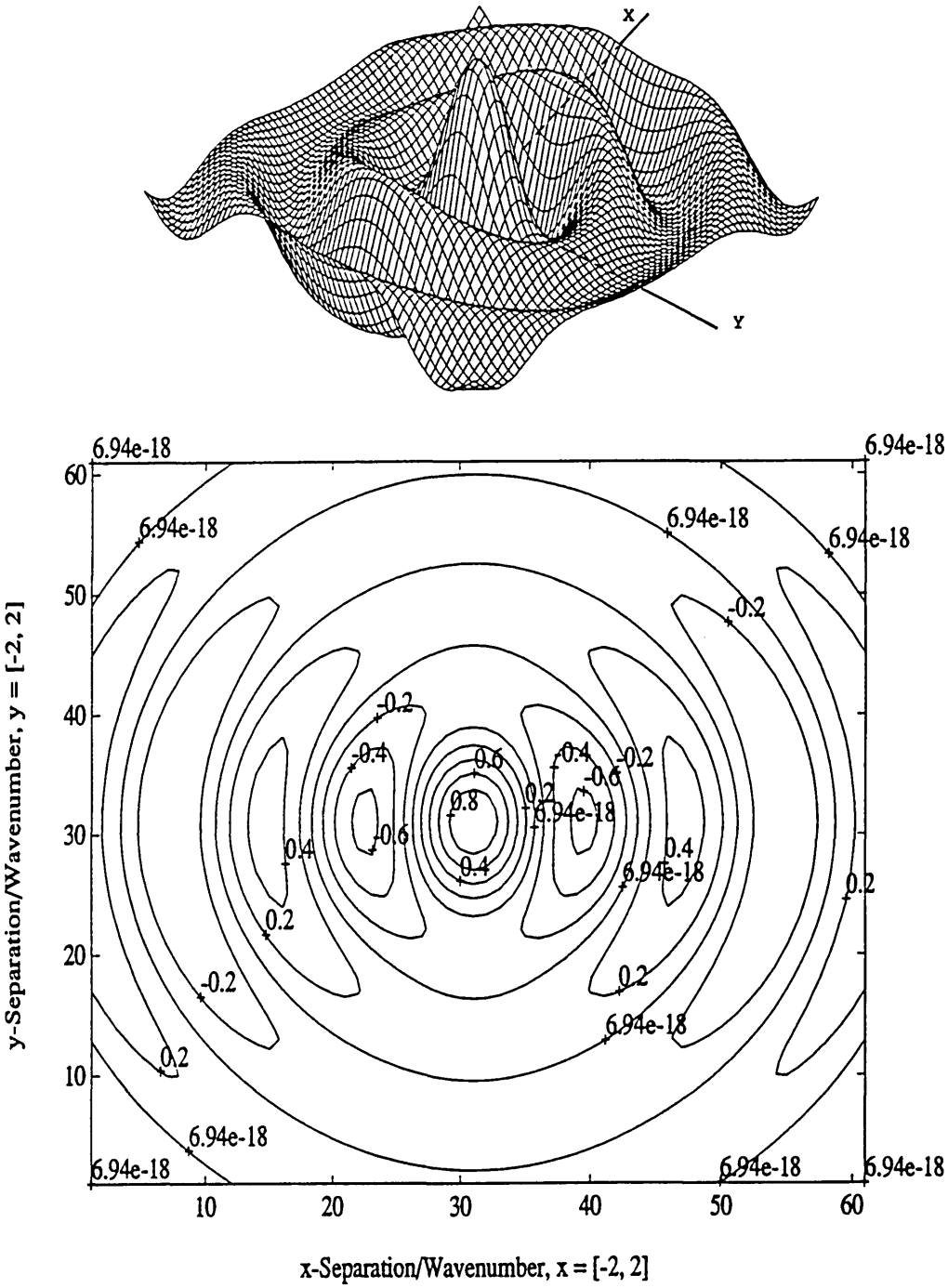

Figure 5.24: Horizontal correlation (scattered field) for $k_s = 0.03\,m^{-1}$, $k_n = 0.09\,m^{-1}$, and $\zeta_s = 90°$.

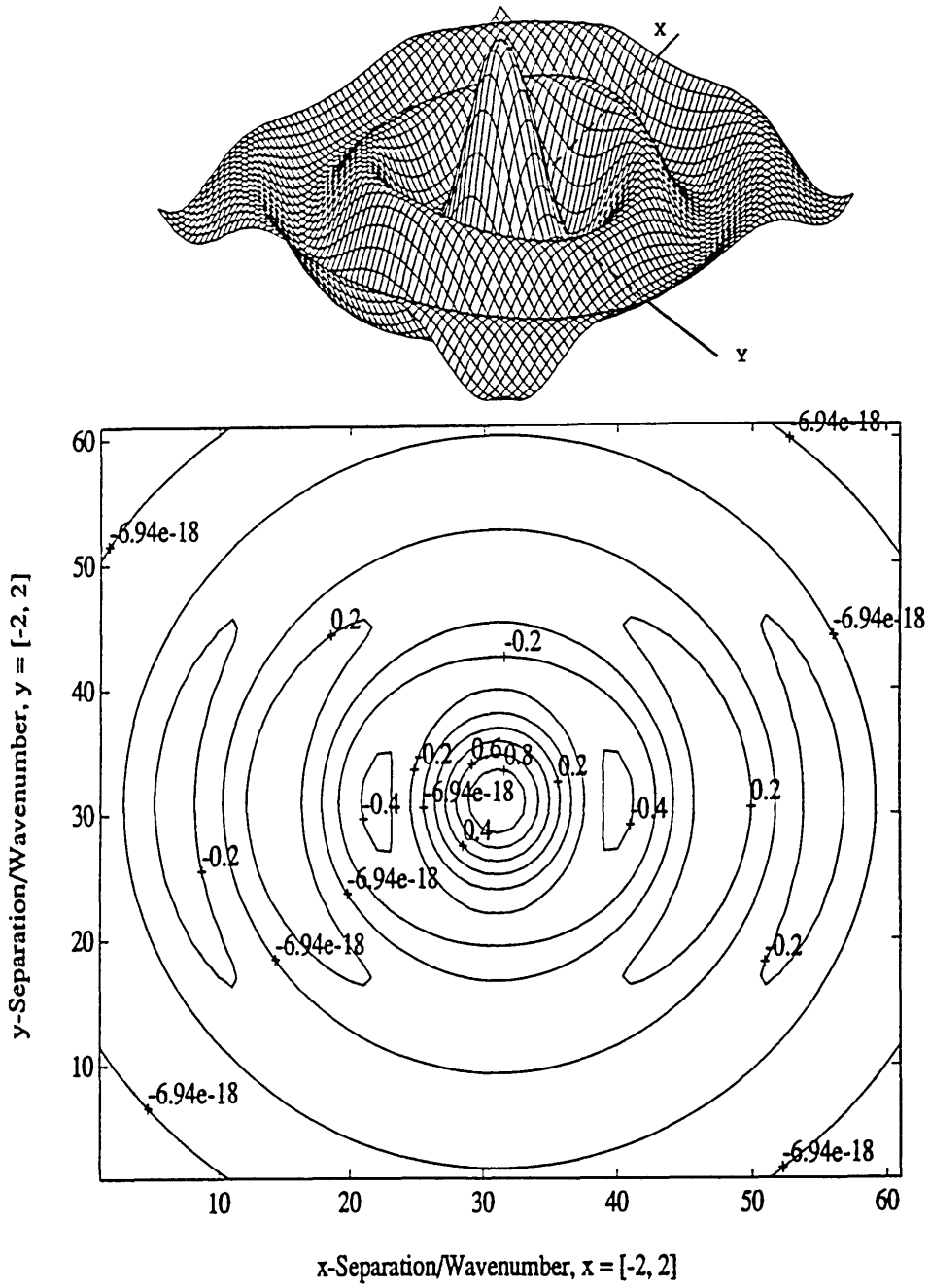

Figure 5.25: Horizontal correlation (total field) for $k_s = 0.03\,m^{-1}$, $k_n = 0.09\,m^{-1}$, and $\zeta_s = 90°$.

shown in Fig. 5.26, which shows that the local strikes are aligned along 60°, counting clockwise from the y-axis. It is seen the scattered noise field is rotated accordingly due to the rotation of the local strikes.

Figure 5.27 presents a case of stronger anisotropy of the sea floor roughness, where $k_s = 0.02\,m^{-1}$, and $k_n = 0.14\,m^{-1}$. The results of the scattered field are shown in Fig. 5.28. The anisotropic features of the scattered noise field are evidently seen in the figure.

Based upon the above results, it is demonstrated that the spatial correlation of the noise field bears a close relationship with the characteristics of the sea floor topography, such as the RMS roughness, seamount orientation, length scales, *etc.* This implies that the spatial properties of the noise field may be used as bases for inversion of sea floor topography at least in a qualitative sense. This presents a promising alternative in the study of geological or morphological properties of the sea floor for which direct measurements of the desired quantities present a great deal of difficulties.

5.7 Summary

We have analyzed the spatial correlation of the noise field. We first demonstrated the interplay between the spatial correlation of the noise field and the correlation length of the roughness using an isotropic roughness spectrum corresponding to an isotropic random field. This was illustrated by the horizontal correlation using the axisymmetric Gaussian roughness spectra in a canonical waveguide environment. It was demonstrated that for roughness correlation lengths shorter than the acoustic wavelength, the scattering has the effect of decreasing the horizontal spatial correlation

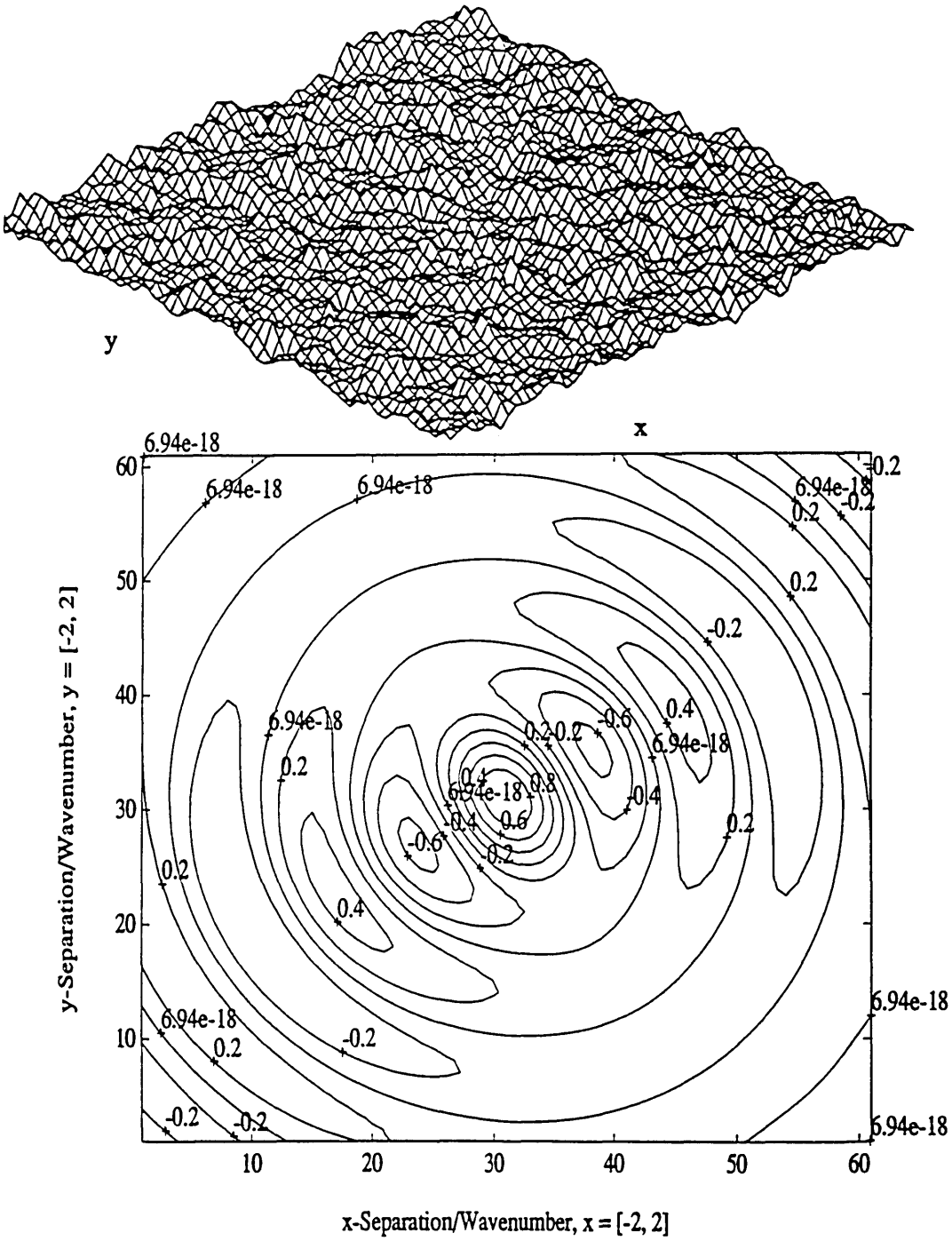

Figure 5.26: Realization for $k_s = 0.03\,m^{-1}$, $k_n = 0.09\,m^{-1}$, and $\zeta_s = 60°$, and its resulting horizontal correlation (scattered field).

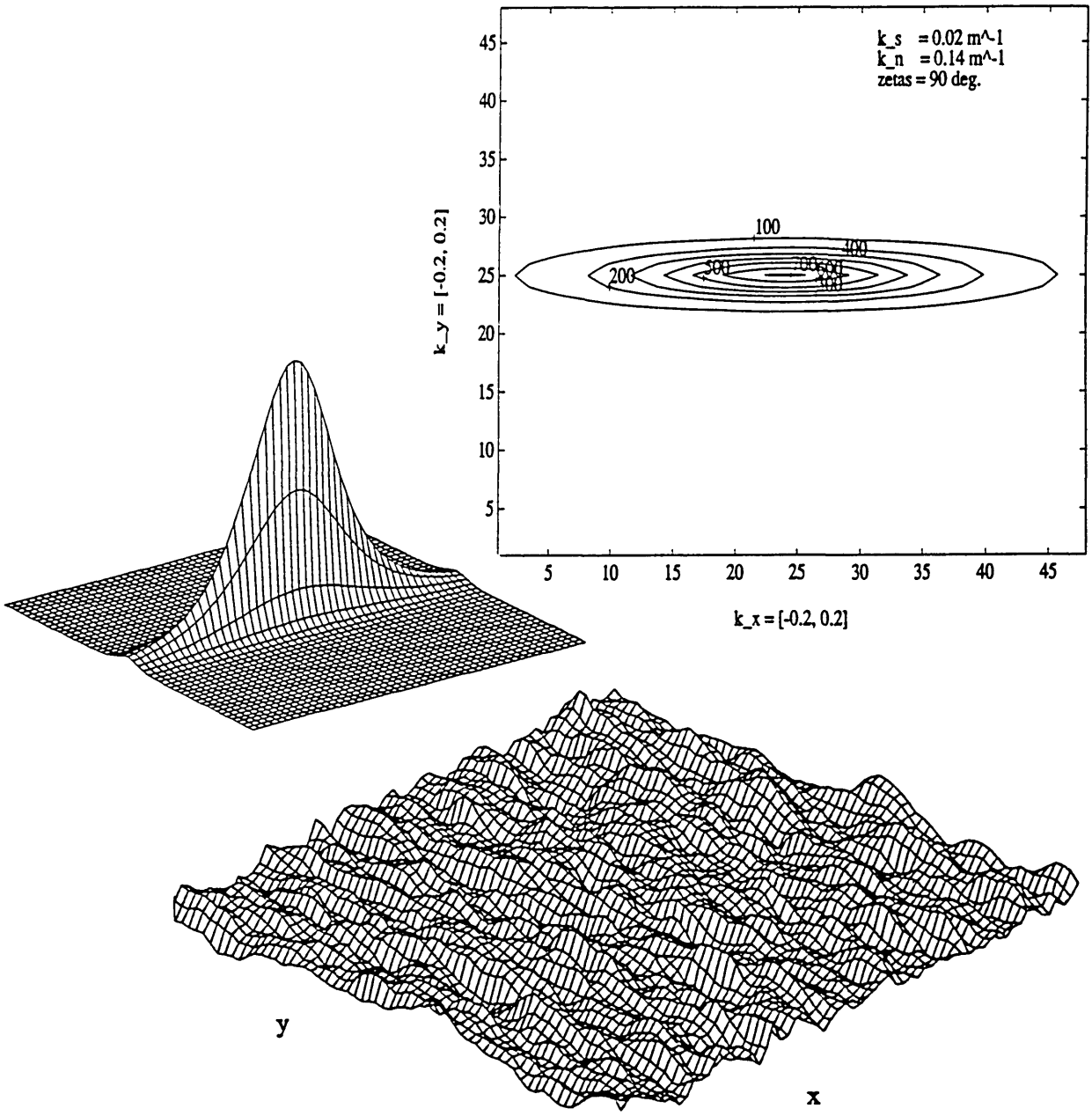

Figure 5.27: Goff-Jordan spectrum and its realization for $k_s = 0.02\,m^{-1}$, $k_n = 0.14\,m^{-1}$, and $\zeta_s = 90°$.

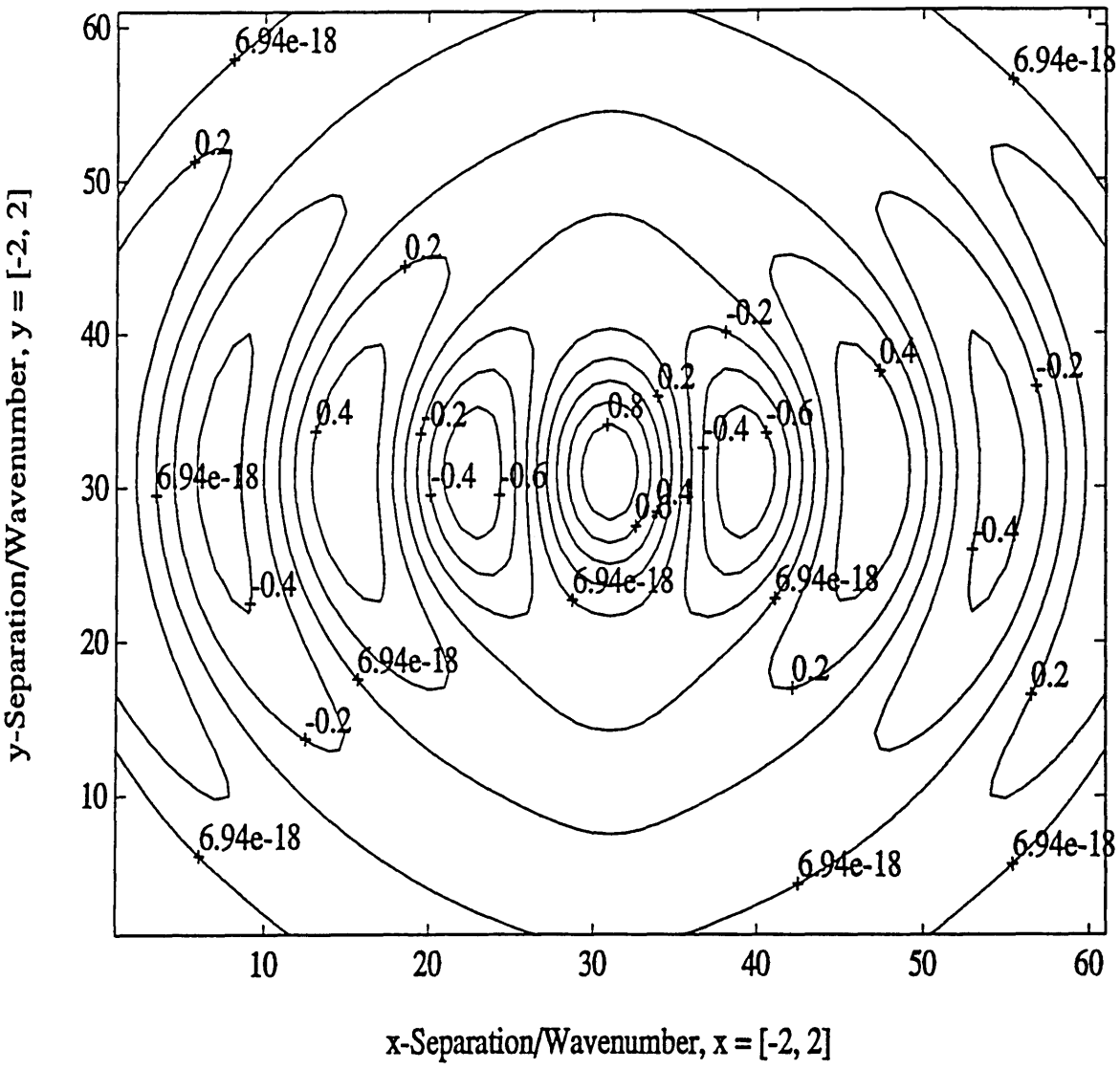

Figure 5.28: Horizontal correlation (scattered field) for $k_s = 0.02\,m^{-1}$, $k_n = 0.14\,m^{-1}$, and $\zeta_s = 90°$.

of the total noise field relative to the plane stratified case.

Then, the vertical correlation was studied. The results showed that the overall vertical correlation is of order of acoustic wavelength. Near the rough surface, the vertical correlation is slightly altered by a strong scattering field, but the effect is much smaller than for the horizontal correlation. The effects of employing different roughness spectra were also investigated. The results indicated that with different roughness spectra the resultant difference is in general small for the frequency regime of our interest. The effect of excess depth for a deep ocean waveguide was examined. The results showed that the lower-order modes in the mean noise field may be trapped in the upper part of the water column. However, in general, there still exist many modes which may escape from the sound channel and reach the bottom to interact with the roughness. Thus, rough bottom scattering still plays an important role in deep ocean noise generation, even in a waveguide with an excess depth.

Finally we extended our analysis to a three-dimensional noise field resulting from anisotropy of the sea floor topography. By employing the Goff-Jordan roughness model, in which the anisotropy may be clearly specified through the choice of the model parameters, the scattered noise field was accordingly varied, and the directivity of the noise field was then be explored. The above results suggested that the spatial correlation of the deep ocean noise field may form the basis for inversion of subbottom geological or morphological properties.

Chapter 6

Conclusions and Further Developments

— in which we summarize what we have shown, and what needs to be shown.

6.1 Conclusions

The motivation of this research project stems from recent experimental observations which demonstrate a strong evidence that the seismic interface waves are important carriers of ambient noise in a deep ocean. It has been our primary goal to search for a plausible explanation of this phenomenon. This was accomplished in a series of investigation throughout the course of this study.

The implementation of this research follows closely the objectives stated in Sec. 1.2,

where at each stage a specialized investigation has been performed, leading to an overall understanding of the problem.

The accomplishments and conclusions of this study can be summarized as follows:

- A wave-theoretical model which combines two previously developed theories for rough interface scattering and surface-generated ambient noise in a stratified ocean has been developed. The result of the derivation is in terms of the cross-spectral correlation function, which is allowed for computation of the various quantities of our interests.

- The canonical seismo-acoustic waveguide problem of an ocean bounded above by a pressure-release surface and below by an elastic bottom has been used to illustrate the spectral redistribution of the ambient noise provided by rough interface scattering in the sea bed. The results have shown that the existence of rough interfaces provides a mechanism for the excitation of Scholte waves in both *shallow* or *deep* ocean environments.

- It is demonstrated that since the secondary sources provided by the roughness are placed close to the bottom interfaces where the seismic interface waves have their maximum excitation, these waves dominate not only the scattered field, but also the total noise field. As a result, the model predicts an increase in the noise level close to the bottom, which is consistent with experimental observations.

- The overall noise intensity is shown to be dominated by the mean noise field in the upper part of the ocean, and by the scattered seismic interface waves near the sea bed.

- The noise spectra have been computed for a deep ocean environment represent-

ing a real experimental oceanic scenario. The effects of roughness statistics, and sediment properties and thickness has been analyzed. It has been demonstrated that the distinct transition frequency within the infrasonic regime (1 to 20 Hz) observed in the experimental data can be associated with the transition frequency for the seismic interface waves in a stratified sea bed, indicating that this spectral feature is attributable to the sediment shear speed and thickness. The interface roughness provides the critical mechanism for the excitation of the seismic components, but the effect of the actual roughness statistics is mainly quantitative in terms of the spectral levels.

- It is demonstrated that for roughness correlation lengths shorter than the acoustic wavelength, the scattering has the effect of decreasing the horizontal spatial correlation of the total noise field relative to the plane stratified case. This in turn suggests that the spatial correlation of the deep ocean noise field may be used as a basis for inversion for subbottom roughness. The model indicates that the horizontal spatial coherence of the near-bottom noise field is reduced by small scale roughness. Moreover, the results of rough surface scattering due to fully three-dimensional, anisotropic random field may account for the directivity of the noise field.

- Rough sea bed scattering has only a minor effect on the vertical correlation in contrast to the effect on the horizontal correlation for which it is greatly influenced by roughness scattering.

- In a deep ocean waveguide with an upward refracting sound speed profile, even though the lower-order modes in the mean noise field may be trapped in the upper part of the water column, being presented from interaction with the roughness, the coupling into the seismic waves is still important in general because sufficient number of modes may escape from the sound channel and

reach the bottom to excite the interface waves. Thus, rough surface scattering is still an important factor in considering the noise generation in a deep ocean, even with an excess depth.

- The difference between the results employing different roughness spectra (Gaussian vs. power law) is not significant in the infrasonic regime; thus, details of roughness can cause only a small difference, generally within $2\,dB$.

It should be stressed that the current study has employed several assumptions such as the Born approximation, and those assumptions embedded in Eq. (2.19) as discussed in Sec. 2.4.1 for waveguide scattering. It is expected that elimination of these assumptions can only affect the present results quantitatively, but not qualitatively. Also, the use of white noise spectrum for the random surface sources may not realistic in view of the fact that the surface wave spectrum associated with the source mechanism is generally colored. Thus, caution should be used when interpreting the results. For example, although it has been demonstrated that for certain selected bottom parameters, the present theory can in fact account entirely for the observed spectral composition, it is not by any means our intent to suggest that the surface source spectrum is white. Instead it has been our goal to illustrate the importance of the waveguide propagation and the rough interface scattering mechanism in shaping the spectral composition of the total noise field.

In terms of understanding the role of the roughness scattering in ambient noise generation in a deep ocean, with the supports of the above conclusions, our objectives for this study have been fulfilled.

6.2 Major Contributions of the Thesis Work

This thesis may be regarded as a continuation of the ongoing research in the areas of wave propagation in a stochastic waveguide conducted by Kuperman and Schmidt, *e.g.*, Ref. [7], in which the primary interest has been in the effects of rough surfaces on the waveguide propagation due to the *discrete* sources. The present study is an extension of Ref. [7], where the *distributed* sources are the noise generators, providing a distinct physical problem which allows the investigation of the scattered noise field attributable to the natural processes near the ocean surface such as wind-generated waves. Mathematically, the results from Ref. [7] provide a Green's function for the present study.

On the other hand, this research may also be viewed as pursuing along the work by Kuperman and Ingenito, *e.g.*, Ref. [8], where the noise field generated by random sources near the ocean surface in a *smooth* waveguide was treated. The present work directly extends its stochastic formalism to include the roughness interface scattering, thereby its derivation bears a close similarity in the functional form as in Ref. [8], except the scattering-related quantities which are absent in the smooth interface case.

Both the above two theories, individually, failed to account for the observed experimental data. By combining them we are able to simulate the noise field generated by the roughness scattering of surface-generated ambient noise, and thus appropriately interpreting the roles of the distributed noise sources as well as the interface roughness in modifying the noise field composition. This combined noise-scattering model has offered a deep insight into the coupling mechanisms between the random surface sources and the seismic waves, and is an important contribution towards the understanding of the ambient noise generation in a deep ocean environment.

In summary, the major contributions of this thesis work include the following:

1. Develop a noise-scattering model suitable for studying the noise fields generated by a distribution of random sources in a fluid/elastic stratified medium with rough interfaces.

2. Establish the coupling mechanisms between the surface-generated ambient noise and the seismic waves in a deep ocean environment.

3. Identify the controlling parameters and offer a physical interpretation for the transition frequency and low-frequency rise of infrasonic ambient-noise frequency spectrum.

4. Account for the effect of rough interface scattering on the spatial correlation and directivity of deep ocean ambient noise.

6.3 Further Developments

6.3.1 Theoretical Studies

The theory developed in this study is general in nature as far as the geometry of the environment is concerned, except subject to some generally accepted assumption such as horizontal stratification. However, many numerical results were derived for the purpose of qualitative analysis at the expense of numerical simplification. Even though these assumptions do not expect to damage the analysis as a whole, the amount of influence should be assessed before a full-scale application such as ambient noise prediction based upon the present model may be applied.

To refine the analysis or conduct research along this line, the following investigations are suggested:

- Quantify the fundamental assumptions including the errors introduced by the Born approximation and the contributions due to the higher-order terms in the perturbation procedure.
- Include a realistic random surface source spectrum and multiple-scale rough surfaces.
- Establish the noise spatial structure in relation to the sea floor properties for the investigation of the inverse problems.

As mentioned above, potential application of this study is to solve the inverse problems, for example, determination of sea floor geological or morphological properties from the measured noise sound fields. However, not until every phase of the proposed model is examined quantitatively should attempt be made for the inverse analysis.

6.3.2 Experimental Studies

The most direct verification of a theory is through experimentation. In this study, we have compared our theoretical prediction of frequency spectra with available experimental data, and found the gross behavior of the both results are in general consistent. Also, we have been able to interpret the experimental observations with the present model. However due to the lack of experimental data on spatial correlation for 3D scattered field in a deep ocean environment, we are unable to make a similar comparison for the spatial correlation and the directivity of the noise field.

Thus experimental implementation for the present study in an actual ocean or under simulated environment may be included in the further pursuit.

Appendix A

Derivation of the Boundary Operators for a Deep Ocean Waveguide

This appendix is cited on Page 98.

The derivation of the linear systems for the deep ocean waveguide shown in Fig. 4.1 is parallel to that for the three-layer canonical problem presented in Sec. 3.3. The depth-dependent solutions of the field potentials are still the exponential functions for the elastic media, but those for the water column are now the solutions of the pseudo-linear sound speed profile, which are the Airy functions $Ai(\zeta)$ and $Bi(\zeta)$.

Using the similar nomenclature as in Sec. 3.3, the wavefields are represented by the wavenumber integrals:

$$\phi_2(\mathbf{r},z) \;=\; \frac{1}{2\pi}\int d^2\mathbf{k}e^{-j\mathbf{k}\cdot\mathbf{r}}\left[(Ai(\zeta)+iBi(\zeta))A_2^-(\mathbf{k})+Ai(\zeta)A_2^+(\mathbf{k})\right],$$

$$
\begin{aligned}
\phi_3(\mathbf{r},z) &= \frac{1}{2\pi}\int d^2\mathbf{k}e^{-j\mathbf{k}\cdot\mathbf{r}}\left[Ai(\zeta)A_3^-(\mathbf{k})+(Ai(\zeta)+iBi(\zeta))A_3^+(\mathbf{k})\right],\\
\phi_4(\mathbf{r},z) &= \frac{1}{2\pi}\int d^2\mathbf{k}e^{-j\mathbf{k}\cdot\mathbf{r}}\left[e^{-\alpha_4 z}A_4^-(\mathbf{k})+e^{\alpha_4 z}A_4^+(\mathbf{k})\right],\\
\psi_4(\mathbf{r},z) &= \frac{1}{2\pi}\int d^2\mathbf{k}e^{-j\mathbf{k}\cdot\mathbf{r}}\left[e^{-\beta_4 z}B_4^-(\mathbf{k})+e^{\beta_4 z}B_4^+(\mathbf{k})\right],\\
\Lambda_4(\mathbf{r},z) &= \frac{1}{2\pi}\int d^2\mathbf{k}e^{-j\mathbf{k}\cdot\mathbf{r}}\left[e^{-\beta_4 z}C_4^-(\mathbf{k})+e^{\beta_4 z}C_4^+(\mathbf{k})\right],\\
\phi_5(\mathbf{r},z) &= \frac{1}{2\pi}\int d^2\mathbf{k}e^{-j\mathbf{k}\cdot\mathbf{r}}e^{-\alpha_5 z}A_5^-(\mathbf{k}),\\
\psi_5(\mathbf{r},z) &= \frac{1}{2\pi}\int d^2\mathbf{k}e^{-j\mathbf{k}\cdot\mathbf{r}}e^{-\beta_5 z}B_5^-(\mathbf{k}),\\
\Lambda_5(\mathbf{r},z) &= \frac{1}{2\pi}\int d^2\mathbf{k}e^{-j\mathbf{k}\cdot\mathbf{r}}e^{-\beta_5 z}C_5^-(\mathbf{k}),
\end{aligned}
\tag{A.1}
$$

where the kernels for ϕ_2 and ϕ_3 are chosen appropriately according to the asymptotic behavior of the Airy functions for a large argument, which in turn lend themselves to ensuring numerical stability of the resulted linear system [38]. For simplicity, the modified independent solution, $Ai(\zeta)+iBi(\zeta)$, of Eq. (4.6) will be represented by $Ci(\zeta)$ in the following presentation. The radiation conditions are applied to eliminate the upgoing components in the layer 5.

The wavefields must be supplemented by a source field if a source is present in a particular layer. In the present analysis, we assume that the sources are in the water column at depth z_s. In this case, the field generated by a point source in a pseudo-linear sound speed profile is [38]

$$
\begin{aligned}
\hat{\phi}_i(\mathbf{r},z) &= \frac{1}{2\pi}\int d^2\mathbf{k}e^{-j\mathbf{k}\cdot\mathbf{r}}\\
&\times\begin{cases}
-\frac{S_\omega}{4\pi}\frac{2c_i^{-1/3}Ci(\zeta_{z_s})}{A_i'(\zeta_{z_s})Ci(\zeta_{z_s})-Ai(\zeta_{z_s})Ci'(\zeta_{z_s})}Ai(\zeta), & a_i(z-z_s)<0\\
-\frac{S_\omega}{4\pi}\frac{2c_i^{-1/3}Ai(\zeta_{z_s})}{A_i'(\zeta_{z_s})Ci(\zeta_{z_s})-Ai(\zeta_{z_s})Ci'(\zeta_{z_s})}Ci(\zeta), & a_i(z-z_s)\geq 0
\end{cases}
\end{aligned}
\tag{A.2}
$$

where $\zeta_{z_s}=c_i^{-2/3}[k^2-\rho_w\omega^2(a_iz_s+b_i)]$, for $i=2,3$.

Again, the unknown wavefield amplitudes are determined from the boundary conditions. We shall here employ the local coordinate system for each layer; *i.e.*,

the coordinate system has an origin at the top interface of each layer. Thus the boundary conditions are:

At the sea surface (layer 1 and 2):

$$\sigma_{zz,2}|_{z=0} = 0. \tag{A.3}$$

At the sea/sea interface (layer 2 and 3):

$$w_2|_{z=t_2} = w_3|_{z=0}, \tag{A.4}$$

$$\sigma_{zz,2}|_{z=t_2} = \sigma_{zz,3}|_{z=0}. \tag{A.5}$$

$$\tag{A.6}$$

At the sea/sediment interface (layer 3 and 4):

$$w_3|_{z=t_3} = w_4|_{z=0}, \tag{A.7}$$

$$\sigma_{zz,3}|_{z=t_3} = \sigma_{zz,4}|_{z=0}, \tag{A.8}$$

$$\sigma_{zx,4}|_{z=t_3} = 0, \tag{A.9}$$

$$\sigma_{zy,4}|_{z=t_3} = 0. \tag{A.10}$$

At the sediment/subbottom interface (layer 4 and 5):

$$w_4|_{z=t_4} = w_5|_{z=0}, \tag{A.11}$$

$$u_4|_{z=t_4} = u_5|_{z=0}, \tag{A.12}$$

$$v_4|_{z=t_4} = v_5|_{z=0}, \tag{A.13}$$

$$\sigma_{zz,4}|_{z=t_4} = \sigma_{zz,5}|_{z=0}, \tag{A.14}$$

$$\sigma_{zx,4}|_{z=t_4} = \sigma_{zx,5}|_{z=0}, \tag{A.15}$$

$$\sigma_{zy,4}|_{z=t_4} = \sigma_{zy,5}|_{z=0}, \tag{A.16}$$

where $t_i = z_i - z_{i-1}$ is the thickness of layer i, for $i = 2, 3, 4$.

When the above displacements and stresses are written in terms of potentials, and the related kernels are inserted, these conditions result in a linear system of equations in the wavefield amplitudes

$$\tilde{B}_g(\mathbf{k})\tilde{\chi}_g^{\mp}(\mathbf{k}) = \tilde{C}(\mathbf{k}), \tag{A.17}$$

where $\tilde{\chi}_g^{\mp}(\mathbf{k})$ is a column vector containing the unknown amplitudes

$$\begin{aligned}\{\tilde{\chi}_g^{\mp}(\mathbf{k})\}^T \;=\; & \{\tilde{\phi}_2^-(\mathbf{k}), \tilde{\phi}_2^+(\mathbf{k}), \tilde{\phi}_3^-(\mathbf{k}), \tilde{\phi}_3^+(\mathbf{k}), \tilde{\phi}_4^-(\mathbf{k})\tilde{\phi}_4^+(\mathbf{k}), \\ & \tilde{\psi}_4^-(\mathbf{k}), \tilde{\psi}_4^+(\mathbf{k}), \tilde{\Lambda}_4^-(\mathbf{k}), \tilde{\Lambda}_4^+(\mathbf{k}), \tilde{\phi}_5^-(\mathbf{k}), \tilde{\psi}_5^-(\mathbf{k}), \tilde{\Lambda}_5^-(\mathbf{k})\},\end{aligned} \tag{A.18}$$

and $\tilde{B}_g(\mathbf{k})$ is the global coefficient matrix assembled by the local operators $\tilde{B}_{i;i+1}(\mathbf{k})$ involving layer i and $i+1$ given below

$$\widetilde{B}_g(\mathbf{k}) = \begin{bmatrix} \widetilde{B}_{1;2}^{(i,j)} & & \mathbf{0} \\ & \widetilde{B}_{2;3}^{(i,j)} & \\ & & \widetilde{B}_{3;4}^{(i,j)} \\ \mathbf{0} & & \widetilde{B}_{4;5}^{(i,j)} \end{bmatrix}$$

with

$$\tilde{B}_{1;2}^{(j,k)}(\mathbf{k}) = \begin{bmatrix} -\rho_w\omega^2 Ci(\zeta_{o_2}) & -\rho_w\omega^2 Ai(\zeta_{o_2}) \end{bmatrix},$$

$$\tilde{B}_{2;3}^{(j,k)}(\mathbf{k}) = \begin{bmatrix} -c_2^{1/3}Ci'(\zeta_{t_2}) & -c_2^{1/3}A_i'(\zeta_{t_2}) & c_3^{1/3}A_i'(\zeta_{o_3}) & -c_3^{1/3}Ci'(\zeta_{o_3}) \\ -\rho_w\omega^2 Ci(\zeta_{t_2}) & -\rho_w\omega^2 Ai(\zeta_{t_2}) & \rho_w\omega^2 Ai(\zeta_{o_3}) & \rho_w\omega^2 Ci(\zeta_{o_3}) \end{bmatrix},$$

$$\widetilde{B}_{3;4}^{(j,k)}(\mathbf{k}) = \left[\begin{array}{cccc} -c_3^{1/3}A_i'(\zeta_{t_3}) & -c_3^{1/3}Ci'(\zeta_{t_3}) & \alpha_4 & -\alpha_4 \\ -\rho_w\omega^2 Ai(\zeta_{t_3}) & -\rho_w\omega^2 Ci(\zeta_{t_3}) & \lambda_4 k_{p,4}^4 - 2\mu_4\alpha_4^2 & \lambda_4 k_{p,4}^4 - 2\mu_4\alpha_4^2 \\ 0 & 0 & 2j\mu_4 k_x\alpha_4 & -2j\mu_4 k_x\alpha_4 \\ 0 & 0 & 2j\mu_4 k_y\alpha_4 & -2j\mu_4 k_y\alpha_4 \end{array}\right.$$

$$\left.\begin{array}{cccc} 0 & 0 & -k^2 & -k^2 \\ 0 & 0 & 2\mu_4\beta_4 k^2 & -2\mu_4\beta_4 k^2 \\ j\mu_4 k_y\beta_4 & -j\mu_4 k_y\beta_4 & -j\mu_4 k_x(2k^2 - k_{s,4}^2) & -j\mu_4 k_x(2k^2 - k_{s,4}^2) \\ -j\mu_4 k_x\beta_4 & j\mu_4 k_x\beta_4 & -j\mu_4 k_y(2k^2 - k_{s,4}^2) & -j\mu_4 k_y(2k^2 - k_{s,4}^2) \end{array}\right],$$

$$\widetilde{B}_{4;5}^{(j,k)}(\mathbf{k}) = \left[\begin{array}{ccc} -\alpha_4 e^{\alpha_4 t_4} & \alpha_4 e^{-\alpha_4 t_4} & 0 \\ -jk_x e^{-\alpha_4 t_4} & -jk_x e^{\alpha_4 t_4} & -jk_y e^{-\beta_4 t_4} \\ -jk_y e^{-\alpha_4 t_4} & -jk_y e^{\alpha_4 t_4} & jk_x e^{-\beta_4 t_3} \\ (-\lambda_4 k_{p,4}^2 + 2\mu_4\alpha_4^2)e^{-\alpha_4 t_4} & (-\lambda_4 k_{p,4}^2 + 2\mu_4\alpha_4^2)e^{\alpha_4 t_4} & 0 \\ 2j\mu_4 k_x\alpha_4 e^{-\alpha_4 t_4} & -2j\mu_4 k_x\alpha_4 e^{\alpha_4 t_4} & j\mu_4 k_y\beta_4 e^{-\beta_4 t_4} \\ 2j\mu_4 k_y\alpha_4 e^{-\alpha_4 t_4} & -2j\mu_4 k_y\alpha_4 e^{\alpha_4 t_4} & -j\mu_4 k_y\beta_4 e^{-\beta_4 t_4} \end{array}\right.$$

$$\left.\begin{array}{ccc} 0 & k^2 e^{-\beta_4 t_4} & k^2 e^{\beta_4 t_4} \\ -jk_y e^{\beta_4 t_4} & jk_x\beta_4 e^{-\beta_4 t_4} & -jk_x\beta_4 e^{\beta_4 t_4} \\ jk_x e^{\beta_4 t_4} & jk_y\beta_4 e^{-\beta_4 t_4} & -jk_y\beta_4 e^{\beta_4 t_4} \\ 0 & -2\mu_4 k^2\beta_4 e^{-\beta_4 t_4} & 2\mu_4 k^2\beta_4 e^{\beta_4 t_4} \\ -j\mu_4 k_y\beta_4 e^{\beta_4 t_4} & -j\mu_4 k_x(2k^2 - k_{s,4}^2)e^{-\beta_4 t_4} & -j\mu_4 k_x(2k^2 - k_{s,4}^2)e^{\beta_4 t_4} \\ j\mu_4 k_x\beta_4 e^{\beta_4 t_4} & -j\mu_4 k_y(2k^2 - k_{s,4}^2)e^{-\beta_4 t_4} & -j\mu_4 k_y(2k^2 - k_{s,4}^2)e^{\beta_4 t_4} \end{array}\right]$$

$$\left.\begin{array}{ccc} \alpha_5 & 0 & -k^2 \\ jk_x & jk_y & -jk_x\beta_5 \\ jk_y & -jk_x & -jk_y\beta_5 \\ \lambda_5 k_{p,5}^2 - 2\mu_5\alpha_5^2 & 0 & 2\mu_5 k^2\beta_5 \\ -2j\mu_5 k_x\alpha_5 & -j\mu_5 k_y\beta_5 & j\mu_5 k_x(2k^2 - k_{s,5}^2) \\ -2j\mu_5 k_y\alpha_5 & j\mu_5 k_x\beta_5 & j\mu_5 k_y(2k^2 - k_{s,5}^2) \end{array}\right],$$

where

$$\zeta_{o_i} = c_i^{-2/3}(k^2 - \rho_w \omega^2 b_i), \tag{A.19}$$

$$\zeta_{t_i} = c_i^{-2/3}[k^2 - \rho_w \omega^2 (a_i t_i + b_i)], \tag{A.20}$$

for $i = 2$, 3, and

$$\alpha_i = \sqrt{k^2 - k_{p,i}^2}\,, \tag{A.21}$$

$$\beta_i = \sqrt{k^2 - k_{s,i}^2}\,, \tag{A.22}$$

$$k^2 = k_x^2 + k_y^2\,, \tag{A.23}$$

for $i = 4$, 5.

The column vector $\tilde{C}(\mathbf{k})$ representing the integration kernel for the source field for a source in the water column at depth z_s, assuming in the layer 2, is

$$\tilde{C}(\mathbf{k}) = \left\{ \begin{array}{c} -\frac{S_\omega \rho_w \omega^2}{4\pi} \frac{2c_2^{-1/3} Ci(\zeta_{z_s}) Ai(\zeta_{o_2})}{A_i'(\zeta_{z_s}) Ci(\zeta_{z_s}) - Ai(\zeta_{z_s}) Ci'(\zeta_{z_s})} \\ -\frac{S_\omega \rho_w \omega^2}{4\pi} \frac{2Ai(\zeta_{z_s}) Ci'(\zeta_{t_2})}{A_i'(\zeta_{z_s}) Ci(\zeta_{z_s}) - Ai(\zeta_{z_s}) Ci'(\zeta_{z_s})} \\ -\frac{S_\omega \rho_w \omega^2}{4\pi} \frac{2c_2^{-1/3} Ai(\zeta_{z_s}) Ci(\zeta_{t_2})}{A_i'(\zeta_{z_s}) Ci(\zeta_{z_s}) - Ai(\zeta_{z_s}) Ci'(\zeta_{z_s})} \\ 0 \\ 0 \\ 0 \\ 0 \\ 0 \\ 0 \\ 0 \\ 0 \\ 0 \\ 0 \end{array} \right\}.$$

The rotation boundary operator $\tilde{b}_i(\mathbf{k})$ is derived in a similar way, representing the discontinuities of the following field parameters according to Eq. (2.13):

$$\tilde{b}_{i,x}(\mathbf{k})\tilde{\chi}^{\mp}_{i;i+1}(\mathbf{k}) = \left\{ \begin{array}{c} -\tilde{u}_i + \tilde{u}_{i+1} \\ \tilde{w}_i - \tilde{w}_{i+1} \\ 0 \\ -2\tilde{\sigma}_{xz,i} + 2\tilde{\sigma}_{xz,i+1} \\ \tilde{\sigma}_{zz,i} - \tilde{\sigma}_{xx,i} - \tilde{\sigma}_{zz,i+1} + \tilde{\sigma}_{xx,i+1} \\ -\tilde{\sigma}_{xy,i} + \tilde{\sigma}_{xy,i+1} \end{array} \right\}, \tag{A.24}$$

$$\tilde{b}_{i,y}(\mathbf{k})\tilde{\chi}^{\mp}_{i;i+1}(\mathbf{k}) = \left\{ \begin{array}{c} -\tilde{v}_1 + \tilde{v}_{i+1} \\ 0 \\ \tilde{w}_i - \tilde{w}_{i+1} \\ -2\tilde{\sigma}_{yz,i} + 2\tilde{\sigma}_{yz,i+1} \\ -\tilde{\sigma}_{xy,i} + \tilde{\sigma}_{xy,i+1} \\ \tilde{\sigma}_{zz,i} - \tilde{\sigma}_{yy,i} - \tilde{\sigma}_{zz,i+1} + \tilde{\sigma}_{yy,i+1} \end{array} \right\}, \tag{A.25}$$

for $i = 3, 4$. By inserting the wavenumber kernel for the displacements and stresses, we get the rotational operators as

$$\tilde{b}_{3,x}(\mathbf{k}) = \left[\begin{array}{cccc} jk_xAi(\zeta_{t_3}) & jk_xCi(\zeta_{t_3}) & -jk_x & -jk_x \\ 0 & 0 & 4j\mu_4 k_x\alpha_4 & -4j\mu_4 k_x\alpha_4 \\ 0 & 0 & -2\mu_4(k_x^2+\alpha_4^2) & -2\mu_4(k_x^2+\alpha_4^2) \\ 0 & 0 & -2\mu_4 k_xk_y & -2\mu_4 k_xk_y \end{array} \right.$$

$$\left. \begin{array}{cccc} -jk_y & -jk_y & jk_x\beta_4 & -jk_x\beta_4 \\ 2j\mu_4 k_y\beta_4 & -2j\mu_4 k_y\beta_4 & -2j\mu_4 k_x(2k^2-k_{s,4}^2) & -2j\mu_4 k_x(2k^2-k_{s,4}^2) \\ -2\mu_4 k_xk_y & -2\mu_4 k_xk_y & 2\mu_4\beta_4(2k_x^2+k_y^2) & -2\mu_4\beta_4(2k_x^2+k_y^2) \\ \mu_4(k_x^2-k_y^2) & \mu_4(k_x^2-k_y^2) & 2\mu_4\beta_4 k_xk_y & -2\mu_4\beta_4 k_xk_y \end{array} \right],$$

$$\tilde{b}_{3,y}(\mathbf{k}) = \begin{bmatrix} jk_yAi(\zeta_{t_3}) & jk_yCi(\zeta_{t_3}) & -jk_y & -jk_y \\ 0 & 0 & 4j\mu_4k_y\alpha_4 & -4j\mu_4k_y\alpha_4 \\ 0 & 0 & -2\mu_4k_xk_y & -2\mu_4k_xk_y \\ 0 & 0 & -2\mu_4(k_x^2+\alpha_4^2) & -2\mu_4(k_x^2+\alpha_4^2) \end{bmatrix}$$

$$\begin{bmatrix} jk_x & jk_x & jk_y\beta_4 & -jk_y\beta_4 \\ -2j\mu_4k_x\beta_4 & 2j\mu_4k_x\beta_4 & -2j\mu_4k_y(2k^2-k_{s,4}^2) & j2\mu_4k_y(2k^2-k_{s,4}^2) \\ \mu_4(k_x^2-k_y^2) & \mu_4(k_x^2-k_y^2) & 2\mu_4\beta_4k_xk_y & -2\mu_4\beta_4k_xk_y \\ 2\mu_4k_xk_y & 2\mu_4k_xk_y & 2\mu_4\beta_4(2k_x^2+k_y^2) & -2\mu_4(2k_x^2+k_y^2) \end{bmatrix},$$

$$\tilde{b}_{4,x}(\mathbf{k}) = \begin{bmatrix} jk_xe^{-\alpha_4t_4} & jk_xe^{\alpha_4t_4} & jk_ye^{-\beta_4t_4} \\ -\alpha_4e^{-\alpha_4t_4} & \alpha_4e^{-\alpha_4t_4} & 0 \\ 0 & 0 & 0 \\ -4j\mu_4k_x\alpha_4e^{-\alpha_4t_4} & 4j\mu_4k_x\alpha_4e^{\alpha_4t_4} & -2j\mu_4k_y\beta_4e^{-\beta_4t_4} \\ 2\mu_4(k_x^2+\alpha_4^2)e^{-\alpha_4t_4} & 2\mu_4(k_x^2+\alpha_4^2)e^{\alpha_4t_4} & 2\mu_4k_xk_ye^{-\beta_4t_4} \\ 2\mu_4k_xk_ye^{-\alpha_4t_4} & 2\mu_4k_xk_ye^{\alpha_4t_4} & -\mu_4(k_x^2-k_y^2)e^{-\beta_4t_4} \end{bmatrix}$$

$$\begin{bmatrix} jk_ye^{\beta_4t_4} & -jk_x\beta_4e^{-\beta_4t_4} & jk_x\beta_4e^{\beta_4t_4} \\ 0 & k^2e^{-\beta_4t_4} & k^2e^{\beta_4t_4} \\ 0 & 0 & 0 \\ 2j\mu_4k_y\beta_4e^{\beta_4t_4} & 2j\mu_4k_x(2k^2-k_{s,4}^2)e^{-\beta_4t_4} & 2j\mu_4k_x(2k^2-k_{s,4}^2)e^{\beta_4t_4} \\ 2\mu_4k_xk_ye^{\beta_4t_4} & -2\mu_4\beta_4(2k_x^2+k_y^2)e^{-\beta_4t_4} & 2\mu_4\beta_4(2k_x^2+k_y^2)e^{\beta_4t_4} \\ -\mu_4(k_x^2-k_y^2)e^{-\beta_4t_4} & -2\mu_4\beta_4k_xk_ye^{-\beta_4t_4} & 2\mu_4\beta_4k_xk_ye^{\beta_4t_4} \end{bmatrix}$$

$$\begin{bmatrix} -jk_x & -jk_y & jk_x\beta_5 \\ \alpha_5 & 0 & -k^2 \\ 0 & 0 & 0 \\ 4\mu_5 k_x \alpha_5 & 2\mu_5 k_y \beta_5 & -2\mu_5 k_x (2k^2 - k_{s,5}^2) \\ -2\mu_5 (k_x^2 + \alpha_5^2) & -2\mu_5 k_x k_y & 2\mu_5 \beta_5 (2k_x^2 + k_y^2) \\ -2\mu_5 k_x k_y & \mu_5 (k_x^2 - k_y^2) & 2\mu_5 k_x k_y \beta_5 \end{bmatrix},$$

$$\tilde{b}_{4,y}(\mathbf{k}) = \begin{bmatrix} jk_y e^{-\alpha_4 t_4} & jk_y e^{\alpha_4 t_4} & -jk_x e^{-\beta_4 t_4} \\ 0 & 0 & 0 \\ -\alpha_4 e^{-\alpha_4 t_4} & \alpha_4 e^{\alpha_4 t_4} & 0 \\ -4j\mu_4 k_y \alpha_4 e^{-\alpha_4 t_4} & 4j\mu_4 k_y \alpha_4 e^{\alpha_4 t_4} & 2j\mu_4 k_y \beta_4 e^{-\beta_4 t_4} \\ 2\mu_4 k_x k_y e^{-\alpha_4 t_4} & 2\mu_4 k_x k_y e^{\alpha_4 t_4} & -\mu_4 (k_x^2 - k_y^2) e^{-\beta_4 t_4} \\ 2\mu_4 (k_y^2 + \alpha_4^2) e^{-\alpha_4 t_4} & 2\mu_4 (k_y^2 + \alpha_4^2) e^{\alpha_4 t_4} & -2\mu_4 k_x k_y e^{-\beta_4 t_4} \end{bmatrix}$$

$$\begin{matrix} -jk_y e^{\beta_4 t_4} & -jk_y \beta_4 e^{-\beta_4 t_4} & jk_x \beta_4 e^{\beta_4 t_4} \\ 0 & 0 & 0 \\ 0 & k^2 e^{-\beta_4 t_4} & k^2 e^{\beta_4 t_4} \\ -2j\mu_4 k_x \beta_4 e^{\beta_4 t_4} & 2j\mu_4 k_y (2k^2 - k_{s,4}^2) e^{-\beta_4 t_4} & 2j\mu_4 k_y (2k^2 - k_{s,4}^2) e^{\beta_4 t_4} \\ -\mu_4 (k_x^2 - k_y^2) e^{-\beta_4 t_4} & -2\mu_4 \beta_4 k_x k_y e^{-\beta_4 t_4} & 2\mu_4 \beta_4 k_x k_y e^{\beta_4 t_4} \\ -2\mu_4 k_x k_y e^{\beta_4 t_4} & -2\mu_4 \beta_4 (k_x^2 + 2k_y^2) e^{-\beta_4 t_4} & 2\mu_4 \beta_4 (k_x^2 + 2k_y^2) e^{\beta_4 t_4} \end{matrix}$$

$$\begin{bmatrix} -jk_y & jk_x & jk_x\beta_5 \\ 0 & 0 & 0 \\ \alpha_5 & 0 & -k^2 \\ 4j\mu_5 k_y \alpha_5 & -2j\mu_5 k_x \beta_5 & -2j\mu_5 k_y (2k^2 - k_{s,5}^2) \\ -2\mu_5 k_x k_y & \mu_5 (k_x^2 - k_y^2) & 2\mu_5 k_x k_y \beta_5 \\ -2\mu_5 (k_x^2 + \alpha_5^2) & 2\mu_5 k_x k_y & 2\mu_5 \beta_5 (k_x^2 + 2k_y^2) \end{bmatrix}.$$

The depth derivative of the operators, $\tilde{B}_{3;4}^{(j,k)}$ and $\tilde{B}_{4;5}^{(j,k)}$, is obtained by simply multiplying the columns corresponding to $\tilde{\phi}_i^-$,$\tilde{\phi}_i^+$,..., with $-\alpha_i$, α_i, *etc.*, except those elements involving Airy functions, A_i and B_i, are now replaced by the product of $-c_i^{1/3}$ and the derivative with respect to its argument of the related Airy functions.

References

[1] M. S. Longuet-Higgins, "A theory on the origin of microseisms," Philos. Trans. Roy. Soc., Ser. A **243**, 1-35 (1950).

[2] K. A. Hasselmann, "A statistical analysis of the generation of microseism," Rev. Geophysic. Space Phys., **1**, 177-210 (1963).

[3] A. E. Schreiner and L. M. Dorman, "Coherence lengths of seafloor noise: Effect of ocean bottom structure," J. Acoust. Soc. Am. **88**, 1503-1514 (1990).

[4] A. C. Kibblewhite and K. C. Ewans, "Wave-wave interactions, microseisms, an infrasonic ambient noise in the ocean," J. Acoust. Soc. Am. **78**, 981-994 (1986).

[5] Henrik Schmidt and W. A. Kuperman, "Estimation of surface noise source level from low-frequency seismoacoustic ambient noise measurements," J. Acoust. Soc. Am. **84**, 2153-2162 (1988).

[6] J.A. Ogilvy, "Wave scattering from rough surface," Rep. Prog. Phys. *50*, 1553-1608 (1987).

[7] W. A. Kuperman and Henrik Schmidt, "Self-consistent perturbation approach to rough surface scattering in stratified elastic media," J. Acoust. Soc. Am. **86**, 1511-1522 (1989).

[8] W. A. Kuperman and F. Ingenito, "Spatial correlation of surface generated noise in a stratified ocean," J. Acoust. Soc. Am. **67**, 1988-1996 (1980).

[9] Lord Rayleigh, *The Theory of Sound* (New York: Dover, 1945) (1st edition, 1877, New York: Macmillan).

[10] Lord Rayleigh, "On the dynamical theory of gratings," Proc. Roy. Soc., **A 79**, 399-416 (1907).

[11] Eric I. Thorsos and Darrell R. Jackson, "The validity of the perturbation approximation for rough surface scattering using a Gaussian roughness spectrum," J. Acoust. Soc. Am. **86**, 261-277 (1989).

[12] G.R. Kirchhoff, *Vorlesung uber mathematische physik*, Vol. II (Leipzig:Teubner, 1891).

[13] F. M. Labianca and E. Y. Harper, "Connection between various small-waveheight solutions of the problem of the problem of scattering from ocean surface," J. Acoust. Soc. Am., **62**, 1144-1157 (1977).

[14] P. M. Morse and H. Feshbach, *Methods of Theoretical Physics*, Vols. I and II (New York: McGraw-Hill, 1953).

[15] Y.-H. Pao and C.-C. Mow, *Diffraction of Elastic Waves and Dynamic Stress Concentrations* (London: Hilger).

[16] P. Beckmann and A. Spizzichino, *The Scattering of Electromagnetic Waves from Rough Surfaces*, (Oxford: Pergamon, 1963).

[17] P. Beckmann, "Scattering of light by rough surfaces", Progress in Optics, Vol. VI, E. Wolf editor, (Amsterdam: North Holland, 1967).

[18] F. G. Bass and I. M. Fuks, *Wave Scattering from Statistically Rough Surfaces* (Oxford: Pergamon, 1979).

[19] J. A. Ogilvy, *Theory of Wave Scattering from Random Rough Surfaces* (Adam Hilger, 1991).

[20] F. Fortuin, "Survey of literature on reflection and scattering of sound waves at the sea surface," J. Acoust. Soc. Am. **47**, 1209-1228 (1969).

[21] C. W. Horton, "A review of reverberation, scattering and echo structure," J. Acoust. Soc. Am. **51**, 1049-1061 (1972).

[22] A. Ishimaru, *Wave Propagation and Scattering in Random Media*, Vol. II (Academic Press, 1978), Chap. 21.

[23] W. A. Kuperman, "Coherent component of specular reflection and transmission at a randomly rough two-fluid interface," J. Acoust. Soc. Am. **58**, 365-370 (1975).

[24] W. A. Kuperman and F. Ingenito, "Attenuation of the coherent component of sound propagation in shallow water with rough boundaries," J. Acoust. Soc. Am. **61**, 1178-1187 (1977).

[25] H. Medwin, "Speed of sound in water: A simple equation for realistic parameters," J. Acoust. Soc. Am., **58**, 1318-1319 (1975).

[26] Ivan Tolstoy and C. S. Clay, *Ocean Acoustics, Theory and Experiment in Underwater Sound,* Acoust. Soc. of Am., p. 6 (1987).

[27] C. L. Pekeris, "Theory of propagation of explosive sound in shallow water," Mem. Geol. Soc. Am., **No. 27** (1948).

[28] W. S. Jardetzky, "Period equation for an N-layered halfspace and some related questions," Tech. Rep. Seism. **No. 29**, Columbia University, Lamont-Doherty Geological Observatory, 1953.

[29] W. M. Ewing, W. S. Jardetzky, and F. Press, *Elastic Waves in Layered Media* (McGraw-Hill, 1957).

[30] W. T. Thomson, "Transmission of elastic waves through a stratified solid medium," J. Appl. Phys. **21**, 89-93 (1950).

[31] N. A. Haskell, "The dispersion of surface waves on multilayered media," Bull. Seismol. Soc. Am., **43**, 17-34 (1953).

[32] B. L. N. Kennett, "Reflections, rays, and reverberations," Bull. Seism. Soc. Am., **65**, 1685-1696 (1974).

[33] B. L. N. Kennett, *Seismic Wave Propagation in Stratified Media* (Cambridge Univ. Press, 1983).

[34] J. Ha, "Recurrence relations for computing P and SV seismograms," Geophys. J. R. Astr. Soc., **79**, 863-874 (1984).

[35] Henrik Schmidt and F. B. Jensen, "An efficient numerical solution technique for wave propagation in horizontally stratified environments," Comp. Math. Appl. **11**, 699-716 (1985).

[36] H. Schmidt and G. Tango, "Efficient global matrix approach to the computation of synthetic seismograms," Geophys. J. R. astr. Soc. **84**, 331-359 (1986).

[37] O. C. Zienkiewitz, *The Finite Element Method*, 3rd edition (McGraw-Hill, 1977).

[38] Henrik Schmidt, *SAFARI - Seismo-Acoustic Fast Field Algorithm for Range-Independent Environment, User's Guide*, SR 113 (SACLANT ASW Research Centre, La Spezia, Italy, 1987).

[39] L. M. Brekhovskikh, *Waves in Layered Media*, 2nd edition (Prentice-Hall, 1980).

[40] Keiiti Aki and Paul G. Richards, *Quantitative Seismology Theory and Methods*, Vol I (Freeman, 1980).

[41] W. A. Kuperman and Henrik Schmidt, "Rough surface elastic wave scattering in a horizontally stratified ocean," J. Acoust. Soc. Am. **79**, 1767-1777 (1986).

[42] Henrik Schmidt and Finn B. Jensen, "A full wave solution for propagation in multilayered viscoelastic media with application to Gaussian beam reflection at fluid-solid interfaces," J. Acoust. Soc. Am. **77**, 813-825 (1985).

[43] H. Schmidt and J. Glattetre, "A fast field model for three-dimensional wave propagation in stratified environments based on the global matrix method," J. Acoust. Soc. Am. **78**, 2105-2114 (1985).

[44] T.H. Bell, "Statistical features of sea floor topography," Deep Sea Res., **22**, 883-892, (1975b).

[45] T.H. Bell, "Mesoscale sea floor roughness," Deep Sea Res., Part A. **26**, 65-76 (1975).

[46] C. G. Fox and D. E. Hayes, "Quantitative methods for analyzing the roughness of the seafloor," Rev. Geophys., **23**, 1-48 (1985).

[47] John A. Goff and Thomas H. Jordan, "Stochastic modeling of seafloor morphology: Inversion of Sea Beam data for second-order statistics," J. Geophys. Res., **93**, No. B11, 13,589-13,608 (1988).

[48] B.B. Mandelbrot, *The Fractal Geometry of Nature* (W.H. Freeman, NY, 1985).

[49] S. A. Kitaigorodskii, *Physika Vsaimodesstiviya i Okeana*, (Physics of Ocean-Atmosphere Interaction) (Gidrometeoizdat, Leningrad, 1970).

[50] T. P. Barnett and J. C. Wilkerson, "On the generation of ocean wind waves as inferred from airborne radar measurements of fetch-limited spectra," J. Mar. Res., **25**, 292-328 (1967).

[51] W. J. Pierson, Jr. and L. Moskovitz, "A proposed spectral form for fully developed wind seas based on the similarity theory of S. A. Kitaigorodskii," J. Geophys. Res., **69**, 5181-5190 (1964).

[52] W. J. Pierson, Jr., "Wind-generated gravity waves," in *Advances in Geophysics,* **2**, 93-178 (Academic Press, 1955).

[53] T. R. Thomas (ed), *Rough Surfaces* (Longman, 1982).

[54] G.P. Agapova, "Quantitative characteristics of bottom slope angles in seas and oceans," Oceanology, Engl. Trans., 5(4), 135-138 (1965).

[55] H. H. Heezen and T. L. Holcombe, "Geographic distribution of bottom roughness in the North Atlantic," 41 pp., Bell Teleph. Lab., Holmdel, N.J., and Lamont-Doherty Geol. Observ., Columbia Univ., Palisades, N.Y., (1965).

[56] D. C. Krause and H. W. Menard, "Depth distribution and bathymetric classification of some sea floor profiles," Mar. Geol., **3**, 169-193 (1965).

[57] R. L. Larson and F. N. Spiess, "Slope distributions of the East Pacific Rise crest," SIO Ref. 70-8, Scripps Inst. Oceanogr., Univ. of Calif., San Diego (1970).

[58] D. C. Krause, P. J. Grim, and H. W. Menard, "Quantitative marine geomorphology of the East Pacific Rise," NOAA Tech. Rep., ERL 275-AOML 10, 1-73 (1973).

[59] N. S. Neidell, "Spectral studies of marine geophysical profiles," Geophysics, **31**, 122-134 (1966).

[60] J. M. Berkson, "Statistical properties of ocean bottom roughness, power spectra of ocean bottom roughness (abstract)," J. Acoust. Soc., Am., **58** (S1), 587 (1975).

[61] M.F. McDonald and E.J. Katz, "Quantitative methods for describing the regional topography of the ocean floor," J. Geophys. Res., **74**, 2597-2607 (1969).

[62] C. S. Clay and W. K. Leong, "Acoustic estimates of the topography and roughness spectrum of the sea floor southeast of the Iberian Peninsula," *Physics of Sound in Marine Sediments*, edited by L. Hampton (John Wiley 1977).

[63] T. Akal and J. Hovem, "Two-dimensional space series analysis for sea-floor roughness," Mar. Geotechnol., 3(2), 171-182 (1978).

[64] J. J. Naudin and R. Prud'homme, "L'analyse cartographique: Etude numérique des caractéristiques morphologiques des surfaces," Sci. Terre Ser. Inf. Geol., **25** 47-71 (1980).

[65] J. M. Berkson and J. E. Matthews, "Statistical properties of seafloor roughness," in *Acoustics in the Sea-Bed,* edited by N. G. Pace, 215-223 (Bath University Press, Bath, England, 1983).

[66] J. Miklowitz, *The Theory of Elastic Waves and Waveguides* (North-Holland, New York, 1984).

[67] Henrik Schmidt and S. Krenk, "Asymmetric vibration of a circular elastic half-space," Int. J. Solids Struct., **18**, 91-105 (1982).

[68] M. J. Beran and G. B. Parrent, Jr., *Theory of Partial Coherence* (Prentice-Hall, Englewood Cliffs, 1964), p. 58.

[69] Finn. B. Jensen, W.A. Kuperman, M. B. Porter, and H. Schmidt, *Computational Ocean Acoustics* (Springer-Verlag, to be published); also class notes of courses 13.861 and 13.863 at MIT by Professor Henrik Schmidt.

[70] M. Abramowitz and I. A. Stegun, *Handbook of Mathematical Functions* (Dover, New York, 1965).

[71] G. L. D'Spain, W. S. Hodgkiss, and G. L. Edmonds, "Energetics of the deep ocean's infrasonic field," J. Acoust. Soc. Am. **89**, 1134-1158 (1991).

[72] Henrik Schmidt, "Excitation and propagation of interface waves in a stratified sea-bed", 327-334 in *Acoustics and the Sea-Bed* edited by N.G. Page, Conference Proceedings (Bath U. Press, Bath UK, 1983).

[73] R. D. Mindlin, *An Introduction to Mathematical Theory of Vibration of Elastic Plates* (Fort Monmouth, NY. U.S. Army Signal Corps. Engineering Laboratories, 1955).

[74] L. M. Brekhovskikh and Yu. P. Lysanov, *Fundamentals of Ocean Acoustics*, 2nd edi. (Springer-Verlag, 1991).